Controlling Polymer Microstructure using Multiblock Copolymers *via* Reversible Addition−Fragmentation Chain Transfer Polymerization

Junliang Zhang

A thesis submitted in partial fulfilment of the requirements of the degree of

Doctor of Philosophy in Chemistry

Department of Chemistry

University of Warwick

July 2017

Table of Contents

List of Figures

List of Tables

List of Schemes

Abbreviations

3D	Three dimensional
ACVA	4, 4′-azobis(4-cyanovaleric acid)
AFM	Atomic force microscopy
ATRP	Atom transfer radical polymerisation
$CDCl_3$	Deuterated chloroform
$CHCl_3$	Chloroform
CTA	Chain transfer agent
Đ	Dispersity
DBA	Benzene-1,4-diboronic acid
DBTDL	Dibutyltin dilaurate
DCM	Dichloromethane
D_h	Hydrodynamic diameter
DP	Degree of polymerization
DLS	Dynamic light scattering
DMAP	4-dimethylaminopyridine
DMF	Dimethylformamide
DMSO	Dimethyl sulfoxide
DRI	Differential refractive index
DSC	Differential scanning calorimetry
EDC.HCl	1-(3-Dimethylaminopropyl)-3-ethylcarbodiimide hydrochloride
EGMEA	Ethylene glycol methyl ether acrylate
<*G*>	Compaction parameter
GLA	Glycerol acrylate
GPC	Gel permeation chromatography

HEA	2-hydroxyethyl acrylate
MBCP	multiblock copolymer
MDI	4, 4′-Methylenebis(phenyl isocyanate)
MeOH	Nethanol
$\boldsymbol{M_n}$	Number average molar mass
MPABTC	Methoxy-(propanoic acid)yl butyl trithiocarbonate
$\mathbf{Na_2SO_4}$	Sodium sulphate
$\mathbf{N_{eff}}$	Effective number of monomer units
NMP	Nitroxide mediated polymerisation
NAM	4-acryloylmorpholine
NMR	Nuclear magnetic resonance
ODT	Order-disorder transition
PABTC	2-(((butylthio)-carbonothioyl)thio)propanoic acid (called (propanoic acid)yl butyl trithiocarbonate
PB	Polybutadiene
PNAM	Poly(4-Acryloylmorpholine)
PS	Polystyrene
***p*TI**	*p*-tolyl isocyanate
RAFT	Reversible addition fragmentation chain transfer
$\mathbf{R_h}$	Radius hydrodynamic
RDRP	Reversible deactivation radical polymerization
SAXS	Small angel X-ray scattering
SCNP	Single chain nanoparticle
SCJNP	Single chain Janus nanoparticle
SEC	Size exclusion chromatography

T_g	Glass transition temperature
TEM	Transmission electron microscopy
***t*BA**	*tert*-butyl acrylate
TEA	Triethylamine
THF	Tetrahydrofuran
UV	Ultraviolet
VA-044	2, 2′-azobis[2-(2-imidazolin-2-yl)propane]dihydrochloride
V601	Dimethyl 2, 2′-azobis(2-methylpropionate)

Acknowledgements

I would like to take this opportunity to thank all the people who provided me great help during my PhD study.

First and foremost, I would like to thank my supervisor, Professor Sébastien Perrier, for giving me this opportunity to pursue my PhD study in this great group and for being a great mentor to let me have the freedom to explore my ability to uncover the mystery of science. I cannot thank you enough for what you have done for me: from before I joined the group, throughout the whole process of my PhD study, and the help and support when I was looking for a job. Thank you very much for your guidance during my PhD researches, your encouragement when I met difficulties, your advices when I needed them, and help in finding ways for my PhD going to the promising direction. Thank you for providing me the opportunities to participate conferences to improve my presentation skills and meet scientists from different places of the world. Thank you very much for choosing me as your student even my background was not relevant to the research of the group. Thank you for everything you have done for me!

I would also like to extend my acknowledgement to Professor David M. Haddleton for giving me useful suggestions and guidance for my PhD research. Thank you very much for your help and support when I was applying for fellowship and jobs. Thank you for being my PhD thesis examiner and the useful suggestions and discussions.

Also thanks Dr. Remzi Becer from Queen Mary, University of London for being my PhD thesis examiner and the suggestions and corrections for my thesis. I would also like to thank Dr. David Fox for giving me suggestions in my first two years' annual reports. Special thanks to my Masters' study supervisor Professor Hui Xu for the great mentor and continuous supports with my PhD study.

I would also like to thank Dr. Guillaume Gody, the master of RAFT polymerization. Thank you for teaching me the knowledge of RAFT polymerization and synthesis of multiblock copolymers, answering me questions, and help and guidance for my first PhD project. I cannot forget the way you carry out scientific research, the integrity you showed in doing scientific research.

Also, I would like to express my great gratitude to Dr. Matthias Hartlieb for the help throughout my PhD. I learned a lot from you about analysing data and writing scientific publications. Thank you for the help of my PhD researches and writing manuscripts. Especially thanks for the help when I was applying for jobs.

Thanks also go to Mr. Robert Deubler and Professor Dr. Felix H. Schacher from Friedrich-Schiller-University Jena for the SAXS analysis of my samples and contributions of the writing of the manuscript. Many thanks to Ms. Elena Patyukova and Dr. Paul D. Topham from Aston University for the theoretical study and the data analysis of my results and the contributions to the writing of manuscript.

I also would like to express my enormous and special thanks to Mr. Joji Tanaka. Thank you very much for the nice ideas and help in my PhD research. Many thanks for getting involved and contributions in my PhD projects. I will always remember the many nights of working until very late in the labs and office with you. Thank you so much for your kind explanations of both scientific and non-scientific questions without complaining. Thanks for being so modest. It has been a really nice pleasure working with you.

Big thanks also goes to Dr. Johannes C. Brendel for the ideas and suggestions for my PhD research and the help when I was applying for the job in University Jena. Also thanks Dr. Sylvain Catrouillet for the help in my research and manuscript writing. Thanks Mr. Pratik Gurnani for carrying out the TEM analysis and help in my research. Many thanks to Mr. Liam

Martin for the fruitful discussion about the RAFT polymerization and help for my research. Thanks Dr. Paul Wilson for the corrections of the manuscript.

The NMR analysis for my samples by Dr. Ivan Prokes is really appreciated. Thanks Dr. Neil Wilson for providing training and the access of the AFM equipment. Great appreciation to Dr. Daniel Lester for the help and maintenance of the GPC. Thanks Mr. David Hammond and Mr. Patrick De Jongh for the help in DSC analysis. Huge thanks to Mr. Jason Noone for solving the IT problems for me.

I would also like to thank all the colleagues and friends (Dr. Chongyu Zhu, Mr. Sangho Won, and Mr. Nuttapol Risangud) across the corridor. Many thanks to all the Perrier group members for the help in my PhD study, for making my life here colourful and enjoyable. I will miss the time of playing football together with you (cheers, football teammates!), group outing, and group seminars. I will remember everyone, especially Majda's laugh. Yes, that's the one!

Finally, I would like to thank all my family members for the encouragement, support and the endless love throughout the years. Especially, sincerely thanks to my beautiful, lovely wife, Pei Zhou, for the companion of so many years, all the support, encouragement, and understanding. I could achieve nothing without you.

Declaration

Experimental work contained in this thesis is original research carried out by the author, unless otherwise stated, in the Department of Chemistry at the University of Warwick, October 2013 and July 2017. No material contained herein has been submitted for any other degree, or at any other institution.

Results from other authors are referenced in the usual manner throughout the text.

Date:

_____

Junliang Zhang

Abstract

Reversible addition fragmentation chain transfer (RAFT) polymerization is a very versatile way to generate synthetic polymeric materials. Multiblock copolymers have received enormous scientific interest recently due to the ability to mimic the sequence-regulated microstructure of biopolymers. The objective of this thesis was to investigate RAFT polymerization and explore its potential in the synthesis of sequence-controlled multiblock polymeric chains, and their use to tune the micro-structure of the polymers, engineer single chain polymeric nanoparticles, and fabricate functional polymeric nanomaterials.

This work firstly addresses the investigation of the enormous ability of sequence-controlled multiblock copolymer to tune the physical properties by altering their microstructure. A series of sequence controlled multiblock copolymers were synthesized by RAFT polymerization using ethylene glycol methyl ether acrylate and tert-butyl acrylate as monomers. These block copolymers were synthesized with an alternating order of the two monomers with a similar total degree of polymerization. The number of blocks was varied by decreasing the length of each block while keeping the ratio of monomers constant. Their microphase separation was studied by investigating the glass transition temperature utilizing differential scanning calorimetry analysis. Small angel X-ray scattering analysis was also applied to investigate the transition of the microphase separation with the variation of the segmentations of these multiblock copolymers. The study found the microstructure was significantly affected by the number of segments of the polymer chain whilst keeping the total length constant.

Having demonstrated the enormous potential of sequence controlled multiblock copolymers to access defined microstructures, further studies were focused on mimicking the controlled folding process of the peptide chain to a secondary and tertiary structure using

sequence controlled multiblock copolymers. RAFT polymerization was used to produce multiblock copolymers, which are decorated with pendant cross-linkable groups in foldable sections, separated by non-functional spacer blocks in between. An external cross linker was then used to cause the folding of the specific domains. A chain extension-folding sequence was applied to create polymer chains having individual folded subdomains. In order to achieve a further step on the way to copy nature's ability to synthesize highly defined bio-macromolecules with a distinct three dimensional structure, linear diblock copolymer precursors were synthesized by RAFT polymerization. One block of the precursor with pendant functional groups was folded using an external cross-linker to form tadpole-like single chain nanoparticles (SCNPs). These tadpole-like SCNPs could then self-assemble into a more complex stimuli responsive 3D structure by adaptation to environmental pH changes. The stimuli responsive assemblies were found to be able to dissociate responding to low pH or exposure to glucose.

Chapter 1 *Introduction*

1.1 RAFT polymerization

1.1.1 The mechanism of RAFT polymerization

Reversible addition-fragmentation chain transfer (RAFT) polymerization was first reported by Moad, Rizzardo, and Thang in 1998.[1] RAFT has since become one of the most powerful and versatile tools for the synthesis of polymers in the area of reversible deactivation radical polymerization (RDRP).[2-4] RAFT polymerization is a process similar to a conventional free-radical system (monomer and initiator) with the exception of requiring the introduction of a dithioester compound as chain transfer agent (CTA). The generally accepted mechanism of RAFT polymerization based on addition-fragmentation[5-10] is depicted in **Scheme 1.1**, which consists of several elementary steps, including: initiation, chain transfer, re-initiation, chain equilibration, and termination.

The radicals generated by the decomposition of the initiator react with the monomer which is called initiation step (step I, k_i, the radicals may add directly to the RAFT agent before react with any monomer). The propagating radicals ($P_m^{\bullet}$, growing polymer chains) add onto the thiolcarbonyl double bond (C=S) of the RAFT agent (**1**) to form the radical intermediate (**2**, step II, k_{add}). The intermediate **2** subsequently fragments into a macro chain transfer agent (Macro-CTA, **3**) and a new reinitiating radical $R^{\bullet}$ (chain transfer step, step II, k_β). The formed $R^{\bullet}$ group will re-initiate the polymerization by reacting with other monomers to start another polymer chain $P_1^{\bullet}$ ($k_{re\text{-}in}$, step III), which subsequently either forms a new propagating group $P_n^{\bullet}$ (k_p, step III) or reacts with the Macro-CTA (k_β, step II). When the initial CTA is completely consumed, the main equilibrium (IV) will be established by degenerative chain transfer

between the active ($P_n^{\bullet}$ or $P_m^{\bullet}$) and dormant chains (thiocarbonyl-thio capped **3** or **5**). This equilibrium will provide all chains equal probability to grow and, therefore, lead to the formation of polymers with narrow molar mass distribution. The intermediate radicals **2** will also be involved in reactions of termination with other radicals by combination (k_{tc}, step V).

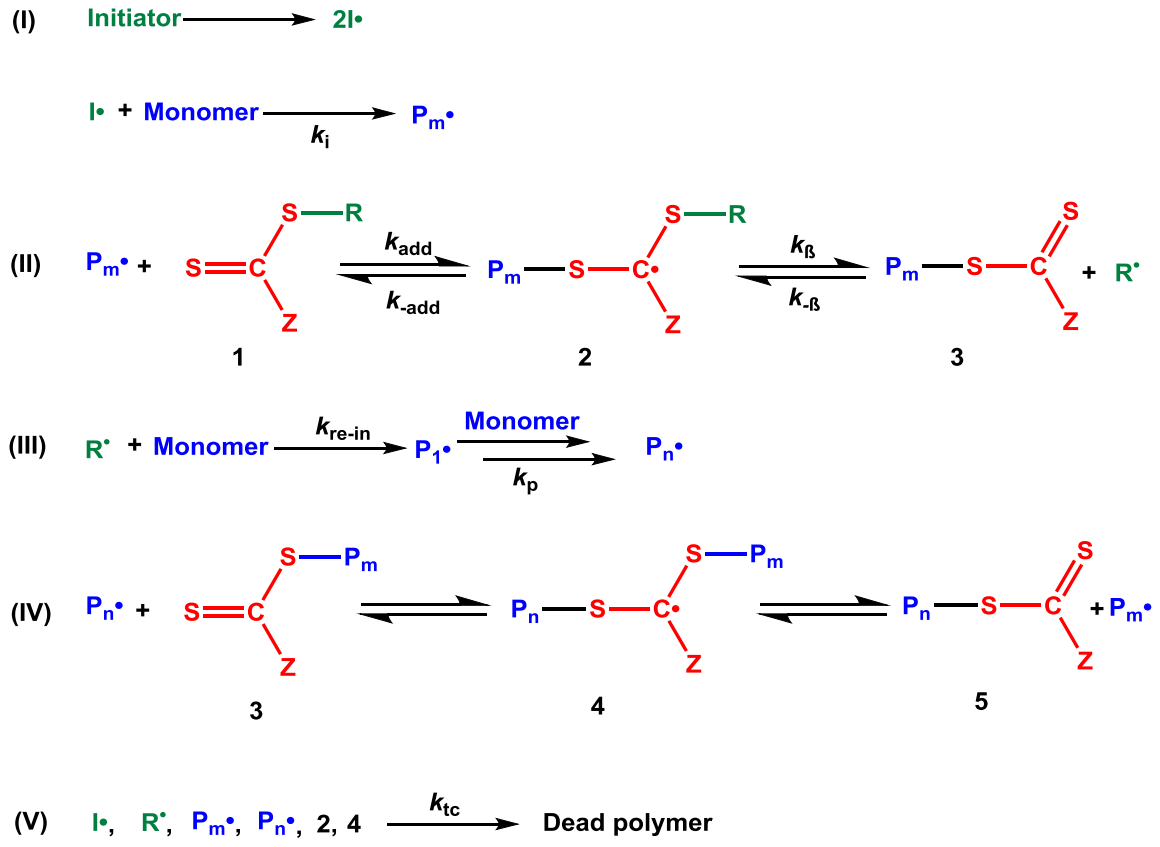

Scheme 1.1 Mechanism of reversible addition-fragmentation chain transfer (RAFT) polymerization: I) initiation step; II) propagation and fragmentation step; III) re-initiation step; IV) equilibration step; V) termination step.

As RAFT polymerization is carried out under experimental conditions which are almost identical to those used in conventional radical polymerization, it exhibits most of the advantages of a free radical process. These advantages include its applicability to a large variety of monomers (e.g., (meth)acrylates, (meth)acrylamides, styrene derivatives, dienes, vinyl esters).[3] Besides, various solvents ranging from aqueous conditions[11-13] to organic solvents[5, 14] and a wide range of temperatures, from -15 to 180 °C.[12, 15-19] can be employed for the polymerization. In addition, RAFT process is tolerant to different functional groups, including

hydroxyl, acid, and tertiary amino groups.[1, 5] RAFT polymerization can be performed in solution, bulk, suspension or emulsion, with the possibility to achieve a wide range of molar masses.[5]

Although RAFT polymerization is not a pure living technique (termination occurs in the system, step V in **Scheme 1.1**), it still has the living character which is maintained by the reversible addition fragmentation process mediated by the transfer of the S=C(Z)S- group between the active and dormant chains.[1] The living character of RAFT process can be assessed by the following parameters: (a) the product should have narrow polydispersity; (b) the evolution of molecular weight versus conversion should be linear; (c) the molecular weight should be predictable by the ratio of monomer consumed to CTA; (d) further monomer addition should produce block (co)polymer.[20]

1.1.2 Selection of RAFT agents

The influence of CTA is critical for the RAFT process in terms of controlling the molecular weight and maintaining narrow molecular weight distribution (*Đ*). The molecular weight distribution (*Đ*) is calculated according to **Equation 1.1**. In order to ensure a narrow dispersity, the CTA should have a high chain transfer constant (C_{tr}) which means the transfer rate constant (k_{tr}) of the CTA should be relative high compared to the propagation constant (k_p) of the monomer (**Equation 1.2**).

$$Đ = 1 + \frac{1}{C_{tr}} \qquad \text{(Equation 1.1)}$$

$$C_{tr} = \frac{k_{tr}}{K_p} \qquad \text{(Equation 1.2)}$$

The transfer rate constant (k_{tr}) of the CTA depends on several factors according to **Scheme 1.1** and **Equation 1.3**: the addition rate of the monomer to the dithioester (k_{add}), the

fragmentation rate of the intermediate **2** to release radical R$^{\bullet}$ (k_{β}), and the rate of the intermediate **2** re-fragmenting back the propagating monomer (k_{-add}).

$$k_{tr} = k_{add}\frac{k_{\beta}}{k_{-add}+k_{\beta}} \qquad \text{(Equation 1.3)}$$

A wide range of CTAs have been discovered (e.g. dithioesters,[1] xanthates,[21, 22] dithiocarbamates,[23, 24] trithiocarbonates,[20, 25] and phosphoryl-/(thiophosphoryl)dithioformates[26]) to control the polymerization of a large variety of monomers (**Figure 1.1**).

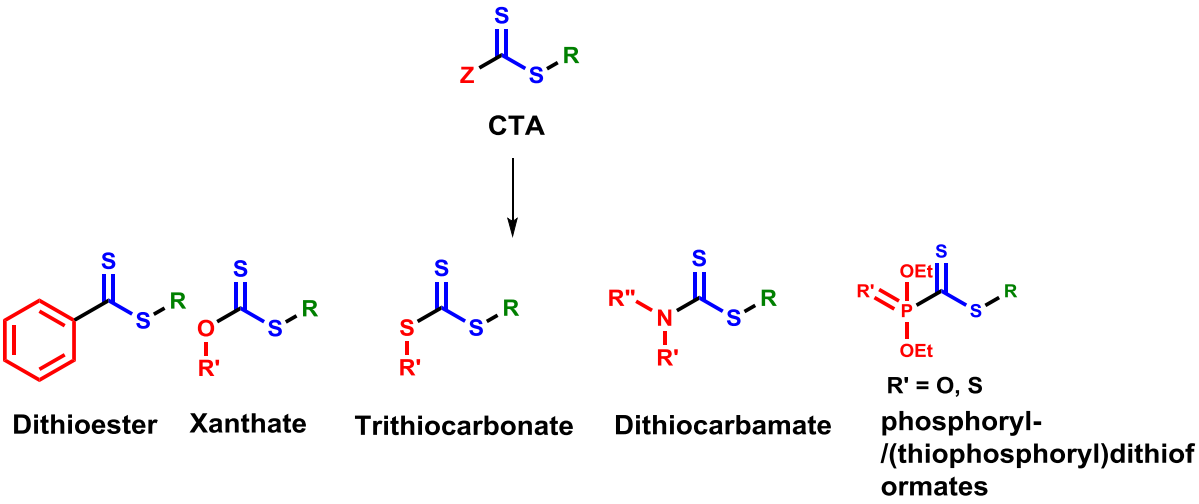

Figure 1.1 General structures and examples of RAFT agents with different functional units of the Z group.

There are two requirements for a RAFT agent to be effective.[23] One is both, addition and fragmentation rate need to be relatively fast compared to the propagation rate of the monomer to ensure the initial RAFT agent to be rapidly consumed, and a fast equilibration between the active and dormant chains . The second requirement is that the expelled radical (R$^{\bullet}$) should be able to reinitiate the polymerization to ensure chain growth. Z and R groups are crucial in the choice of the RAFT agent to ensure the success of polymerization.

The Z group strongly affects the stability of the intermediate radicals and the reactivity of the thiolcarbonyl double bond (C=S).[6, 14, 23, 27] Therefore, the Z group should ideally activate (or not deactivate) the C=S motif towards radical addition (k_{add}). Several studies investigating

the influence of the Z group on the polymerization of various monomers have been published.[19, 23, 24, 28-31] Based on this research, the phenyl group has been identified as an ideal Z group for most monomers because it can keep the balance between the radical intermediate stability and the reactivity to form propagating radicals. Also, the following order has been suggested by the experimental data[19, 23, 24, 28-32] and *ab initio* calculations[33] when choosing the Z group of a CTA: addition rates decrease and fragmentation rates increase from left to right (**Figure 1.2**).

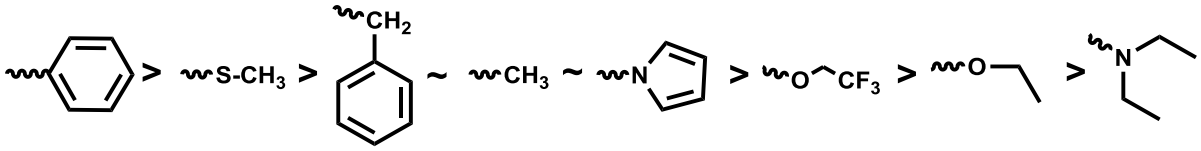

Figure 1.2 Guidelines for the selection of the Z group for a CTA for various polymerization: addition rates decrease and fragmentation rates increase from left to right.

The R group of the CTA should be an excellent free-radical leaving group. At the same time, R• should effectively reinitiate the free radical polymerization. When choosing the R group, the stability of the expelled radical, polarity, and steric bulk should also be considered.[4] There have been many studies investigating the importance of the R group for the polymerizations of different monomers.[14, 27, 34-41] Cumyl or cyanoisopropyl units have been found to be the most efficient for the reinitiation step.[24] All the above experimental data and the *ab initio* calculations[33] give the following guidelines for choosing the R group of the CTA for various polymerizations: fragmentation rates decrease from left to right (**Figure 1.3**).

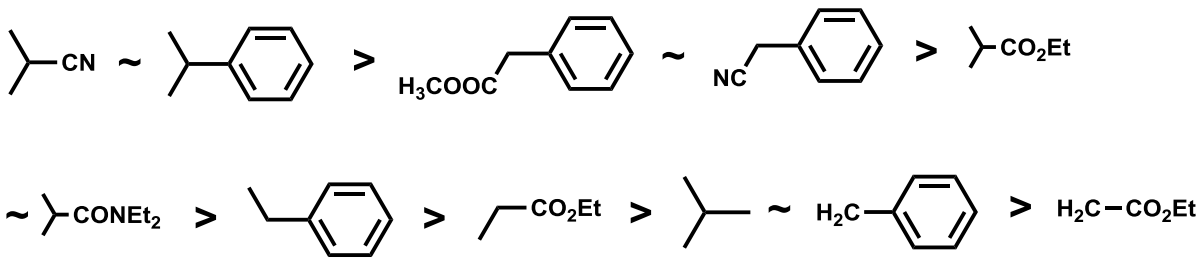

Figure 1.3 Guidelines for the selection of the R group for a CTA: fragmentation rates decrease from left to right.

1.2 Multiblock copolymers by RAFT polymerization

1.2.1 General considerations about multiblock copolymers by RAFT polymerization

As mentioned above, RAFT polymerization has living character originating from the ability of the S=C(Z)S- moiety to transfer radicals between dormant and active chains.[5] Considering most of the chains generated from RAFT process possess a S=C(Z)S- end group (as minimum amount of initiator was used for the polymerization), polymerization will be able to continue in the presence of additional monomers to afford block copolymers.[5] Synthesizing block copolymers is one of the main advantages of RAFT polymerization over a free radical polymerization. Multiblock copolymers which have a higher level of structural control are polymers in which the sequence of the large number of monomers/functionalities is regulated along the polymer chain. This characteristic of multiblock copolymers enables them to mimic the properties and structural features of biopolymers, such as proteins and nucleic acids.[42-44] The highly specific functions of these macromolecules originate from the elegantly controlled primary structure along the polymer backbone.[45] By incorporating a wide range of functional groups in specific domains of a polymer chain, highly ordered materials with unique properties will be generated.

A basic requirement for the synthesis of block copolymers with a narrow molecular weight distribution in a RAFT polymerization is that the polymeric thiocarbonylthio compound (Macro-CTA) formed in the former block should have a high chain transfer constant in the following polymerization to form the subsequent block. This will require the propagating radical $P_m^{\bullet}$ (formed from the former block) to have a comparable or higher leaving ability than

that of the new (later formed) propagating radical $P_n^{\bullet}$ under the polymerization conditions (**Scheme 1.2**).[5]

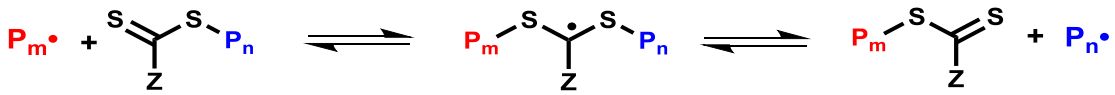

Scheme 1.2 Simplified mechanism and structures of the propagating radicals and intermediate radicals in RAFT polymerization.

However, since free radical intermediates are formed in the process of RAFT polymerization, radical-radical termination is unavoidable.[46] Therefore, dead polymer chains derived from initiator radicals will be formed ultimately. In order to synthesize multiblock copolymers, keeping a high fraction of living chains is of major significance. To achieve polymers with narrow polydispersities and a high number of living chains, the priority is to minimize the consumed initiator and, as a result, to minimize the number of initiator-derived chains.[6] The polymerization usually needs to be stopped at low to moderate monomer conversions to preserve a high livingness, which will severely limit the practice of the synthesis of multiblock copolymers.[47] There are several different parameters which can be optimized in order to maintain a high level of livingness in a RAFT polymerization process, e.g. monomer concentration,[48] solvent,[49-52] reaction temperature,[51, 53] and pressure.[53, 54] For example, increasing the monomer concentration will increase the Arrhenius pre-exponential factor which will accelerate the speed of polymerization.[48, 55] Choosing a polar solvent (i.e. water) will help stabilizing the transition state of the propagating radicals, which will lower the termination rate and the activation energy, therefore increase the speed of propagation.[49] Furthermore, the propagation rate constant (k_p), is considered to be chemically affected and therefore to be significantly controlled by temperature and pressure.[56]

1.2.2 Calculation of the theoretical livingness in multiblock copolymers

The livingness (the number fraction of living chains which have the CTA end group, *L*) in the synthesis of multiblock copolymers is calculated according to **Equation 1.4**.

$$L = \frac{[\mathrm{CTA}]_0}{[\mathrm{CTA}]_0 + 2f[I]_0(1-\mathrm{e}^{-k_d t})(1-\frac{f_c}{2})} \qquad \text{(Equation 1.4)}$$

where *L* is the number fraction of living chains, $[\mathrm{CTA}]_0$ and $[I]_0$ are the initial concentrations of CTA and initiator, respectively. The term '2' represents that one molecule of azo initiator degrades into two primary radicals with a certain efficiency *f* (taken as 0.5 in this thesis). k_d is the decomposition rate coefficient of the initiator. The term $(1 - f_c/2)$ represents the number of chains produced in a radical–radical termination event with f_c the coupling factor (f_c = 1 means 100% bimolecular termination by combination, f_c = 0 means 100% bimolecular termination by disproportionation). Using this equation, it is possible to predict the amount of chains possessing the CTA end group and the structures of generated block copolymers.

1.2.3 Advances and highlights of multiblock copolymers by RAFT polymerization

Multiblock copolymers have received considerable attention in recent years as they aid to understand the relationship between the monomer sequence of a polymer chain and the resulting structure and functionality.[57-62] For instance, the self-assembly of block copolymers in solution or in bulk can lead to the formation of different types of objects with tailored microstructures.[63-71] Although having great promises, the synthesis of sequence controlled multiblock copolymers by RAFT polymerization still remains challenging. This is attributed to the inevitably loss of chain ends during polymerization as a result from the termination reactions due to the requirement of an external radical source which will cause the overall livingness to be lower than in other RDRP techniques. Considering that the amount of dead

chains only corresponds to the amount of radicals derived from the decomposed initiator in the RAFT polymerization (depicted in **Equation 1.1**), it is possible to reach quantitative monomer conversions with a high fraction of living chains by keeping the decomposed initiator at a minimum concentration. However, lowering the initiator concentration will slow down the polymerization rate and will therefore prolong the reaction time.[2] This drawback can be overcome by optimizing other reaction parameters.

Recently, our group developed an approach which enables the synthesis of highly complex multiblock copolymers with near full monomer conversion for each block extension and good control of molecular weight distributions. This strategy employed a one-pot approach *via* sequential monomers addition to synthesize multiblock copolymers using RAFT polymerization by optimizing the reaction parameters.[18] A dodecablock and an amphiphilic hexablock copolymer were synthesized by utilizing carefully selected conditions to polymerize acrylamide (high k_p) monomers using AIBN as the initiator and a trithiocarbonate as the CTA (low retardation) using dioxane as solvent at 65 ˚C. Near full monomer conversion (> 99%) was obtained within 24 h for each chain extension with a final theoretical livingness of up to 95%. In order to avoid the lengthy reaction time to reach full monomer conversion, an initiator which decomposes much faster than AIBN (2,2'-azobis[2-(2-imidazolin-2-yl)propane]dihydrochloride (VA-044)) was employed. This approach demonstrated the high versatility by synthesizing the first reported icosablock (20 blocks, 2 h per block at 70 ˚C in H_2O) copolymer with ~ 98 – 99% conversion for each chain extension and a remarkable control of the molecular weight with a final dispersity of 1.4 and a 93.8% theoretical livingness. This study illustrates the great potential of using RAFT polymerization to the synthesis of highly complex functional polymers with precisely distribution of monomers sequence along the polymer chain. These approaches, however, still have limitation, i.e. not suitable for monomers with low k_p (styrene and methacrylates).

Very recently, the Haddleton group reported the synthesis of sequence-controlled multiblock copolymers using various methacrylate monomers *via* a sulfur-free emulsion RAFT polymerization technic.[72] Despite the significant challenge of using methacrylates for the fabrication of complex multiblock copolymers, several higher order multiblock copolymers (up to 24 blocks) were successfully obtained with low molecular weight distribution ($Đ < 1.5$) in a facile, rapid, quantitative, and scalable approach (up to 80 g).

All the above approaches offer new perspective for building sequence controlled synthetic polymers which have great potential in the wide range of applications, including nanostructured materials, microphase separation, and single chain folding.

1.3 Single Chain Nanoparticles (SCNPs)

The advances of multiblock copolymers enable the access to well defined complex architectures as a further step on the way to control the sequence of synthetic polymers. Recently, mimicking the highly specific sequence of biopolymers (e.g. proteins and nucleic acids) has attracted substantial interest in the field of the polymer synthesis.[44, 73, 74] These sequence controlled biomacromolecules are significant to the development, functioning and reproduction of all living systems.[72] The wide variety of functionalities of natural polymers result from their sophisticated structures which originate from the controlled folding of polymer chain.[45] Inspired by this elegant folding process, considerable attention has been drawn to employ synthetic polymers to reproduce this precision, which is folding a single polymer chain into a single chain nanoparticles (SCNPs). SCNPs are a promising type of materials which can mimic the structure and function of biopolymers.[75] They have various potential bioinspired applications in nanomedicine,[76] bioimaging,[77] biosensing,[78, 79] and catalysis.[80, 81]

1.3.1 Synthetic strategies of SCNPs

Considering the RAFT technique can be employed to polymerize various monomers and there are relative few side reactions involved which will interfere with the RAFT process, polymer scaffolds with functional groups which can be modified by post-polymerization can easily be accessed without protection/deprotection of monomers.[82, 83] Well-defined SCNPs have been accessible by single chain folding of synthetic polymer chains with controlled composition, molecular weight, and molecular weight distribution.[84]

The general strategy for the synthesis of SCNPs is based on the intramolecular single chain collapse of a polymer. There are three main approaches to induce a polymer chain collapse: homo-functional chain folding, hetero-bifunctional chain folding, and cross-linker mediated chain folding. In addition to the folding of a whole polymer chain, the folding process can also be performed within one block of a diblock or triblock copolymer, which leads the formation of SCNPs with different shapes, e.g. tadpole-like SCNPs.[85]

In the homo-functional intra-chain cross-linking approach, the linear copolymer chain is decorated with one type of reactive functional groups (e.g. double bonds) which can react with each other to cause the intramolecular cross-linking. The hetero-bifunctional chain folding strategy is similar to the homo-functional chain collaps but requires two different but complementary functional pendant groups along the polymer backbone. However, it is usually difficult to synthesize such copolymers. In both these methods, the cross-linking reaction needs to be carried out under ultra-dilute conditions in order to avoid the competing intermolecular cross-linking. The concentration of the functional groups is usually in the region of 10^{-5} – 10^{-6} mol/L.[86] This drawback severely precludes the synthesis of SCNPs in a large scale. Utilizing a bifunctional cross-linker to react with the pendant reactive units present in the polymer chain offers opportunity to overcome this drawback. The cross-linker induced single chain collapse

is a widely employed approach to generate SCNPs efficiently as the synthesis of the linear precursor is easier considering a wide variety of functional groups can be introduced into the polymer chain. Besides, extra functional groups can be incorporated into the polymer backbone by the cross-linking reagent. Also, cross-linker mediated single chain folding can either be performed under ultra-dilute conditions or employing a "slow-addition" method, as developed by Hawker *et. al.*.[86] This method allows the synthesis of SCNPs in a large quantity and avoids intermolecular interactions which are still evident even under dilute conditions.

1.3.2 Cross-linking chemistries for the generation of SCNPs

A wide variety of reactions have been used for the intramolecular cross-linking of linear polymer chains to synthesize SCNPs which include covalent chemistry, non-covalent chemistry, and dynamic covalent chemistry.[87-92]

Covalent chemistry is the most widely utilized approach to generate SCNPs as it is very versatile in terms of functional groups and reaction conditions (e.g. temperature and solvent). **Table 1.1** summarizes the frequently used covalent strategies which have been developed for the generation of SCNPs, including Friedel Crafts reaction, free radical coupling, Diels-Alder ligation, copper-catalysed azide-alkyne cycloaddition (CuAAC), Tetrazole-ene Cycloaddition, isocyanate amine coupling, Thiol-Yne coupling, amide formation, etc.. Covalent cross-linking generates SCNPs with desired structures which remain stable upon exposed to the environmental changes. In addition to this advantage, the covalent conjugations have specific disadvantages, for instance, harsh conditions may be required during cross linking (e.g. high temperature), or the requirement of a catalyst or initiator (for radical induced cross-linking).[93] The irreversible nature of covalent cross-linking also limits their biomimetic functions which rely on folding/unfolding processes.

Table 1.1 Irreversible covalent cross-linking reactions for the synthesis of SCNPs.

Cross-linking chemistry and mode*	Functional group precursors	Cross-linked structure	References
Friedel Crafts reaction (Het)	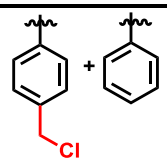	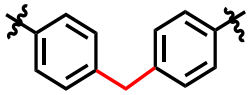	Sillescu[94]
Free radical coupling (Hom)	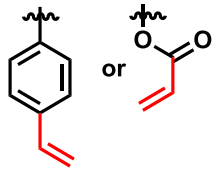	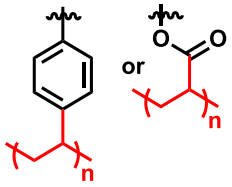	Thayumanavan,[95] Miller,[96] Du Prez.[97]
Photoinduced Diels-Alder ligation (Het)	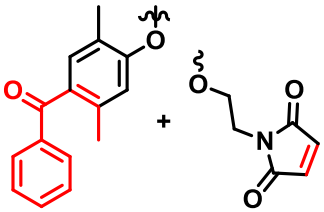	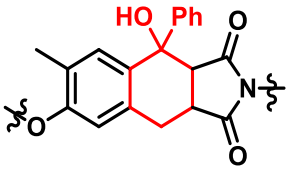	Barner-Kowollik[98]
Photoinduced Tetrazole-ene Cycloaddition (Het)	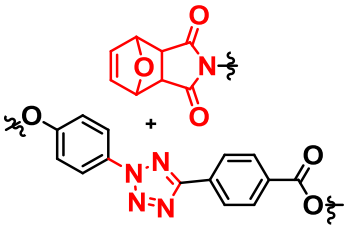	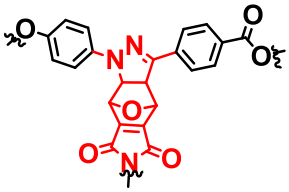	Barner-Kowollik[99]
Photo-cross-linking of cinnamoyl groups (Hom)	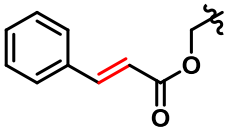	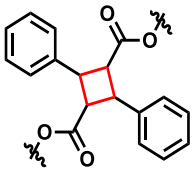	Liu,[100, 101] Chen,[102, 103] Khan.[104]
Tetrazine-norbornene reaction (XL)	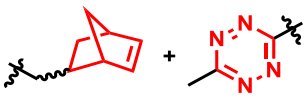	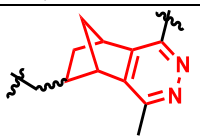	O'Reilly[105]
Isocyanate amine coupling (XL)	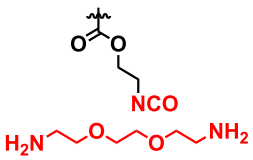	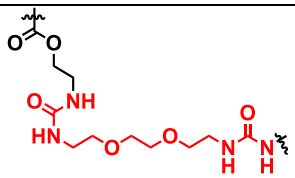	Hawker[106]
Azide-alkyne click chemistry (Het or XL)	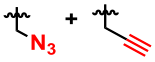	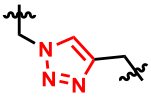	Loinaz,[107, 108] Pomposo,[109, 110] Odriozola,[77] Yagci,[111] Lutz.[85]

Table 1.1 continued

Cross-linking chemistry and mode*	Functional group precursors	Cross-linked structure	References
Thiol-Yne coupling chemistry (XL)	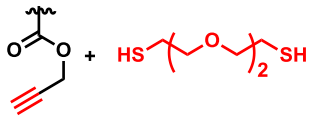	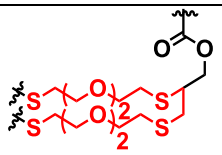	Pomposo[112]
Amide formation (XL)	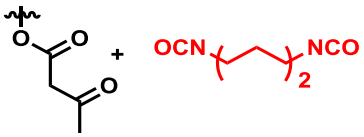	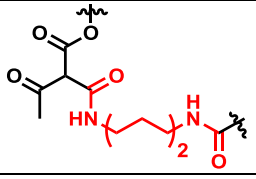	Pomposo[113]
Olefin metathesis		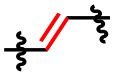	Coates[114]

* Hom represents homofunctional cross-linking; Het represents heterofunctional cross-linking; XL represents cross-linker medidated cross-linking reaction.

In order to realize the folding/unfolding process as displayed by biomacromolecules (e.g. proteins), non-covalent interaction which are also called supramolecular interactions, including hydrogen bonds, host-gest interactions, metal-ligand coordination, etc. can be used to produce bio-mimicking SCNPs. **Table 1.2** summarizes the frequently used non-covalent bonds to synthesize SCNPs. The reversible cross linking is regulated by temperature, pH, UV light, redox potential, concentration, pressure, competing chemical agents, etc.[91, 115] SCNPs generated by non-covalent bonds have great potential applications in self-healing materials, biosensors, and smart adaptable systems. However, the advantages can sometimes be disadvantages. Some non-covalent bonds might be incompatible with certain solvents, for example, the hydrogen bonds are usually disrupted by hydrogen bonding competitor solvents (e.g. DMF).[116]

Table 1.2 Noncovalent cross-linking reactions for the synthesis of SCNPs.

Cross-linking chemistry and mode*	Functional group precursors	Cross-linked structure	References
Thymine-diaminopyridine hydrogen bonding (Het)	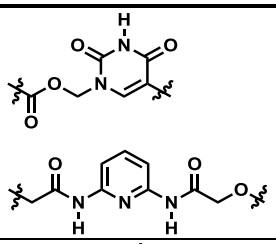	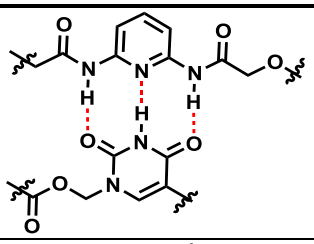	Barner-Kowollik,[117] Rotello.[118]
Upy dimerization hydrogen bonding (Hom)	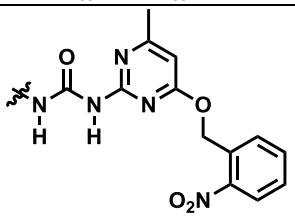	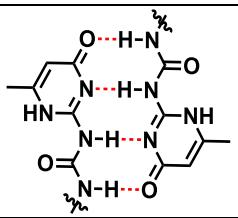	Meijer[119-123]
Pd-complexation (XL)	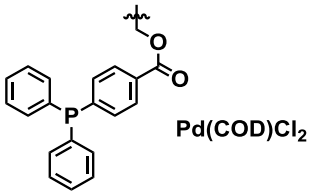	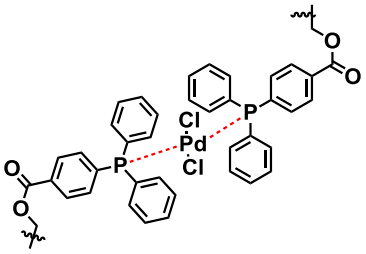	Barner-Kowollik[124]
Cyclodextrins Host-guest Chemistry (Het)	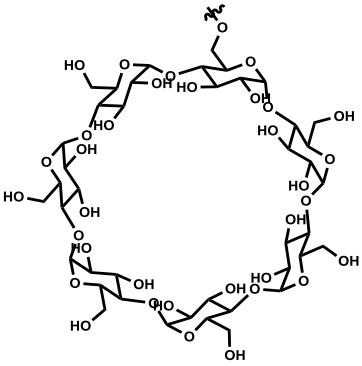	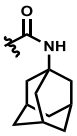	Barner-Kowollik[125]
BTA stacking (Hom)	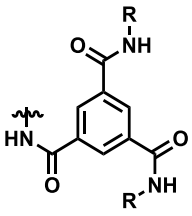	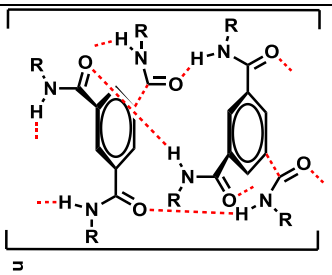	Meijer[126-132]

* Hom represents homofunctional cross-linking; Het represents heterofunctional cross-linking; XL represents cross-linker medidated cross-linking reaction.

Dynamic covalent bonds not only show all the properties that displayed by conventional covalent bonds but also show reversible breaking/reformation in response to the external

stimuli, e.g. oxidizing or reducing reagents, pH, chemical species, etc.[133-135] **Table 1.3** summarizes the frequently used dynamic covalent cross-linking reactions for the fabrication of SCNPs, including disulphide chemistry, hydrazone chemistry, enamine chemistry, imine chemistry, acetal chemistry, boronate ester chemistry, etc. The main property exhibited by dynamic covalent bonds mediated SCNPs is responsive and adaptive behaviour to the changes of their environment. This important property enables a component exchange along the polymer backbone or inside the nanoparticles. The reversible nature allows the nanoparticles to be used in the area of encapsulation and controlled drug delivery/release.[136]

Table 1.3 Dynamic covalent cross-linking reactions for the synthesis of SCNPs.

Cross-linking chemistry and mode*	Functional group precursors	Cross-linked structure	References
Disulfide chemistry (Hom)		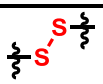	Lutz,[137] Thayumanavan.[138]
Hydrazone chemistry (XL)	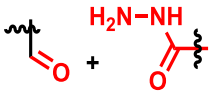	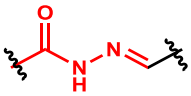	Fulton[139, 140]
Enamine chemistry (XL)	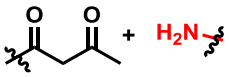	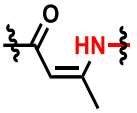	Pomposo[141]
Imine chemistry (XL)	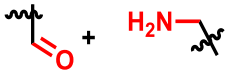	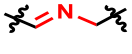	Yang[142]
Acetal chemistry (XL)	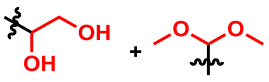	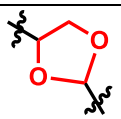	Haag,[143] Tran.[144]
Boronate ester (XL)	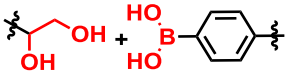	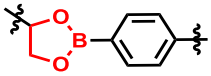	Lam,[145] Wang,[146] Levkin.[147]

* Hom represents homofunctional cross-linking; Het represents heterofunctional cross-linking; XL represents cross-linker medidated cross-linking reaction.

The above mentioned chemistries have been widely employed to construct well-defined SCNPs with tailored structures and functionalities. **Tables 1.1**, **1.2**, and **1.3** could be potentially used as a guideline for the design and synthesis of SCNPs with novel structures and features.

1.4 References

1. Chiefari, J.; Chong, Y. K.; Ercole, F.; Krstina, J.; Jeffery, J.; Le, T. P. T.; Mayadunne, R. T. A.; Meijs, G. F.; Moad, C. L.; Moad, G.; Rizzardo, E.and Thang, S. H. Living Free-Radical Polymerization by Reversible Addition−Fragmentation Chain Transfer: The RAFT Process. *Macromolecules* **1998**, 31 (16), 5559-5562.

2. Hill, M. R.; Carmean, R. N.and Sumerlin, B. S. Expanding the Scope of RAFT Polymerization: Recent Advances and New Horizons. *Macromolecules* **2015**, 48 (16), 5459-5469.

3. Moad, G.; Rizzardo, E.and Thang, S. H. Living Radical Polymerization by the RAFT Process – A Third Update. *Aust. J. Chem.* **2012**, 65 (8), 985-1076.

4. Perrier, S.and Takolpuckdee, P. Macromolecular design via reversible addition–fragmentation chain transfer (RAFT)/xanthates (MADIX) polymerization. *J. Polym. Sci., Part A: Polym. Chem.* **2005**, 43 (22), 5347-5393.

5. Chong, Y. K.; Le, T. P. T.; Moad, G.; Rizzardo, E.and Thang, S. H. A More Versatile Route to Block Copolymers and Other Polymers of Complex Architecture by Living Radical Polymerization: The RAFT Process. *Macromolecules* **1999**, 32 (6), 2071-2074.

6. Moad, G.; Chiefari, J.; Chong, Y. K.; Krstina, J.; Mayadunne, R. T. A.; Postma, A.; Rizzardo, E.and Thang, S. H. Living free radical polymerization with reversible addition – fragmentation chain transfer (the life of RAFT). *Polym. Int.* **2000**, 49 (9), 993-1001.

7. Barner-Kowollik, C.; Davis, T. P.; Heuts, J. P. A.; Stenzel, M. H.; Vana, P.and Whittaker, M. RAFTing down under: Tales of missing radicals, fancy architectures, and mysterious holes. *J. Polym. Sci., Part A: Polym. Chem.* **2003**, 41 (3), 365-375.

8. Moad, G.; Rizzardo, E.and Thang, S. H. Living Radical Polymerization by the RAFT Process. *Aust. J. Chem.* **2005**, 58 (6), 379-410.

9. Moad, G.; Rizzardo, E.and Thang, S. H. Living Radical Polymerization by the RAFT ProcessA First Update. *Aust. J. Chem.* **2006**, 59 (10), 669-692.

10. Moad, G.; Rizzardo, E.and Thang, S. H. Living Radical Polymerization by the RAFT Process A Second Update. *Aust. J. Chem.* **2009**, 62 (11), 1402-1472.

11. Li, M.; Li, H.; De, P.and Sumerlin, B. S. Thermoresponsive Block Copolymer–Protein Conjugates Prepared by Grafting-from via RAFT Polymerization. *Macromol. Rapid Commun.* **2011**, 32 (4), 354-359.

12. Martin, L.; Gody, G.and Perrier, S. Preparation of complex multiblock copolymers via aqueous RAFT polymerization at room temperature. *Polym. Chem.* **2015**, 6 (27), 4875-4886.

13. Hoff, E. A.; Abel, B. A.; Tretbar, C. A.; McCormick, C. L.and Patton, D. L. Aqueous RAFT at pH zero: enabling controlled polymerization of unprotected acyl hydrazide methacrylamides. *Polym. Chem.* **2017**.

14. Benaglia, M.; Rizzardo, E.; Alberti, A.and Guerra, M. Searching for More Effective Agents and Conditions for the RAFT Polymerization of MMA: Influence of Dithioester Substituents, Solvent, and Temperature. *Macromolecules* **2005**, 38 (8), 3129-3140.

15. Sun, X.-L.; He, W.-D.; Li, J.; Li, L.-Y.; Zhang, B.-Y.and Pan, T.-T. RAFT cryopolymerizations of N,N-dimethylacrylamide and N-isopropylacrylamide in moderately frozen aqueous solution. *J. Polym. Sci., Part A: Polym. Chem.* **2009**, 47 (24), 6863-6872.

16. Sun, X.-L.; He, W.-D.; Pan, T.-T.; Ding, Z.-L.and Zhang, Y.-J. RAFT cryopolymerizations of acrylamides and acrylates in dioxane at −5 °C. *Polymer* **2010**, 51 (1), 110-114.

17. Paulus, R. M.; Becer, C. R.; Hoogenboom, R.and Schubert, U. S. High Temperature Initiator-Free RAFT Polymerization of Methyl Methacrylate in a Microwave Reactor. *Aust. J. Chem.* **2009**, 62 (3), 254-259.

18. Gody, G.; Maschmeyer, T.; Zetterlund, P. B.and Perrier, S. Rapid and quantitative one-pot synthesis of sequence-controlled polymers by radical polymerization. *Nat. Commun.* **2013**, 4, 2505.

19. Quinn, J. F.; Rizzardo, E.and Davis, T. P. Ambient temperature reversible addition-fragmentation chain transfer polymerisation. *Chem. Commun.* **2001**, (11), 1044-1045.

20. Mayadunne, R. T. A.; Rizzardo, E.; Chiefari, J.; Krstina, J.; Moad, G.; Postma, A.and Thang, S. H. Living Polymers by the Use of Trithiocarbonates as Reversible Addition−Fragmentation Chain Transfer (RAFT) Agents: ABA Triblock Copolymers by Radical Polymerization in Two Steps. *Macromolecules* **2000**, 33 (2), 243-245.

21. Ladavière, C.; Dörr, N.and Claverie, J. P. Controlled Radical Polymerization of Acrylic Acid in Protic Media. *Macromolecules* **2001**, 34 (16), 5370-5372.

22. Francis, R.and Ajayaghosh, A. Minimization of Homopolymer Formation and Control of Dispersity in Free Radical Induced Graft Polymerization Using Xanthate Derived Macro-photoinitiators. *Macromolecules* **2000**, 33 (13), 4699-4704.

23. Mayadunne, R. T. A.; Rizzardo, E.; Chiefari, J.; Chong, Y. K.; Moad, G.and Thang, S. H. Living Radical Polymerization with Reversible Addition−Fragmentation Chain Transfer (RAFT Polymerization) Using Dithiocarbamates as Chain Transfer Agents. *Macromolecules* **1999**, 32 (21), 6977-6980.

24. Destarac, M.; Charmot, D.; Franck, X.and Zard, S. Z. Dithiocarbamates as universal reversible addition-fragmentation chain transfer agents. *Macromol. Rapid Commun.* **2000**, 21 (15), 1035-1039.

25. Mayadunne, R. T. A.; Jeffery, J.; Moad, G.and Rizzardo, E. Living Free Radical Polymerization with Reversible Addition−Fragmentation Chain Transfer (RAFT Polymerization): Approaches to Star Polymers. *Macromolecules* **2003**, 36 (5), 1505-1513.

26. Laus, M.; Papa, R.; Sparnacci, K.; Alberti, A.; Benaglia, M.and Macciantelli, D. Controlled Radical Polymerization of Styrene with Phosphoryl- and (Thiophosphoryl)dithioformates as RAFT Agents. *Macromolecules* **2001**, 34 (21), 7269-7275.

27. Donovan, M. S.; Lowe, A. B.; Sumerlin, B. S.and McCormick, C. L. Raft Polymerization of N,N-Dimethylacrylamide Utilizing Novel Chain Transfer Agents Tailored for High Reinitiation Efficiency and Structural Control. *Macromolecules* **2002**, 35 (10), 4123-4132.

28. Destarac, M.; Bzducha, W.; Taton, D.; Gauthier-Gillaizeau, I.and Zard, S. Z. Xanthates as Chain-Transfer Agents in Controlled Radical Polymerization (MADIX): Structural Effect of the O-Alkyl Group. *Macromol. Rapid Commun.* **2002**, 23 (17), 1049-1054.

29. Barner-Kowollik, C.; Quinn, J. F.; Nguyen, T. L. U.; Heuts, J. P. A.and Davis, T. P. Kinetic Investigations of Reversible Addition Fragmentation Chain Transfer Polymerizations: Cumyl Phenyldithioacetate Mediated Homopolymerizations of Styrene and Methyl Methacrylate. *Macromolecules* **2001**, 34 (22), 7849-7857.

30. Chiefari, J.; Mayadunne, R. T. A.; Moad, C. L.; Moad, G.; Rizzardo, E.; Postma, A.and Thang, S. H. Thiocarbonylthio Compounds (SC(Z)S−R) in Free Radical Polymerization with Reversible Addition-Fragmentation Chain Transfer (RAFT Polymerization). Effect of the Activating Group Z. *Macromolecules* **2003**, 36 (7), 2273-2283.

31. Davis, T. P.; Barner-Kowollik, C.; Nguyen, T. L. U.; Stenzel, M. H.; Quinn, J. F.and Vana, P., Influences of the Structural Design of RAFT Agents on Living Radical Polymerization Kinetics. In *Advances in Controlled/Living Radical Polymerization*, American Chemical Society: 2003; Vol. 854, pp 551-569.

32. Adamy, M.; van Herk, A. M.; Destarac, M.and Monteiro, M. J. Influence of the Chemical Structure of MADIX Agents on the RAFT Polymerization of Styrene. *Macromolecules* **2003**, 36 (7), 2293-2301.

33. Coote, M. L.and Henry, D. J. Effect of Substituents on Radical Stability in Reversible Addition Fragmentation Chain Transfer Polymerization: An ab Initio Study. *Macromolecules* **2005**, 38 (4), 1415-1433.

34. Schilli, C.; Lanzendörfer, M. G.and Müller, A. H. E. Benzyl and Cumyl Dithiocarbamates as Chain Transfer Agents in the RAFT Polymerization of N-Isopropylacrylamide. In Situ FT-NIR and MALDI−TOF MS Investigation. *Macromolecules* **2002**, 35 (18), 6819-6827.

35. Perrier, S.; Takolpuckdee, P.; Westwood, J.and Lewis, D. M. Versatile Chain Transfer Agents for Reversible Addition Fragmentation Chain Transfer (RAFT) Polymerization to Synthesize Functional Polymeric Architectures. *Macromolecules* **2004**, 37 (8), 2709-2717.

36. Perrier, S.; Barner-Kowollik, C.; Quinn, J. F.; Vana, P.and Davis, T. P. Origin of Inhibition Effects in the Reversible Addition Fragmentation Chain Transfer (RAFT) Polymerization of Methyl Acrylate. *Macromolecules* **2002**, 35 (22), 8300-8306.

37. Chong, Y. K.; Krstina, J.; Le, T. P. T.; Moad, G.; Postma, A.; Rizzardo, E.and Thang, S. H. Thiocarbonylthio Compounds [SC(Ph)S−R] in Free Radical Polymerization with Reversible Addition-

Fragmentation Chain Transfer (RAFT Polymerization). Role of the Free-Radical Leaving Group (R). *Macromolecules* **2003**, 36 (7), 2256-2272.

38. Lebreton, P.; Ameduri, B.; Boutevin, B.and Corpart, J.-M. Use of Original ω-Perfluorinated Dithioesters for the Synthesis of Well-Controlled Polymers by Reversible Addition-Fragmentation Chain Transfer (RAFT). *Macromol. Chem. Phys.* **2002**, 203 (3), 522-537.

39. Farmer, S. C.and Patten, T. E. (Thiocarbonyl-α-thio)carboxylic acid derivatives as transfer agents in reversible addition–fragmentation chain-transfer polymerizations. *J. Polym. Sci., Part A: Polym. Chem.* **2002**, 40 (4), 555-563.

40. Takolpuckdee, P.; Mars, C. A.; Perrier, S.and Archibald, S. J. Novel Amide-Based Chain Transfer Agent for Reversible Addition Fragmentation Chain Transfer Polymerization. *Macromolecules* **2005**, 38 (4), 1057-1060.

41. Li, C.and Benicewicz, B. C. α-Cyanobenzyl dithioester reversible addition–fragmentation chain-transfer agents for controlled radical polymerizations. *J. Polym. Sci., Part A: Polym. Chem.* **2005**, 43 (7), 1535-1543.

42. ten Brummelhuis, N. Controlling monomer-sequence using supramolecular templates. *Polym. Chem.* **2015**, 6 (5), 654-667.

43. Badi, N.and Lutz, J. F. Sequence control in polymer synthesis. *Chem. Soc. Rev.* **2009**, 38 (12), 3383-90.

44. Lutz, J.-F.; Ouchi, M.; Liu, D. R.and Sawamoto, M. Sequence-Controlled Polymers. *Science* **2013**, 341 (6146), 1238149.

45. Dobson, C. M. Protein folding and misfolding. *Nature* **2003**, 426 (6968), 884-890.

46. Rodlert, M.; Harth, E.; Rees, I.and Hawker, C. J. End-group fidelity in nitroxide-mediated living free-radical polymerizations. *J. Polym. Sci., Part A: Polym. Chem.* **2000**, 38 (S1), 4749-4763.

47. Gody, G.; Maschmeyer, T.; Zetterlund, P. B.and Perrier, S. Exploitation of the Degenerative Transfer Mechanism in RAFT Polymerization for Synthesis of Polymer of High Livingness at Full Monomer Conversion. *Macromolecules* **2014**, 47 (2), 639-649.

48. Beuermann, S.; Buback, M.; Hesse, P.; Kukučková, S.and Lacık, I. Propagation Kinetics of Free-Radical Methacrylic Acid Polymerization in Aqueous Solution. The Effect of Concentration and Degree of Ionization. *Macromol. Symp.* **2007**, 248 (1), 23-32.

49. Valdebenito, A.and Encinas, M. V. Effect of solvent on the free radical polymerization of N,N-dimethylacrylamide. *Polym. Int.* **2010**, 59 (9), 1246-1251.

50. Read, E.; Guinaudeau, A.; James Wilson, D.; Cadix, A.; Violleau, F.and Destarac, M. Low temperature RAFT/MADIX gel polymerisation: access to controlled ultra-high molar mass polyacrylamides. *Polym. Chem.* **2014**, 5 (7), 2202-2207.

51. Gody, G.; Maschmeyer, T.; Zetterlund, P. B.and Perrier, S. Pushing the Limit of the RAFT Process: Multiblock Copolymers by One-Pot Rapid Multiple Chain Extensions at Full Monomer Conversion. *Macromolecules* **2014**, 47 (10), 3451-3460.

52. Puttick, S.; Davis, A. L.; Butler, K.; Irvine, D. J.; Licence, P.and Thurecht, K. J. The influence of domain segregation in ionic liquids upon controlled polymerisation mechanisms: RAFT polymerisation. *Polym. Chem.* **2013**, 4 (5), 1337-1344.

53. Arita, T.; Buback, M.and Vana, P. Cumyl Dithiobenzoate Mediated RAFT Polymerization of Styrene at High Temperatures. *Macromolecules* **2005**, 38 (19), 7935-7943.

54. Rzayev, J.and Penelle, J. HP-RAFT: A Free-Radical Polymerization Technique for Obtaining Living Polymers of Ultrahigh Molecular Weights. *Angew. Chem.* **2004**, 116 (13), 1723-1726.

55. Lacík, I.; Beuermann, S.and Buback, M. PLP−SEC Study into Free-Radical Propagation Rate of Nonionized Acrylic Acid in Aqueous Solution. *Macromolecules* **2003**, 36 (25), 9355-9363.

56. Buback, M. Propagation Kinetics in Radical Polymerization Studied via Pulsed Laser Techniques. *Macromol. Symp.* **2009**, 275–276 (1), 90-101.

57. Lutz, J.-F.; Ouchi, M.; Liu, D. R.and Sawamoto, M. Sequence-Controlled Polymers. *Science* **2013**, 341 (6146), 628-636.

58. Börner, H. G. Precision Polymers—Modern Tools to Understand and Program Macromolecular Interactions. *Macromol. Rapid Commun.* **2011**, 32 (2), 115-126.

59. Lutz, J.-F. Sequence-controlled polymerizations: the next Holy Grail in polymer science? *Polym. Chem.* **2010**, 1 (1), 55.

60. Schmidt, B. V. K. J.and Barner-Kowollik, C. Polymer chemistry: Macromolecules made to order. *Nat Chem* **2013**, 5 (12), 990-992.

61. Benoit, D.; Hawker, C. J.; Huang, E. E.; Lin, Z.and Russell, T. P. One-Step Formation of Functionalized Block Copolymers. *Macromolecules* **2000**, 33 (5), 1505-1507.

62. Pfeifer, S.and Lutz, J.-F. A Facile Procedure for Controlling Monomer Sequence Distribution in Radical Chain Polymerizations. *J. Am. Chem. Soc.* **2007**, 129 (31), 9542-9543.

63. BATES, F. S. Polymer-Polymer Phase Behavior. *Science* **1991**, 251 (4996), 898-905.

64. Förster, S.and Plantenberg, T. From Self-Organizing Polymers to Nanohybrid and Biomaterials. *Angew. Chem. Int. Ed.* **2002**, 41 (5), 688-714.

65. Hamley, I. W. Nanotechnology with Soft Materials. *Angew. Chem. Int. Ed.* **2003**, 42 (15), 1692-1712.

66. Kubowicz, S.; Baussard, J.-F.; Lutz, J.-F.; Thünemann, A. F.; von Berlepsch, H.and Laschewsky, A. Multicompartment Micelles Formed by Self-Assembly of Linear ABC Triblock Copolymers in Aqueous Medium. *Angew. Chem. Int. Ed.* **2005**, 44 (33), 5262-5265.

67. Li, Z.; Kesselman, E.; Talmon, Y.; Hillmyer, M. A.and Lodge, T. P. Multicompartment Micelles from ABC Miktoarm Stars in Water. *Science* **2004**, 306 (5693), 98-101.

68. Arotçaréna, M.; Heise, B.; Ishaya, S.and Laschewsky, A. Switching the Inside and the Outside of Aggregates of Water-Soluble Block Copolymers with Double Thermoresponsivity. *J. Am. Chem. Soc.* **2002**, 124 (14), 3787-3793.

69. Du, J.and O'Reilly, R. K. Advances and challenges in smart and functional polymer vesicles. *Soft Matter* **2009**, 5 (19), 3544-3561.

70. Lutz, J.-F.; Geffroy, S.; von Berlepsch, H.; Bottcher, C.; Garnier, S.and Laschewsky, A. Investigation of a dual set of driving forces (hydrophobic + electrostatic) for the two-step fabrication of defined block copolymer micelles. *Soft Matter* **2007**, 3 (6), 694-698.

71. Hadjiantoniou, N. A.; Triftaridou, A. I.; Kafouris, D.; Gradzielski, M.and Patrickios, C. S. Synthesis and Characterization of Amphiphilic Multiblock Copolymers: Effect of the Number of Blocks on Micellization. *Macromolecules* **2009**, 42 (15), 5492-5498.

72. Engelis, N. G.; Anastasaki, A.; Nurumbetov, G.; Truong, N. P.; Nikolaou, V.; Shegiwal, A.; Whittaker, M. R.; Davis, T. P.and Haddleton, D. M. Sequence-controlled methacrylic multiblock copolymers via sulfur-free RAFT emulsion polymerization. *Nat Chem* **2017**, 9 (2), 171-178.

73. Lutz, J.-F. Aperiodic Copolymers. *ACS Macro Letters* **2014**, 3 (10), 1020-1023.

74. Hibi, Y.; Ouchi, M.and Sawamoto, M. A strategy for sequence control in vinyl polymers via iterative controlled radical cyclization. *Nat. Commun.* **2016**, 7, 11064.

75. Hanlon, A. M.; Martin, I.; Bright, E. R.; Chouinard, J.; Rodriguez, K. J.; Patenotte, G. E.and Berda, E. B. Exploring structural effects in single-chain "folding" mediated by intramolecular thermal Diels-Alder chemistry. *Polym. Chem.* **2017**.

76. Sanchez-Sanchez, A.; Akbari, S.; Moreno, A. J.; Verso, F. L.; Arbe, A.; Colmenero, J.and Pomposo, J. A. Design and Preparation of Single-Chain Nanocarriers Mimicking Disordered Proteins for Combined Delivery of Dermal Bioactive Cargos. *Macromol. Rapid Commun.* **2013**, 34 (21), 1681-1686.

77. Perez-Baena, I.; Loinaz, I.; Padro, D.; Garcia, I.; Grande, H. J.and Odriozola, I. Single-chain polyacrylic nanoparticles with multiple Gd(iii) centres as potential MRI contrast agents. *J. Mater. Chem.* **2010**, 20 (33), 6916-6922.

78. Gillissen, M. A. J.; Voets, I. K.; Meijer, E. W.and Palmans, A. R. A. Single chain polymeric nanoparticles as compartmentalised sensors for metal ions. *Polym. Chem.* **2012**, 3 (11), 3166-3174.

79. Latorre-Sanchez, A.and Pomposo, J. A. A simple, fast and highly sensitive colorimetric detection of zein in aqueous ethanol via zein-pyridine-gold interactions. *Chem. Commun.* **2015**, 51 (86), 15736-15738.

80. Terashima, T.; Mes, T.; De Greef, T. F. A.; Gillissen, M. A. J.; Besenius, P.; Palmans, A. R. A.and Meijer, E. W. Single-Chain Folding of Polymers for Catalytic Systems in Water. *J. Am. Chem. Soc.* **2011**, 133 (13), 4742-4745.

81. Perez-Baena, I.; Barroso-Bujans, F.; Gasser, U.; Arbe, A.; Moreno, A. J.; Colmenero, J.and Pomposo, J. A. Endowing Single-Chain Polymer Nanoparticles with Enzyme-Mimetic Activity. *ACS Macro Letters* **2013**, 2 (9), 775-779.

82. Gauthier, M. A.; Gibson, M. I.and Klok, H.-A. Synthesis of Functional Polymers by Post-Polymerization Modification. *Angew. Chem. Int. Ed.* **2009**, 48 (1), 48-58.

83. Iha, R. K.; Wooley, K. L.; Nyström, A. M.; Burke, D. J.; Kade, M. J.and Hawker, C. J. Applications of Orthogonal "Click" Chemistries in the Synthesis of Functional Soft Materials. *Chem. Rev.* **2009**, 109 (11), 5620-5686.

84. Beck, J. B.; Killops, K. L.; Kang, T.; Sivanandan, K.; Bayles, A.; Mackay, M. E.; Wooley, K. L.and Hawker, C. J. Facile Preparation of Nanoparticles by Intramolecular Cross-Linking of Isocyanate Functionalized Copolymers. *Macromolecules* **2009**, 42 (15), 5629-5635.

85. Schmidt, B. V.; Fechler, N.; Falkenhagen, J.and Lutz, J. F. Controlled folding of synthetic polymer chains through the formation of positionable covalent bridges. *Nat. Chem.* **2011**, 3 (3), 234-238.

86. Harth, E.; Horn, B. V.; Lee, V. Y.; Germack, D. S.; Gonzales, C. P.; Miller, R. D.and Hawker, C. J. A Facile Approach to Architecturally Defined Nanoparticles via Intramolecular Chain Collapse. *J. Am. Chem. Soc.* **2002**, 124 (29), 8653-8660.

87. Aiertza, M.; Odriozola, I.; Cabañero, G.; Grande, H.-J.and Loinaz, I. Single-chain polymer nanoparticles. *Cell. Mol. Life Sci.* **2012**, 69 (3), 337-346.

88. Sanchez-Sanchez, A.; Perez-Baena, I.and Pomposo, J. A. Advances in click chemistry for single-chain nanoparticle construction. *Molecules* **2013**, 18 (3), 3339-3355.

89. Lyon, C. K.; Prasher, A.; Hanlon, A. M.; Tuten, B. T.; Tooley, C. A.; Frank, P. G.and Berda, E. B. A brief user's guide to single-chain nanoparticles. *Polym. Chem.* **2015**, 6 (2), 181-197.

90. Altintas, O.and Barner-Kowollik, C. Single chain folding of synthetic polymers by covalent and non-covalent interactions: current status and future perspectives. *Macromol. Rapid Commun.* **2012**, 33 (11), 958-971.

91. Sanchez-Sanchez, A.and Pomposo, J. A. Single-Chain Polymer Nanoparticles via Non-Covalent and Dynamic Covalent Bonds. *Particle & Particle Systems Characterization* **2014**, 31 (1), 11-23.

92. Altintas, O.and Barner-Kowollik, C. Single-Chain Folding of Synthetic Polymers: A Critical Update. *Macromol. Rapid Commun.* **2016**, 37 (1), 29-46.

93. Altintas, O.and Barner-Kowollik, C. Single Chain Folding of Synthetic Polymers by Covalent and Non-Covalent Interactions: Current Status and Future Perspectives. *Macromol. Rapid Commun.* **2012**, 33 (11), 958-971.

94. Antonietti, M.; Sillescu, H.; Schmidt, M.and Schuch, H. Solution properties and dynamic bulk behavior of intramolecular cross-linked polystyrene. *Macromolecules* **1988**, 21 (3), 736-742.

95. Jiang, J.and Thayumanavan, S. Synthesis and Characterization of Amine-Functionalized Polystyrene Nanoparticles. *Macromolecules* **2005**, 38 (14), 5886-5891.

96. Mecerreyes, D.; Lee, V.; Hawker, C. J.; Hedrick, J. L.; Wursch, A.; Volksen, W.; Magbitang, T.; Huang, E.and Miller, R. D. A Novel Approach to Functionalized Nanoparticles: Self-Crosslinking of Macromolecules in Ultradilute Solution. *Adv. Mater.* **2001**, 13 (3), 204-208.

97. Renterghem, L. M. V.; Lammens, M.; Dervaux, B.; Viville, P.; Lazzaroni, R.and Prez, F. E. D. Design and Use of Organic Nanoparticles Prepared from Star-Shaped Polymers with Reactive End Groups. *J. Am. Chem. Soc.* **2008**, 130 (32), 10802-10811.

98. Altintas, O.; Willenbacher, J.; Wuest, K. N. R.; Oehlenschlaeger, K. K.; Krolla-Sidenstein, P.; Gliemann, H.and Barner-Kowollik, C. A Mild and Efficient Approach to Functional Single-Chain Polymeric Nanoparticles via Photoinduced Diels–Alder Ligation. *Macromolecules* **2013**, 46 (20), 8092-8101.

99. Willenbacher, J.; Wuest, K. N. R.; Mueller, J. O.; Kaupp, M.; Wagenknecht, H.-A.and Barner-Kowollik, C. Photochemical Design of Functional Fluorescent Single-Chain Nanoparticles. *ACS Macro Letters* **2014**, 3 (6), 574-579.

100. Tao, J.and Liu, G. Polystyrene-block-poly(2-cinnamoylethyl methacrylate) Tadpole Molecules. *Macromolecules* **1997**, 30 (8), 2408-2411.

101. Njikang, G.; Liu, G.and Curda, S. A. Tadpoles from the Intramolecular Photo-Cross-Linking of Diblock Copolymers. *Macromolecules* **2008**, 41 (15), 5697-5702.

102. Zhou, F.; Xie, M.and Chen, D. Structure and Ultrasonic Sensitivity of the Superparticles Formed by Self-Assembly of Single Chain Janus Nanoparticles. *Macromolecules* **2014**, 47 (1), 365-372.

103. Xie, M. X.; Jiang, L.; Xu, Z. P.and Chen, D. Y. Monofunctional polymer nanoparticles prepared through intramolecularly cross-linking the polymer chains sparsely grafted on the surface of sacrificial silica spheres. *Chem. Commun.* **2015**, 51 (10), 1842-1845.

104. Hecht, S.and Khan, A. Intramolecular Cross-Linking of Helical Folds: An Approach to Organic Nanotubes. *Angew. Chem.* **2003**, 115 (48), 6203-6206.

105. Hansell, C. F.; Lu, A.; Patterson, J. P.and O'Reilly, R. K. Exploiting the tetrazine-norbornene reaction for single polymer chain collapse. *Nanoscale* **2014**, 6 (8), 4102-7.

106. Beck, J. B.; Killops, K. L.; Kang, T.; Sivanandan, K.; Bayles, A.; Mackay, M. E.; Wooley, K. L.and Hawker, C. J. Facile Preparation of Nanoparticles by Intramolecular Crosslinking of Isocyanate Functionalized Copolymers. *Macromolecules* **2009**, 42 (15), 5629-5635.

107. de Luzuriaga, A. R.; Ormategui, N.; Grande, H. J.; Odriozola, I.; Pomposo, J. A.and Loinaz, I. Intramolecular Click Cycloaddition: An Efficient Room-Temperature Route towards Bioconjugable Polymeric Nanoparticles. *Macromol. Rapid Commun.* **2008**, 29 (12–13), 1156-1160.

108. Ormategui, N.; Garcia, I.; Padro, D.; Cabanero, G.; Grande, H. J.and Loinaz, I. Synthesis of single chain thermoresponsive polymer nanoparticles. *Soft Matter* **2012**, 8 (3), 734-740.

109. de Luzuriaga, A. R.; Perez-Baena, I.; Montes, S.; Loinaz, I.; Odriozola, I.; García, I.and Pomposo, J. A. New Route to Polymeric Nanoparticles by Click Chemistry Using Bifunctional Cross-Linkers. *Macromol. Symp.* **2010**, 296 (1), 303-310.

110. Oria, L.; Aguado, R.; Pomposo, J. A.and Colmenero, J. A versatile "click" chemistry precursor of functional polystyrene nanoparticles. *Adv. Mater.* **2010**, 22 (28), 3038-3041.

111. Cengiz, H.; Aydogan, B.; Ates, S.; Acikalin, E.and Yagci, Y. Intramolecular Cross-linking of Polymers Using Difunctional Acetylenes via Click Chemistry. *Des. Monomers Polym.* **2011**, 14 (1), 69-78.

112. Perez-Baena, I.; Asenjo-Sanz, I.; Arbe, A.; Moreno, A. J.; Lo Verso, F.; Colmenero, J.and Pomposo, J. A. Efficient Route to Compact Single-Chain Nanoparticles: Photoactivated Synthesis via Thiol–Yne Coupling Reaction. *Macromolecules* **2014**, 47 (23), 8270-8280.

113. Sanchez-Sanchez, A.and Pomposo, J. A. Efficient Synthesis of Single-Chain Polymer Nanoparticles via Amide Formation. *Journal of Nanomaterials* **2015**, 2015, 7.

114. Cherian, A. E.; Sun, F. C.; Sheiko, S. S.and Coates, G. W. Formation of Nanoparticles by Intramolecular Cross-Linking: Following the Reaction Progress of Single Polymer Chains by Atomic Force Microscopy. *J. Am. Chem. Soc.* **2007**, 129 (37), 11350-11351.

115. Fischer, T. S.; Schulze-Sünninghausen, D.; Luy, B.; Altintas, O.and Barner-Kowollik, C. Stepwise Unfolding of Single-Chain Nanoparticles by Chemically Triggered Gates. *Angew. Chem. Int. Ed.* **2016**, 55 (37), 11276-11280.

116. Catrouillet, S.; Fonteneau, C.; Bouteiller, L.; Delorme, N.; Nicol, E.; Nicolai, T.; Pensec, S.and Colombani, O. Competition Between Steric Hindrance and Hydrogen Bonding in the Formation of Supramolecular Bottle Brush Polymers. *Macromolecules* **2013**, 46 (19), 7911-7919.

117. Altintas, O.; Rudolph, T.and Barner-Kowollik, C. Single chain self-assembly of well-defined heterotelechelic polymers generated by ATRP and click chemistry revisited. *J. Polym. Sci., Part A: Polym. Chem.* **2011**, 49 (12), 2566-2576.

118. Carroll, J. B.; Waddon, A. J.; Nakade, H.and Rotello, V. M. "Plug and Play" Polymers. Thermal and X-ray Characterizations of Noncovalently Grafted Polyhedral Oligomeric Silsesquioxane (POSS)−Polystyrene Nanocomposites. *Macromolecules* **2003**, 36 (17), 6289-6291.

119. Foster, E. J.; Berda, E. B.and Meijer, E. W. Metastable Supramolecular Polymer Nanoparticles via Intramolecular Collapse of Single Polymer Chains. *J. Am. Chem. Soc.* **2009**, 131 (20), 6964-6966.

120. Foster, E. J.; Berda, E. B.and Meijer, E. W. Tuning the size of supramolecular single-chain polymer nanoparticles. *J. Polym. Sci., Part A: Polym. Chem.* **2011**, 49 (1), 118-126.

121. Berda, E. B.; Foster, E. J.and Meijer, E. W. Toward Controlling Folding in Synthetic Polymers: Fabricating and Characterizing Supramolecular Single-Chain Nanoparticles. *Macromolecules* **2010**, 43 (3), 1430-1437.

122. Stals, P. J. M.; Gillissen, M. A. J.; Nicolay, R.; Palmans, A. R. A.and Meijer, E. W. The balance between intramolecular hydrogen bonding, polymer solubility and rigidity in single-chain polymeric nanoparticles. *Polym. Chem.* **2013**, 4 (8), 2584-2597.

123. Beijer, F. H.; Sijbesma, R. P.; Kooijman, H.; Spek, A. L.and Meijer, E. W. Strong Dimerization of Ureidopyrimidones via Quadruple Hydrogen Bonding. *J. Am. Chem. Soc.* **1998**, 120 (27), 6761-6769.

124. Willenbacher, J.; Altintas, O.; Trouillet, V.; Knofel, N.; Monteiro, M. J.; Roesky, P. W.and Barner-Kowollik, C. Pd-complex driven formation of single-chain nanoparticles. *Polym. Chem.* **2015**, 6 (24), 4358-4365.

125. Willenbacher, J.; Schmidt, B. V. K. J.; Schulze-Suenninghausen, D.; Altintas, O.; Luy, B.; Delaittre, G.and Barner-Kowollik, C. Reversible single-chain selective point folding via cyclodextrin driven host-guest chemistry in water. *Chem. Commun.* **2014**, 50 (53), 7056-7059.

126. Mes, T.; van der Weegen, R.; Palmans, A. R.and Meijer, E. W. Single-chain polymeric nanoparticles by stepwise folding. *Angew. Chem. Int. Ed. Engl.* **2011**, 50 (22), 5085-5089.

127. Artar, M.; Terashima, T.; Sawamoto, M.; Meijer, E. W.and Palmans, A. R. A. Understanding the catalytic activity of single-chain polymeric nanoparticles in water. *J. Polym. Sci., Part A: Polym. Chem.* **2014**, 52 (1), 12-20.

128. Huerta, E.; Stals, P. J. M.; Meijer, E. W.and Palmans, A. R. A. Consequences of Folding a Water-Soluble Polymer Around an Organocatalyst. *Angew. Chem. Int. Ed.* **2013**, 52 (10), 2906-2910.

129. Huerta, E.; van Genabeek, B.; Stals, P. J. M.; Meijer, E. W.and Palmans, A. R. A. A Modular Approach to Introduce Function into Single-Chain Polymeric Nanoparticles. *Macromol. Rapid Commun.* **2014**, 35 (15), 1320-1325.

130. Gillissen, M. A. J.; Terashima, T.; Meijer, E. W.; Palmans, A. R. A.and Voets, I. K. Sticky Supramolecular Grafts Stretch Single Polymer Chains. *Macromolecules* **2013**, 46 (10), 4120-4125.

131. Stals, P. J. M.; Gillissen, M. A. J.; Paffen, T. F. E.; de Greef, T. F. A.; Lindner, P.; Meijer, E. W.; Palmans, A. R. A.and Voets, I. K. Folding Polymers with Pendant Hydrogen Bonding Motifs in Water: The Effect of Polymer Length and Concentration on the Shape and Size of Single-Chain Polymeric Nanoparticles. *Macromolecules* **2014**, 47 (9), 2947-2954.

132. Hosono, N.; Palmans, A. R. A.and Meijer, E. W. "Soldier-Sergeant-Soldier" triblock copolymers: revealing the folded structure of single-chain polymeric nanoparticles. *Chem. Commun.* **2014**, 50 (59), 7990-7993.

133. Rowan, S. J.; Cantrill, S. J.; Cousins, G. R. L.; Sanders, J. K. M.and Stoddart, J. F. Dynamic Covalent Chemistry. *Angew. Chem. Int. Ed.* **2002**, 41 (6), 898-952.

134. Wojtecki, R. J.; Meador, M. A.and Rowan, S. J. Using the dynamic bond to access macroscopically responsive structurally dynamic polymers. *Nat Mater* **2011**, 10 (1), 14-27.

135. Corbett, P. T.; Leclaire, J.; Vial, L.; West, K. R.; Wietor, J.-L.; Sanders, J. K. M.and Otto, S. Dynamic Combinatorial Chemistry. *Chem. Rev.* **2006**, 106 (9), 3652-3711.

136. Mavila, S.; Eivgi, O.; Berkovich, I.and Lemcoff, N. G. Intramolecular Cross-Linking Methodologies for the Synthesis of Polymer Nanoparticles. *Chem. Rev.* **2016**, 116 (3), 878-961.

137. Shishkan, O.; Zamfir, M.; Gauthier, M. A.; Borner, H. G.and Lutz, J.-F. Complex single-chain polymer topologies locked by positionable twin disulfide cyclic bridges. *Chem. Commun.* **2014**, 50 (13), 1570-1572.

138. Song, C.; Li, L.; Dai, L.and Thayumanavan, S. Responsive single-chain polymer nanoparticles with host–guest features. *Polym. Chem.* **2015**, 6 (26), 4828-4834.

139. Murray, B. S.and Fulton, D. A. Dynamic Covalent Single-Chain Polymer Nanoparticles. *Macromolecules* **2011**, 44 (18), 7242-7252.

140. Whitaker, D. E.; Mahon, C. S.and Fulton, D. A. Thermoresponsive Dynamic Covalent Single-Chain Polymer Nanoparticles Reversibly Transform into a Hydrogel. *Angew. Chem. Int. Ed.* **2013**, 52 (3), 956-959.

141. Sanchez-Sanchez, A.; Fulton, D. A.and Pomposo, J. A. pH-responsive single-chain polymer nanoparticles utilising dynamic covalent enamine bonds. *Chem. Commun.* **2014**, 50 (15), 1871-1874.

142. Tan, H.; Jin, H.; Mei, H.; Zhu, L.; Wei, W.; Wang, Q.; Liang, F.; Zhang, C.; Li, J.; Qu, X.; Shangguan, D.; Huang, Y.and Yang, Z. PEG-urokinase nanogels with enhanced stability and controllable bioactivity. *Soft Matter* **2012**, 8 (9), 2644-2650.

143. Steinhilber, D.; Rossow, T.; Wedepohl, S.; Paulus, F.; Seiffert, S.and Haag, R. A Microgel Construction Kit for Bioorthogonal Encapsulation and pH-Controlled Release of Living Cells. *Angew. Chem. Int. Ed.* **2013**, 52 (51), 13538-13543.

144. Bulmus, V.; Chan, Y.; Nguyen, Q.and Tran, H. L. Synthesis and Characterization of Degradable p(HEMA) Microgels: Use of Acid-Labile Crosslinkers. *Macromol. Biosci.* **2007**, 7 (4), 446-455.

145. Li, Y.; Xiao, W.; Xiao, K.; Berti, L.; Luo, J.; Tseng, H. P.; Fung, G.and Lam, K. S. Well-Defined, Reversible Boronate Crosslinked Nanocarriers for Targeted Drug Delivery in Response to Acidic pH Values and cis-Diols. *Angew. Chem. Int. Ed.* **2012**, 51 (12), 2864-2869.

146. Chen, W.; Cheng, Y.and Wang, B. Dual-Responsive Boronate Crosslinked Micelles for Targeted Drug Delivery. *Angew. Chem. Int. Ed.* **2012**, 51 (22), 5293-5295.

147. Li, L.; Bai, Z.and Levkin, P. A. Boronate–dextran: An acid-responsive biodegradable polymer for drug delivery. *Biomaterials* **2013**, 34 (33), 8504-8510.

Chapter 2 *Evolution of microphase separation with variations of segments of sequence-controlled multiblock copolymers*

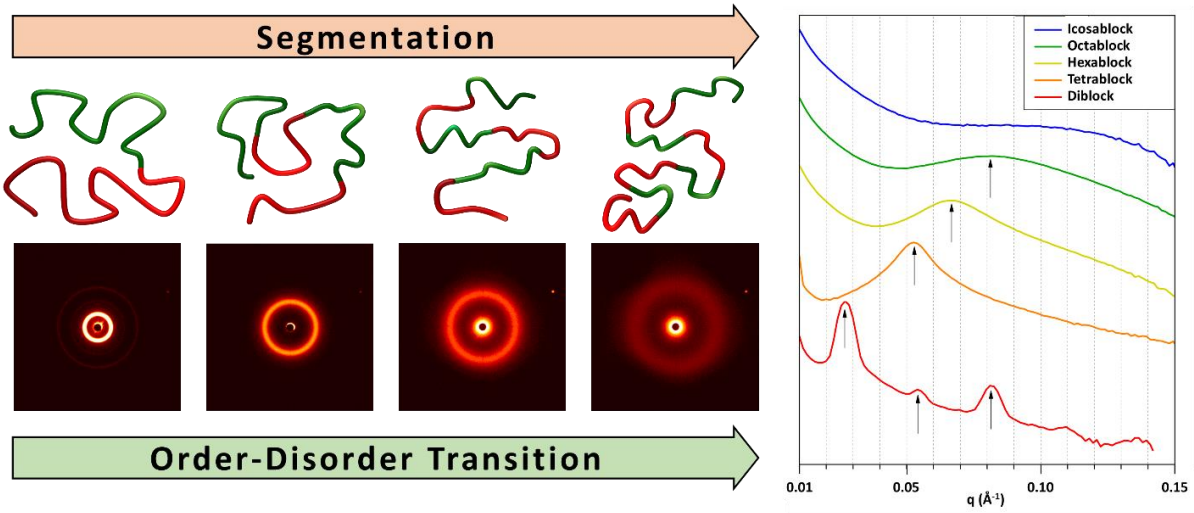

Multiblock copolymers (MBCPs) are emerging class of materials that are becoming more accessible in recent years. However, to date there is still a lack of fundamental understanding of their physical properties. In particular, the glass transition temperature (T_g) which is known to be affected by the phase separation has not been well characterised experimentally. In this chapter, the first experimental study on the evolution of the T_gs and the corresponding phase separation of linear MBCPs with increasing number of blocks whilst keeping the overall degree of polymerisation (DP) constant (DP = 200) was carried out. Ethylene glycol methyl ether acrylate (EGMEA) and tert-butyl acrylate (tBA) were chosen as monomers for reversible addition-fragmentation chain transfer polymerization to synthesise MBCPs. The T_gs (as measured by Differential Scanning Calorimetry) of EGMEA and tBA segments within the MCBPs were found to converge with increasing number of blocks and decreasing block length, correlating with the loss of the heterogeneity as observed from Small Angel X-ray Scattering (SAXS) analysis. The T_gs of the multiblock copolymers were also

compared to the T_gs of the polymer blends of the corresponding homopolymers, and the T_gs of the polymer blends were found to be similar to those of the respective homopolymers, as expected. SAXS experiments further demonstrated microphase separation of multiblock copolymers. This work demonstrates the enormous potential of multiblock architectures to tune the physical properties of synthetic polymers, by changing their glass transition temperature and their morphologies obtained from microphase separation, with domain sizes reaching under 10 nm.

2.1 Introduction

Sequence regulated synthetic macromolecules, called multiblock copolymers (MBCPs), form an interesting class of materials, where the properties and functionality can be controlled on demand.[1, 2] Multiblock copolymers have opened up a new perspective for building functional polymer architectures with tailored morphologies.[3-5] Advances in the synthesis of multiblock copolymers have offered a novel platform to manipulate the microdomain structures (e.g. spherical, cylindrical or lamellar domains) of synthetic materials in terms of block length, polymer architecture, or choice of monomers.[1, 6-11] Microphase separated block copolymers have appealing properties (for applications such as nanoscale lithography, ionic conductivity, or energy storage) that are influenced significantly by their microdomain structures.[12-20] Tuning the molecular composition of the block copolymer can influence both type and domain size of the respective bulk morphologies upon self-assembly in the solid state and this might allow for the generation of materials with designed properties for nanotechnology applications.[21-24]

Phase behavior in $(AB)_n$ multiblock copolymers has been a subject of ongoing theoretical[25-32] and experimental[30, 33-37] research over recent twenty years. It was shown that $(AB)_n$ linear multiblock copolymer phase behavior qualitatively is similar to that of AB diblock copolymers[25, 26] and is governed by the composition f of the block copolymer (where f_A is the volume fraction of the A block), and the product χN_{eff} (where χ is the Flory-Huggins parameter describing excluded volume interactions between A and B blocks, and N_{eff} is the effective number of monomer units in a diblock copolymer obtained by dissecting the multiblock copolymer under study into constituent diblocks). Thus, depending on the composition of the multiblock copolymer and the degree of segregation, ordered lamellar, cylindrical, bcc spherical, hcp spherical, gyroid and Fddd phases are expected to be observed. These theoretical predictions are in perfect agreement with experimental observations.[30, 33-37]

The largest difference in terms of phase behaviour of multiblock copolymers with respect to diblock copolymer systems is expected when operating close to the order-disorder transition (ODT).[30, 32] It was shown that ordering in multiblock copolymers occurs at lower values of χN_{eff} compared to diblock copolymers with the same value of χN. This is explained by the lower value of both translational and conformational entropy of a multiblock copolymer system compared to the equivalent diblock copolymer system. Interestingly, it was shown by Wu *et al.* that taking into account fluctuations shifts ODT in $(AB)_n$ multiblock copolymers upwards relative to the mean-field prediction by the value independent of number of blocks in a multiblock.[30]

However, understanding phase behaviour is just the first step on the way fully understanding about multiblock copolymer properties relevant for applications. The material properties of synthetic polymers are to a large extent dependent on the thermal response, such as glass transition or crystallization behaviour.[38]

The glass transition temperature (T_g) plays a significant role in the applications of synthetic materials and the T_g values are useful for a variety of purposes,[39-42] e.g. intelligent medical devices,[43] implants for minimally invasive surgery,[44, 45] producing 'breathable clothing',[46] or fabricating devices with high ionic conductivity using soft (low T_g) polymers featuring rapid segmental motion and low rigidity.[47]

A large body of work has focused on studying the correlation between the structure of block copolymers and the glass transition temperature in order to further investigate the microdomain morphologies and physical properties.[48-53] Recently, Zuckermann *et al.* synthesized a series of sequence-defined peptoid diblock copolymers by solid-phase synthesis and investigated the nanoscale phase separation of these materials.[14] With this approach it was possible to tune the intra- and intermolecular interactions of block copolymers, proving the system to be useful for fundamental studies of block copolymer self-assembly. More recently,

Gao et al. reported the investigation of the effect of monomer sequence on the T_g of segmented hyperbranched copolymers,[54] proving that segmentation significantly affects the glass transition.

Dependence of the number and length of blocks on the glass transition of linear multiblock copolymers was studied in works of Spontak *et al.*[37] and Lee *et al.*[34] In the former, symmetrical Poly(styrene-*b*-isoprene)$_n$ ($1 \leq n \leq 4$) multiblock copolymers were studied. They considered two multiblock copolymer series: one with constant block length and the second with constant overall multiblock chain length. All samples showed long range lamellar order where the domain size decreased as $n^{0.8}$ for the series with constant chain molecular mass. For the first series, domain size also decreased with increase in the number of blocks but this dependence was not as strong. Multiblock copolymer samples showed interesting thermal behaviour. The authors found that the lower (isoprenic) glass transition was insensitive to the number of blocks, however the higher (styrenic) glass transition temperature showed a decrease on increase in n. The effect was more pronounced for the second series in their study.

Lee *et al.*[34] studied the phase behavior of Poly(styrene-*b*-butadiene)$_n$ multiblock copolymers with alternating (n = 7, 8, 11, 15) and random (n = 16, 21, 24, 25) sequence and volume fraction of PS block in the range 69%-85% PS. The length of block was fixed and the number of blocks was varied. They found lamellar for alternating tetrablock copolymer. All other samples were disordered, but inhomogeneous. They found a slight decrease in the higher glass transition temperatures and an increase in the lower T_g compared to the glass transition temperatures of the corresponding homopolymers. These small differences increased with decreasing block length. Shifts in T_g were attributed to microphase mixing of PS and PB blocks.

In this work, synthesis and study of microphase separation and thermal properties of symmetric Poly(ethylene glycol methyl ether acrylate-*b*-*tert*-butyl acrylate) [(EGMEA-tBA)$_n$] multiblock copolymers with overall fixed degree of polymerisation but different number of

blocks was carried out. In contrast to study of Spontak, *et al.*,[37] this work considers short blocks and probe the region near order-disorder transition. This study demonstrates the T_gs of the segments to converge with increasing number of blocks and decreasing block length, correlating with the loss of the heterogeneity as observed from Small Angel X-ray Scattering (SAXS) analysis. This approach highlights the potential of MBCP for tuning the physical properties of synthetic polymers.

2.2 Results and Discussion

Very recently, our group developed a simple and scalable approach to synthesize well-defined sequence controlled multiblock copolymers with quantitative monomer conversions using a wide range of monomers in a one-pot approach, which showed enormous potential to generate synthetic polymers with complex architectures.[1, 8] Herein, this method was applied to systematically explore the effect of the segmentation on the T_g dependence and nanoscale phase separation in linear multiblock copolymers.

A series of sequence controlled multiblock copolymers (diblock, tetrablock, hexablock, octablock and icosablock) based on two different monomers, ethylene glycol methyl ether acrylate (EGMEA, **A**) and *tert*-butyl acrylate (*t*BA, **B**), as well as their corresponding homopolymers and statistical copolymers were synthesized by RAFT polymerization. The block copolymers were synthesized with alternating order of the two monomers (e.g. ABAB for a tetrablock). Importantly, the total targeted degree of polymerization (DP) of each copolymer was set at 200 with a monomer ratio of 1:1, in order to keep the overall chemical composition of each multiblock copolymer constant while the degree of segmentation was varied (**Scheme 2.1a, Table 2.1**).

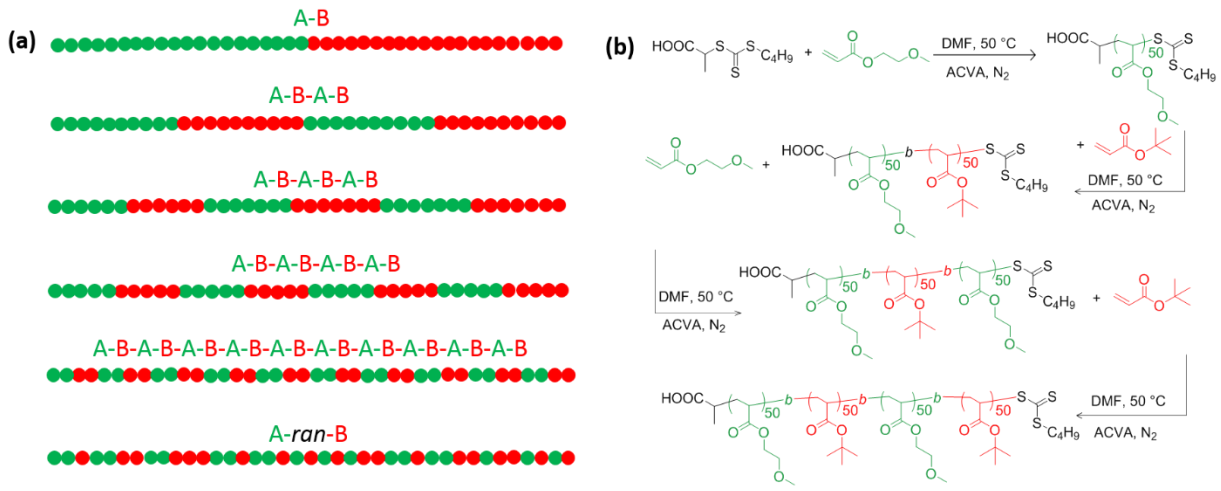

Scheme 2.1 a) Schematic Representation of Multiblock Copolymers Investigated in this Study. b) Synthesis of the Tetrablock Copolymer of $\mathbf{A_{50}B_{50}A_{50}B_{50}}$ by RAFT Polymerization (where A and B represent EGMEA and tBA, respectively).

All MBCPs were synthesized by RAFT polymerization in a one pot approach using sequential monomer addition for each block. In order to avoid side reactions of the acrylate monomers during the polymerization, all polymerizations were carried out in DMF at a relatively low temperature (50 °C) using 2-((butylthio)-carbonothioyl) thio propanoic acid (referred to as (propanoic acid)yl butyl trithiocarbonate (PABTC) in this paper) as chain transfer agent (CTA) and 4, 4′-azobis(4-cyanovaleric acid) (ACVA) as initiator. **Scheme 2.1b** illustrates the synthesis of the tetrablock copolymer of $\mathbf{A_{50}B_{50}A_{50}B_{50}}$. The detailed synthetic procedures of these multiblock copolymers can be found in the experimental part (**Tables 2.2-2.7**). MBCPs were analysed by ^{1}H NMR and SEC to determine conversion after each step and confirm the successful chain extension.

^{1}H NMR spectra of MBCPs showed near quantitative monomer conversion (≥ 96%, see **Figure 2.10-2.15**, see **Figure 2.11** for a detailed structural assignment for the ^{1}H NMR spectrum of the diblock copolymer $\mathbf{A_{100}B_{100}}$ as an example) for each block extension. The molecular weight distributions were characterized by Size Exclusion Chromatography (SEC, see **Figures 2.16-2.20**), revealing asymmetrical distributions with a clear shift to higher

molecular weights after each monomer addition. However, some low-molecular-weight tailing was observed after each chain extension, which can be ascribed to the accumulation of initiator-derived dead chains, termination through coupling reactions, or possible interactions of the multiblock copolymer with the SEC column.[1, 8, 9] These findings are more prevalent for the icosablock (20 blocks) system; as a higher number of blocks was targeted, a higher initial initiator concentration was required to reach full monomer conversion after each step.[9] The increased propagating radical concentration, however, also increases the number of termination events (initiator derived chains).[55] However, assuming that the segment lengths of the individual blocks are similar, the presence of dead chains with different number of segments surely affects the overall dispersity, but not necessarily the (*vide infra*) self-assembly in the bulk. The high molecular weight shoulder detected by SEC is likely associated to the copolymerization of macromonomer formed by the propagating radical undergoing backbiting β-scission, which occurs during the radical polymerization of acrylates.[9, 56-58]

Table 2.1 Characterization of the Multiblock Copolymers by ^{1}H NMR, $CHCl_3$-SEC and DSC.

	Sample	$M_{n,th}$[c] g mol^{-1}	$M_{n,SEC}$[d] g mol^{-1}	$Đ$[d]	P(A) T_g[e] °C	P(B) T_g[e] °C
	A_{200}[a]	26,300	24,700	1.11	-32.3±0.2	-
	B_{200}[b]	25,900	24,500	1.09	-	47.9±0.3
BCP^{di}	$A_{100}B_{100}$	26,100	24,800	1.17	-30.9±0.3	39.1±0.2
BCP^{tetra}	$A_{50}B_{50}A_{50}B_{50}$	26,100	22,700	1.26	-28.1±0.1	23.3±0.2
BCP^{hexa}	$A_{33}B_{33}A_{33}B_{33}A_{33}B_{33}$	25,800	21,200	1.37	-26.6±0.6	10.1±0.4
BCP^{octa}	$A_{25}B_{25}A_{25}B_{25}A_{25}B_{25}A_{25}B_{25}$	26,100	23,300	1.34	-22.6±1.0	3.1±0.6
BCP^{icosa}	$(A_{10}B_{10}A_{10}B_{10}A_{10}B_{10}A_{10}B_{10}A_{10}B_{10})_2$	26,100	21,200	1.67	-9.9±0.4	-9.9±0.4
CP^{ran}	A_{100}-*ran*-B_{100}	26,100	25,300	1.10	-6.5±0.2	

[a] A represents the monomer EGMEA

[b] B represents the monomer tBA

[c] $M_{n,th} = ([M]_0 \times p \times M_M)/[CTA]_0 + M_{CTA}$, where p is the monomer conversion

[d] Determined by SEC in $CHCl_3$ with PMMA used as molecular weight standards

[e] Data represent mean ± SD (n = 3).

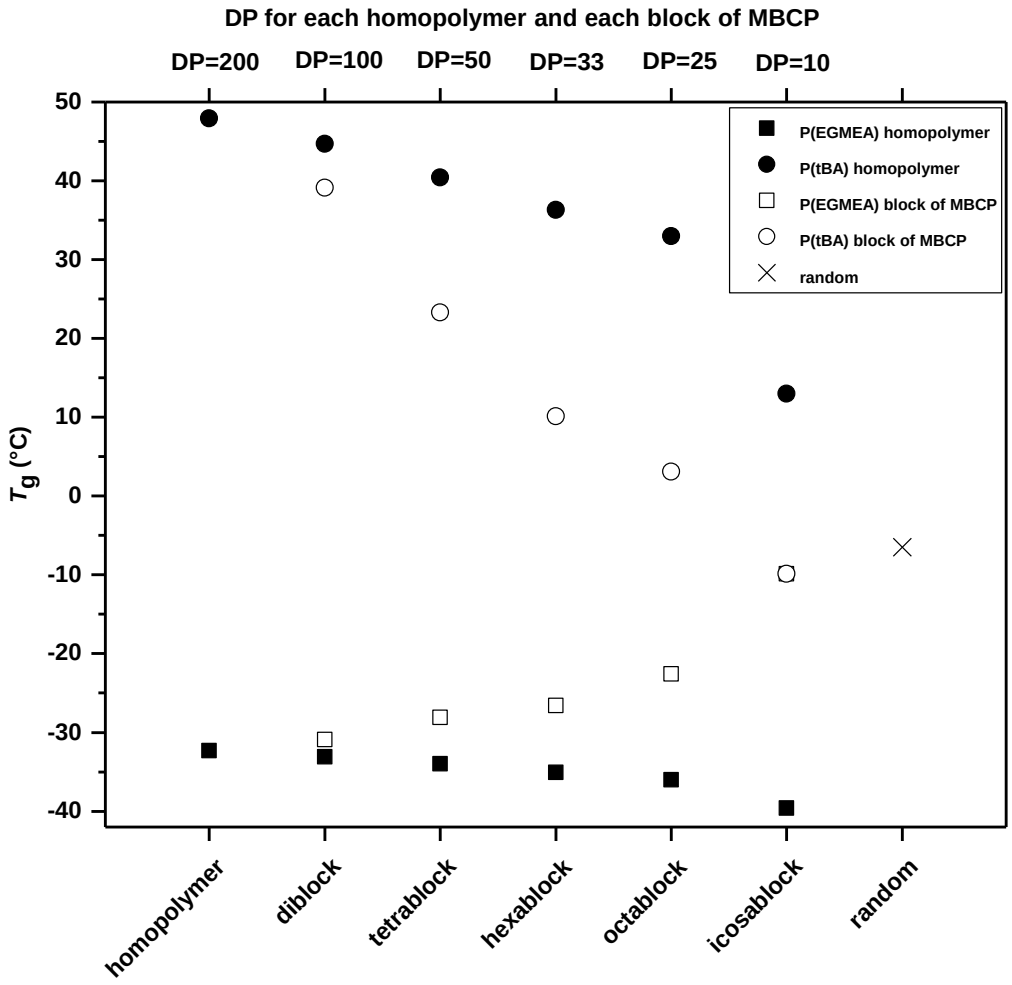

Figure 2.1 Comparison of Tg values of multiblock copolymers (total DP = 200), homopolymers EGMEA and tBA (DP = 200, 100, 50, 33, 25, 10, respectively) and statistical copolymer of EGMEA and tBA (DP = 200). Data represent mean values only (error bars within point size, see **Tables 2.1** and **2.9** for SD).

The microphase separation of MBCPs and the influence of the segmentation on the T_g were investigated using DSC measurements. The results are shown in **Table 2.1**, **Figure 2.1** and DSC curves are depicted in the experimental part (**Figures 2.21-2.25**). Based on all of the DSC traces of the MBCPs, melting peaks and crystallization exotherms were not observed, showing that all of these MBCPs are noncrystalline.[14, 18, 59]

As a control, a statistical copolymer with a DP of 200 (DP 100 for each monomer) was synthesized as well. Based on the polymerization kinetic study (**Figures 2.26-2.28**), the two

monomers **A** and **B** had the similar reactivity, which indicates a random distribution along the copolymer chain.

The DSC thermogram of random copolymer (**CP^{ran}**) showed one single T_g value of -6.5 °C (**Table 2.1**, **Figure 2.29**) which means there was no microphase separation occurring as expected for a random copolymer. On the other hand, the diblock copolymer **BCP^{di}** (**$A_{100}B_{100}$**) showed two distinct T_gs at -30.9 °C and 39.1 °C (**Table 2.1, Figure 2.21**) indicative of phase separation. The tetrablock copolymer **BCP^{tetra}** (**$A_{50}B_{50}A_{50}B_{50}$**) was synthesized with a decreased DP of each block (from 100 to 50) and an increased segmentation number (from 2 to 4). The DSC thermogram of the tetrablock copolymer **BCP^{tetra}** also displayed two T_gs of -28.1 °C and 23.3 °C (**Table 2.1**, **Figure 2.22**), again demonstrating the occurrence of phase separation. The hexablock, **BCP^{hexa}** (**$A_{33}B_{33}A_{33}B_{33}A_{33}B_{33}$**), with a DP of 33 for each block and segmentation number of 6 still shows two T_g values, -26.6 °C and 10.1 °C (**Table 2.1, Figure 2.23**). With a further decreased DP of 25 for each block and a more segmented polymer chain, the 8 blocks containing octablock copolymer (**BCP^{octa}**) still exhibits two T_g values, -22.6 °C and 3.1 °C (**Table 2.1**, **Figure 2.24**). It is however noteworthy that these latter T_g values were not as clearly observable as for the other aforementioned MBCPs (DSC thermograms shown in **Figure 2.24**). Overall it is apparent that the T_g values of the MBCPs shift towards that of the statistical copolymer with increasing segmentation. In order to investigate the effect of segmentation on MBCP microphase separation further, an icosablock copolymer (**BCP^{isoca}**, DP 10 for each block) was synthesised and analysed. The DSC analysis of **BCP^{isoca}** demonstrated only one T_g value of -9.9 °C (**Table 2.1, Figure 2.25**) which indicates the absence of phase separation. These results show that these multiblock copolymers up to octamer sample have two glass transition temperatures which shows that they are microscopically inhomogeneous.

In addition, homopolymers of each monomer with a DP equal to each block of the multiblock copolymers were synthesized [**Tables 2.8** and **2.9**, for ^{1}H NMR spectra see **Figures**

2.30-2.36), for SEC traces see (**Figures 2.37 and 2.38**)] and subsequently analysed by DSC. As expected, the T_g values of the homopolymers decreased with decreasing molecular weight (**Figure 2.1**). As the DP decreased from 200 to 10: **A_{200}** was shown to have a T_g of -32.3 °C, while the T_g values of **A_{100}**, **A_{50}**, **A_{33}**, **A_{25}** and **A_{10}** were -33.1 °C, -34.0 °C, -35.1 °C, -36.0 °C and -39.6 °C, respectively (**Table 2.9, Figures 2.39-2.44**). The T_g values of homopolymers of **B** also decreased with decreasing DP. The T_gs decreased from 47.8 °C for **B_{200}** to 44.7 °C, 40.4 °C, 36.3 °C, 33 °C and 13 °C for **B_{100}**, **B_{50}**, **B_{33}**, **B_{25}** and **B_{10}**, respectively (**Table 2.9, Figures 2.45-2.50**). Compared to the homopolymers of **A**, the difference is more pronounced. This is attributed to larger flexibility of homopolymer **A**, which means that it is difficult to change the T_g dramatically. These results are corroborated by well-known theory, based on the Fox-Flory equation (Equation 1).[60, 61]

$$T_g = T_{g,\infty} - K/M_n \qquad \text{(Equation 2.1)}$$

where

$$K = 2\frac{\rho N_A \theta}{\alpha} \qquad \text{(Equation 2.2)}$$

where ρ is density, N_A is Avogadro number, θ is an average free volume content per chain, α is the thermal expansion coefficient, $T_{g,\infty}$ is the T_g for the (hypothetical) polymer with an infinite molecular weight and K is an empirical parameter for a specific polymer species. Decreasing molecular weight consequently increases the chain-end concentration. The end groups, however, exhibit greater free volume than units within the chain and possess deficient intermolecular constraints, which will lead to higher segmental mobility and cause a lower T_g.[62-67] Fitting of our experimental data with Equation 1 gives approximations of $T_{g(A),\infty}$ = -32 °C, $K_{(A)}$ = 1.3 × 10^4 K and $T_{g(B),\infty}$ = 50 °C, $K_{(B)}$ = 5.5 × 10^4 K (see **Figures 2.2** and **2.3**).

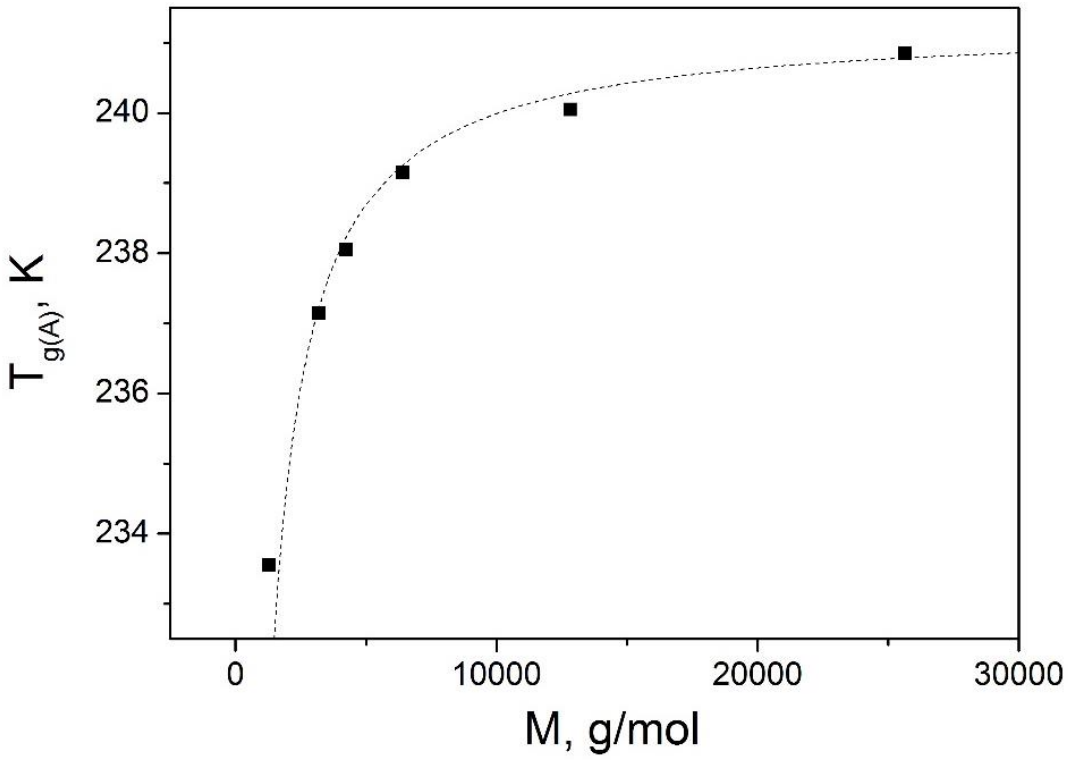

Figure 2.2 Dependence of thermal glass transition temperature of polymer A on the molecular weight of homopolymer. Fitting with Fox-Flory equation gives $T_{Ag,\infty}$ = -32 °C, K_A = 1.3·10^4 K.

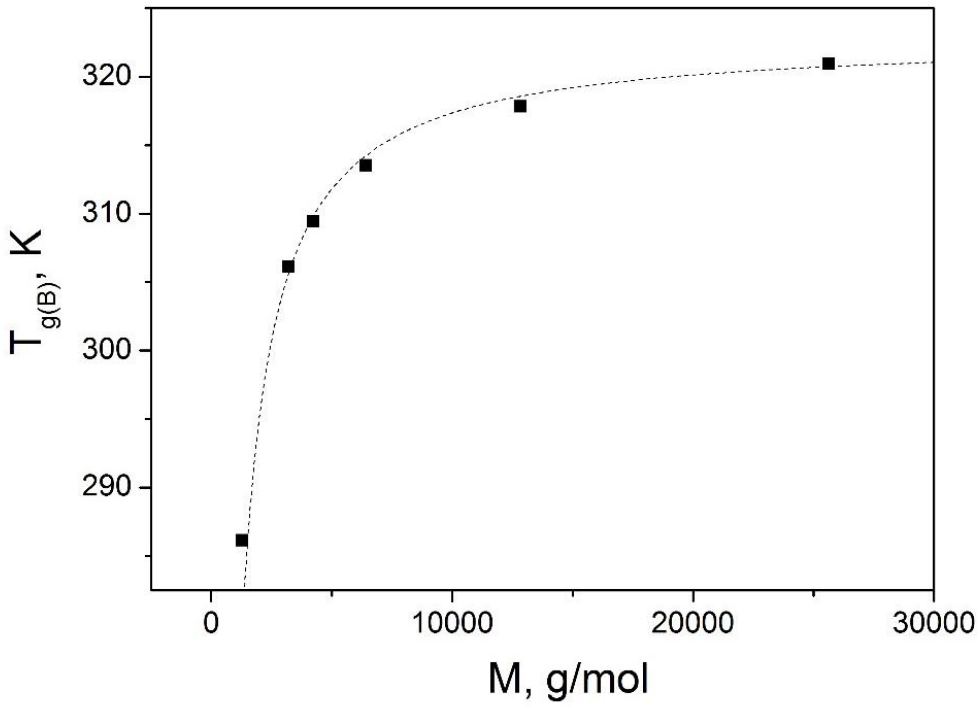

Figure 2.3 Dependence of thermal glass transition temperature of polymer B on the molecular weight of homopolymer. Fitting with Fox-Flory equation gives $T_{Bg,\infty}$ = 50 °C, K_B = 5.5·10^4 K.

As shown in **Figure 2.1**, the comparison between the multiblock copolymers and the homopolymers is particularly striking. The T_g of the **B** block dropped significantly from 39.4 °C for $\mathbf{B_{100}}$ in $\mathbf{BCP^{di}}$ to -9.9 °C for $\mathbf{B_{10}}$ in $\mathbf{BCP^{isoca}}$ while it only decreased from 44.7 °C for homopolymer $\mathbf{B_{100}}$ to 13 °C for homopolymer $\mathbf{B_{10}}$. Interestingly, an opposing trend was observed for the T_g values of the **A** block, which increased for the MBCPs yet decreased for the homopolymers with decreasing DP (**Figure 2.1**). The T_g of the $\mathbf{A_{100}}$ block in the diblock copolymer $\mathbf{BCP^{di}}$ was -30.9 °C and increased to -9.9 °C for $\mathbf{A_{10}}$ block in the icosablock copolymer $\mathbf{BCP^{icosa}}$**,** whereas it decreased from -33.1 °C for homopolymer $\mathbf{A_{100}}$ to -39.6 °C for homopolymer $\mathbf{A_{10}}$. As the number of blocks in multiblock copolymer increases and their length correspondingly goes down, degree of segregation in the system also decreases. Boundaries between domains rich in A and B become smoother and mixing between species increases. This leads to the decrease of difference in T_gs of A-rich and B-rich areas of the melt and increase of corresponding breadths of glass transitions. Both $\mathbf{A_{10}B_{10}}$ diblock copolymers (see below) and icosablock demonstrate one glass transition temperature indicating the presence large degree of homogeneity in theses samples compared to other multiblocks. However, the fact that the breadth of glass transition in both cases is larger than for random copolymer sample allows us to conclude that concentration fluctuations in Both $\mathbf{A_{10}B_{10}}$ diblock and icosablock are stronger than in randomly mixed system.

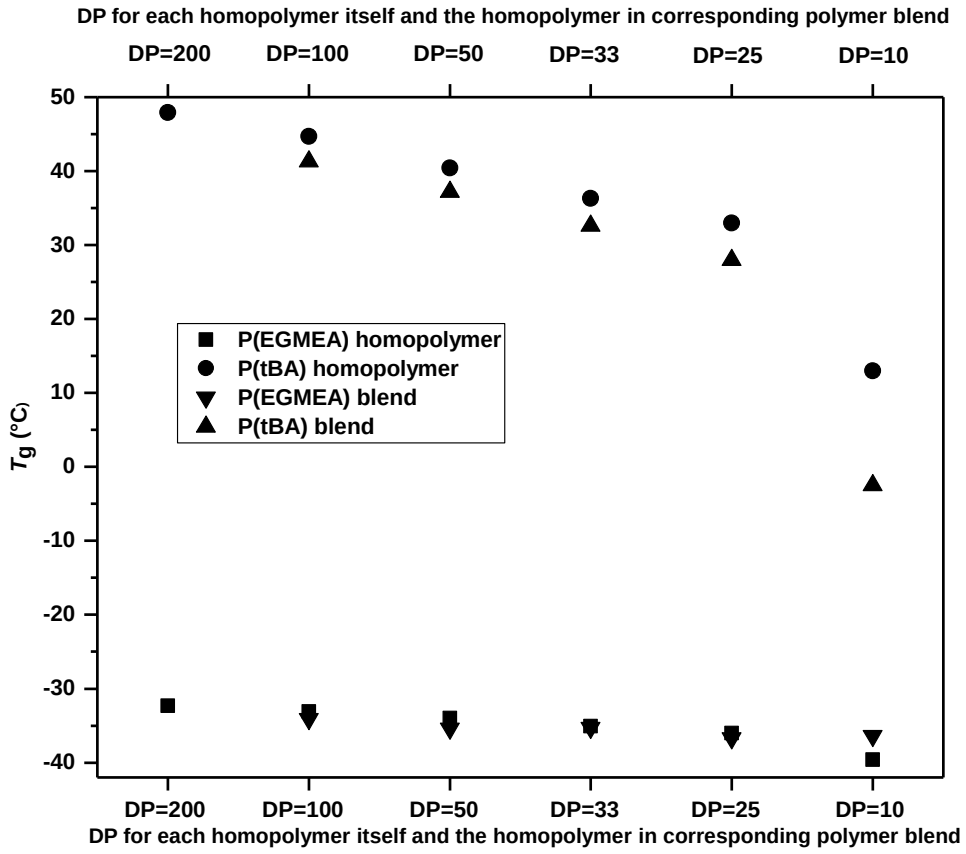

Figure 2.4 The comparison of T_g values of homopolymers (DP=200, 100, 50, 33, 25 and 10) and corresponding polymer blends. Data represent mean values only (error bars within point size, see **Tables 2.1** and **2.9** for SD).

Polymer blends of the two different homopolymers with the same DP were also investigated by DSC (**Table 2.9**, **Figures 2.51-2.55**). Based on the DSC thermograms, all blends investigated displayed two different T_gs, even at DP 10. Compared to the corresponding pristine homopolymers (**Figure 2.4**, for the comparison to the multiblock copolymers, see **Figure 2.5**), most of the T_g values of the **A** component in the polymer blends were similar but a slight decrease in the T_g values of the **B** portion was observed in the polymer blends. Most notably, the **B** portion in the polymer blend of DP 10 showed a more pronounced decrease (from 13 °C for the homopolymer to -2.5 °C for the blend) compared to the polymer blends composed of longer homopolymer chains. This phenomenon can be explained by the fact that the fraction of **A** polymer inside the **B**-rich phase and the fraction of **B** polymer inside the **A**-rich phase increases upon decrease in chain length affecting the observed glass transition

temperatures. In order to make a rough estimation of this effect, concentrations of **A**-rich and **B**-rich phases were calculated using the Flory-Huggins expression for the free energy of the mixture[68,81] and then the obtained concentration was used to predict shifts in glass transition temperatures using the Fox equation.[69] Comparison of calculations with experimental data can be found in **Figure 2.6**. Qualitatively, the dependence of glass transition temperatures of the homopolymer mixtures on their length is closely matched, however, the reduction in the higher glass transition temperature of mixtures of longer homopolymers compared to pure polymer **B** is not yet fully aligned and requires the development of a more suitable theoretical model.

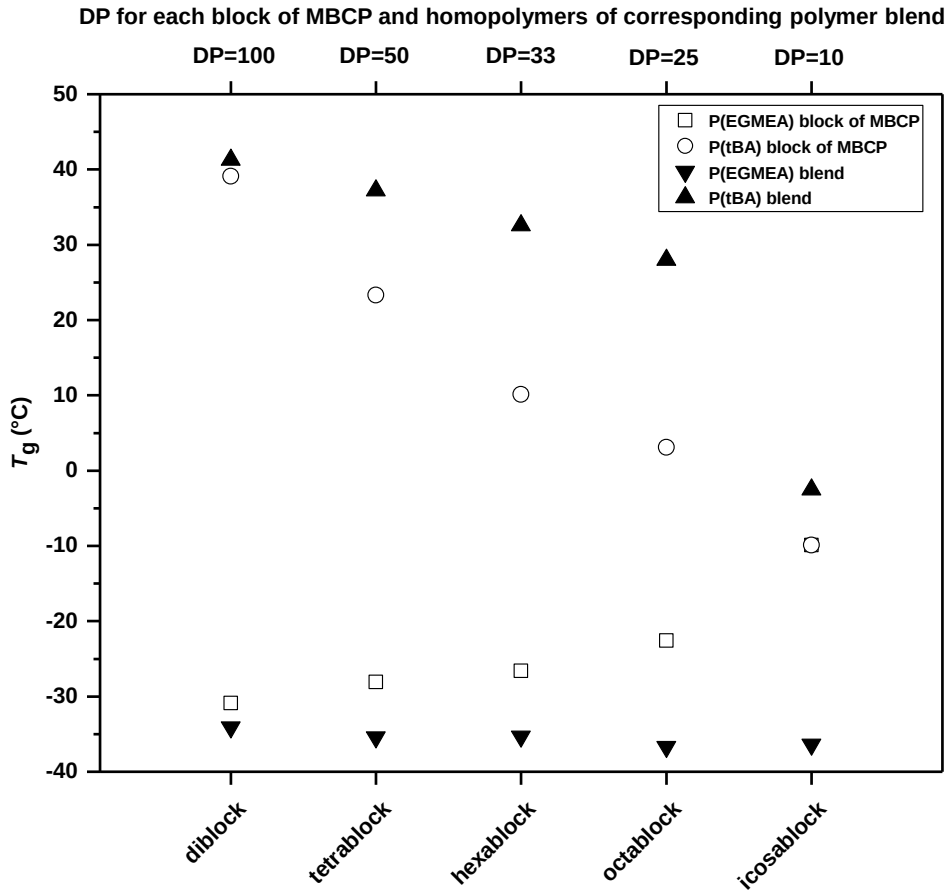

Figure 2.5 The comparison of T_g values of multiblock copolymers (total DP=200) and polymer blends. Data represent mean values only (error bars within point size, see **Tables 2.1** and **2.9** for SD).

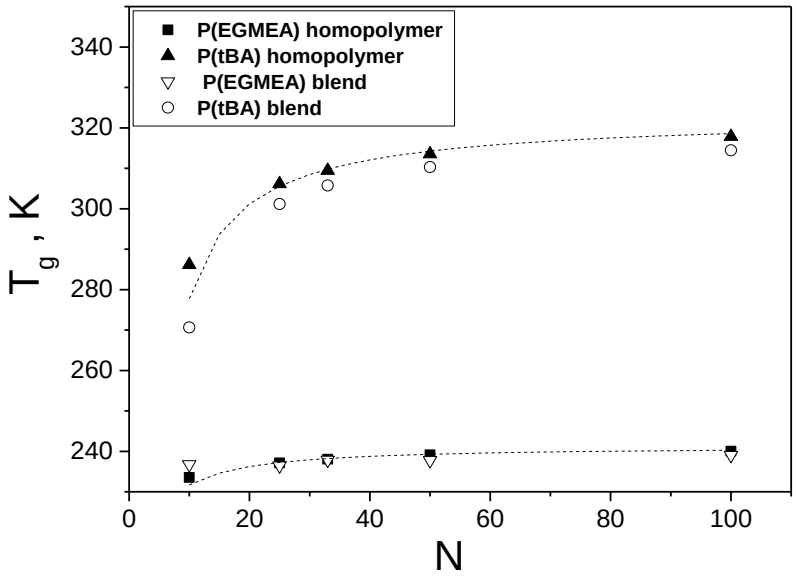

Figure 2.6 Experimental glass transition temperatures for pure homopolymers (solid square and solid triangle), mixtures of homopolymers (hollow triangle and hollow circle), and predictions of glass transition temperatures for mixtures (dash lines, $\chi = 0.25$).

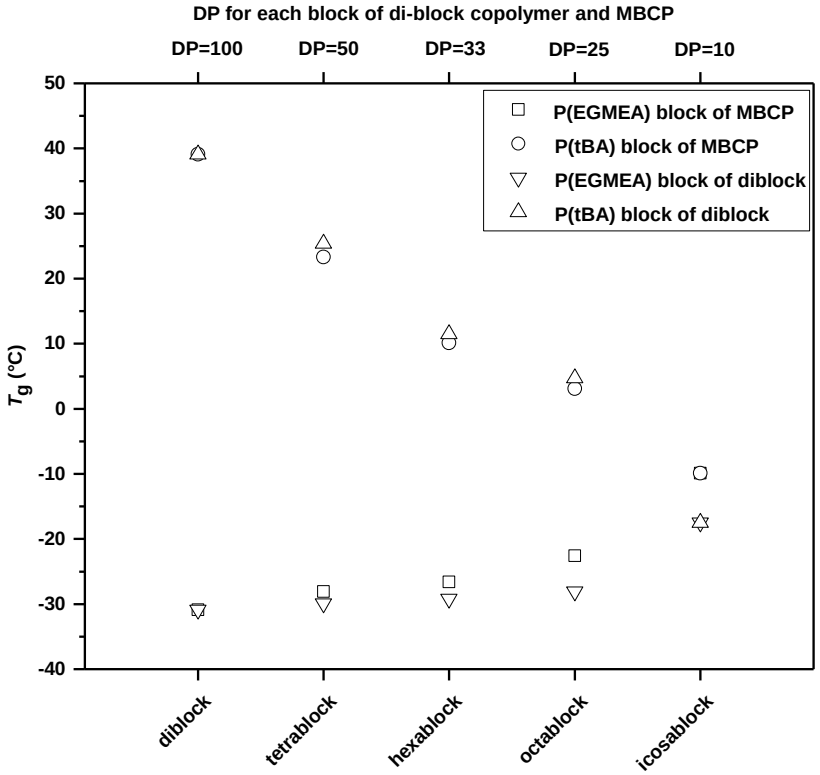

Figure 2.7 The comparison of T_g values of diblock copolymers (DP=100, 50, 33, 25 and 10 for each block) and multiblock copolymers (total DP=200). Data represent mean values only (error bars within point size, see **Tables 2.1** and **2.9** for SD).

In order to investigate the influence of the overall molecular weight on the phase separation, diblock copolymers with segment size matching those of the MBCPs (e.g. **$A_{10}B_{10}$** corresponding to **BCP^{icosa}** and **$A_{25}B_{25}$** corresponding to **BCP^{octa}**) were synthesized and analysed by DSC (**Figures 2.21, 2.56-2.59**). Importantly, all diblock copolymers showed similar T_g values to the corresponding MBCPs (**Table 2.9**, **Figure 2.7**), which suggests similar molecular environments[70] in agreement with overall similarities in the phase behaviour of diblock copolymers and $(AB)_n$ multiblock copolymers.

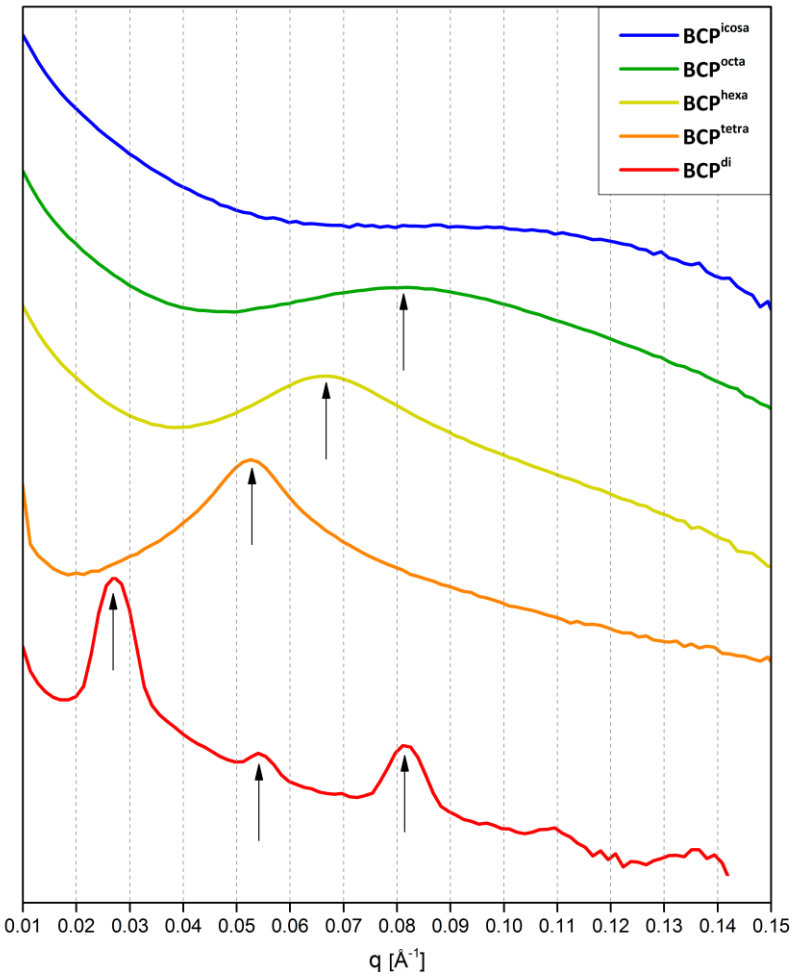

Figure 2.8 Radially integrated Small angle X-ray scattering data for different MBCPs, the measurements were carried out at -30 °C for the **BCP^{hexa}**, **BCP^{octa}**, and **BCP^{icosa}** – all measurements were performed for 2 h.

The microphase separation of the MBCPs with varying degrees of segmentation was also investigated using small angle X-ray scattering (**Figure 2.8**). As can be seen, three distinct

reflexes can be observed for the diblock copolymer **$A_{100}B_{100}$** with [100] : [200] : [300] = 0.027 $Å^{-1}$: 0.054 $Å^{-1}$: 0.081 $Å^{-1}$, indicative of a lamellar morphology in the bulk state, with an overall long period of d = 23 nm (calculated using the Bragg equation according to the reflection assigned as [100]; $d = 2\pi/q$, where q is the scattering vector of the peak). Structure factors of all other samples demonstrate only one main peak indicating the absence of long-range order. The tetrablock, **$A_{50}B_{50}A_{50}B_{50}$**, shows one distinctly broader reflection at q = 0.052 $Å^{-1}$, which corresponds to a characteristic length scale of monomer density fluctuations of 12 nm. This trend continues for the hexablock copolymer, where an even broader reflection at q = 0.068 $Å^{-1}$ is found, showing that the presence of compositional heterogeneity, albeit being far less pronounced (d = 9 nm). It should be noted that for this sample, as for the octa- and icosablock copolymer, the measurement was carried out at -30 °C to account for the rather oily consistency of the material at room temperature and, in addition, phase separation might be more pronounced at lower temperatures (due to the associated increase in the Flory-Huggins interaction parameter between the two blocks, $\chi_{A\text{-}B}$). In the case of the octablock copolymer, the observed reflection with a maximum in intensity at q = 0.081 $Å^{-1}$ increases further in width and shows that there is much less order in the system and the interfaces between the **A**-rich and **B**-rich domains are significantly less well-defined. The icosablock copolymer which has one glass transition temperature according to DSC measurements shows structure factor with extremely broad and weak peak. So it can be concluded that in this case a preferable wavelength of fluctuations in the system cannot be determined due to the high degree of homogeneity. Here it is worth to mention that as molecular weight distribution can significantly affect the phase behaviour of block copolymers,[71-73] the high dispersity of the **BCP^{icosa}** ($Đ$ = 1.67) could also influence the phase separation and explain the presence of one single T_g. However, considering the segment lengths are similar even with a high dispersity and the fact that the diblock copolymer **$A_{10}B_{10}$** has a low dispersity ($Đ$ = 1.15) but also displays only one T_g (**Table 2.9**,

Figure 2.59), it can be speculated that dispersity is not the main driving force to prevent phase separation for **BCP^{icosa}**. Summarising it can be concluded that all multiblock samples except diblock copolymer **$A_{100}B_{100}$** are in a disordered state, however, as far as tetrablock, hexablock and octablock copolymers show two distinct glass transition temperatures these disordered states are microscopically inhomogeneous and may have *liquid-like* order with the domain size $d = 2\pi/q^*$ defined by the position of the peak q^* of structure factor.

According to the mean-field theory dimensions of block copolymers in a disordered state must be Gaussian for flexible chains[74] and correspondingly the domain size should scale as $N^{0.5}$ with number of segments in a chain. However, the plot of log d *versus* log N_{eff} (**Figure 2.9**) for the multiblock copolymer series where $d = 2\pi/q^*$ and N_{eff} is the total degree of polymerization of the diblock copolymer obtained by cutting the multiblock copolymer at even junctions between blocks (as shown in **Figure 2.9b**), gives an approximate linear correlation (regression value, $r^2 \sim 0.98$) with an α value of 0.78 indicating non-Gaussian (more extended) conformation of the chains, which is in line with other reports on diblock copolymers.[75-79]

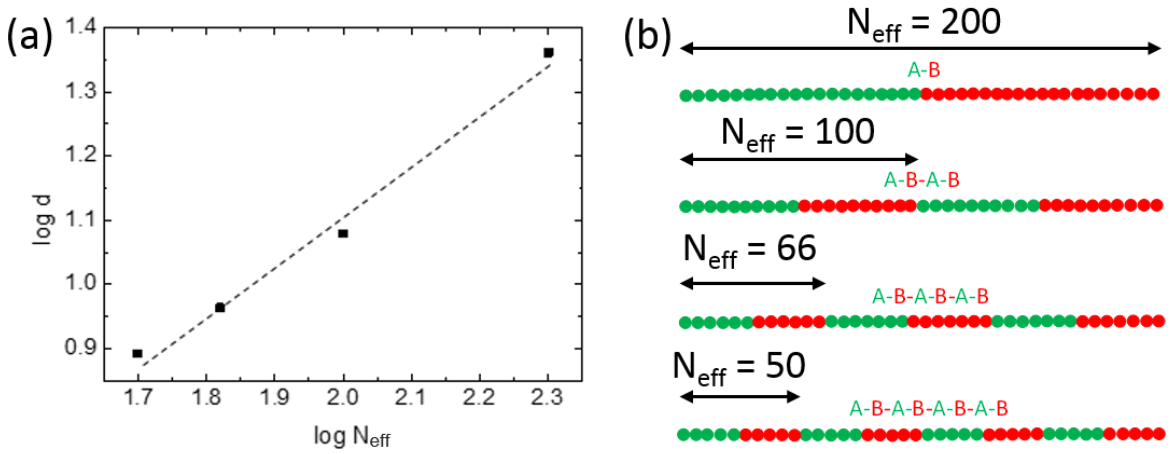

Figure 2.9 (a) Plot of log d *versus* log N for the amorphous domains in the multiblock copolymer series (**BCP^{di}**, **BCP^{tetra}**, **BCP^{hexa}**, **BCP^{octa}**), where the domain spacing is the distance between like polymer phases (taken from SAXS data) and N_{eff} is the total degree of polymerization of the diblock copolymer obtained by cutting the multiblock copolymer at even junctions between blocks [as shown in (b)]. The dashed line is a linear fit of the data points with a gradient of 0.78 and a regression value (r^2) of 0.98.

2.3 Conclusions

In summary, a series of sequence controlled multiblock copolymers using EGMEA and tBA were synthesized by RAFT polymerization and their microphase separation was studied by investigating the glass transition temperatures using DSC analysis. Compared to the homopolymers and homopolymer blends, the glass transition temperatures of the multiblock copolymers displayed a more distinct trend which evolves according to the size of segments. A counter trend behavior of the T_gs of the polyEGMEA blocks was observed in the multiblock copolymers compared to the homopolymers with decreasing DP. Diblock copolymers composed of blocks of the same length as the segments of the multiblock copolymers displayed similar thermal characteristics to their corresponding multiblock copolymers. In addition, SAXS analyses showed that all multiblock copolymers except diblock copolymers (which show lamellae morphology) are in a disordered inhomogeneous state (up to and including octablock copolymers) with a characteristic size of inhomogeniety decreasing when lowering the size of the blocks with a dependence of $N_{eff}^{0.78}$, where N_{eff} is the total length of two of the polymer blocks. Our findings show that the glass transition temperatures of the multiblocks are akin to that of individual diblock copolymers of equivalent block lengths. This approach therefore can be used to modulate the T_g and domain sizes of a block copolymer by keeping the ratio of monomer and overall DP of each monomer constant, but varying the number of segments in the copolymer.

2.4 Experimental

2.4.1 Materials

DMF (≥99.9%) was obtained from Sigma Aldrich and used as received. Ethylene glycol methyl ether acrylate (EGMEA, 98%, referred as "**A**" in this chapter) and tert-Butyl acrylate (tBA, 98%, referred as "**B**" in this chapter) were obtained from Sigma Aldrich and filtered through a basic aluminium oxide (activated, basic, BrockmannI, standard grade, B150 mesh, 58Å) column to remove the radical inhibitor before use. 4, 4′-Azobis(4-cyanovaleric acid) (ACVA, ≥98.0%) was obtained from Sigma Aldrich and used without further purification. All polymerizations were carried out under a nitrogen atmosphere. Milli-Q water and methanol (99.6%, obtained from Sigma Aldrich and used as received) were used for polymer precipitation. Chloroform-*d* ($CDCl_3$, 99.8% D atom) obtained from Sigma Aldrich was used for ^{1}H NMR analysis. RAFT agent of 2-(((butylthio)-carbonothioyl)thio)propanoic acid (called (propanoic acid)yl butyl trithiocarbonate (PABTC) in this paper) was prepared according to a previously reported procedure.[80]

2.4.2 Methods

2.4.2.1 Proton Nuclear Magnetic Resonance (^{1}H NMR) spectroscopy

^{1}H NMR Spectra were recorded on a Bruker Avance III 300 spectrometer (300 MHz) at 27 °C in deuterated chloroform ($CDCl_3$). Chemical shift values (δ) are reported in ppm. The residual proton signal of the solvent (δ_H = 7.26 ppm in $CDCl_3$) was used as internal reference.

2.4.2.2 Determination of monomer conversions

The conversions of the monomers were determined by comparing the integration of the vinyl protons (δ ~ 6.50–5.50 ppm) before and after reaction. The integration of the three methyl protons belonging to the Z group of the PABTC chain transfer agent (–CH_2–C$\underline{H_3}$) was used as reference.

2.4.2.3 Size Exclusion Chromatography (SEC)

Number-average molar masses ($M_{n,SEC}$) and dispersity values ($Đ$) were determined using size exclusion chromatography with $CHCl_3$ as an eluent. The $CHCl_3$ Agilent 390-LC MDS instrument was equipped with differential refractive index (DRI), and two wavelength UV detectors. The system was equipped with 2 x PLgel Mixed D columns (300 x 7.5 mm) and a PLgel 5 µm guard column. The eluent was $CHCl_3$ with 2 % TEA (triethylamine) additive. Samples were run at 1 mL min^{-1} at 30 °C. Poly(methyl methacrylate) ranging from MW = 1010 g mol^{-1} to 955000 g mol^{-1} and polystyrene standards ranging from MW = 162 g mol^{-1} to 483400 g mol^{-1} (Agilent Easy Vials) were used for calibration. Analysed samples were filtered through a PVDF membrane with 0.22 µm pore size before injection. Respectively, experimental molar mass ($M_{n,SEC}$) and dispersity ($Đ$) values of synthesized polymers were determined by conventional calibration using Agilent GPC/SEC software.

2.4.2.4 Calculation of $M_{n,th}$

The theoretical number average molar mass ($M_{n,th}$) is calculated using equation (Equation 2.3).

$$M_{\mathrm{n,th}} = \frac{[\mathrm{M}]_0\, p M_M}{[\mathrm{CTA}]_0} + M_{\mathrm{CTA}} \qquad \text{(Equation 2.3)}$$

where $[M]_0$ and $[CTA]_0$ are the initial concentrations (in mol L^{-1}) of monomer and chain transfer agent respectively; p is the monomer conversion as determined by ^{1}H NMR, M_M and M_{CTA} are the molar masses (g mol^{-1}) of the monomer and chain transfer agent respectively.

2.4.2.5 Calculation of the Theoretical Number Fraction of Living Chains (L)

The theoretical number fraction of living chains is calculated using equation (Equation 2.4).

$$L = \frac{[CTA]_0}{[CTA]_0 + 2f[I]_0(1-e^{-k_d t})(1-\frac{f_c}{2})} \quad \text{(Equation 2.4)}$$

where L is the number fraction of living chains, $[CTA]_0$ and $[I]_0$ are the initial concentrations of CTA and initiator, respectively. The term '2' represents that one molecule of azo initiator degrades into two primary radicals with a certain efficiency f (taken as 0.5 in this study). k_d is the decomposition rate coefficient of the initiator. The term $1 - f_c/2$ represents the number of chains produced in a radical–radical termination event with f_c the coupling factor (f_c = 1 means 100% bimolecular termination by combination, f_c = 0 means 100% bimolecular termination by disproportionation). In this study, a value of f_c = 0 was assumed.

2.4.2.6 Differential Scanning Calorimetry (DSC)

The experiments were performed to determine the thermal behavior of the synthesized polymers on a Mettler Toledo DSC1. In all tests, a scan rate of 10 K/min was used in the temperature range of -100 to 100 °C for three heating and cooling cycles. Three different samples of each polymer were analysed. The T_g value is the maxima of the first derivative of (d_H/d_T). The T_g values were presented with an average value ± standard deviation (mean ± SD, n = 3).

2.4.2.7 Small angle X-ray scattering (SAXS)

SAXS measurements were performed on a Bruker AXS Nanostar (Bruker, Karlsruhe, Germany), equipped with a microfocus X-ray source (Incoatec IμSCu E025, Incoatec, Geesthacht, Germany), operating at λ = 1.54 Å. A setup with three pinholes of 750 μm, 400 μm, and 1,000 μm (with the 1,000 μm hole closest to the sample) was used and the sample-to-detector distance was 107 cm. Samples were mounted on a metal rack using Scotch tape. In case of the multi-block copolymers with 6, 8, or 20 segments the measurements were also carried out at -30 °C, as the consistency of the materials at room temperature was rather waxy. The scattering patterns were background corrected (Scotch tape) prior to evaluation if necessary. Temperature during the measurements was adjusted using a connected Peltier element. The measurement time per isothermal measurement was set to 2 h.

2.4.3 Multiblock copolymer synthesis by RAFT polymerization.

2.4.3.1 General procedures for the synthesis of the first block

CTA, monomer, solvent (DMF) and azoinitiator were charged into a flask having a magnetic stirring bar. The flask was sealed with a rubber septum and degassed with nitrogen for ca. 15 minutes. The solution was then allowed to stir at 50 ˚C in a thermo-stated oil bath for the desired time. A sample was taken for ^{1}H NMR (to determine monomer conversion) and SEC analysis (to determine $M_{n.SEC}$ and $Đ$). After reaction, the mixture is cooled down in cold water to room temperature and open to air.

2.4.3.2 General procedures for the synthesis of the following blocks

For the iterative chain extension, monomer, initiator and solvent is added to the previous polymerization medium and well mixed. The mixture is then degassed by bubbling nitrogen

through the solution for ca. 15 minutes, and the polymerization mixture was allowed to polymerize at 50 ˚C for the desired time with stirring. Before each new block, a sample was withdrawn from the polymerization medium using a degassed syringe for ^{1}H NMR and SEC analysis. This step is performed as many times as needed following the number of block desired. At any time before a new iterative chain extension, the polymerization can be stopped by storing the flask in the fridge until further chain extension.

2.4.3.3 Preparation of polymer blends

The polymer blends were prepared by mixing the same amount (mol) of the corresponding homopolymer of **A** and **B** with the same DP.

2.4.4 Supporting Information

Table 2.2 Experimental conditions used for the synthesis and characterization data of the diblock copolymer: **$A_{100}B_{100}$**.

	$A_{100}B_{100}$	
	1st block	2nd block
$[Monomer]_0$ (mol.L^{-1})	A	B
	5.00	2.38
$[CTA]_0/[ACVA]_{consumed}$	40.7	14.8
$[ACVA]_0$ (mol.L^{-1})	2.00×10^{-2}	4.00×10^{-2}
DP targeted	100	100
$m_{CTA\ added}$ (mg)	9.16	-
$m_{monomer\ added}$ (mg)	500	492
$m_{ACVA\ added}$ (mg)	4.31	14.03
$V_{DMF\ added}$ (mL)	0.131	0.001
reaction time (h)	15	9.7
monomer conversion[a]	99%	98%
$M_{n,th}$[b] (g mol^{-1})	13,300	26,100
$M_{n,SEC}$[c] (g mol^{-1})	14,200	24,800
$Đ$[c]	1.08	1.17
L[d] (%)	97.60	93.68
Cumulative L[e] (%)	97.60	91.43

[a] Determined by ^{1}H NMR

[b] $M_{n,th} = [M]_0 \times p \times M_M/[CTA]_0 + M_{CTA}$, p is the monomer conversion

[c] Determined by SEC in $CHCl_3$ with PMMA used as molecular weight standards

[d] theoretical estimation of the fraction of living chains per block (e.g. extendable chain having the Z group)

[e] theoretical estimation of the cumulated fraction of living chains

Table 2.3 Experimental conditions used for the synthesis and characterization data of the tetrablock copolymer: **$A_{50}B_{50}A_{50}B_{50}$**.

	$A_{50}B_{50}A_{50}B_{50}$			
	1st block	2nd block	3rd block	4th block
$[Monomer]_0$ ($mol.L^{-1}$)	A	B	A	B
	5.00	2.62	1.72	1.17
$[CTA]_0/[ACVA]_{consumed}$	80.5	38.4	26.4	13.2
$[ACVA]_0$ ($mol.L^{-1}$)	3.00×10^{-2}	3.00×10^{-2}	3.00×10^{-2}	3.90×10^{-2}
DP targeted	50	50	50	50
$m_{CTA\ added}$ (mg)	14.65	-	-	-
$m_{monomer\ added}$ (mg)	400	394	400	394
$m_{ACVA\ added}$ (mg)	5.17	4.91	5.62	14.25
$V_{DMF\ added}$ (mL)	0.047	0.0103	0.032	0.096
reaction time (h)	10	11	10.5	11
monomer conversion[a]	100%	98%	99%	98%
$M_{n,th}$[b] ($g\ mol^{-1}$)	6,700	13,200	19,700	26,100
$M_{n,SEC}$[c] ($g\ mol^{-1}$)	7,000	12,800	18,800	22,700
$Đ$[c]	1.07	1.10	1.15	1.26
L[d] (%)	98.77	97.46	96.35	92.98
Cumulative L[e] (%)	98.77	96.27	92.75	86.23

[a] Determined by ^1H NMR

[b] $M_{n,th} = [M]_0 \times p \times M_M/[CTA]_0 + M_{CTA}$, p is the monomer conversion

[c] Determined by SEC in $CHCl_3$ with PMMA used as molecular weight standards

[d] theoretical estimation of the fraction of living chains per block (e.g. extendable chain having the Z group)

[e] theoretical estimation of the cumulated fraction of living chains

Table 2.4 Experimental conditions used for the synthesis and characterization data of the hexablock copolymer: **$A_{33}B_{33}A_{33}B_{33}A_{33}B_{33}$.**

	$A_{33}B_{33}A_{33}B_{33}A_{33}B_{33}$					
	1st block	2nd block	3rd block	4th block	5th block	6th block
$[Monomer]_0$ ($mol.L^{-1}$)	A	B	A	B	A	B
	5.50	2.75	1.77	1.29	0.996	0.81
$[CTA]_0/[ACVA]_{consumed}$	118.7	70.5	35.9	23.9	17.4	10.9
$[ACVA]_0$ ($mol.L^{-1}$)	3.00×10^{-2}	3.16×10^{-2}	3.15×10^{-2}	3.70×10^{-2}	4.40×10^{-2}	4.40×10^{-2}
DP targeted	33	33	33	33	33	33
$m_{CTA\ added}$ (mg)	22.20	-	-	-	-	-
$m_{monomer\ added}$ (mg)	400	394	400	394	400	394
$m_{ACVA\ added}$ (mg)	4.70	5.43	5.75	10.18	14.39	10.11
$V_{DMF\ added}$ (mL)	0.007	0.000	0.028	0.000	0.015	0.046
reaction time (h)	11.3	9	11.5	10.7	9.5	12.5
monomer conversion[a]	98%	99%	98%	99%	98%	98%
$M_{n,th}$[b] (g mol^{-1})	4,500	8,800	13,100	17,300	21,600	25,800
$M_{n,SEC}$[c] (g mol^{-1})	4,500	8,800	12,800	17,100	20,200	21,200
$Đ$[c]	1.11	1.08	1.13	1.15	1.21	1.37
L[d] (%)	99.16	98.60	97.29	95.98	94.57	91.57
Cumulative L[e] (%)	99.16	97.78	95.13	91.31	86.35	79.07

[a] Determined by ^1H NMR

[b] $M_{n,th} = [M]_0 \times p \times M_M/[CTA]_0 + M_{CTA}$, p is the monomer conversion

[c] Determined by SEC in $CHCl_3$ with PMMA used as molecular weight standards

[d] theoretical estimation of the fraction of living chains per block (e.g. extendable chain having the Z group)

[e] theoretical estimation of the cumulated fraction of living chains

Table 2.5 Experimental conditions used for the synthesis and characterization data of the octablock copolymer: **$A_{25}B_{25}A_{25}B_{25}A_{25}B_{25}A_{25}B_{25}$.**

	$A_{25}B_{25}A_{25}B_{25}A_{25}B_{25}A_{25}B_{25}$							
	1st block	2nd block	3rd block	4th block	5th block	6th block	7th block	8th block
$[Monomer]_0$ ($mol.L^{-1}$)	A	B	A	B	A	B	A	B
	5.90	2.95	1.93	1.43	1.11	0.75	0.66	0.57
$[CTA]_0/[ACVA]_{consumed}$	146.9	78.5	54.3	34.9	25.1	16.2	12.3	7.2
$[ACVA]_0$ ($mol.L^{-1}$)	4.30×10^{-2}	3.30×10^{-2}	3.80×10^{-2}	3.30×10^{-2}	4.50×10^{-2}	4.50×10^{-2}	5.20×10^{-2}	6.00×10^{-2}
DP targeted	25	25	25	25	25	25	25	25
$m_{CTA\ added}$ (mg)	29.31	-	-	-	-	-	-	-
$m_{monomer\ added}$ (mg)	400	394	400	394	400	394	400	394
$m_{ACVA\ added}$ (mg)	6.28	3.61	7.77	3.57	15.98	17.87	18.60	25.04
$V_{DMF\ added}$ (mL)	0.001	0.000	0.000	0.037	0.060	0.500	0.000	0.000
reaction time (h)	9	11	9	12	9.5	10	10	13
monomer conversion[a]	98%	98%	98%	97%	97%	96%	96%	98%
$M_{n,th}$[b] (g mol^{-1})	3,500	6,700	9,900	13,200	16,400	19,600	22,900	26,100
$M_{n,SEC}$[c] (g mol^{-1})	3,600	6,600	10,300	13,800	15,700	18,500	20,500	23,300
$Đ$[c]	1.11	1.09	1.09	1.08	1.18	1.23	1.31	1.34
L[d] (%)	99.32	98.74	98.19	97.22	96.16	94.18	92.46	87.73
Cumulative L[e] (%)	99.32	98.08	96.30	93.63	90.03	84.79	78.40	68.78

[a] Determined by ^1H NMR

[b] $M_{n,th} = [M]_0 \times p \times M_M/[CTA]_0 + M_{CTA}$, p is the monomer conversion

[c] Determined by SEC in $CHCl_3$ with PMMA used as molecular weight standards

[d] theoretical estimation of the fraction of living chains per block (e.g. extendable chain having the Z group)

[e] theoretical estimation of the cumulated fraction of living chains

Table 2.6 Experimental conditions used for the synthesis and characterization data of the icosablock copolymer: **$A_{10}B_{10}A_{10}B_{10}A_{10}B_{10}A_{10}B_{10}A_{10}B_{10}A_{10}B_{10}A_{10}B_{10}A_{10}B_{10}A_{10}B_{10}A_{10}B_{10}$** (blocks 1-10).

	$A_{10}B_{10}A_{10}B_{10}A_{10}B_{10}A_{10}B_{10}A_{10}B_{10}A_{10}B_{10}A_{10}B_{10}A_{10}B_{10}A_{10}B_{10}A_{10}B_{10}$									
	1st block	2nd block	3rd block	4th block	5th block	6th block	7th block	8th block	9th block	10th block
$[Monomer]_0$ (mol.L^{-1})	A	B	A	B	A	B	A	B	A	B
	5.90	2.95	1.97	1.42	1.13	0.94	0.80	0.69	0.61	0.54
$[CTA]_0/[ACVA]_{consumed}$	224.2	111.8	70.3	56.7	39.6	33.2	29.8	27.2	22.6	18.9
$[ACVA]_0$ (mol.L^{-1})	3.00×10^{-2}	3.80×10^{-2}	4.35×10^{-2}	5.50×10^{-2}	4.18×10^{-2}	4.10×10^{-2}	3.94×10^{-2}	3.80×10^{-2}	4.50×10^{-2}	4.50×10^{-2}
DP targeted	10	10	10	10	10	10	10	10	10	10
$m_{CTA\ added}$ (mg)	64.11	-	-	-	-	-	-	-	-	-
$m_{monomer\ added}$ (mg)	350	344.7	350	344.7	350	344.7	350	344.7	350	344.7
$m_{ACVA\ added}$ (mg)	3.83	6.22	7.64	13.66	0.00	6.70	6.67	6.94	17.21	10.12
$V_{DMF\ added}$ (mL)	0.033	0.000	0.0336	0.000	0.143	0.000	0.101	0.0745	0.020	0.0428
reaction time (h)	21.7	17	15.7	11	16.7	17	16.7	16.3	14.5	15.5
monomer conversion[a]	99%	98%	99%	97%	99%	99%	98%	97%	97%	98%
$M_{n,th}$[b] (g mol^{-1})	1,500	2,800	4,100	5,400	6,700	8,000	9,300	10,600	11,900	13,200
$M_{n,SEC}$[c] (g mol^{-1})	1,600	2,400	3,800	5,100	6,800	7,700	8,600	9,800	11,100	12,500
$Đ$[c]	1.14	1.15	1.16	1.15	1.13	1.16	1.17	1.20	1.23	1.26
L[d] (%)	99.56	99.11	98.60	98.27	97.53	97.08	96.57	96.46	95.77	94.98
Cumulative L[e] (%)	99.56	98.67	97.29	95.60	93.25	90.52	87.58	84.47	80.90	76.84

[a] Determined by ^{1}H NMR

[b] $M_{n,th} = [M]_0 \times p \times M_M/[CTA]_0 + M_{CTA}$, p is the monomer conversion

[c] Determined by SEC in $CHCl_3$ with PMMA used as molecular weight standards

[d] theoretical estimation of the fraction of living chains per block (e.g. extendable chain having the Z group)

[e] theoretical estimation of the cumulated fraction of living chains

Table 2.7 Experimental conditions used for the synthesis and characterization data of the icosablock copolymer: **$A_{10}B_{10}A_{10}B_{10}A_{10}B_{10}A_{10}B_{10}A_{10}B_{10}A_{10}B_{10}A_{10}B_{10}A_{10}B_{10}A_{10}B_{10}A_{10}B_{10}$** (blocks 11-20).

	$A_{10}B_{10}A_{10}B_{10}A_{10}B_{10}A_{10}B_{10}A_{10}B_{10}A_{10}B_{10}A_{10}B_{10}A_{10}B_{10}A_{10}B_{10}A_{10}B_{10}$									
	11th block	12th block	13th block	14th block	15th block	16th block	17th block	18th block	19th block	20th block
$[Monomer]_0$ ($mol.L^{-1}$)	A	B	A	B	A	B	A	B	A	B
	0.49	0.44	0.41	0.38	0.35	0.33	0.30	0.29	0.27	0.25
$[CTA]_0/[ACVA]_{consumed}$	17.3	15.6	13.8	11.4	10.9	10.7	9.2	8.7	7.8	7.23
$[ACVA]_0$ ($mol.L^{-1}$)	4.30×10^{-2}	4.57×10^{-2}	4.70×10^{-2}	4.60×10^{-2}	4.86×10^{-2}	4.95×10^{-2}	5.00×10^{-2}	5.05×10^{-2}	5.30×10^{-2}	5.35×10^{-2}
DP targeted	10	10	10	10	10	10	10	10	10	10
$m_{CTA\ added}$ (mg)	-	-	-	-	-	-	-	-	-	-
$m_{monomer\ added}$ (mg)	350	344.7	350	344.7	350	344.7	350	344.7	350	344.7
$m_{ACVA\ added}$ (mg)	7.68	15.57	14.29	10.70	19.14	16.67	16.06	17.46	24.47	20.41
$V_{DMF\ added}$ (mL)	0.1153	0.0004	0.0612	0.0491	0.0006	0.000	0.000	0.0001	0.0281	0.0206
reaction time (h)	16	15.2	15.3	17.5	16.2	15	16.2	16	16	16
monomer conversion[a]	98%	96%	97%	97%	97%	98%	98%	97%	98%	97%
$M_{n,th}$[b] (g mol^{-1})	14,500	15,700	17,000	18,300	19,600	20,900	22,200	23,500	24,800	26,100
$M_{n,SEC}$[c] (g mol^{-1})	13,700	14,900	16,200	17,000	18,400	20,200	20,500	20,700	21,200	21,200
$Đ$[c]	1.27	1.28	1.29	1.38	1.43	1.43	1.47	1.53	1.53	1.67
L[d] (%)	94.55	93.97	93.25	91.96	91.56	91.45	90.22	89.65	88.57	87.84
Cumulative L[e] (%)	72.65	68.27	63.66	58.54	53.60	49.01	44.22	39.65	35.11	30.84

[a] Determined by ^1H NMR

[b] $M_{n,th} = [M]_0 \times p \times M_M/[CTA]_0 + M_{CTA}$, p is the monomer conversion

[c] Determined by SEC in $CHCl_3$ with PMMA used as molecular weight standards

[d] theoretical estimation of the fraction of living chains per block (e.g. extendable chain having the Z group)

[e] theoretical estimation of the cumulated fraction of living chains

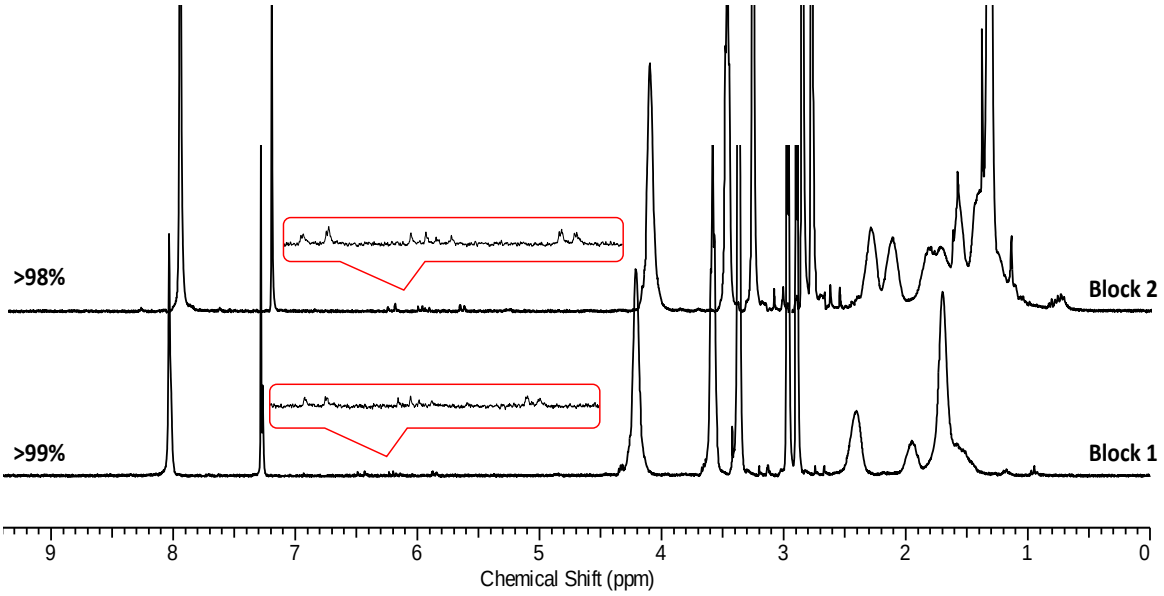

Figure 2.10 ^{1}H NMR spectrum ($CDCl_3$, 300 MHz) of: $\mathbf{A_{100}B_{100}}$ showing the monomer conversion for each block after iterative RAFT polymerization.

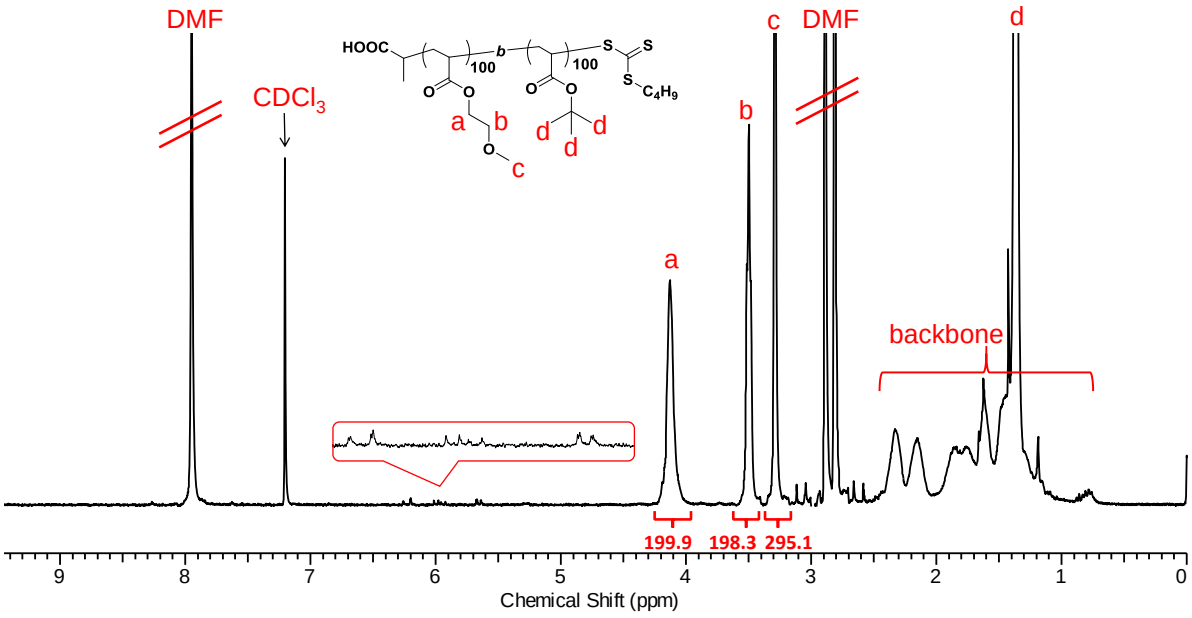

Figure 2.11 Detailed structural assignment of $\mathbf{A_{100}B_{100}}$.

^{1}H NMR (300 MHz, $CDCl_3$, ppm): δ = 4.20 (*s*, –(C=O)–O–C***H*****$_2$**–CH_2–O–CH_3), 3.56 (*s*, –(C=O)–O–CH_2–C***H*****$_2$**–O–CH_3), 3.36 (*s*, –(C=O)–O–CH_2–CH_2–O–C***H*****$_3$**), 1.43 (*s*, –(C=O)–O–C(C***H*****$_3$)$_3$**, 2.73-0.83 (*m*, CH and CH_2 backbone, CH_3 R-group, CH_2 Z-group, CH_3 Z-group).

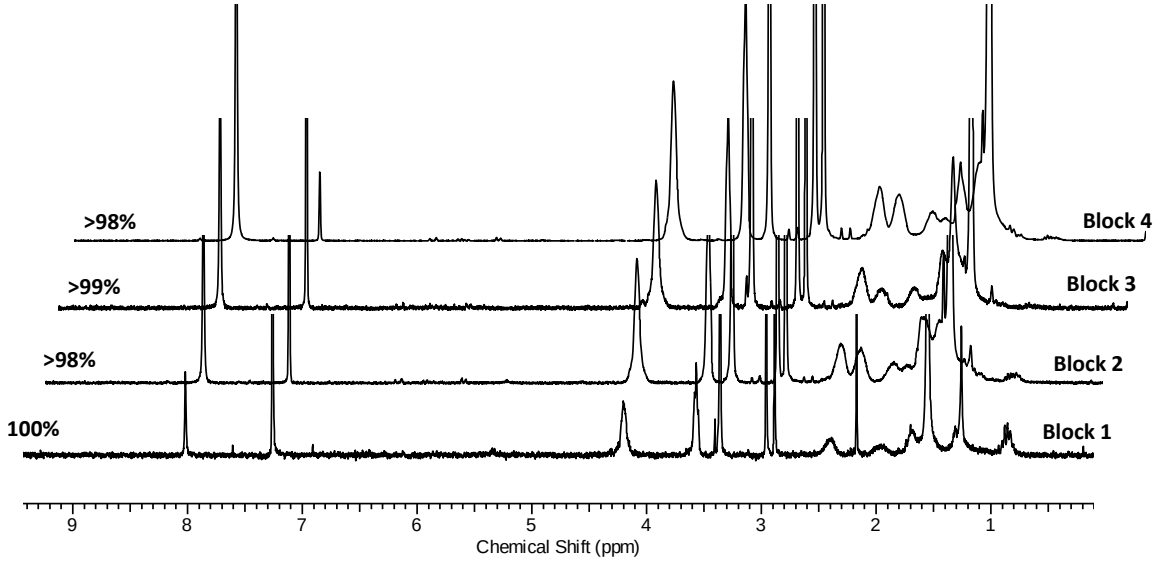

Figure 2.12 ^{1}H NMR spectrum ($CDCl_3$, 300 MHz) of $\mathbf{A_{50}B_{50}A_{50}B_{50}}$ showing the monomer conversion for each block after iterative RAFT polymerization.

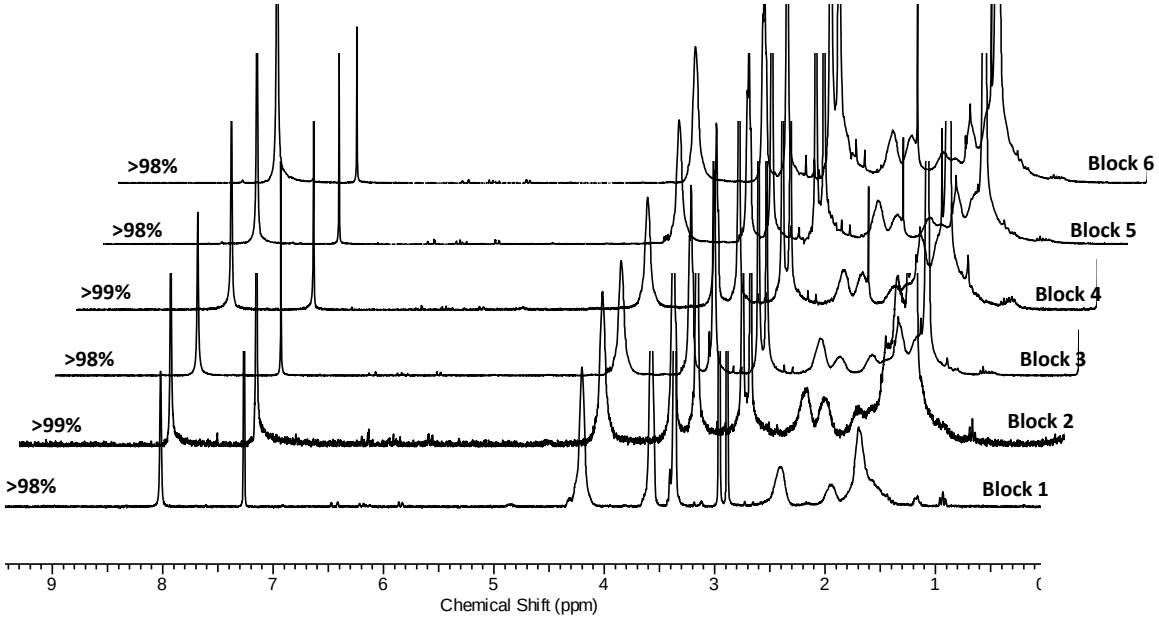

Figure 2.13 ^{1}H NMR spectrum ($CDCl_3$, 300 MHz) of $\mathbf{A_{33}B_{33}A_{33}B_{33}A_{33}B_{33}}$ showing the monomer conversion for each block after iterative RAFT polymerization.

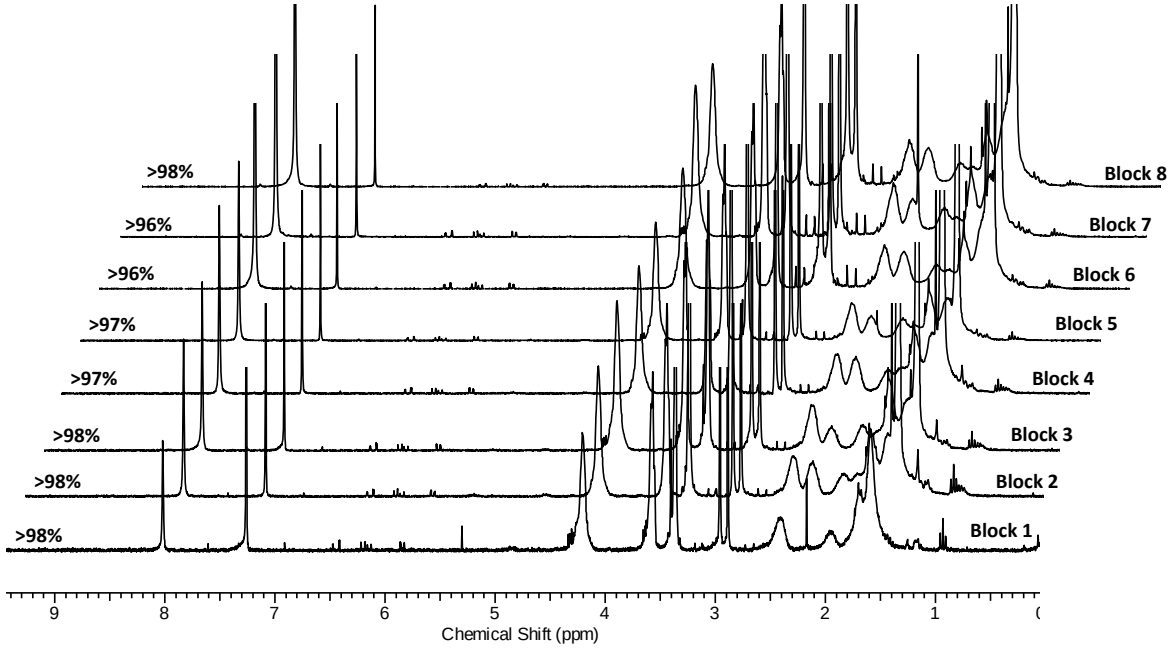

Figure 2.14 ^{1}H NMR spectrum ($CDCl_3$, 300 MHz) of $\mathbf{A_{25}B_{25}A_{25}B_{25}A_{25}B_{25}A_{25}B_{25}}$ showing the monomer conversion for each block after iterative RAFT polymerization.

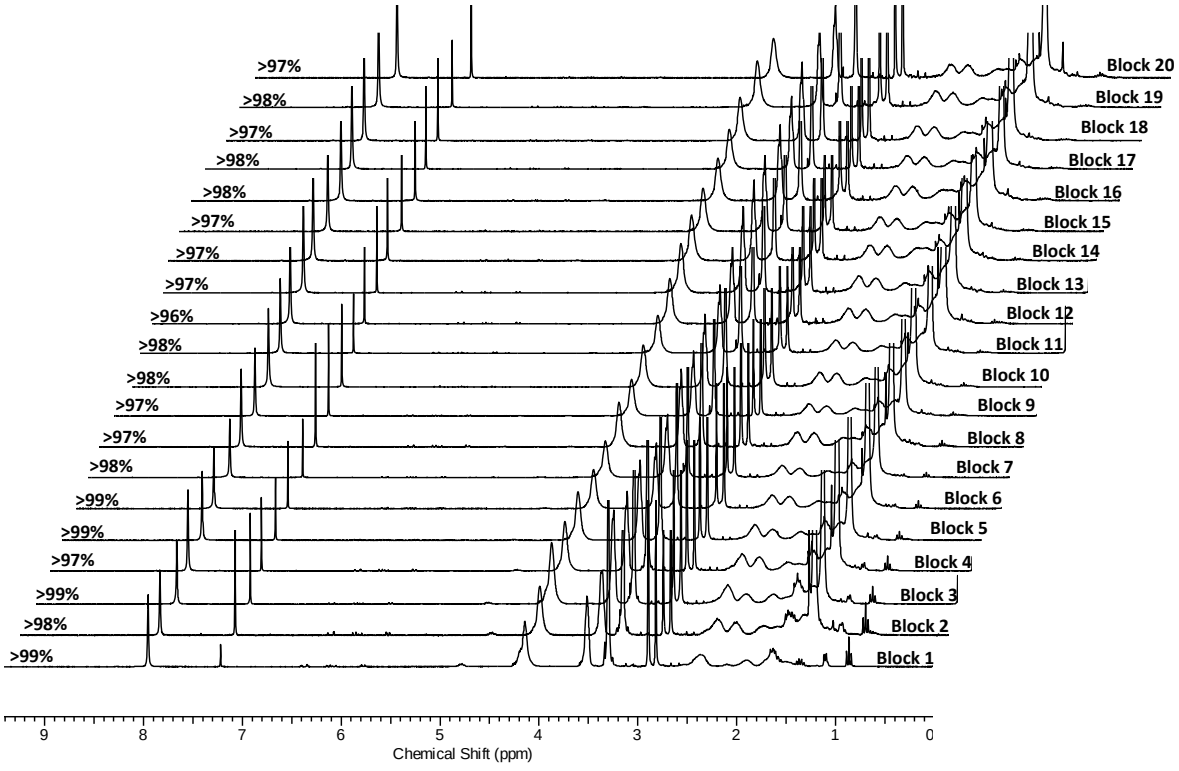

Figure 2.15 ^{1}H NMR spectrum ($CDCl_3$, 300 MHz) of $\mathbf{A_{10}B_{10}A_{10}B_{10}A_{10}B_{10}A_{10}B_{10}A_{10}B_{10}A_{10}B_{10}A_{10}B_{10}A_{10}B_{10}A_{10}B_{10}A_{10}B_{10}}$ showing the monomer conversion for each block after iterative RAFT polymerization.

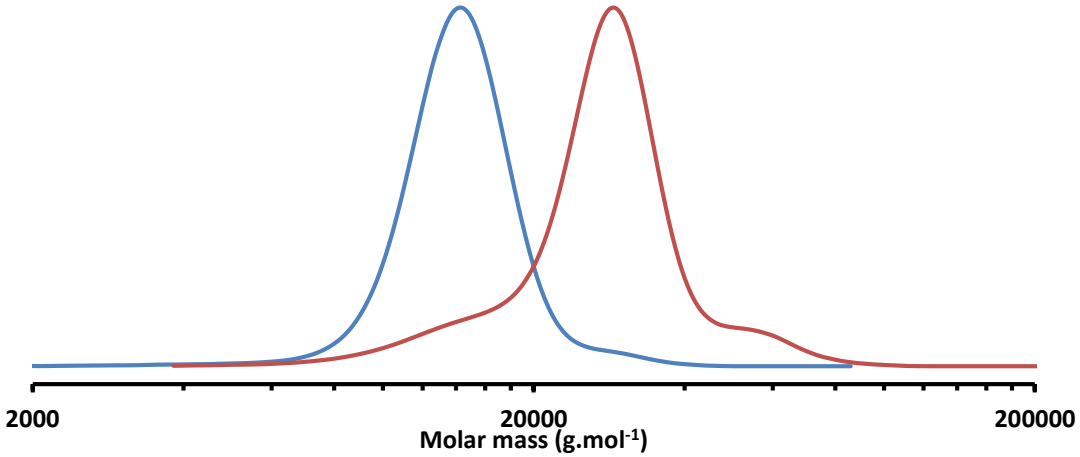

Figure 2.16 Molecular weight distributions for successive block extensions of the diblock copolymer (BCP^{di}:**A$_{100}$B$_{100}$**, SEC RI traces in $CHCl_3$).

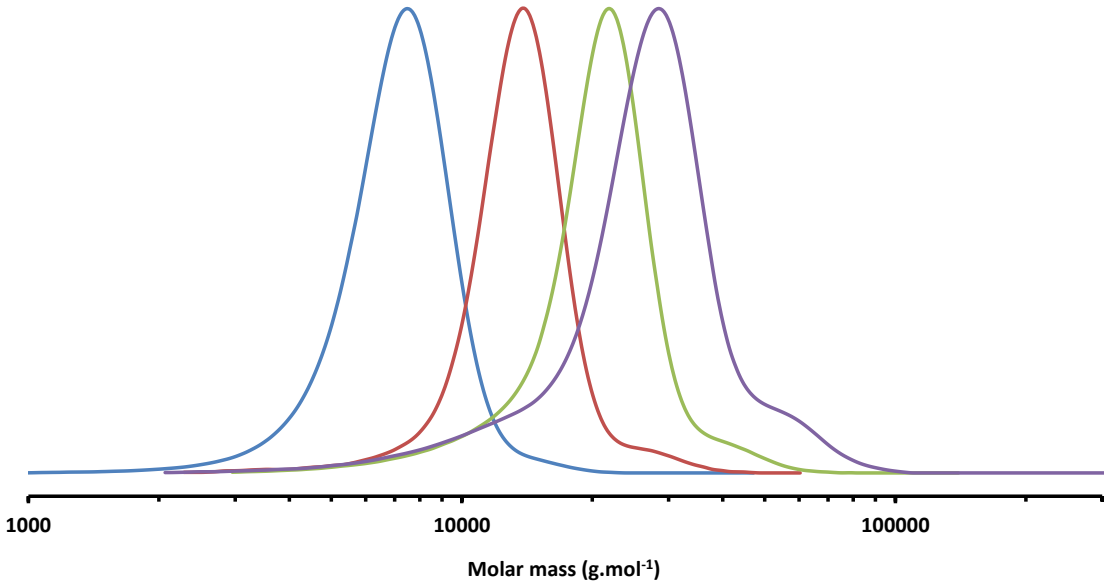

Figure 2.17 Molecular weight distributions for successive block extensions of the tetrablock copolymer (BCP^{tetra}:**A$_{50}$B$_{50}$A$_{50}$B$_{50}$**, SEC RI traces in $CHCl_3$).

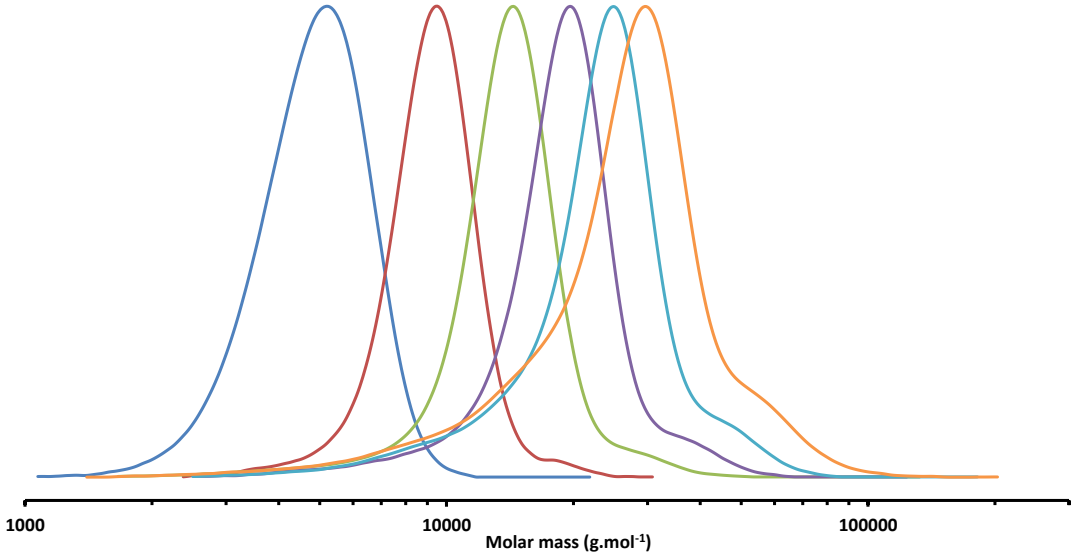

Figure 2.18 Molecular weight distributions for successive block extensions of the hexablock copolymer (BCP^{hexa}:**A$_{33}$B$_{33}$A$_{33}$B$_{33}$ A$_{33}$B$_{33}$**, SEC RI traces in $CHCl_3$).

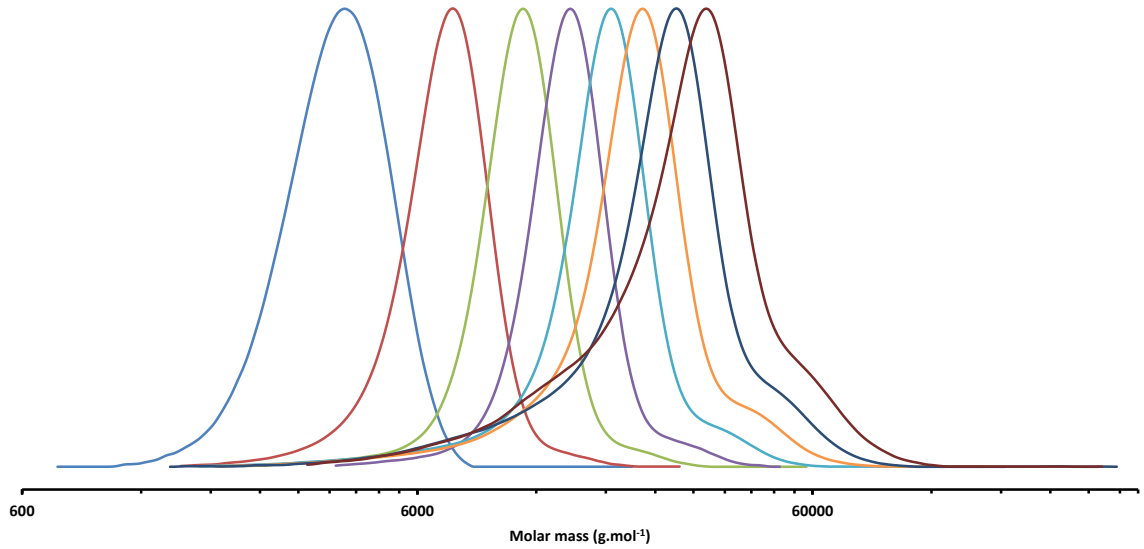

Figure 2.19 Molecular weight distributions for successive block extensions of the octablock copolymer (BCP^{octa}:**A$_{25}$B$_{25}$A$_{25}$B$_{25}$A$_{25}$B$_{25}$A$_{25}$B$_{25}$**, SEC RI traces in $CHCl_3$).

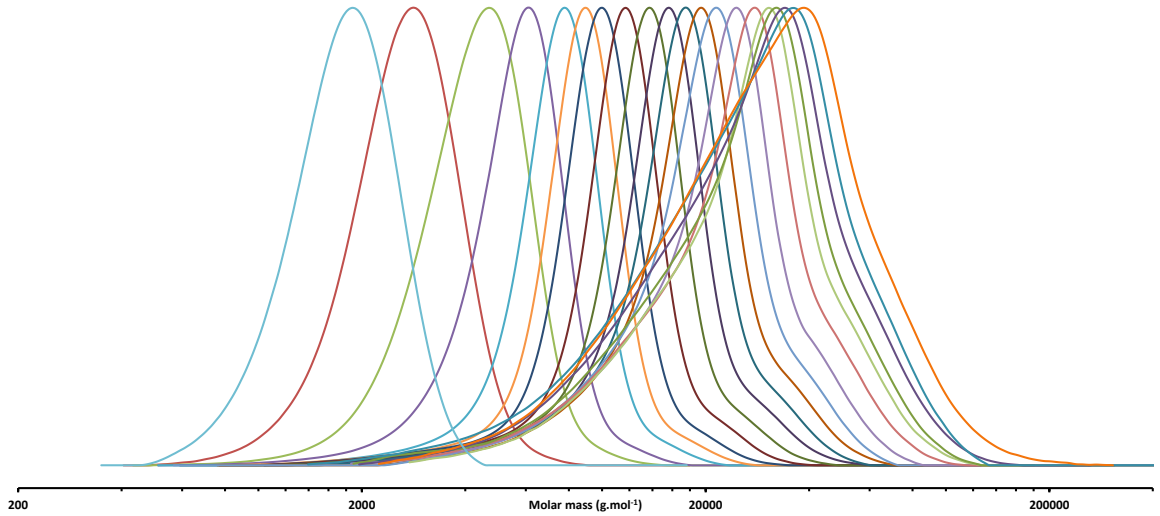

Figure 2.20 Molecular weight distributions for successive block extensions of the icosablock copolymer (BCP^{icosa}:**A$_{10}$B$_{10}$A$_{10}$B$_{10}$A$_{10}$B$_{10}$A$_{10}$B$_{10}$A$_{10}$B$_{10}$A$_{10}$B$_{10}$A$_{10}$B$_{10}$A$_{10}$B$_{10}$A$_{10}$B$_{10}$A$_{10}$B$_{10}$**, SEC RI traces in $CHCl_3$).

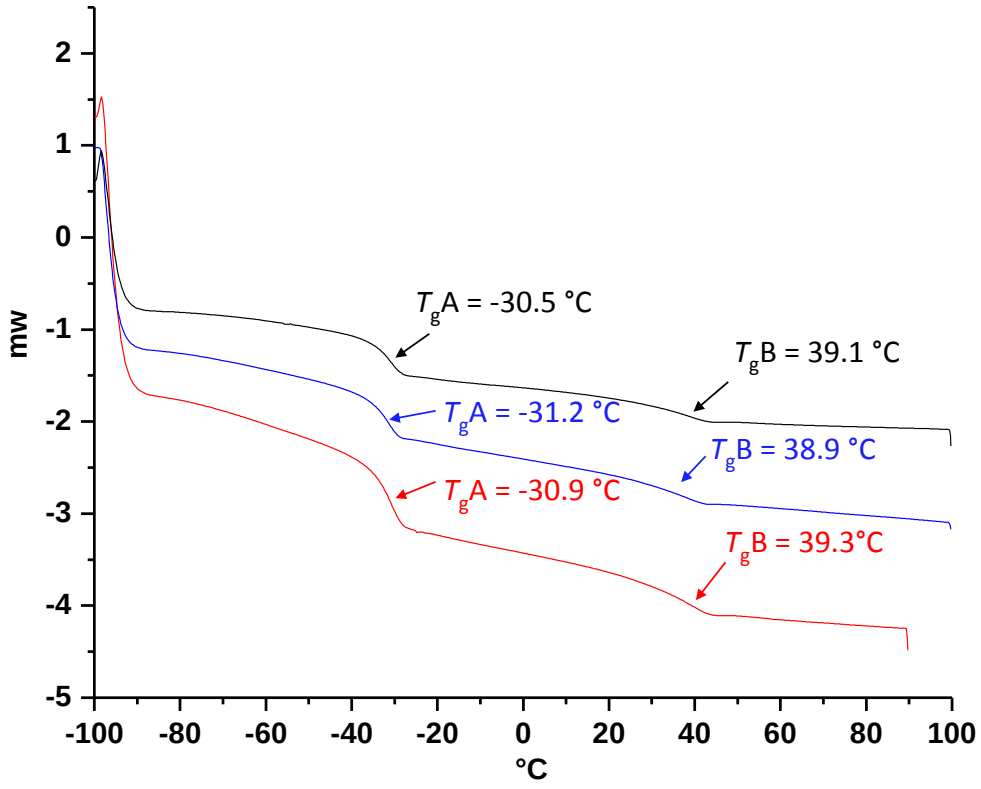

Figure 2.21 DSC curves of the diblock copolymer **A$_{100}$B$_{100}$**.

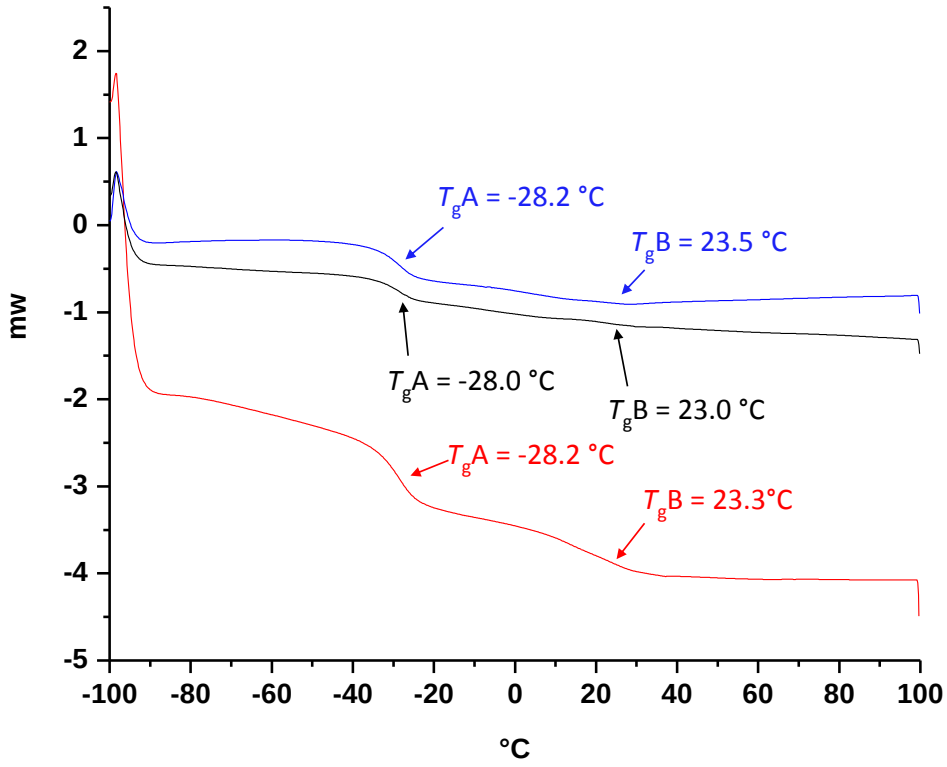

Figure 2.22 DSC curves of the tetrablock copolymer **$A_{50}B_{50}A_{50}B_{50}$**.

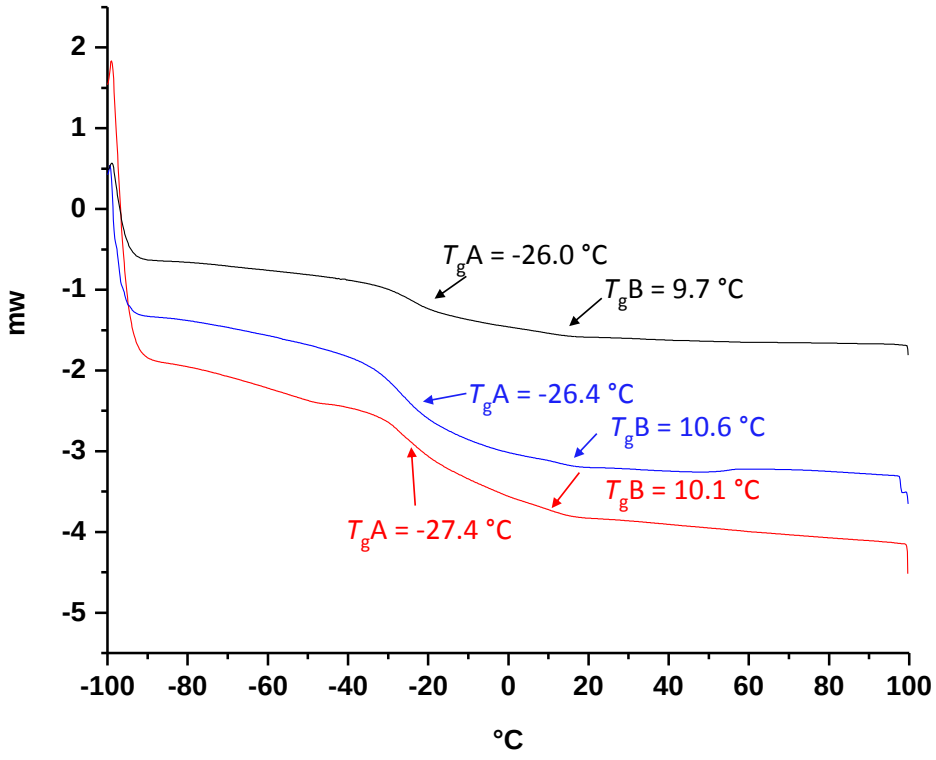

Figure 2.23 DSC curves of the hexablock copolymer **$A_{33}B_{33}A_{33}B_{33}A_{33}B_{33}$**.

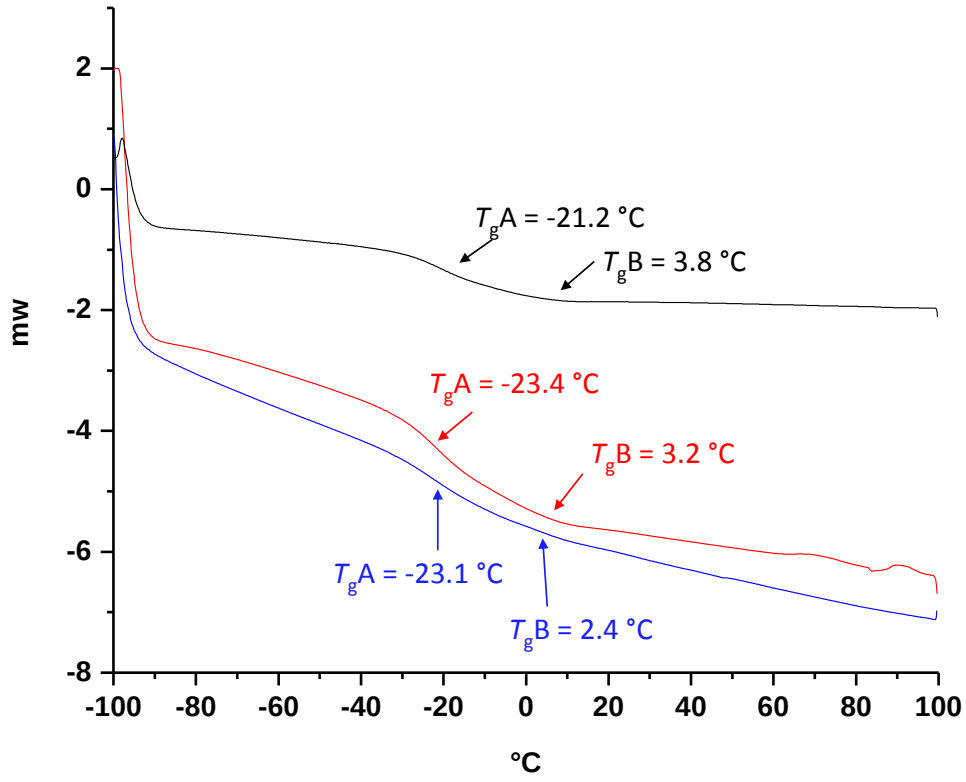

Figure 2.24 DSC curves of the octablock copolymer $\mathbf{A_{25}B_{25}A_{25}B_{25}A_{25}B_{25}A_{25}B_{25}}$.

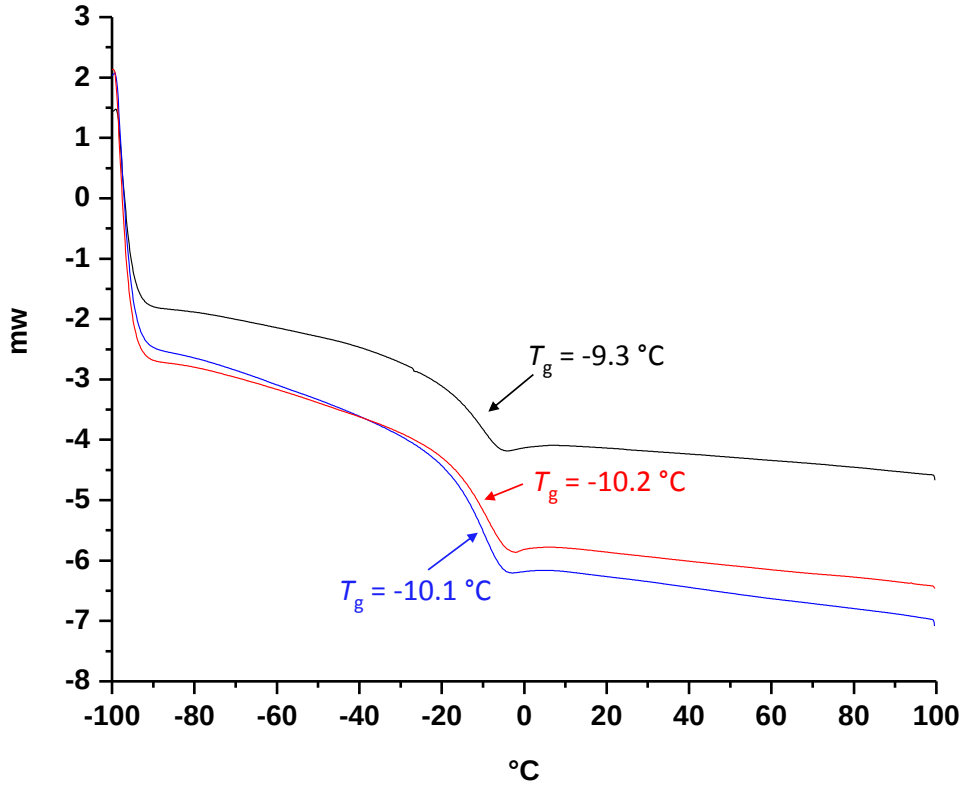

Figure 2.25 DSC curves of the icosablock copolymer $\mathbf{A_{10}B_{10}A_{10}B_{10}A_{10}B_{10}A_{10}B_{10}A_{10}B_{10}A_{10}B_{10}A_{10}B_{10}A_{10}B_{10}A_{10}B_{10}}$.

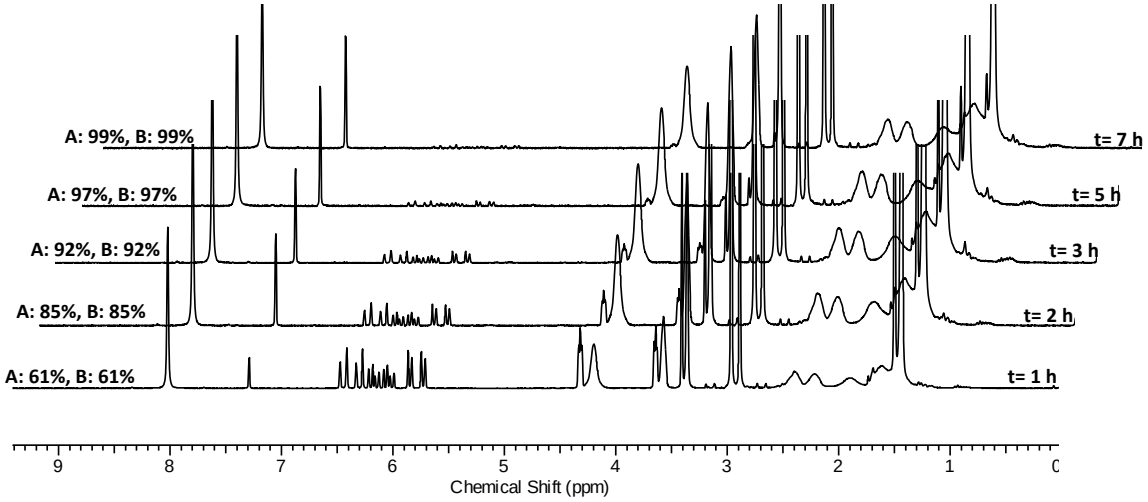

Figure 2.26 ^{1}H NMR of the random copolymer synthesis (samples taken at different time to check the conversions of the two monomers EGMEA and tBA).

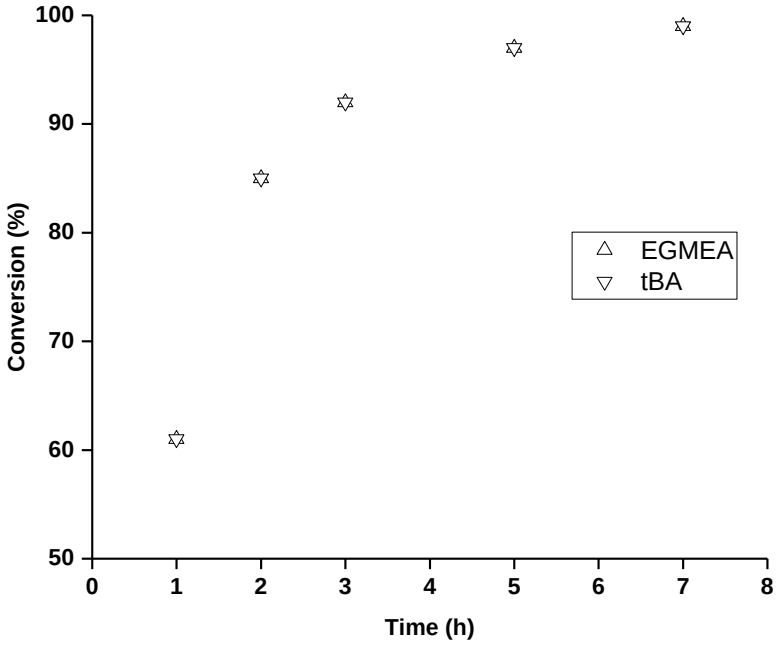

Figure 2.27 Kinetics study (samples taken at different time to check the conversions of the two monomers EGMEA and tBA) of the random copolymer synthesis determined by ^{1}H NMR.

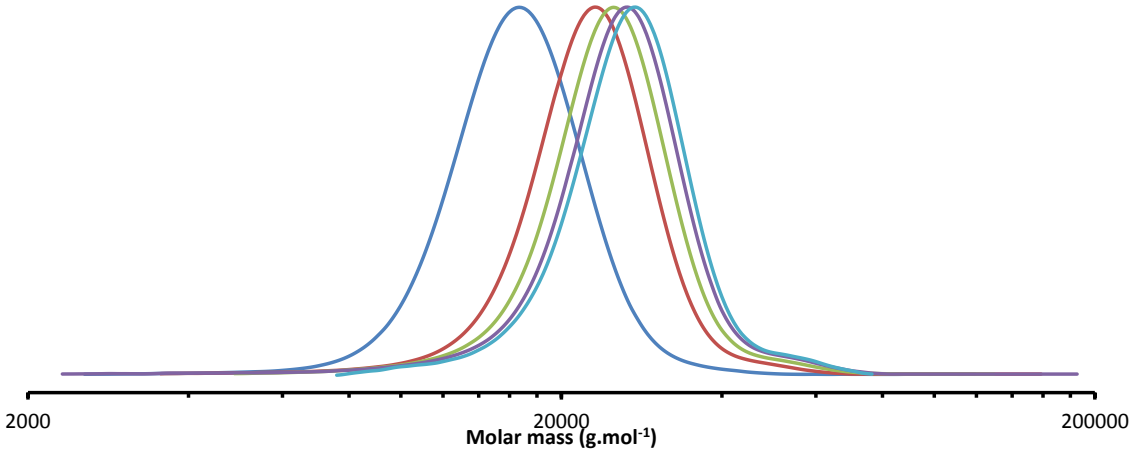

Figure 2.28 Molecular weight distributions for the kinetics (samples taken at different time) of the random copolymer synthesis (SEC RI traces in $CHCl_3$).

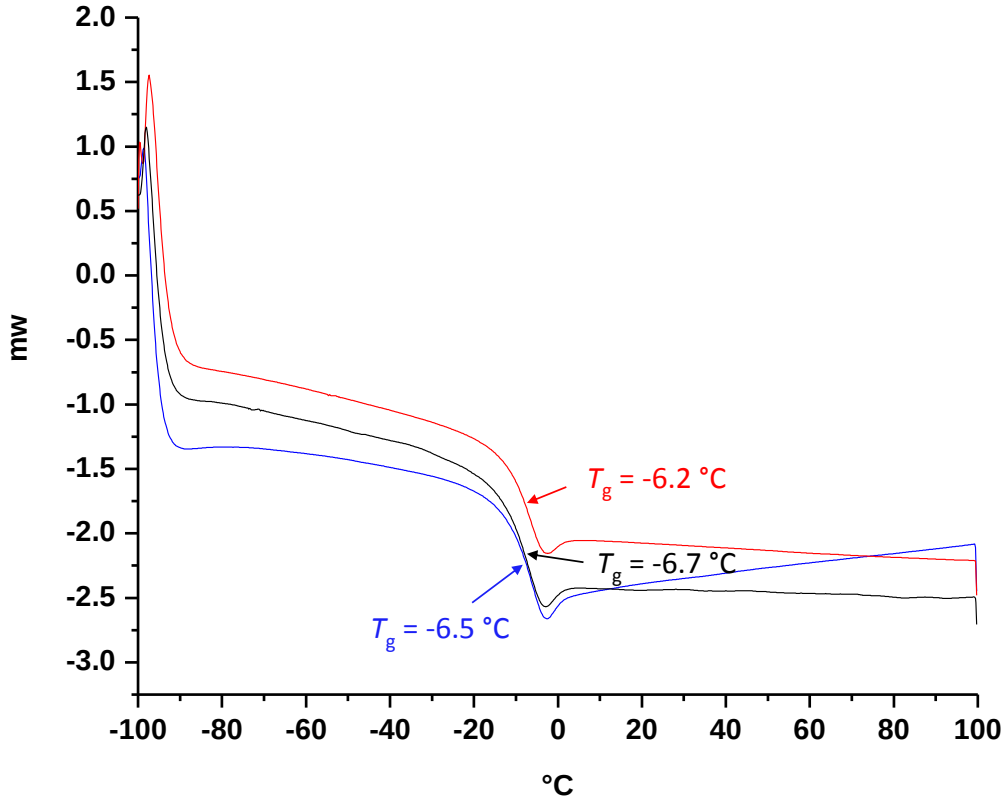

Figure 2.29 DSC curves of the random copolymer **A_{100}-*ran*-B_{100}**.

Table 2.8 Experimental conditions used for the synthesis and characterization data of the homopolymers.

	Homopolymer						
	A_{200}[e]	**B_{200}**	**B_{100}**	**B_{50}**	**B_{33}**	**B_{25}**	**B_{10}**
$[Monomer]_0$ ($mol.L^{-1}$)	A	B	B	B	B	B	B
	5.50	5.50	3.0	4.19	5.11	5.10	5.00
$[CTA]_0/[ACVA]_{consumed}$	21.01	16.81	10.21	38.9	92.02	109.44	161.85
$[ACVA]_0$ ($mol.L^{-1}$)	2.00×10^{-2}	2.50×10^{-2}	2.00×10^{-1}	6.90×10^{-2}	4.50×10^{-2}	4.50×10^{-2}	4.00×10^{-2}
DP targeted	200	200	100	50	33	25	10
$m_{CTA\ added}$ (mg)	7.33	7.44	9.06	18.60	33.82	44.64	74.40
$m_{monomer\ added}$ (mg)	800	800	487	500	600	600	400
$m_{ACVA\ added}$ (mg)	6.27	7.95	71.00	18.02	11.57	11.58	7.00
$V_{DMF\ added}$ (mL)	0.118	0.062	0.000	0.000	0.000	0.001	0.0271
reaction time (h)	16	16	3.5	7.5	9	10	19
monomer conversion[a]	99%	99%	98%	99%	97%	97%	97%
$M_{n,th}$[b] ($g\ mol^{-1}$)	26,300	25,900	13,100	6,600	4,500	3,400	1,500
$M_{n,SEC}$[c] ($g\ mol^{-1}$)	24,700	24,500	12,900	6,400	4,000	3,200	1,200
$Đ$[c]	1.11	1.09	1.09	1.09	1.09	1.09	1.12
L[d] (%)	95.46	94.38	91.08	97.49	98.92	99.09	99.39

[a] Determined by ^1H NMR

[b] $M_{n,th} = [M]_0 \times p \times M_M/[CTA]_0 + M_{CTA}$, p is the monomer conversion

[c] Determined by SEC in $CHCl_3$ with PMMA used as molecular weight standards

[d] theoretical estimation of the fraction of living chains per block (e.g. extendable chain having the Z group)

[e] **A_{100}, A_{50}, A_{33}, A_{25}** and **A_{10}** were synthesized using the same conditions with the synthesis of MBCPs.

Table 2.9 Characterization of the Homopolymers, Polymer Blends and Diblock Copolymers by ^{1}H NMR, $CHCl_3$-SEC and DSC.

Sample	$M_{n,th}$[c] g mol^{-1}	$M_{n,SEC}$[d] g mol^{-1}	$Đ$[d]	P(A) T_g[e] °C	P(B) T_g[e] °C
A_{100}[a]	13,300	14,200	1.08	-33.1±0.2	-
B_{100}[b]	13,100	12,900	1.09	-	44.7±0.5
A_{50}	6,700	7,000	1.07	-34.0±0.2	-
B_{50}	6,600	6,400	1.09	-	40.4±0.4
A_{33}	4,500	4,500	1.11	-35.1±0.3	-
B_{33}	4,500	4,000	1.09	-	36.3±0.4
A_{25}	3,500	3,600	1.11	-36.0±0.3	-
B_{25}	3,400	3,200	1.09	-	33.0±0.3
A_{10}	1,500	1,600	1.14	-39.6±0.6	-
B_{10}	1,500	1,200	1.12	-	13.0±0.4
A_{100}, B_{100} polymer blend	-	-	-	-34.1±0.7	41.3±1.3
A_{50}, B_{50} polymer blend	-	-	-	-35.4±0.3	37.2±0.2
A_{33}, B_{33} polymer blend	-	-	-	-35.3±0.5	32.6±0.2
A_{25}, B_{25} polymer blend	-	-	-	-36.7±0.3	28.0±0.4
A_{10}, B_{10} polymer blend	-	-	-	-36.4±0.4	-2.5±0.5
$A_{50}B_{50}$	13,200	12,800	1.10	-29.9±0.3	25.4±0.2
$A_{33}B_{33}$	8,800	8,800	1.08	-29.2±0.6	11.5±0.3
$A_{25}B_{25}$	6,700	6,600	1.09	-28.1±0.5	4.7±0.2
$A_{10}B_{10}$	2,800	2,400	1.15	-17.5±0.7	

[a] A represents the monomer of EGMEA

[b] B represents the monomer of tBA

[c] $M_{n,th} = [M]_0 \times p \times M_M/[CTA]_0 + M_{CTA}$, p is the monomer conversion

[d] Determined by SEC in $CHCl_3$ with PMMA used as molecular weight standards

[e] Data represent mean ± SD (n = 3).

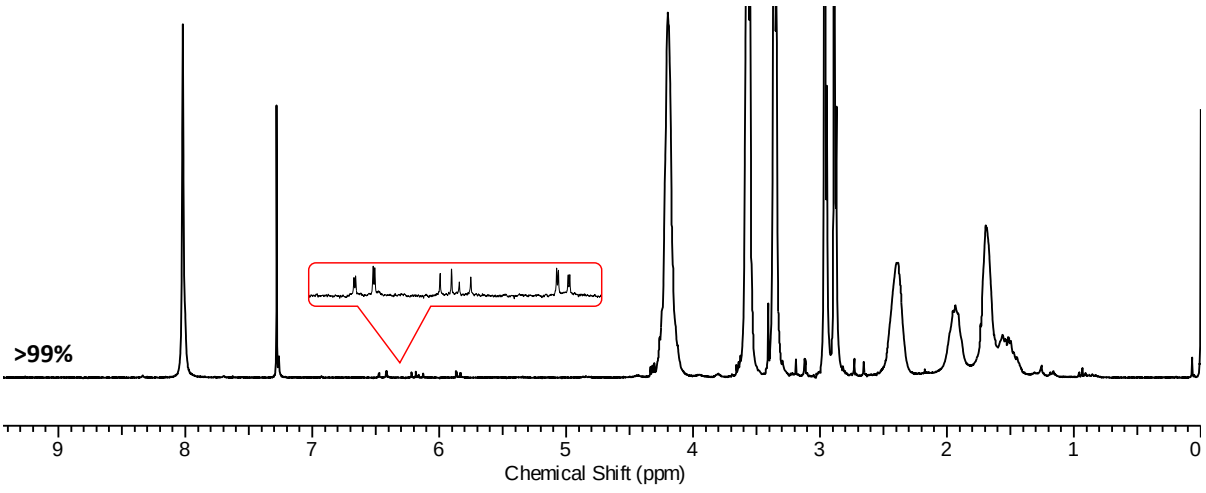

Figure 2.30 ^{1}H NMR spectrum ($CDCl_3$, 300 MHz) of $\mathbf{A_{200}}$ after RAFT polymerization.

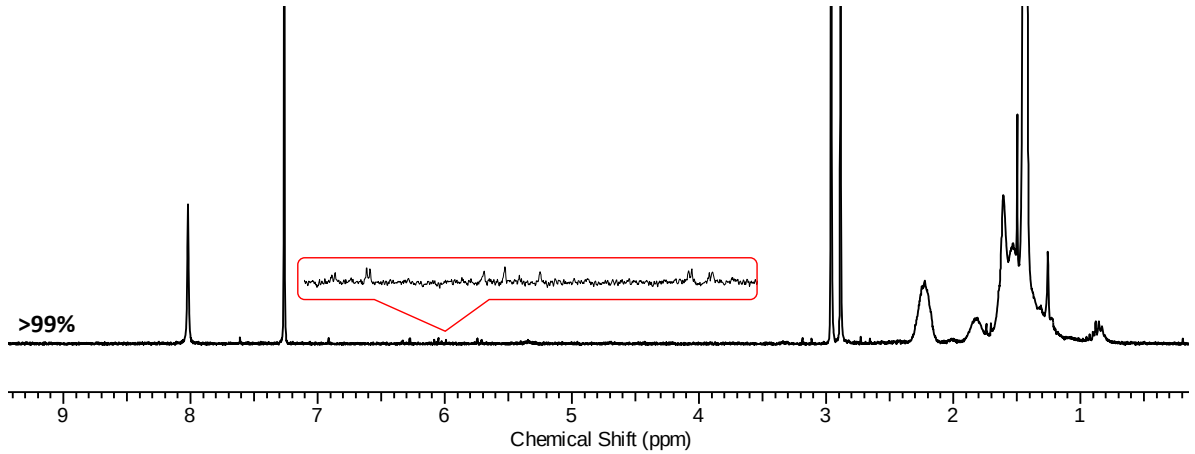

Figure 2.31 ^{1}H NMR spectrum ($CDCl_3$, 300 MHz) of $\mathbf{B_{200}}$ after RAFT polymerization.

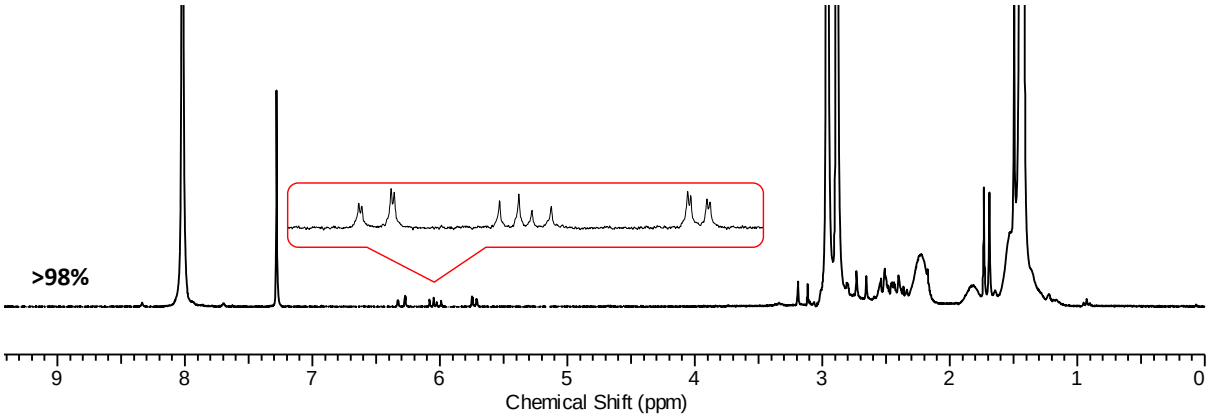

Figure 2.32 ^{1}H NMR spectrum ($CDCl_3$, 300 MHz) of $\mathbf{B_{100}}$ after RAFT polymerization.

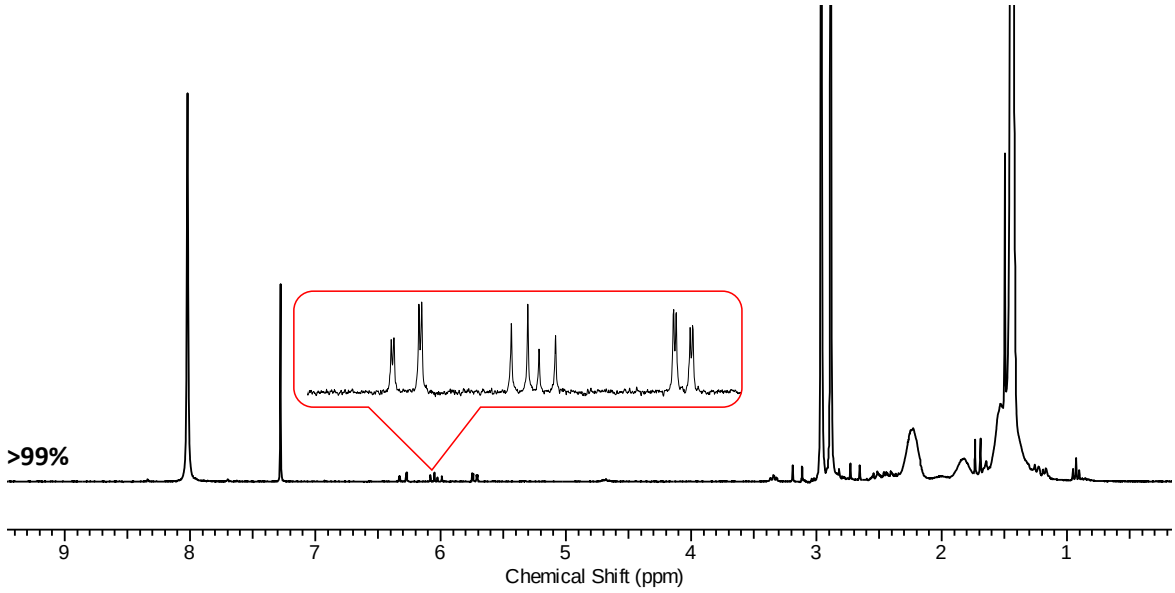

Figure 2.33 ^{1}H NMR spectrum ($CDCl_3$, 300 MHz) of $\mathbf{B_{50}}$ after RAFT polymerization.

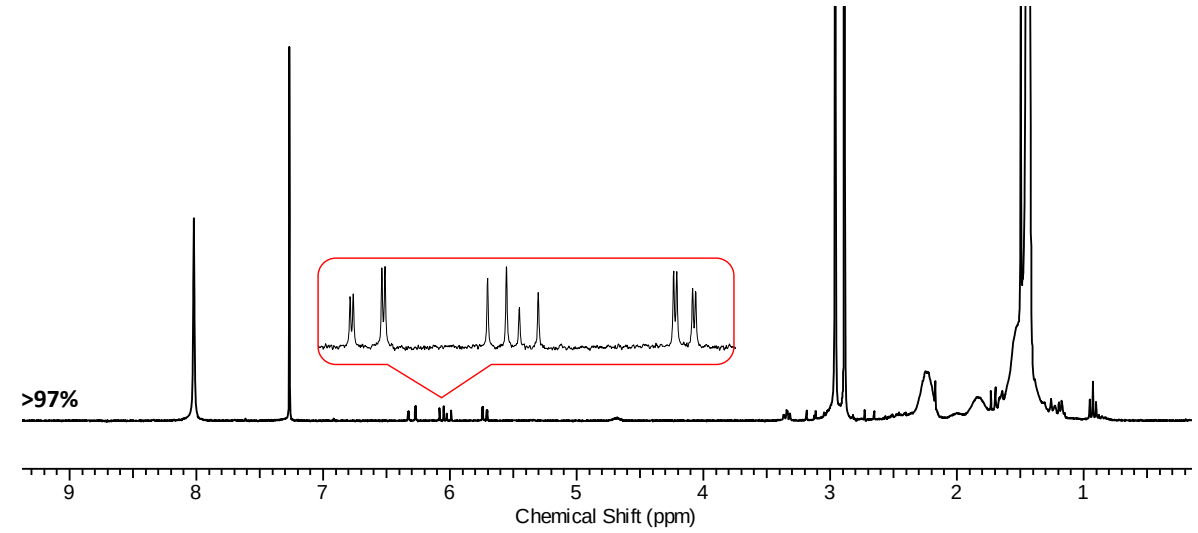

Figure 2.34 ^{1}H NMR spectrum ($CDCl_3$, 300 MHz) of $\mathbf{B_{33}}$ after RAFT polymerization.

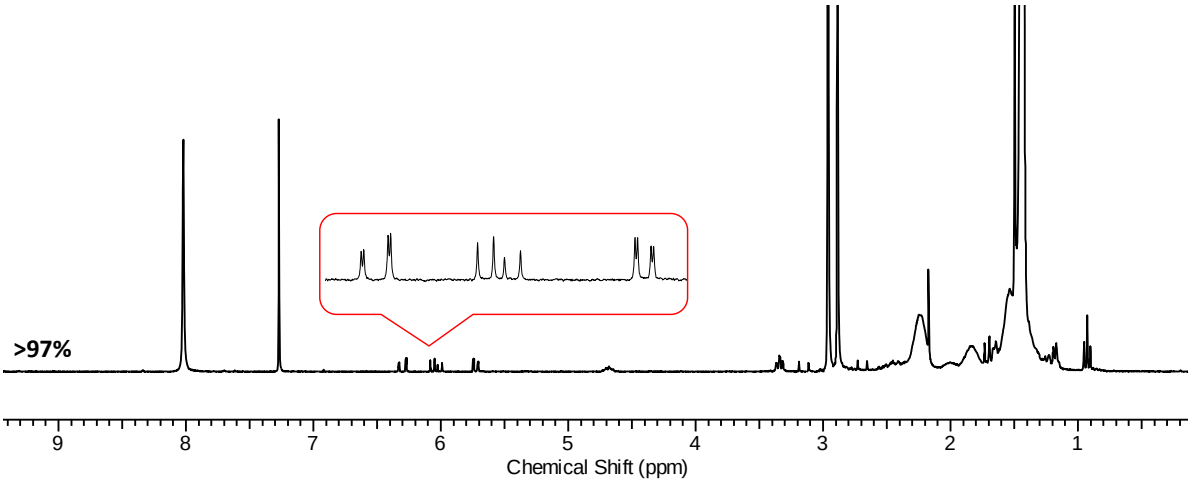

Figure 2.35 ^{1}H NMR spectrum ($CDCl_3$, 300 MHz) of $\mathbf{B_{25}}$ after RAFT polymerization.

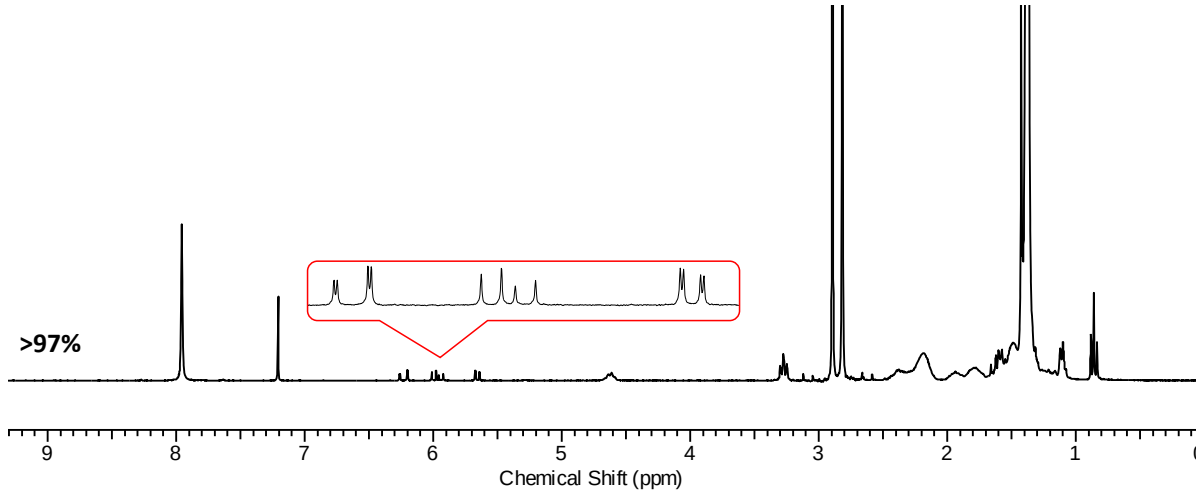

Figure 2.36 ^{1}H NMR spectrum ($CDCl_3$, 300 MHz) of $\mathbf{B_{10}}$ after RAFT polymerization.

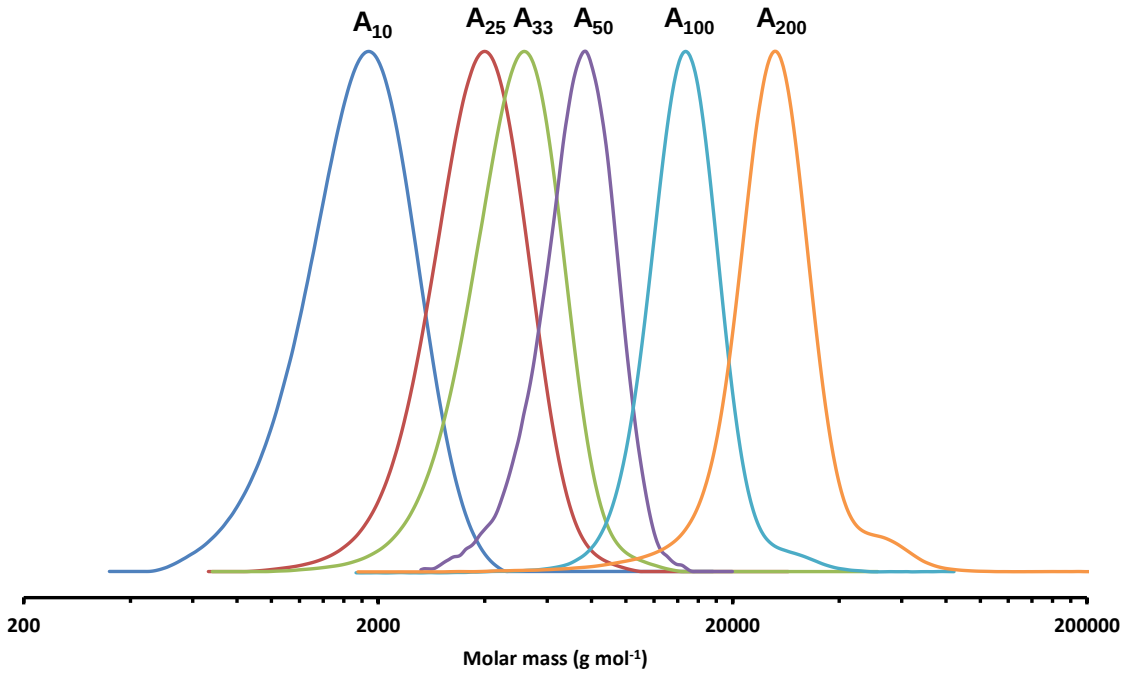

Figure 2.37 Molecular weight distributions for homopolymers: **A**$_{10}$, **A**$_{25}$, **A**$_{33}$, **A**$_{50}$, **A**$_{100}$, and **A**$_{200}$ (SEC RI traces in $CHCl_3$).

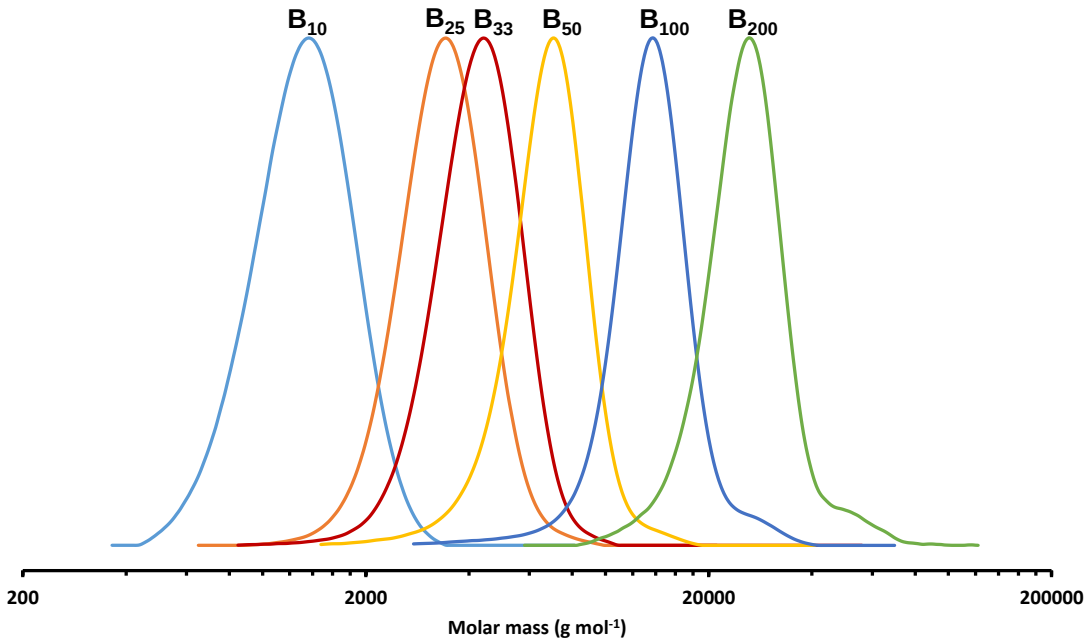

Figure 2.38 Molecular weight distributions for homopolymers: **B**$_{10}$, **B** $_{25}$, **B** $_{33}$, **B** $_{50}$, **B** $_{100}$, and **B** $_{200}$ (SEC RI traces in $CHCl_3$).

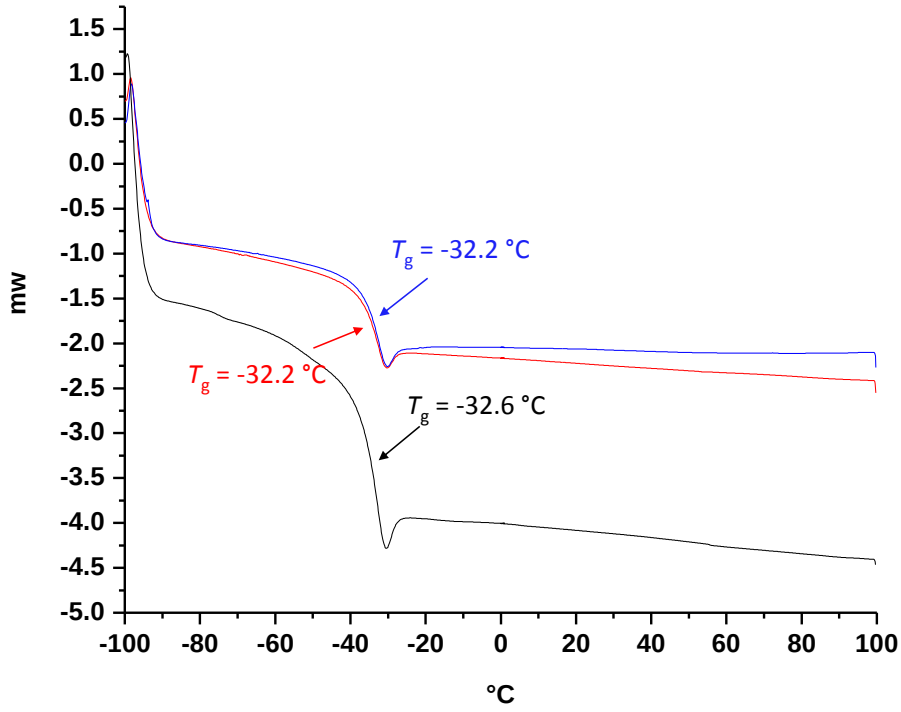

Figure 2.39 DSC curves of the homopolymer **A_{200}**.

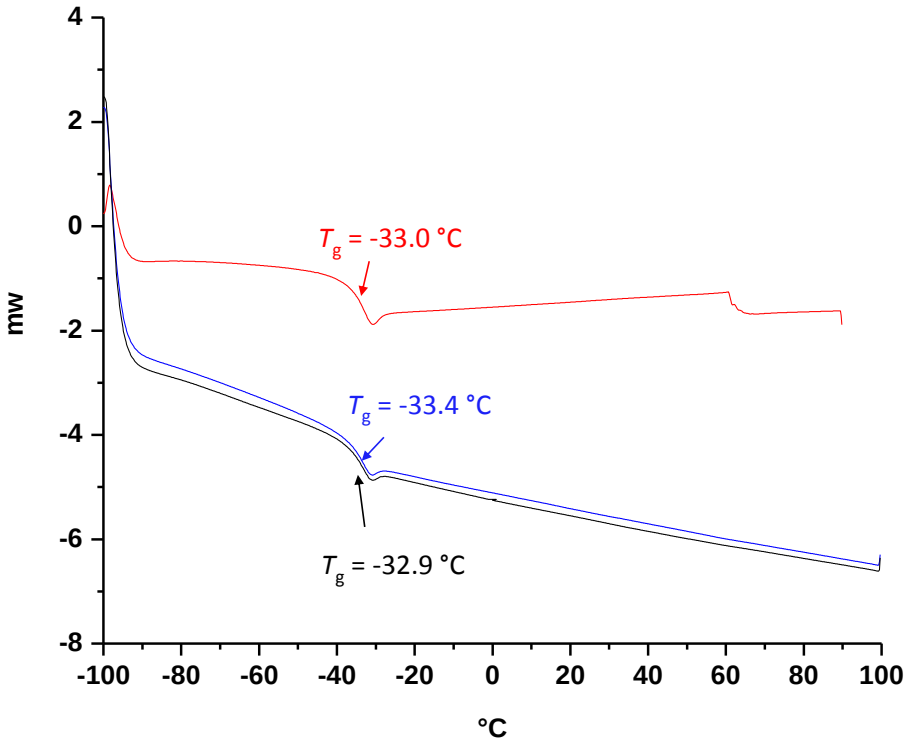

Figure 2.40 DSC curves of the homopolymer **A_{100}**.

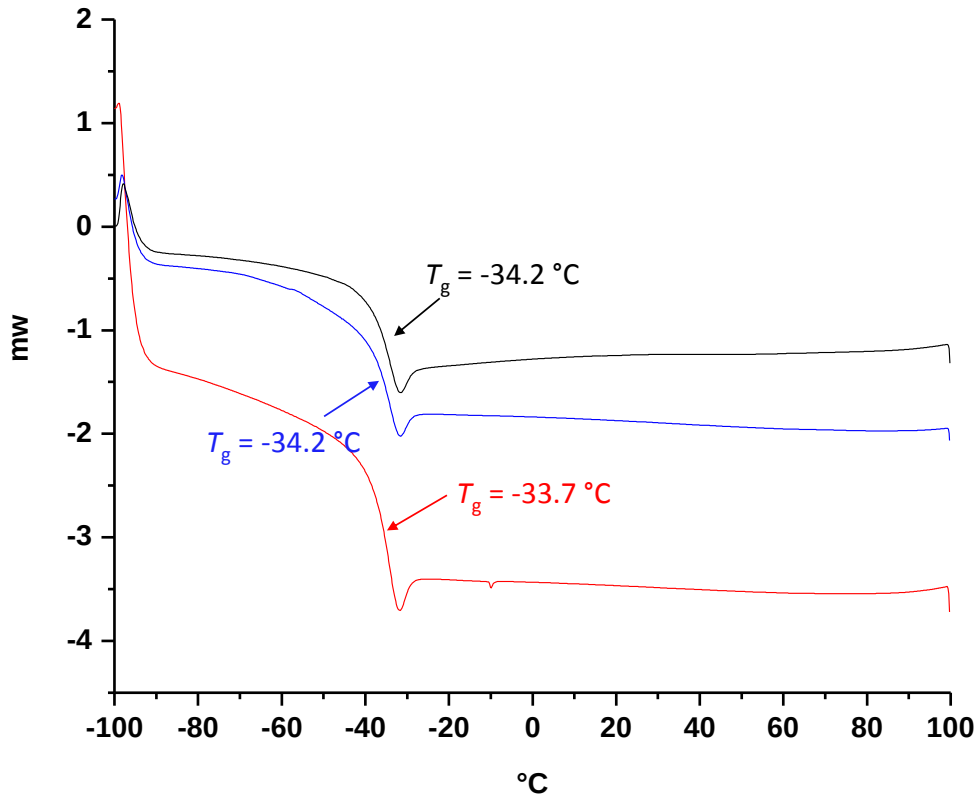

Figure 2.41 DSC curves of the homopolymer **A_{50}**.

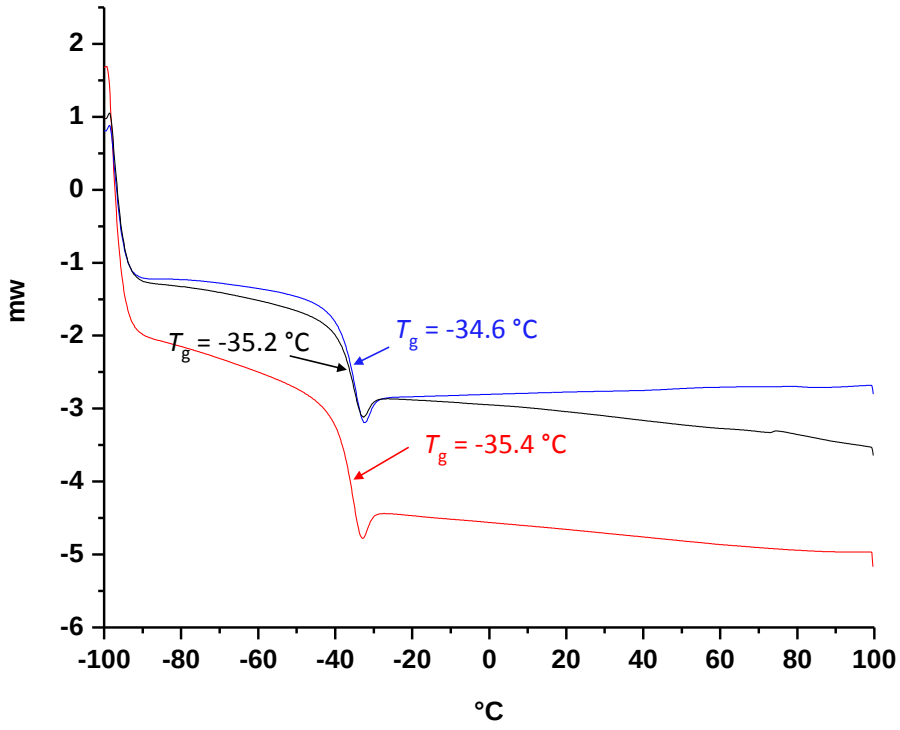

Figure 2.42 DSC curves of the homopolymer **A_{33}**.

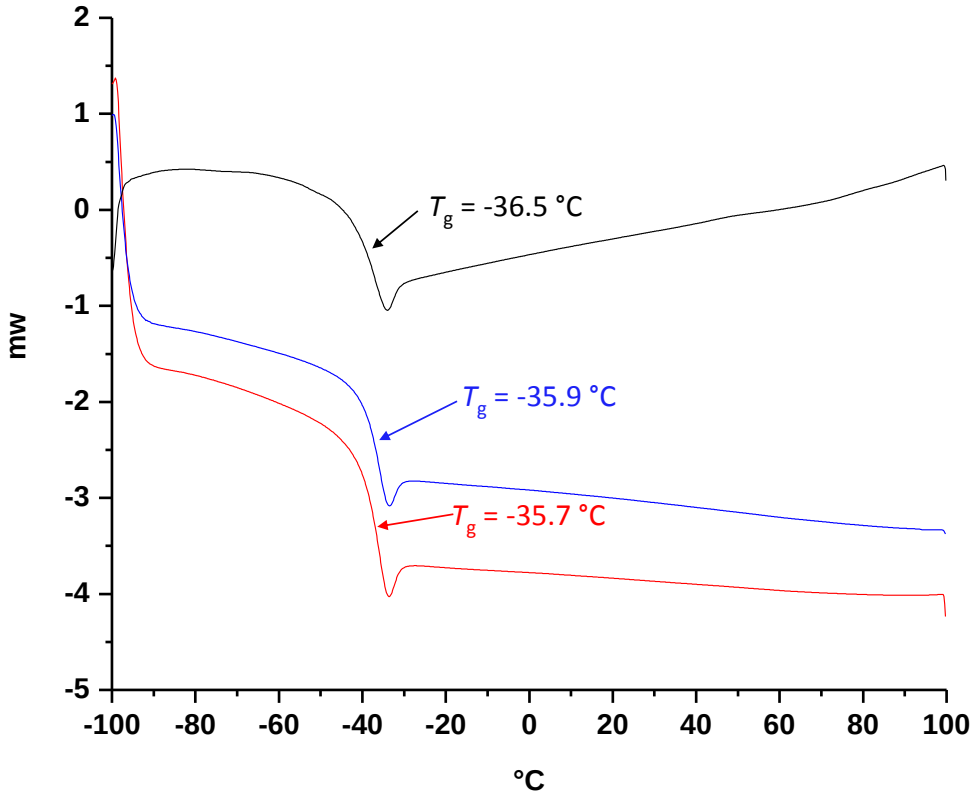

Figure 2.43 DSC curves of the homopolymer **A_{25}**.

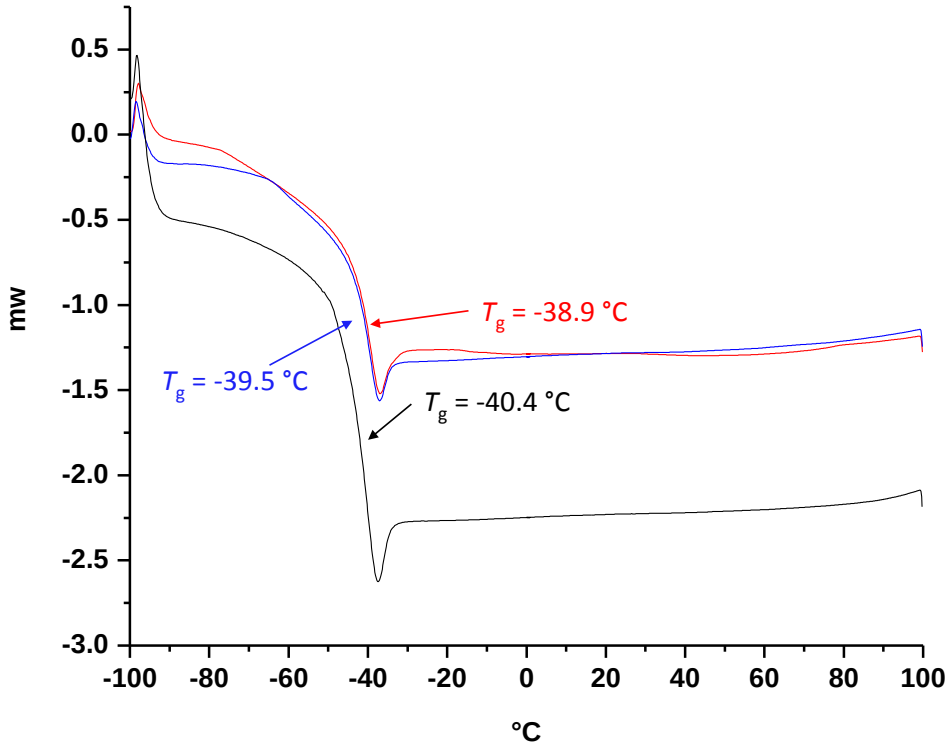

Figure 2.44 DSC curves of the homopolymer **A_{10}**.

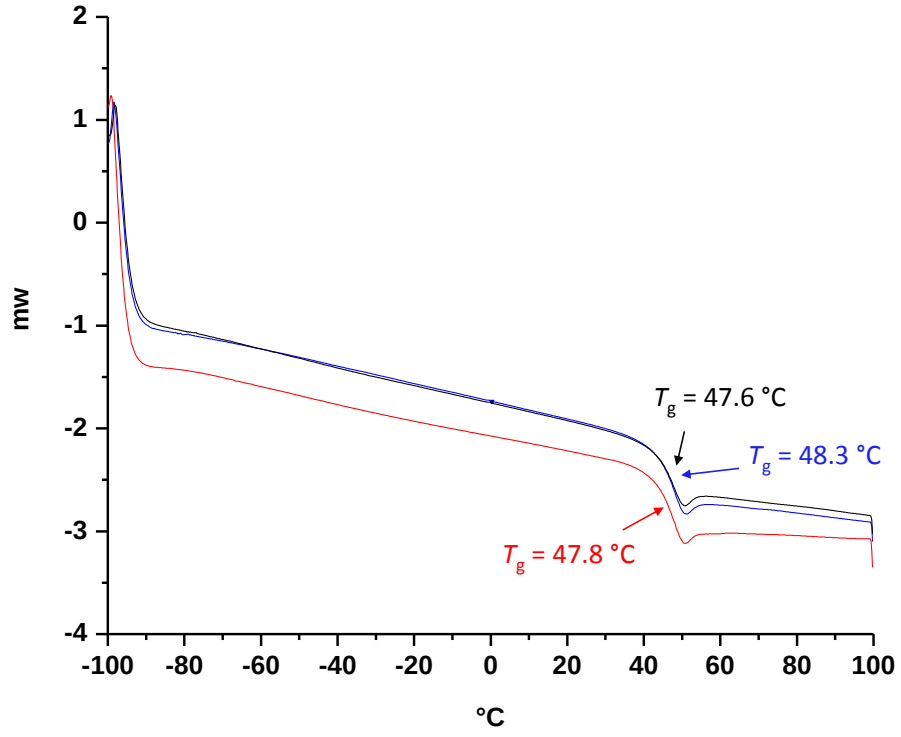

Figure 2.45 DSC curves of the homopolymer **B_{200}**.

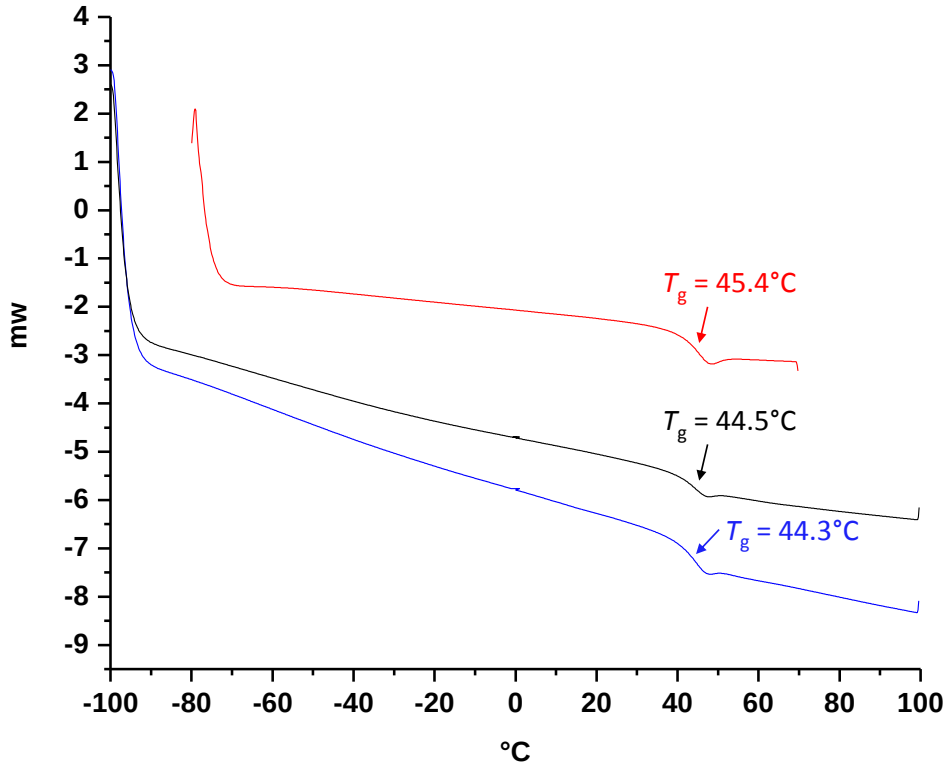

Figure 2.46 DSC curves of the homopolymer **B_{100}**.

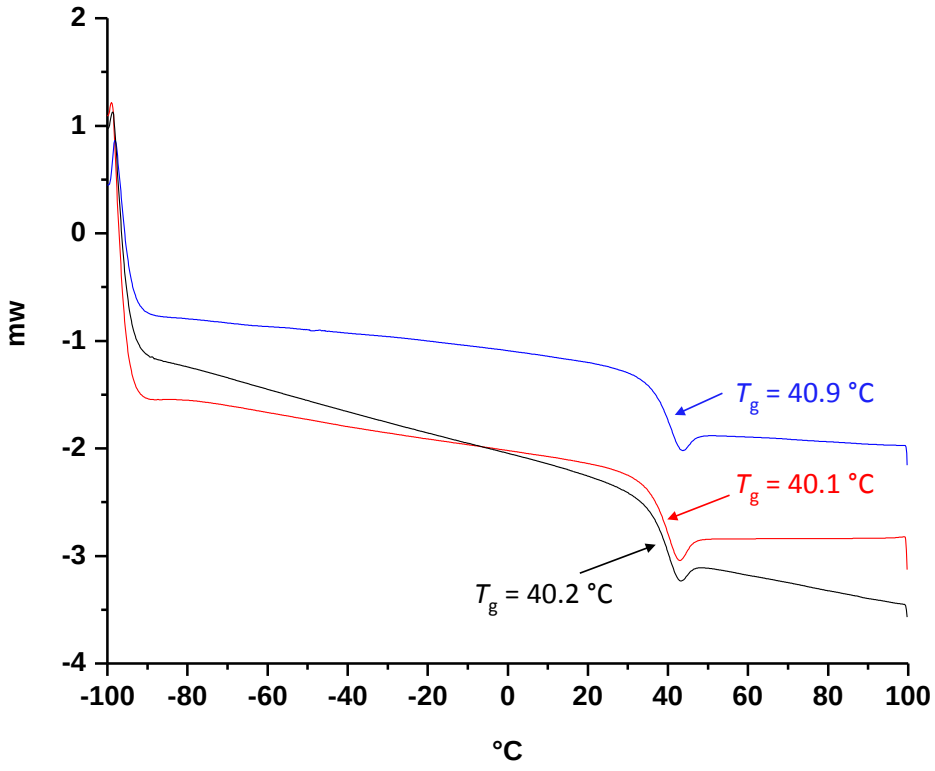

Figure 2.47 DSC curves of the homopolymer **B_{50}**.

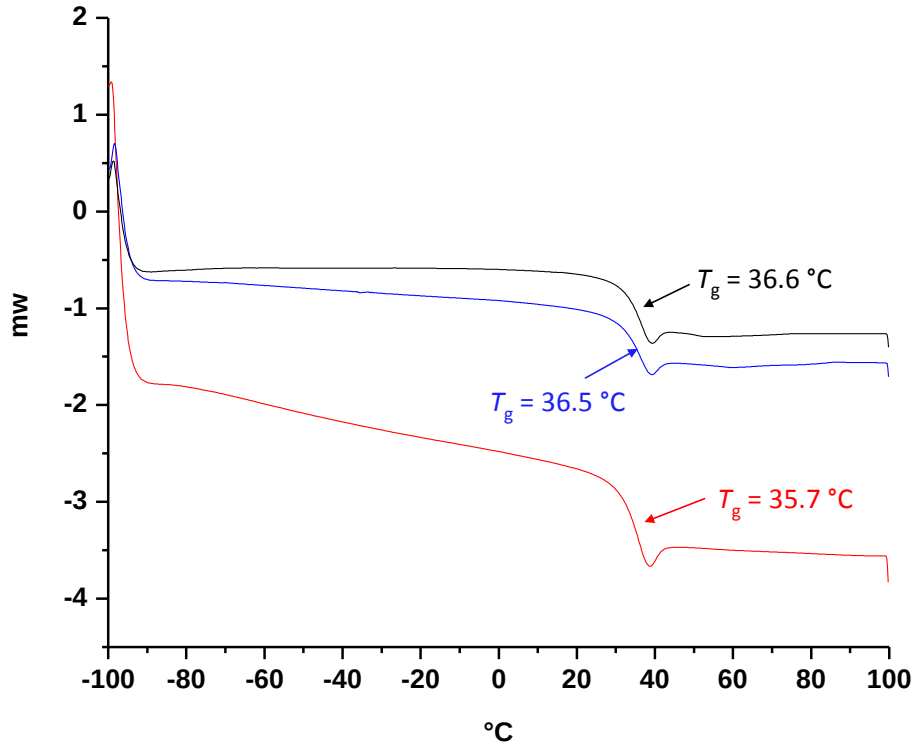

Figure 2.48 DSC curves of the homopolymer **B_{33}**.

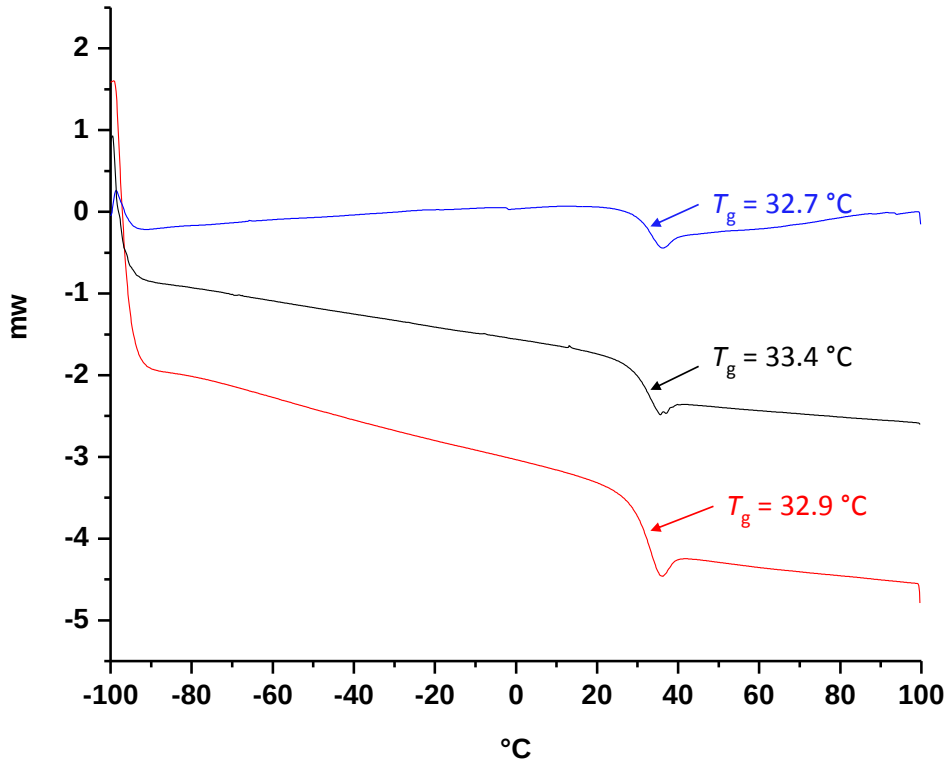

Figure 2.49 DSC curves of the homopolymer **B_{25}**.

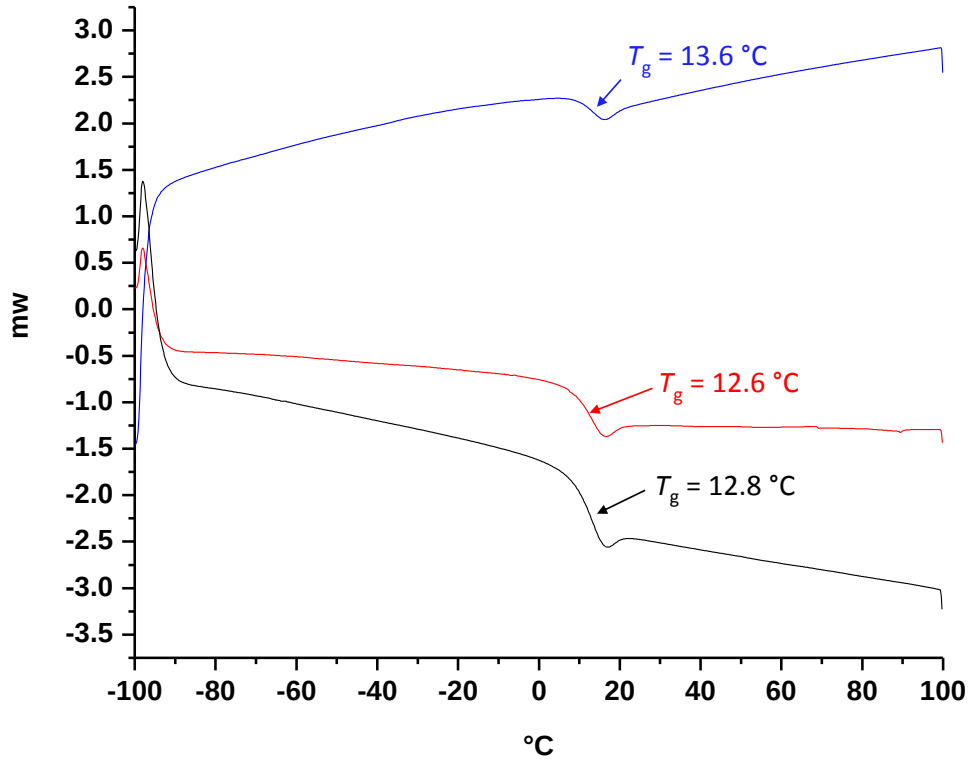

Figure 2.50 DSC curves of the homopolymer **B_{10}**.

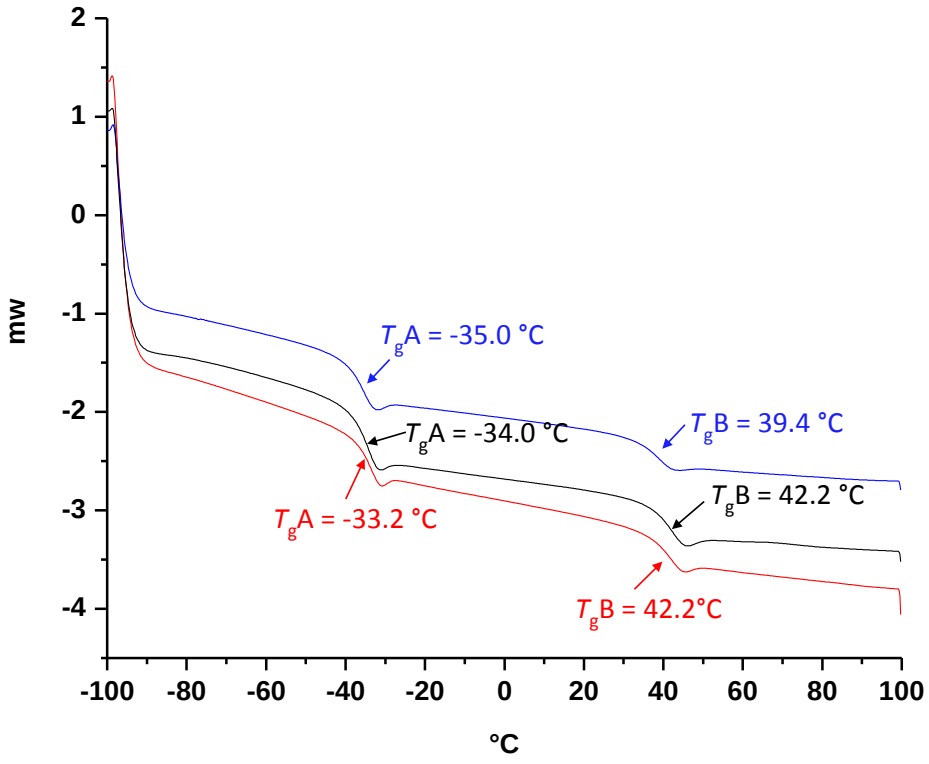

Figure 2.51 DSC curves of the **A_{100}**, **B_{100}** polymer blend.

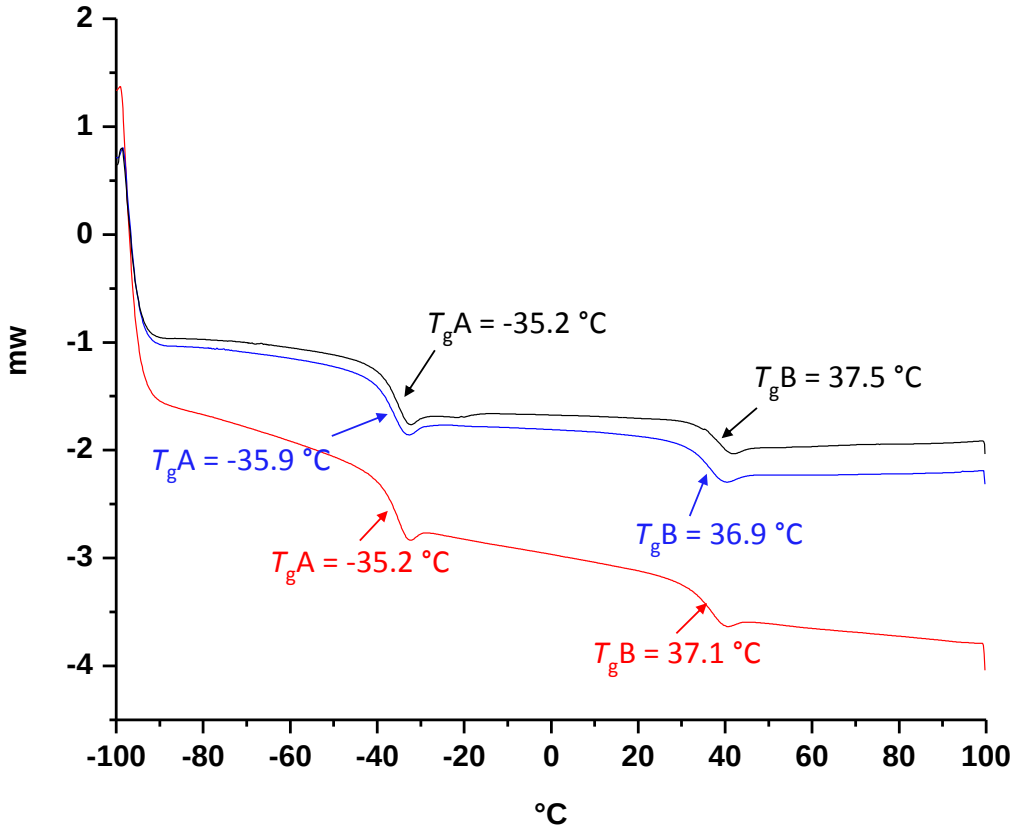

Figure 2.52 DSC curves of the **A_{50}**, **B_{50}** polymer blend.

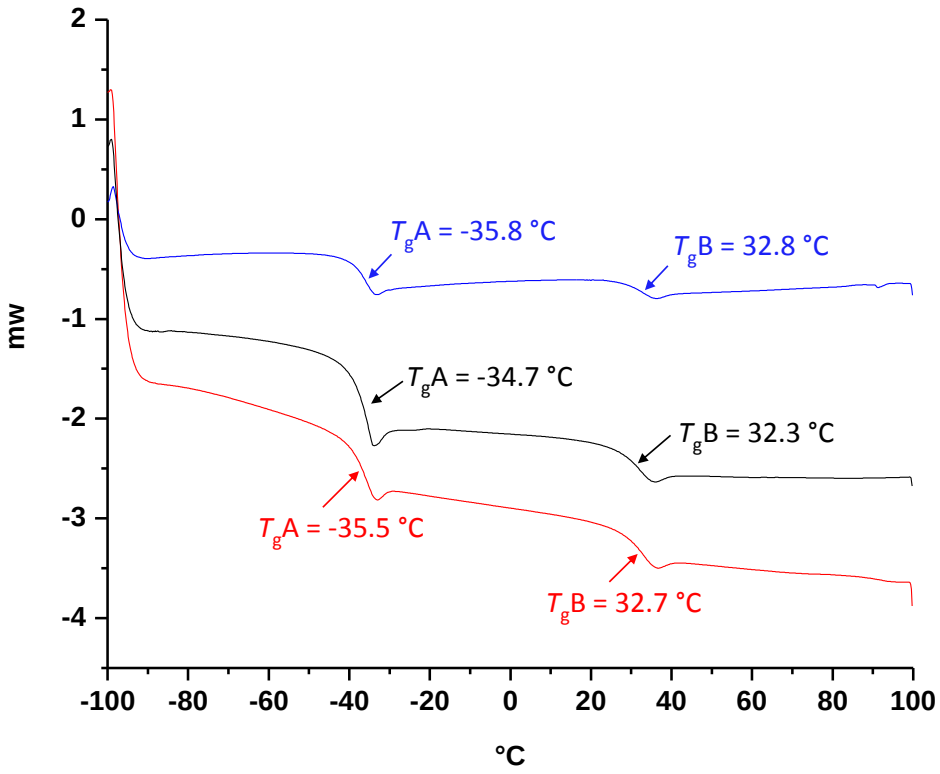

Figure 2.53 DSC curves of the **A**$_{33}$, **B**$_{33}$ polymer blend.

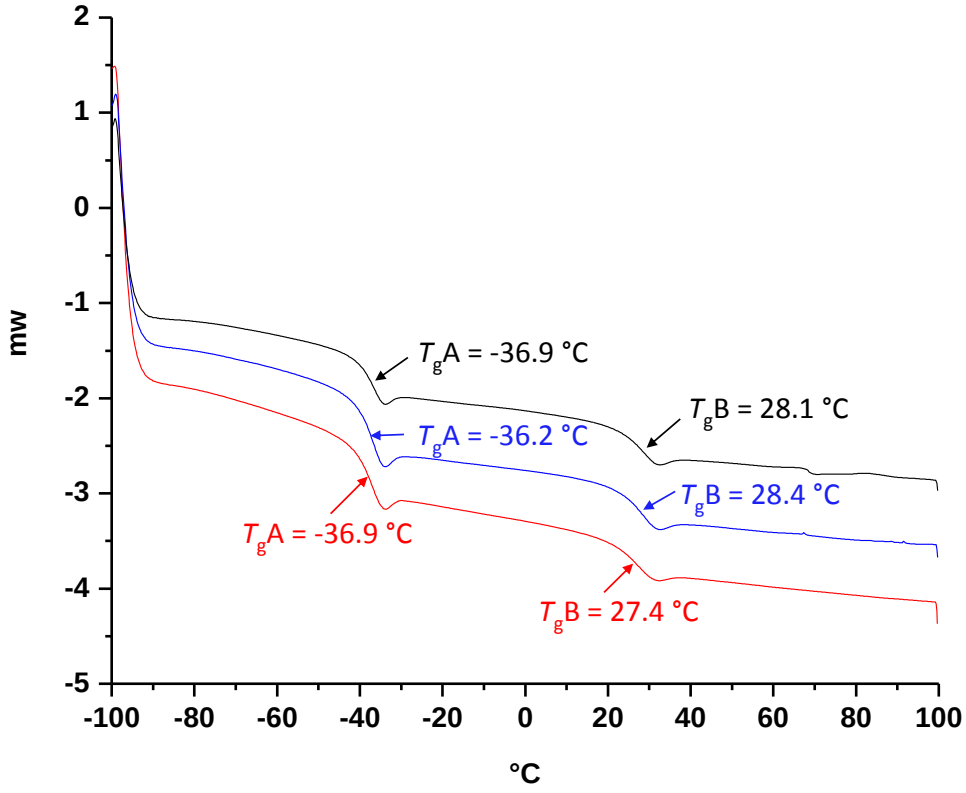

Figure 2.54 DSC curves of the **A**$_{25}$, **B**$_{25}$ polymer blend.

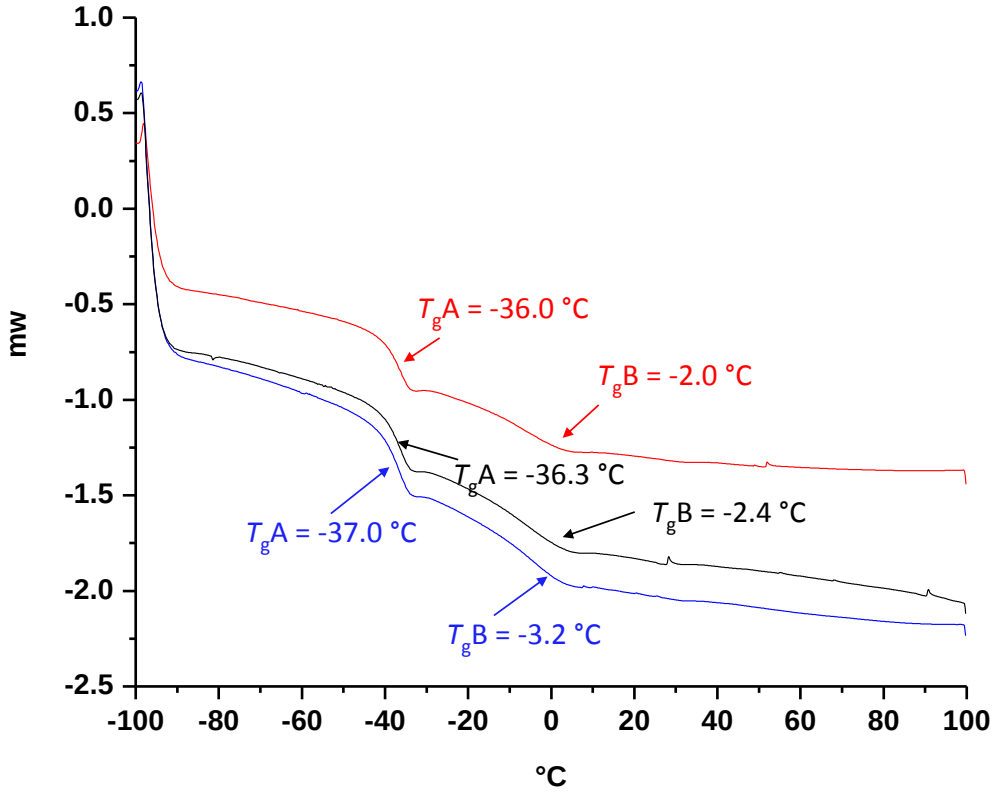

Figure 2.55 DSC curves of the **A_{10}**, **B_{10}** polymer blend.

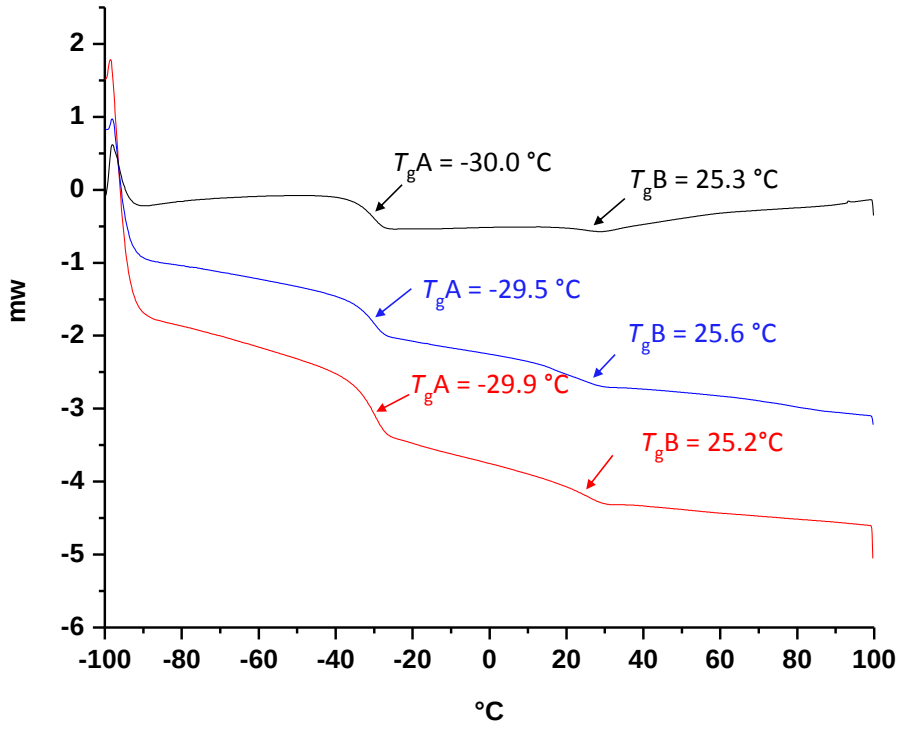

Figure 2.56 DSC curves of the diblock copolymer **$A_{50}B_{50}$**.

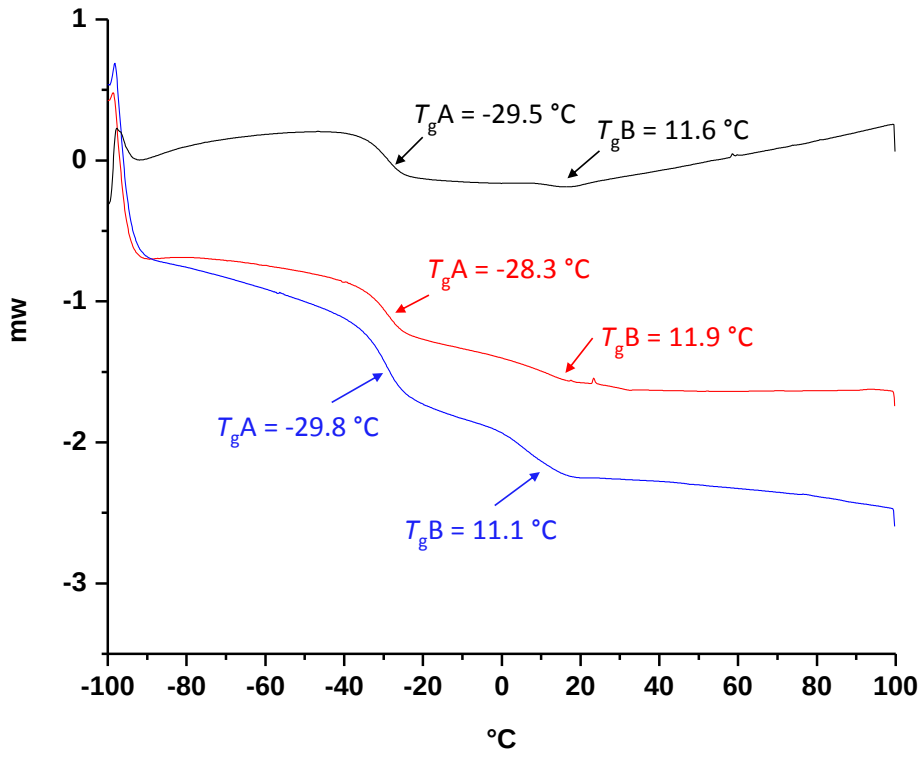

Figure 2.57 DSC curves of the diblock copolymer $\mathbf{A_{33}B_{33}}$.

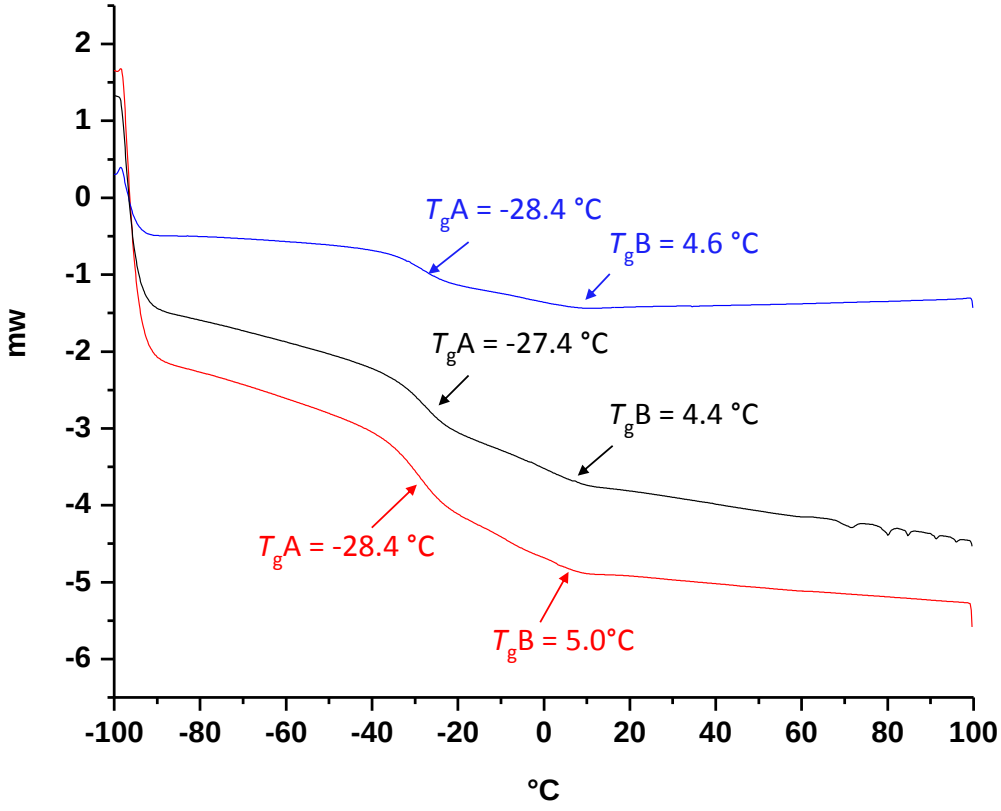

Figure 2.58 DSC curves of the diblock copolymer $\mathbf{A_{25}B_{25}}$.

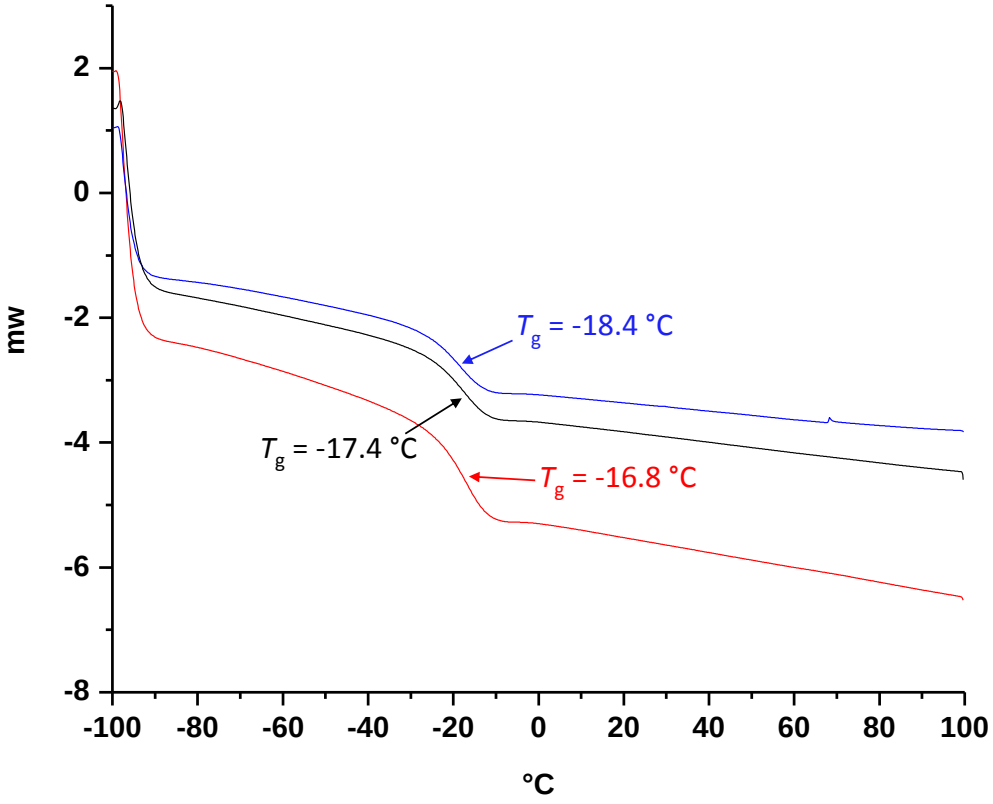

Figure 2.59 DSC curves of the diblock copolymer $\mathbf{A_{10}B_{10}}$.

2.5 References

1. Gody, G.; Maschmeyer, T.; Zetterlund, P. B.and Perrier, S. Rapid and quantitative one-pot synthesis of sequence-controlled polymers by radical polymerization. *Nat. Commun.* **2013**, 4, 2505.

2. Lodge, T. P. Block Copolymers: Past Successes and Future Challenges. *Macromol. Chem. Phys.* **2003**, 204 (2), 265-273.

3. Lutz, J.-F. Sequence-controlled polymerizations: the next Holy Grail in polymer science? *Polym. Chem.* **2010**, 1 (1), 55.

4. Discher, D. E.and Eisenberg, A. Polymer Vesicles. *Science* **2002**, 297 (5583), 967-973.

5. Harada, A.and Kataoka, K. Chain Length Recognition: Core-Shell Supramolecular Assembly from Oppositely Charged Block Copolymers. *Science* **1999**, 283 (5398), 65-67.

6. Badi, N.and Lutz, J. F. Sequence control in polymer synthesis. *Chem. Soc. Rev.* **2009**, 38 (12), 3383-90.

7. Lutz, J.-F.; Ouchi, M.; Liu, D. R.and Sawamoto, M. Sequence-Controlled Polymers. *Science* **2013**, 341 (6146), 628-636.

8. Gody, G.; Maschmeyer, T.; Zetterlund, P. B.and Perrier, S. Exploitation of the Degenerative Transfer Mechanism in RAFT Polymerization for Synthesis of Polymer of High Livingness at Full Monomer Conversion. *Macromolecules* **2014**, 47 (2), 639-649.

9. Gody, G.; Maschmeyer, T.; Zetterlund, P. B.and Perrier, S. Pushing the Limit of the RAFT Process: Multiblock Copolymers by One-Pot Rapid Multiple Chain Extensions at Full Monomer Conversion. *Macromolecules* **2014**, 47 (10), 3451-3460.

10. Pfeifer, S.and Lutz, J.-F. A Facile Procedure for Controlling Monomer Sequence Distribution in Radical Chain Polymerizations. *J. Am. Chem. Soc.* **2007**, 129 (31), 9542-9543.

11. Zamfir, M.and Lutz, J.-F. Ultra-precise insertion of functional monomers in chain-growth polymerizations. *Nat. Commun.* **2012**, 3, 1138.

12. Bita, I.; Yang, J. K. W.; Jung, Y. S.; Ross, C. A.; Thomas, E. L.and Berggren, K. K. Graphoepitaxy of Self-Assembled Block Copolymers on Two-Dimensional Periodic Patterned Templates. *Science* **2008**, 321 (5891), 939-943.

13. Ruiz, R.; Kang, H.; Detcheverry, F. A.; Dobisz, E.; Kercher, D. S.; Albrecht, T. R.; de Pablo, J. J.and Nealey, P. F. Density Multiplication and Improved Lithography by Directed Block Copolymer Assembly. *Science* **2008**, 321 (5891), 936-939.

14. Sun, J.; Teran, A. A.; Liao, X.; Balsara, N. P.and Zuckermann, R. N. Nanoscale Phase Separation in Sequence-Defined Peptoid Diblock Copolymers. *J. Am. Chem. Soc.* **2013**, 135 (38), 14119-14124.

15. Mansky, P.; Liu, Y.; Huang, E.; Russell, T. P.and Hawker, C. Controlling Polymer-Surface Interactions with Random Copolymer Brushes. *Science* **1997**, 275 (5305), 1458-1460.

16. Li, Z.; Kesselman, E.; Talmon, Y.; Hillmyer, M. A.and Lodge, T. P. Multicompartment Micelles from ABC Miktoarm Stars in Water. *Science* **2004**, 306 (5693), 98-101.

17. Park, C.; Yoon, J.and Thomas, E. L. Enabling nanotechnology with self assembled block copolymer patterns. *Polymer* **2003**, 44 (22), 6725-6760.

18. Sun, J.; Stone, G. M.; Balsara, N. P.and Zuckermann, R. N. Structure–Conductivity Relationship for Peptoid-Based PEO–Mimetic Polymer Electrolytes. *Macromolecules* **2012**, 45 (12), 5151-5156.

19. Irwin, M. T.; Hickey, R. J.; Xie, S.; So, S.; Bates, F. S.and Lodge, T. P. Structure–Conductivity Relationships in Ordered and Disordered Salt-Doped Diblock Copolymer/Homopolymer Blends. *Macromolecules* **2016**, 49 (18), 6928-6939.

20. Singh, M.; Odusanya, O.; Wilmes, G. M.; Eitouni, H. B.; Gomez, E. D.; Patel, A. J.; Chen, V. L.; Park, M. J.; Fragouli, P.; Iatrou, H.; Hadjichristidis, N.; Cookson, D.and Balsara, N. P. Effect of Molecular Weight on the Mechanical and Electrical Properties of Block Copolymer Electrolytes. *Macromolecules* **2007**, 40 (13), 4578-4585.

21. Förster, S.and Plantenberg, T. From Self-Organizing Polymers to Nanohybrid and Biomaterials. *Angew. Chem. Int. Ed.* **2002**, 41 (5), 688-714.

22. Hamley, I. W. Nanotechnology with Soft Materials. *Angew. Chem. Int. Ed.* **2003**, 42 (15), 1692-1712.

23. Kubowicz, S.; Baussard, J.-F.; Lutz, J.-F.; Thünemann, A. F.; von Berlepsch, H.and Laschewsky, A. Multicompartment Micelles Formed by Self-Assembly of Linear ABC Triblock Copolymers in Aqueous Medium. *Angew. Chem. Int. Ed.* **2005**, 44 (33), 5262-5265.

24. Stupp, S. I.; LeBonheur, V.; Walker, K.; Li, L. S.; Huggins, K. E.; Keser, M.and Amstutz, A. Supramolecular Materials: Self-Organized Nanostructures. *Science* **1997**, 276 (5311), 384-389.

25. Matsen, M. W. Effect of Architecture on the Phase Behavior of AB-Type Block Copolymer Melts. *Macromolecules* **2012**, 45 (4), 2161-2165.

26. Matsen, M. W.and Schick, M. Stable and Unstable Phases of a Linear Multiblock Copolymer Melt. *Macromolecules* **1994**, 27 (24), 7157-7163.

27. Benoit, H.and Hadziioannou, G. Scattering theory and properties of block copolymers with various architectures in the homogeneous bulk state. *Macromolecules* **1988**, 21 (5), 1449-1464.

28. Kavassalis, T. A.and Whitmore, M. D. On the theory of linear multiblock copolymers. *Macromolecules* **1991**, 24 (19), 5340-5345.

29. Zielinski, J. M.and Spontak, R. J. Confined single-chain model of microphase-separated multiblock copolymers. 1. (AB)n copolymers. *Macromolecules* **1992**, 25 (2), 653-662.

30. Wu, L.; Cochran, E. W.; Lodge, T. P.and Bates, F. S. Consequences of Block Number on the Order−Disorder Transition and Viscoelastic Properties of Linear (AB)n Multiblock Copolymers. *Macromolecules* **2004**, 37 (9), 3360-3368.

31. Rasmussen, K. Ø.; Kober, E. M.; Lookman, T.and Saxena, A. Morphology and bridging properties of (AB)n multiblock copolymers. *J. Polym. Sci., Part B: Polym. Phys.* **2003**, 41 (1), 104-111.

32. Dobrynin, A. V.and Erukhimovich, I. Y. Computer-aided comparative investigation of architecture influence on block copolymer phase diagrams. *Macromolecules* **1993**, 26 (2), 276-281.

33. Lee, I.; Panthani, T. R.and Bates, F. S. Sustainable Poly(lactide-b-butadiene) Multiblock Copolymers with Enhanced Mechanical Properties. *Macromolecules* **2013**, 46 (18), 7387-7398.

34. Lee, I.and Bates, F. S. Synthesis, Structure, and Properties of Alternating and Random Poly(styrene-b-butadiene) Multiblock Copolymers. *Macromolecules* **2013**, 46 (11), 4529-4539.

35. Panthani, T. R.and Bates, F. S. Crystallization and Mechanical Properties of Poly(l-lactide)-Based Rubbery/Semicrystalline Multiblock Copolymers. *Macromolecules* **2015**, 48 (13), 4529-4540.

36. Martello, M. T.; Schneiderman, D. K.and Hillmyer, M. A. Synthesis and Melt Processing of Sustainable Poly(ε-decalactone)-block-Poly(lactide) Multiblock Thermoplastic Elastomers. *ACS Sustainable Chemistry & Engineering* **2014**, 2 (11), 2519-2526.

37. Spontak, R. J.and Smith, S. D. Perfectly-alternating linear (AB)n multiblock copolymers: Effect of molecular design on morphology and properties. *J. Polym. Sci., Part B: Polym. Phys.* **2001**, 39 (9), 947-955.

38. Beck, K. R.; Korsmeyer, R.and Kunz, R. J. An overview of the glass transition temperature of synthetic polymers. *J. Chem. Educ.* **1984**, 61 (8), 668.

39. Fulchiron, R.; Belyamani, I.; Otaigbe, J. U.and Bounor-Legaré, V. A simple method for tuning the glass transition process in inorganic phosphate glasses. *Scientific Reports* **2015**, 5, 8369.

40. Behl, M.and Lendlein, A. Shape-memory polymers. *Mater. Today* **2007**, 10 (4), 20-28.

41. Meng, H.and Li, G. A review of stimuli-responsive shape memory polymer composites. *Polymer* **2013**, 54 (9), 2199-2221.

42. Huang, W. M.; Yang, B.; Zhao, Y.and Ding, Z. Thermo-moisture responsive polyurethane shape-memory polymer and composites: a review. *J. Mater. Chem.* **2010**, 20 (17), 3367-3381.

43. Wache, H. M.; Tartakowska, D. J.; Hentrich, A.and Wagner, M. H. Development of a polymer stent with shape memory effect as a drug delivery system. *J. Mater. Sci. Mater. Med.* **2003**, 14 (2), 109-112.

44. Lendlein, A.and Langer, R. Biodegradable, Elastic Shape-Memory Polymers for Potential Biomedical Applications. *Science* **2002**, 296 (5573), 1673-1676.

45. Metcalfe, A.; Desfaits, A.-C.; Salazkin, I.; Yahia, L. H.; Sokolowski, W. M.and Raymond, J. Cold hibernated elastic memory foams for endovascular interventions. *Biomaterials* **2003**, 24 (3), 491-497.

46. Tobushi, H.; Hara, H.; Yamada, E.and Hayashi, S. In *Thermomechanical properties of shape memory polymer of polyurethane series and their applications*, 1996; 1996; pp 418-423.

47. Boden, N.; Leng, S. A.and Ward, I. M. Ionic conductivity and diffusivity in polyethylene oxode/electrolyte solutions as models for polymer electrolytes. *Solid State Ionics* **1991**, 45 (3–4), 261-270.

48. White, R. P.and Lipson, J. E. G. Polymer Free Volume and Its Connection to the Glass Transition. *Macromolecules* **2016**, 49 (11), 3987-4007.

49. Geng, K.and Tsui, O. K. C. Effects of Polymer Tacticity and Molecular Weight on the Glass Transition Temperature of Poly(methyl methacrylate) Films on Silica. *Macromolecules* **2016**, 49 (7), 2671-2678.

50. Walker, C. N.; Sarapas, J. M.; Kung, V.; Hall, A. L.and Tew, G. N. Multiblock Copolymers by Thiol Addition Across Norbornene. *ACS Macro Letters* **2014**, 3 (5), 453-457.

51. Ellison, C. J.; Mundra, M. K.and Torkelson, J. M. Impacts of Polystyrene Molecular Weight and Modification to the Repeat Unit Structure on the Glass Transition−Nanoconfinement Effect and the Cooperativity Length Scale. *Macromolecules* **2005**, 38 (5), 1767-1778.

52. Boukis, A. C.; Llevot, A.and Meier, M. A. R. High Glass Transition Temperature Renewable Polymers via Biginelli Multicomponent Polymerization. *Macromol. Rapid Commun.* **2016**, 37 (7), 643-649.

53. Vanderlaan, M. E.and Hillmyer, M. A. "Uncontrolled" Preparation of Disperse Poly(lactide)-block-poly(styrene)-block-poly(lactide) for Nanopatterning Applications. *Macromolecules* **2016**, 49 (21), 8031-8040.

54. Shi, Y.; Cao, X.; Luo, S.; Wang, X.; Graff, R. W.; Hu, D.; Guo, R.and Gao, H. Investigate the Glass Transition Temperature of Hyperbranched Copolymers with Segmented Monomer Sequence. *Macromolecules* **2016**, 49 (12), 4416-4422.

55. Zhong, M.and Matyjaszewski, K. How Fast Can a CRP Be Conducted with Preserved Chain End Functionality? *Macromolecules* **2011**, 44 (8), 2668-2677.

56. Postma, A.; Davis, T. P.; Li, G.; Moad, G.and O'Shea, M. S. RAFT Polymerization with Phthalimidomethyl Trithiocarbonates or Xanthates. On the Origin of Bimodal Molecular Weight Distributions in Living Radical Polymerization. *Macromolecules* **2006**, 39 (16), 5307-5318.

57. Moad, G.; Mayadunne, R. T. A.; Rizzardo, E.; Skidmore, M.and Thang, S. H., Kinetics and Mechanism of RAFT Polymerization. In *Advances in Controlled/Living Radical Polymerization*, American Chemical Society: 2003; Vol. 854, pp 520-535.

58. Moad, G.and Barner-Kowollik, C., The Mechanism and Kinetics of the RAFT Process: Overview, Rates, Stabilities, Side Reactions, Product Spectrum and Outstanding Challenges. In *Handbook of RAFT Polymerization*, Wiley-VCH Verlag GmbH & Co. KGaA: 2008; pp 51-104.

59. He, R.and Kyu, T. Effect of Plasticization on Ionic Conductivity Enhancement in Relation to Glass Transition Temperature of Crosslinked Polymer Electrolyte Membranes. *Macromolecules* **2016**, 49 (15), 5637-5648.

60. Fox, T. G.and Flory, P. J. The glass temperature and related properties of polystyrene. Influence of molecular weight. *J. Polym. Sci.* **1954**, 14 (75), 315-319.

61. Fox, T. G.and Flory, P. J. Second-Order Transition Temperatures and Related Properties of Polystyrene. I. Influence of Molecular Weight. *J. Appl. Phys.* **1950**, 21 (6), 581-591.

62. Zhang, L.; Marsiglio, J. A.; Lan, T.and Torkelson, J. M. Dramatic Tunability of the Glass Transition Temperature and Fragility of Low Molecular Weight Polystyrene by Initiator Fragments Located at Chain Ends. *Macromolecules* **2016**, 49 (6), 2387-2398.

63. Hossain, M. D.; Lu, D.; Jia, Z.and Monteiro, M. J. Glass Transition Temperature of Cyclic Stars. *ACS Macro Letters* **2014**, 3 (12), 1254-1257.

64. Rizos, A. K.and Ngai, K. L. Local Segmental Dynamics of Low Molecular Weight Polystyrene: New Results and Interpretation. *Macromolecules* **1998**, 31 (18), 6217-6225.

65. Wooley, K. L.; Hawker, C. J.; Pochan, J. M.and Frechet, J. M. J. Physical properties of dendritic macromolecules: a study of glass transition temperature. *Macromolecules* **1993**, 26 (7), 1514-1519.

66. Roland, C. M.and Nagi, K. L. Segmental Relaxation in Poly(dimethylsiloxane). *Macromolecules* **1996**, 29 (17), 5747-5750.

67. Farrington, P. J.; Hawker, C. J.; Fréchet, J. M. J.and Mackay, M. E. The Melt Viscosity of Dendritic Poly(benzyl ether) Macromolecules. *Macromolecules* **1998**, 31 (15), 5043-5050.

68. Flory, P. J. Thermodynamics of Heterogeneous Polymers and Their Solutions. *The Journal of Chemical Physics* **1944**, 12 (11), 425-438.

69. Fox, T. G. Influence of diluent and of copolymer composition on the glass temperature of a polymer system. *The Bulletin of the American Physical Society* **1956**, 1, 123-132.

70. Lodge, T. P.and McLeish, T. C. B. Self-Concentrations and Effective Glass Transition Temperatures in Polymer Blends. *Macromolecules* **2000**, 33 (14), 5278-5284.

71. Lynd, N. A.; Meuler, A. J.and Hillmyer, M. A. Polydispersity and block copolymer self-assembly. *Prog. Polym. Sci.* **2008**, 33 (9), 875-893.

72. Lynd, N. A.and Hillmyer, M. A. Influence of Polydispersity on the Self-Assembly of Diblock Copolymers. *Macromolecules* **2005**, 38 (21), 8803-8810.

73. Cooke, D. M.and Shi, A.-C. Effects of Polydispersity on Phase Behavior of Diblock Copolymers. *Macromolecules* **2006**, 39 (19), 6661-6671.

74. Leibler, L. Theory of Microphase Separation in Block Copolymers. *Macromolecules* **1980**, 13 (6), 1602-1617.

75. Kim, S.; Nealey, P. F.and Bates, F. S. Directed Assembly of Lamellae Forming Block Copolymer Thin Films near the Order–Disorder Transition. *Nano Lett.* **2014**, 14 (1), 148-152.

76. Erothu, H.; Kolomanska, J.; Johnston, P.; Schumann, S.; Deribew, D.; Toolan, D. T. W.; Gregori, A.; Dagron-Lartigau, C.; Portale, G.; Bras, W.; Arnold, T.; Distler, A.; Hiorns, R. C.; Mokarian-Tabari, P.; Collins,

T. W.; Howse, J. R.and Topham, P. D. Synthesis, Thermal Processing, and Thin Film Morphology of Poly(3-hexylthiophene)–Poly(styrenesulfonate) Block Copolymers. *Macromolecules* **2015**, 48 (7), 2107-2117.

77. Hashimoto, T.; Tsukahara, Y.and Kawai, H. Structure and Properties of Tapered Block Polymers of Styrene and Isoprene II. Dynamic Mechanical Responses and Their Structural Interpretations. *Polym. J.* **1983**, 15 (10), 699-711.

78. Hashimoto, T.; Shibayama, M.and Kawai, H. Domain-Boundary Structure of Styrene-Isoprene Block Copolymer Films Cast from Solution. 4. Molecular-Weight Dependence of Lamellar Microdomains. *Macromolecules* **1980**, 13 (5), 1237-1247.

79. Matsushita, Y.; Mori, K.; Saguchi, R.; Nakao, Y.; Noda, I.and Nagasawa, M. Molecular weight dependence of lamellar domain spacing of diblock copolymers in bulk. *Macromolecules* **1990**, 23 (19), 4313-4316.

80. Ferguson, C. J.; Hughes, R. J.; Nguyen, D.; Pham, B. T. T.; Gilbert, R. G.; Serelis, A. K.; Such, C. H.and Hawkett, B. S. Ab Initio Emulsion Polymerization by RAFT-Controlled Self-Assembly. *Macromolecules* **2005**, 38 (6), 2191-2204.

81. In the Flory-Huggins calculation a reference volume equal to v_0 = 116.5 cm^3/mol was used, which is the average molar volume of A and B polymers. Correspondingly, the effective chain lengths of the polymers changed to $N_{A,eff}$ = 0.9 N_A and $N_{B,eff}$ = 1.1 N_B. The dependence of the Flory-Huggins interaction parameter (χ) was not taken into account and was assumed to be a constant corresponding to some temperature above the upper glass transition temperature of the mixture. The Flory-Huggins parameter was used as an adjustable parameter.

Chapter 3 *Synthesis of Sequence-Controlled Multi-block Single Chain Nanoparticles by a Step-wise Folding-Chain Extension-Folding Process*

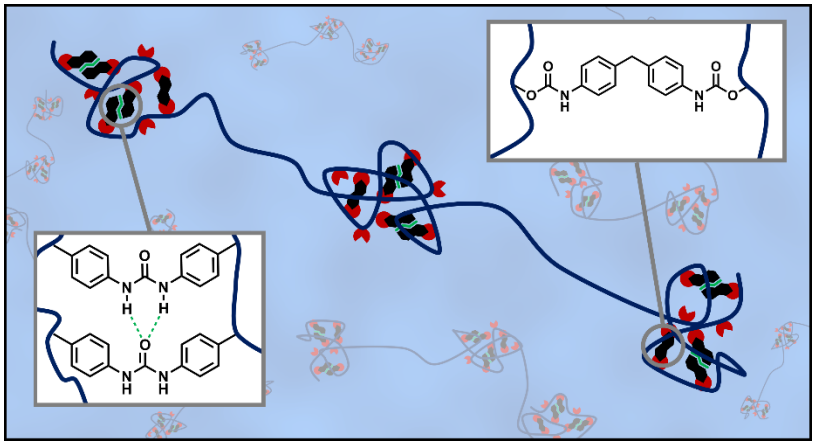

The specific activity of proteins can be traced back to their highly defined tertiary structure, which is a result of a perfectly controlled intra-chain folding process. In this chapter the folding of different distinct domains within a single macromolecule is demonstrated. RAFT polymerization was used to produce multi-block copolymers, which are decorated with pendant hydroxyl groups in foldable sections, separated by non-functional spacer blocks in between. OH-bearing blocks were folded using an isocyanate cross linker prior to chain extension to form single chain nanoparticles (SCNP). After addition of a spacer block and a further OH decorated block, folding was repeated to generate individual SCNP within a polymer chain. Control experiments were performed indicating the absence of inter block cross linking. SCNP were found to be condensed by a combination of covalent and supra molecular (hydrogen bonds) linkage. The approach was used to create a highly complex penta-block copolymer having three individually folded subdomains with an overall dispersity of 1.21. The successful

formation of SCNP was confirmed by size exclusion chromatography, nuclear magnetic resonance, differential scanning calorimetry and atomic force microscopy.

3.1 Introduction

The highly specialized activity of biopolymers, *e.g.* proteins, is determined by the remarkable control of their precise tertiary three-dimensional structure, which arises from the controlled folding of a single polypeptide chain.[1-5] The delicate controlled folding process of proteins is governed by the sophisticated sequence of amino-acid.[3] Reproducing the specific way in which bio-macromolecules fold their linear polymeric chains into perfectly defined nanostructures is a major, yet, challenging goal in the field of macromolecular synthesis.[5-7] Inspired by this model of biopolymers, folding a single linear polymer chain into a single chain nanoparticle (SCNP) has been recognized as a robust strategy for the construction of biopolymeric nanoparticles with potential applications in catalysis, sensing or biotechnology.[8-14] Although the design and synthesis of single chain objects has recently received great attention,[15] the development in this field is still in its initial phase. So far, several types of strategies to mediate the single chain collapse to form SCNPs have been explored,[16-22] ranging from hydrogen bonding,[23-27, 10, 28-31] covalent bonding,[32-36] to dynamic covalent bonding.[37-40] All these recent advances have provided versatile approaches to induce the folding of a single polymer chain. However, the limitation of most of these approaches is the lack of control regarding the polymer sequence and, therefore, lacking precision of the foldable moieties. The controlled folding process, however, is inarguably crucial for the specified functions of the proteins as the incorrect folding of proteins is the origin of a wide variety of pathological conditions and cause of prevalent diseases.[3] In order to mimic the incredible precision of the controlled folding process of biopolymers, controlling the sequence of the polymer chain becomes the first significant issue to address. Multi-block polymers have, therefore, attracted

considerable attentions since the sequences of the multi-block polymers can be controlled on demand. During the last few years, great developments in well-defined multi-block copolymers have been achieved using RAFT, ATRP or NMP.[41-43, 1, 44-46] These polymerization methods enable the synthesis of tailored polymeric chains with well-controlled sequences. By introducing foldable functionalities in a defined region of a single polymer chain, the folding of a specific sequence can then be controlled on demand.

All of the above results have paved the way for synthesizing more elaborated SCNPs to approach the aim of mimicking nature. Recently, Lutz *et al.* reported the intramolecular double compaction of sequence-controlled linear macromolecules into structured random coils at dilute concentrations.[47] This strategy makes a wide variety of tailored polymeric single-chain microstructures attainable and provides new perspective to build complex SCNPs. So far, the investigation about preparing more than two compacted subdomains in one single sequence controlled polymer chain by a repeated "folding-chain extension-folding" process has not been reported.

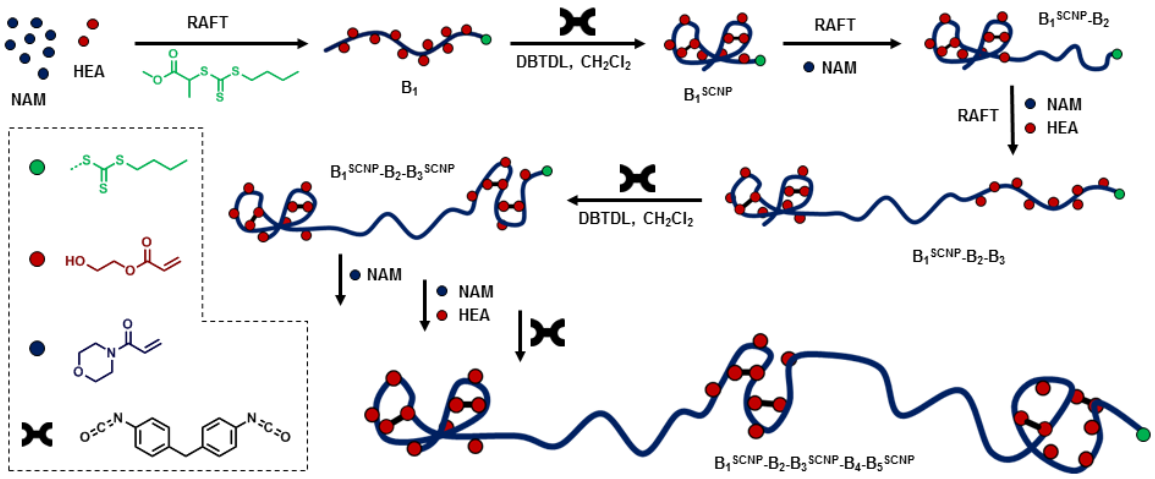

Scheme 3.1 Schematic representation of the synthesis of the multiblock single chain nanoparticles by a repeated folding-chain extension-folding process.

3.2 Results and Discussion

This work depicts the synthesis of multi-block "pearl necklace" shape SCNPs by stepwise "folding- chain extension-folding" of sequence-coded block copolymers. As shown in **Scheme 3.1**, the first step was to synthesize a linear copolymer by RAFT polymerization. In this copolymer, OH-functionalities were introduced as foldable units being able to be cross linked using a bi-functional molecule.

In order to satisfy the demands of the continuous addition method and prevent inter-molecular cross linking, the reaction between the cross linker and the foldable units must proceed rapid.[48] Isocyanates were chosen as they rapidly and quantitatively react with a wide range of nucleophiles (such as amines, thiols, alcohols, and carboxylic acids) under mild reaction conditions, without the production of a by-product.[49] After folding of the first block, a spacer was introduced by chain extension with a non-functional monomer, followed by the introduction of a second foldable block, which again was folded using isocyanates. This procedure was repeated one more time to yield a penta-block consisting of three individual SCNPs each separated by a polymeric spacer representing a molecular pearl necklace.

In this study, hydroxyl groups were used as the cross linkable units. Foldable blocks were produced by copolymerizing a mixture of 2-Hydroxyethyl acrylate (HEA) and N-acryloylmorpholine (NAM) resulting in a polymer decorated with OH functionalities. Methylene diphenyl di-isocyanate (MDI) was used as a cross linker, containing two isocyanate groups, which react rapidly with hydroxyl groups in the presence of a catalyst resulting in SCNP. Subsequently, chain extension using NAM was performed to create a spacer between individual SCNPs, followed by the addition of a further NAM/HEA block. A five block copolymer was synthesized including three blocks consisting of NAM/HEA, folded separately and separated by two NAM blocks.

3.2.1 Synthesis and folding of the first block (B_1 and B_1^{SCNP})

The linear polymer poly(NAM_{39}-*stat*-HEA_{10}) precursor **B_1** (first block) containing statistically distributed pendant hydroxyl units was prepared by RAFT copolymerization of NAM and HEA as depicted in **Scheme 3.1**. Optimized RAFT conditions, previously described for the synthesis of water soluble multi-block copolymers (Azoinitiator: VA-044 at 70 °C in H_2O)[45] were applied to provide a fast and quantitative monomer conversion while maintaining high control over molar mass, narrow dispersity and high theoretical livingness. Particular attention was paid to the use of a non-free COOH chain transfer agent (methoxy-(propanoic acid)yl butyl trithiocarbonate, MPABTC, **Scheme 3.4**, **Figures 3.13** and **3.14**) to avoid any side reactions during the intramolecular cross linking step with MDI. The overall degree of polymerization of the first block was targeted to be 50 with 20% of HEA comonomer to ensure efficient intramolecular cross linking, as well as a high degree of livingness. After 2 h of polymerization, near quantitative monomer conversion (98%) was obtained from ^{1}H NMR analysis for both monomers. Size-exclusion chromatography in $CHCl_3$ revealed a mono-modal distribution and a narrow dispersity ($M_{n,th}$ = 7,000 g mol^{-1}, $M_{n,SEC}$ = 6,200 g mol^{-1}, $Đ$ = 1.12, **Figure 3.1** and **Table 3.1**). The monomer ratio and the DP were determined by ^{1}H-NMR (**Figure 3.15**).

As shown in **Scheme 3.2** the folding of the linear copolymer **B_1** was carried out by the reaction of the statistically distributed pendant cross linkable hydroxyl units using MDI in presence of the catalyst dibutyltin dilaurate (DBTDL) in dry DCM (to limit degradation of the isocyanate group into a primary amine). In order to reduce the competing intermolecular cross linking of multiple chains, such reactions are usually carried out at high dilutions (~10^{-5} – 10^{-6} mol L^{-1}).[48] However, even in dilute conditions, intermolecular cross linking is still unavoidable.[47]

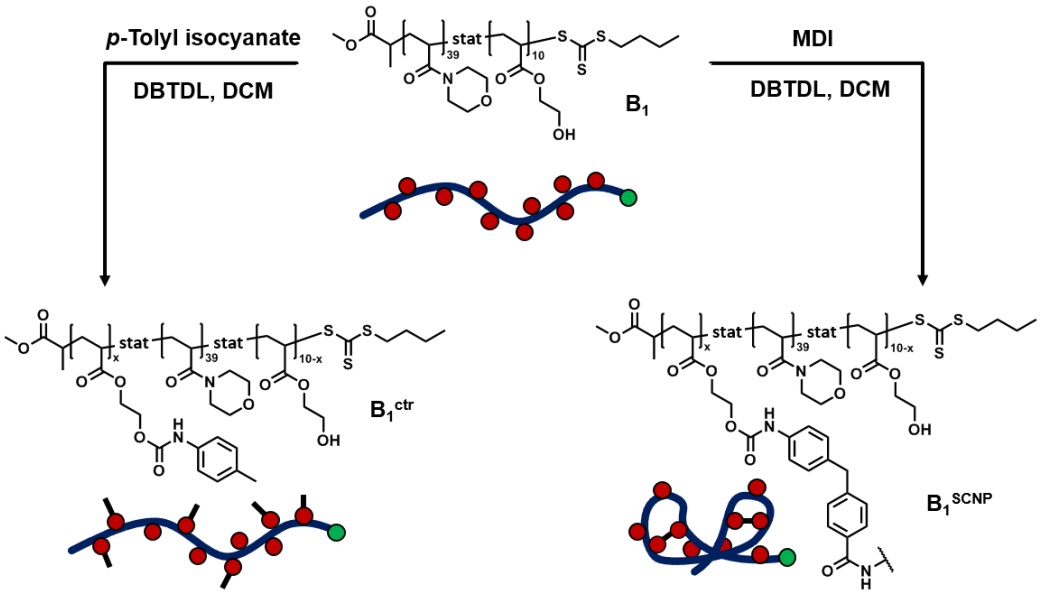

Scheme 3.2 Synthesis of the single chain polymeric nanoparticles $\mathbf{B_1}^{\mathbf{SCNP}}$ and the linear control copolymer $\mathbf{B_1}^{\mathbf{ctr}}$ from the precursor copolymer $\mathbf{B_1}$ (Poly(NAM_{39}-*stat*-HEA_{10})).

A solution to that problem was developed by Hawker *et al.* introducing a continuous addition method (by adding the solution of one reactant dropwise to the solution of the other reactant) to synthesize SCNPs.[48] This strategy also permits the synthesis of well-defined and functionalized SCNPs in a relatively high concentration (ca. 0.01 mol L^{-1}) and bigger quantities. For presented system, the slow addition of the copolymer $\mathbf{B_1}$ ([OH] = 0.01 mol L^{-1}) into a premade solution of the cross linker (MDI, 0.5 equivalent per hydroxyl group) in dry DCM was found to be the most successful approach to avoid intermolecular cross linking reactions. After 24 h remaining isocyanate groups were quenched using methanol to prevent reactions with further blocks.

In order to determine whether the single chain folding was successful and to quantify the number of reacted MDI, SEC and ^{1}H NMR studies were performed. SEC is an ideal technique to monitor any changes in the hydrodynamic volume of a polymer chain allowing to distinguish between linear precursors, intermolecular cross linked species and SCNP.[50, 4, 24, 51, 52] Comparing the SEC chromatogram of the material in chloroform after reaction ($\mathbf{B_1}^{\mathbf{SCNP}}$) with

its parent copolymer **B_1**, a shift towards lower mass (*i.e.* smaller hydrodynamic volume, M_n = 6200 g mol^{-1} to 4800 g mol^{-1}, **Table 3.1**, **Figure 3.1A**) was observed, suggesting the successful formation of single chain polymeric nanoparticles **B_1^{SCNP}**. This result is consistent with previous literature about the intramolecular cross linking of a single polymer chain.[32, 48, 47, 4, 52, 35, 38, 39]

Table 3.1 Characterization of the polymers by ^{1}H NMR and $CHCl_3$-SEC.

Sample	Composition[a]	MDI[a] eq. per chain	*p*TI[a] eq. per chain	Ureth.[a] %	Urea[a] %	NH_2[a] %	M_n[b] g mol^{-1}	$Đ$[b]
B_1	$P(NAM_{39}\text{-}HEA_{10})$	-	-	-	-	-	6,200	1.12
B_1^{SCNP}	$P(NAM_{39}\text{-}HEA_{10})^{SCNP}$	2.4	-	44	36	20	4,800	1.27
B_1^{ctr}	$P(NAM_{39}\text{-}HEA_{10})^{ctr}$	-	4.5	100	0	0	7,500	1.11
B_1^{SCNP}-B_2	$P[(NAM_{39}\text{-}HEA_{10})^{SCNP}\text{-}b\text{-}NAM_{12}]$	2.4	-	44	36	20	7,000	1.19
B_1^{SCNP}-B_2-B_3	$P[(NAM_{39}\text{-}HEA_{10})^{SCNP}\text{-}b\text{-}NAM_{12}\text{-}b\text{-}(NAM_{29}\text{-}HEA_8)]$	2.4	-	44	36	20	11,100	1.15
B_1^{SCNP}-B_2-B_3^{SCNP}	$P[(NAM_{39}\text{-}HEA_{10})]^{SCNP}\text{-}b\text{-}NAM_{12}\text{-}b\text{-}(NAM_{29}\text{-}HEA_8)^{SCNP}]$	4.8	-	43	39	18	9,400	1.25
B_1-B_2-B_3	$P[(NAM_{39}\text{-}HEA_{10})\text{-}b\text{-}NAM_{12}\text{-}b\text{-}(NAM_{29}\text{-}HEA_8)]$	-	-	-	-	-	12,100	1.10
$(B_1\text{-}B_2\text{-}B_3)^{SCNP}$	$P[(NAM_{39}\text{-}HEA_{10})\text{-}b\text{-}NAM_{12}\text{-}b\text{-}(NAM_{29}\text{-}HEA_8)]^{SCNP}$	3.9	-	40	40	20	8,400	1.29
B_1^{SCNP}-B_2-B_3^{SCNP}-B_4	$P[(NAM_{39}\text{-}HEA_{10})^{SCNP}\text{-}b\text{-}NAM_{12}\text{-}b\text{-}(NAM_{29}\text{-}HEA_8)^{SCNP}\text{-}b\text{-}NAM_{12}]$	4.8	-	43	39	18	10,700	1.27
B_1^{SCNP}-B_2-B_3^{SCNP}-B_4-B_5	$P[(NAM_{39}\text{-}HEA_{10})^{SCNP}\text{-}b\text{-}NAM_{12}\text{-}b\text{-}(NAM_{29}\text{-}HEA_8)^{SCNP}\text{-}b\text{-}NAM_{12}\text{-}b\text{-}(NAM_{41}\text{-}HEA_8)]$	4.8	-	43	39	18	17,500	1.20
B_1^{SCNP}-B_2-B_3^{SCNP}-B_4-B_5^{SCNP}	$P[(NAM_{39}\text{-}HEA_{10})^{SCNP}\text{-}b\text{-}NAM_{12}\text{-}b\text{-}(NAM_{29}\text{-}HEA_8)^{SCNP}\text{-}b\text{-}NAM_{12}\text{-}b\text{-}(NAM_{41}\text{-}HEA_8)^{SCNP}]$	6.5	-	57	23	20	16,000	1.21

[a] The degree of polymerization, as well as amount of cross linker were determined by ^{1}H NMR;

[b] Determined by SEC in $CHCl_3$ with PMMA used as molecular weight standards.

In order to investigate whether the observed changes in hydrodynamic volume is associated to the formation of covalent connections or hydrogen bonds between urethane units, a control copolymer **B_1^{ctr}** was synthesized by reacting the linear copolymer **B_1** with a mono-functional isocyanate (*p*-tolyl isocyanate (*p*TI), **Scheme 3.2**). The SEC chromatogram obtained for the polymer **B_1^{ctr}** shows a shift towards higher molar mass (**Figure 3.1A**). The direct comparison of the $CHCl_3$ SEC traces of **B_1^{SCNP}**, **B_1** and **B_1^{ctr}** confirms that the decreased hydrodynamic volume of **B_1^{SCNP}** is due to intramolecular cross linking of **B_1** to obtain a collapsed nanoparticle from a random coil. It has to be noted that all SEC measurements were

conducted using a flow rate marker as internal standard to eliminate SEC measurement errors, and the final pentablock with three subdomain folded copolymer was analyzed for multiple times (see **Figure 3.28**, 5 times in this case) by SEC and the results showed the shift to lower molar mass after cross-linking was due to intramolecular cross-linking.

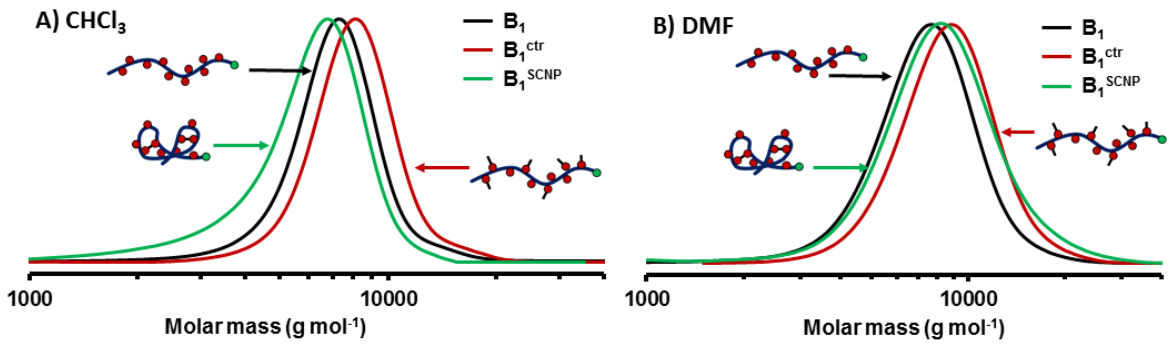

Figure 3.1 SEC RI traces of $\mathbf{B_1}$, $\mathbf{B_1^{SCNP}}$ and $\mathbf{B_1^{ctr}}$ in $CHCl_3$ (A) and in DMF (B).

To visualize whether the observed change in hydrodynamic volume is the result of covalent cross linking or supramolecular interactions (*e.g.* hydrogen bonds), the parent polymer, the SCNP and the control were also investigated by SEC using DMF as eluent, **(Figure 3.1B)**. Due to its high polarity, DMF is a strong hydrogen bonding competitor solvent, which is expected to completely disrupt hydrogen bonds.[53, 54]

Surprisingly, the folded chain $\mathbf{B_1^{SCNP}}$ does have an increased hydrodynamic volume in DMF compared to its parent polymer $\mathbf{B_1}$ and elutes at slightly decreased molecular weight as compared to $\mathbf{B_1^{ctr}}$, which is in contradiction to the results obtained in chloroform at first sight. However, this observation could be explained by the appearance of hydrogen bonds in $CHCl_3$, which are disrupted by DMF. Indeed, covalent cross linking is not expected to be solvent sensitive. The fact that $\mathbf{B_1^{ctr}}$ possesses a slightly higher hydrodynamic volume in DMF than $\mathbf{B_1^{SCNP}}$, indicates that covalent cross linking is involved in the process as well. Otherwise, for a non-covalently cross linked $\mathbf{B_1^{SCNP}}$ a shift of the SEC trace to higher molecular weights as compared to $\mathbf{B_1^{ctr}}$ is expected, as MDI, the cross linking agent of $\mathbf{B_1^{SCNP}}$ has a higher molar

mass than *p*TI, the functionalization agent of $\mathbf{B_1^{ctr}}$. The increased R_h of $\mathbf{B_1^{SCNP}}$ in DMF as compared to $\mathbf{B_1}$ could be a result of the increased molecular weight by the addition of multiple cross-linker molecules. As hydrogen bonds are not expected to occur in DMF, MDI is partially solubilized and contributed to an increased R_h (which contradicts the decreasing effect of R_h caused by covalent cross-linking) compared to the parent polymer.

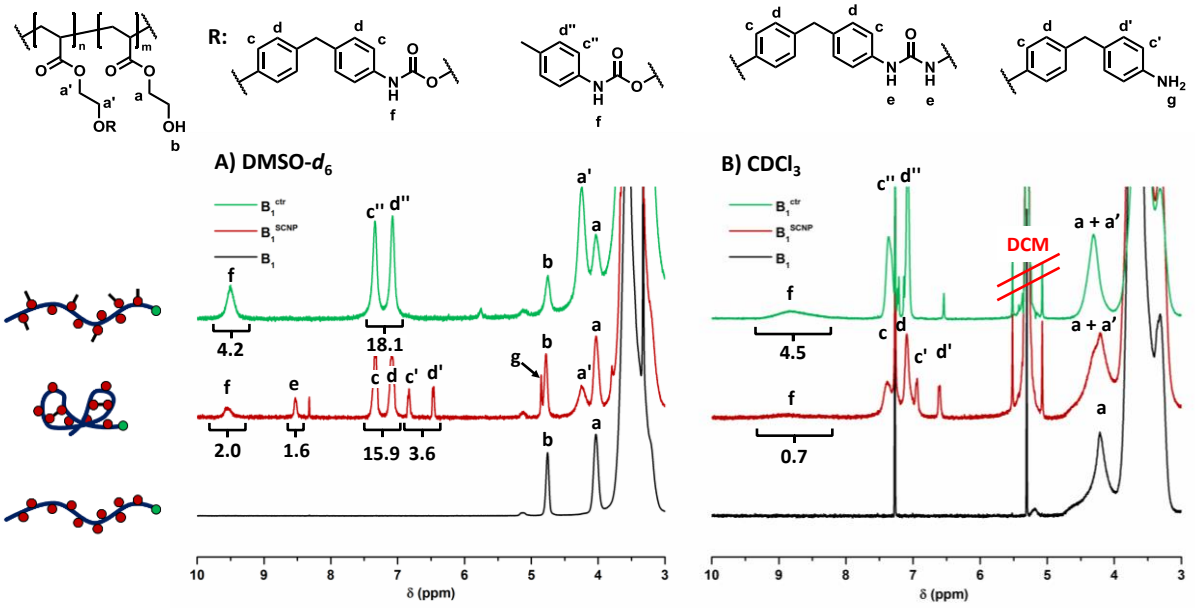

Figure 3.2 ^{1}H NMR spectra (400MHz) of linear polymer $\mathbf{B_1}$, folded polymer $\mathbf{B_1^{SCNP}}$ as well as control polymer $\mathbf{B_1^{ctr}}$ in DMSO-d_6 (A) and $CDCl_3$ (B), respectively.

To prove the involvement of hydrogen bonding in the cross linking process, as well as to assess the amount of reacted cross linker, ^{1}H NMR spectroscopy investigation was carried out (**Figure 3.2**). From the comparison of the spectra of $\mathbf{B_1^{SCNP}}$ and $\mathbf{B_1}$ in DMSO-d_6 (**Figures 3.2A**, **3.15** and **3.16**) the appearance of MDI associated signals is visible (**Figure 3.2A**: signals c & d). However, in addition to the signals expected for a urethane cross linked polymer, signals corresponding to urea and primary amine moieties are visible (**Figure 3.2A**: signals e & g; for a comparison with hydrolysed MDI, as well as methanol reacted MDI see **Figures 3.25**, **3.26** and **3.27**). This can be explained by the hydrophilic nature of the polymer, which leads to presence of water during cross linking reaction even though dry solvents and reagents were

used. The hydrolysis of MDI leads to the presence of primary amines which, in turn, can react with isocyanate moieties to form urea units. Indeed, in the case of $\mathbf{B_1^{SCNP}}$, only 2.4 equivalents MDI per polymer chain have reacted to form urethane (44%), urea (36%) and amine groups (20%), respectively (see **Table 3.1**). For $\mathbf{B_1^{ctr}}$, 4.5 equivalents of isocyanate have reacted with polymeric OH groups forming urethane bonds (**Figures 3.2** and **3.17**). The low efficiency of the reaction of MDI with the polymer in comparison to the control experiment points towards a high steric hindrance of reactive sites on the polymer after folding, which is a possible explanation for the occurrence of urea and amine groups. Once attached to the polymer chain, the remaining isocyanate cannot react with another OH-groups due to steric interaction and is hydrolysed by traces of water.

The formed amine possesses a higher reactivity towards free MDI as compared to OH groups and partially forms urea connections, which, in turn, results in an increase of hydrogen bonding in the SCNP. The presence of free primary amines further indicates the importance of steric hindrance, as the amine group has a higher tendency to react with isocyanates as compared to OH-functionalities. Indeed, the steric hindrance was not surprizing and has been pointed out by Hawker *et al.*,[32] Duxbury *et al.*[55] and Berda *et al.*[51] before. Furthermore, as the cross linking reaction is carried out in dichloromethane, a solvent which does not compete with H-bonds, an additional compaction after the formation of urea and urethane functions is expected.

The presence of hydrogen bonds can also be shown by the difference between ^{1}H NMR spectra measured in DMSO-d_6 and $CDCl_3$ (**Figure 3.2B**). In contrast to DMSO, chloroform is not H-bond competitor solvent. The exchange rate of protons involved in H-bonds is drastically reduced, which leads to a broadening or a disappearance of the signals.[56] This behaviour is seen in **Figure 3.2B**, as signals associated with urea have disappeared accompanied by a decrease in the integral of the urethane signals by 66% is observed.

In the case of $\mathbf{B_1^{ctr}}$, almost no change in the integral of the urethane signal could be detected proving the prevalence of covalent cross linking in the cooperative covalent and supramolecular cross linking observed for $\mathbf{B_1^{SCNP}}$. It is also likely, that the presence of urea moieties (which are known to form strong H-bonds)[57] amplifies the H-bonding potential in the cross linked polymer.

The successful formation of SCNPs can also be indicated by differential scanning calorimetry (DSC) analysis. Due to the intramolecular cross-linking, the chain mobility will decrease compared to the linear polymer resulting in an increased glass transition temperature (T_g) value for SCNP.[48, 58, 59, 37] The T_g value of the $\mathbf{B_1^{SCNP}}$ increased significantly from the initial value of 117.2 °C for linear polymer $\mathbf{B_1}$ to 132.6 °C, while the T_g value of the $\mathbf{B_1^{ctr}}$ only increased slightly to 118.3 °C (**Figure 3.3**).

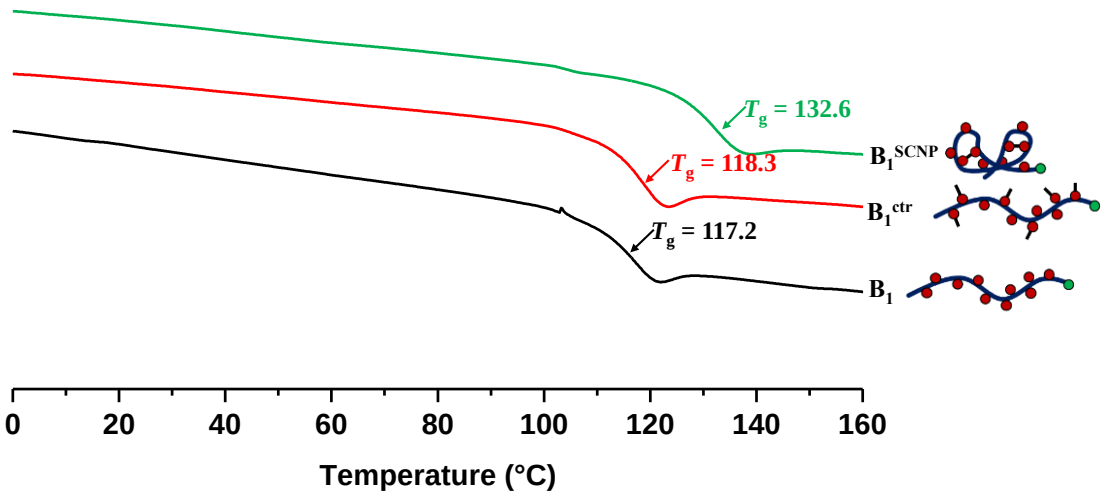

Figure 3.3 DSC curves of linear polymer $\mathbf{B_1}$, control polymer $\mathbf{B_1^{ctr}}$ and folded polymer $\mathbf{B_1^{SCNP}}$.

Dynamic light scattering measurements in chloroform of $\mathbf{B_1^{SCNP}}$ revealed a slightly bigger size ($R_h \approx 3$ nm) than the parent polymer $\mathbf{B_1}$ but a smaller R_h as compared to the control polymer B_1^{ctr} (**Figure 3.4**). These results were similar to the observations of Fulton and co-workers about SCNPs.[52] They proposed possible explanations for the results. One might be a

nonspherical architecture of the SCNPs, different from that of the parent linear polymer resulting in a reduced diffusion speed, thus increasing the calculated particle size. The other explanation was that the folding of linear polymers caused the SCNPs leads to a relatively increased solubility, especially at the periphery of the particle, which contributed the increase of the volume and caused the increased values of D_h. These explanations also apply to this system, especially the increase in solubility of SCNPs compared to the parent linear polymers. In the current system, the cross-linker MDI attached to the polymer chains after cross-linking will highly increase the solubility of the nanoparticle material which in turn increased the value of D_h. However, the difference in size to the control polymer, which was functionalized with a smaller molecule, indicates the formation of the SCNP.

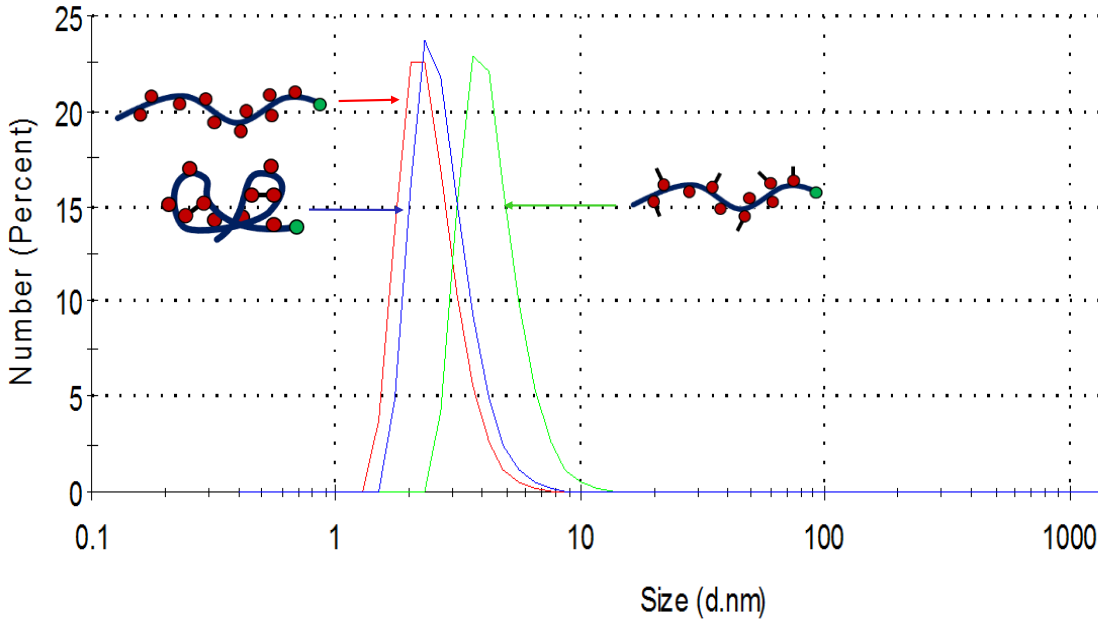

Figure 3.4 DLS for $\mathbf{B_1}$, $\mathbf{B_1^{SCNP}}$and $\mathbf{B_1^{ctr}}$ in chloroform (1 mg/mL).

3.2.2 Synthesis and folding of Triblock copolymer ($\mathbf{B_1^{SCNP}}$-$\mathbf{B_2}$-$\mathbf{B_3^{SCNP}}$)

As demonstrated, folding of the polymer increases steric hindrance, which will inhibit the addition of monomers to the macro-CTA. Consequently, the polymerization rate of the

chain extension will be slower as compared to the polymerization of the first block at same conditions. Therefore, more initiator was required to reach full monomer conversions.

However, an increase in the propagating radical concentration will increase the termination rate and hence decrease the fraction of living chains.[60] The high livingness of the polymer chains is of paramount importance for the chain extension in order to produce multi-block copolymers. Therefore, full conversion of the monomers for the chain extensions was not targeted after the first folding process. Since $\mathbf{B_1^{SCNP}}$ contains hydrophobic MDI moieties, the polymer was water insoluble. In the following chain extensions, dioxane was used as solvent. As shown in **Scheme 3.1**, $\mathbf{B_1^{SCNP}}$ was first chain extended with a block of Poly(NAM) ($\mathbf{B_1^{SCNP}}$-$\mathbf{B_2}$) at 70 °C (**Figure 3.18**). The DP of NAM was targeted to be 20. The monomer conversion was found to be 62% by ^{1}H NMR spectroscopy after 24 h of polymerization. Analysis of the molar mass distributions of $\mathbf{B_1^{SCNP}}$-$\mathbf{B_2}$ by SEC revealed mono-modal distribution with a clear shift to higher molar mass relatively to $\mathbf{B_1^{SCNP}}$ (from 4,800 g mol^{-1} to 7,000 g mol^{-1}, **Table 3.1**, **Figure 3.5**).

In order to skip purification, the polymerization mixture of $\mathbf{B_1^{SCNP}}$-$\mathbf{B_2}$ was used directly for the next chain extension. The next block ($\mathbf{B_3}$) was targeted to have the same composition as the first block ($\mathbf{B_1}$). After 24 h of polymerization, the conversions of NAM and HEA, determined by ^{1}H NMR spectroscopy, were 77% and 76%, respectively. Analysis of the purified $\mathbf{B_1^{SCNP}}$-$\mathbf{B_2}$-$\mathbf{B_3}$ by ^{1}H NMR spectroscopy (**Figure 3.19**) revealed a DP of 8 for HEA and 29 for NAM, slightly lower than expected due to the 77% of conversion of the reaction. The SEC trace of the purified $\mathbf{B_1^{SCNP}}$-$\mathbf{B_2}$-$\mathbf{B_3}$ displayed mono-modal size distribution and a narrow dispersity ($M_{n,SEC}$ = 11,100, $Đ$ = 1.15, **Table 3.1**, **Figure 3.5**) with a clear shift to higher molar mass relative to $\mathbf{B_1^{SCNP}}$-$\mathbf{B_2}$. The folding process of $\mathbf{B_1^{SCNP}}$-$\mathbf{B_2}$-$\mathbf{B_3}$ was carried out using the same conditions used for the synthesis of $\mathbf{B_1^{SCNP}}$ and was monitored by SEC and ^{1}H NMR spectroscopy.

As expected, the SEC trace of the polymer after cross linking reaction revealed a mono-modal chromatogram with a shift toward lower molar mass species relative to the SEC trace of the parent copolymer of $\mathbf{B_1^{SCNP}\text{-}B_2\text{-}B_3}$ (from 11,100 g mol^{-1} to 9,400 g mol^{-1}, **Figure 3.5**, **Table 3.1**). This result indicates that the hydrodynamic volume has decreased due to the cross linking reaction. According to the previous results on $\mathbf{B_1^{SCNP}}$, this reduction in hydrodynamic volume was attributed to the intra-polymer cross-linking through covalent and supramolecular cross-linking.

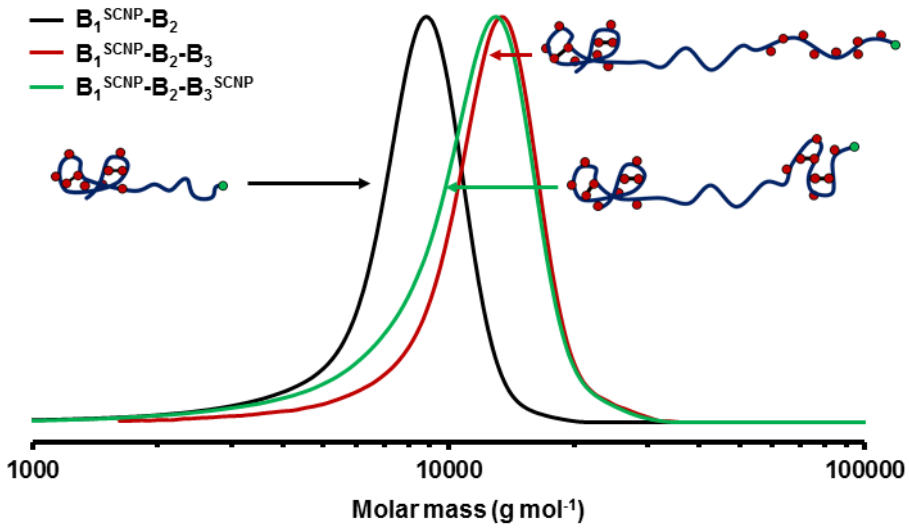

Figure 3.5 SEC chromatograms (RI traces) of $\mathbf{B_1^{SCNP}\text{-}B_2}$, $\mathbf{B_1^{SCNP}\text{-}B_2\text{-}B_3}$ and $\mathbf{B_1^{SCNP}\text{-}B_2\text{-}B_3^{SCNP}}$ in $CHCl_3$.

The folding process was further analysed by ^{1}H NMR spectroscopy of the obtained products (**Figure 3.6**). By comparing the integrals of the MDI with the polymer backbone it was observed that (in addition to the cross linker attached to first block) 2.4 equivalents of MDI have reacted with the polymer bearing 42% of urethane units, 41% of urea units and 17% of primary amines. These values are comparable to the ratios observed for the first folding process and suggest a similar tendency to covalent and H-bond mediated cross linking. The steric hindrance after the folding of the polymer is expected to drastically reduce the reactivity of the

remaining –OH of the first block of **B₁^SCNP-B₂-B₃** with the cross linker. It is, therefore, reasonable to assume that the second folding process only occurs within the third (**B₃**) block.

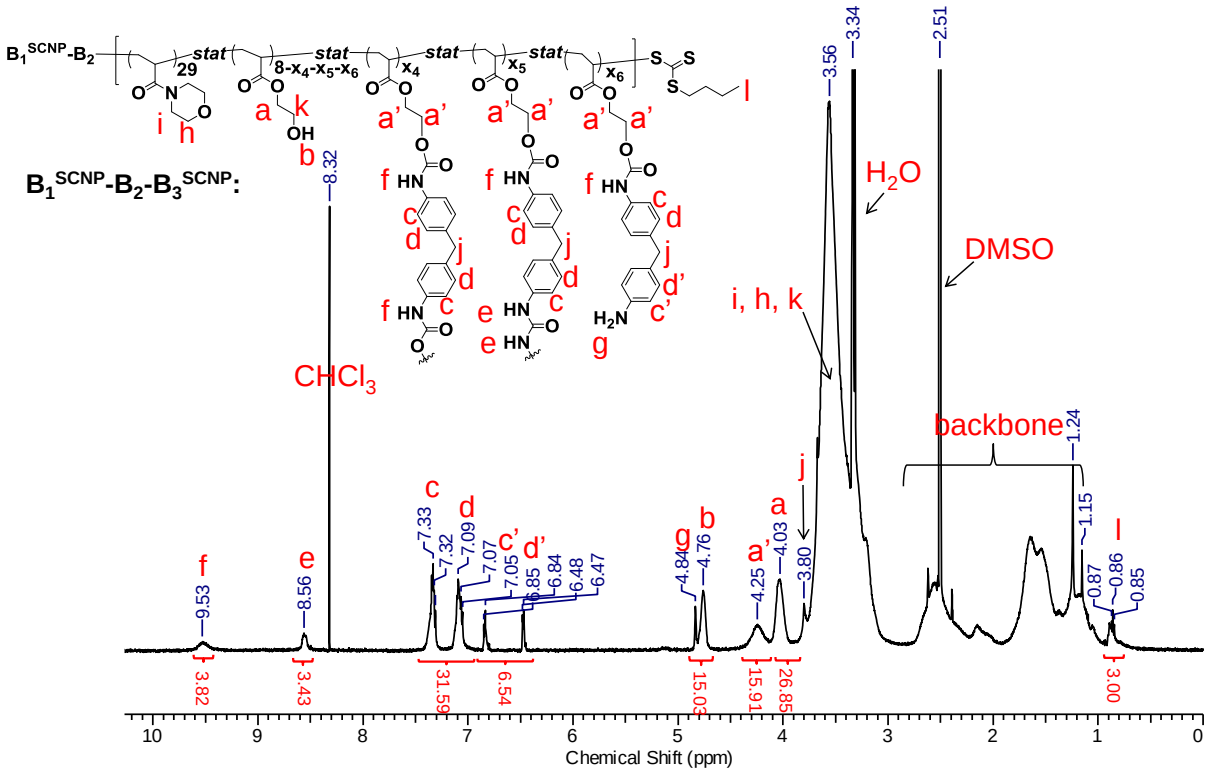

Figure 3.6 ^{1}H NMR spectrum (DMSO-d_6, 600MHz) of single chain nanoparticles **B₁^SCNP-B₂-B₃^SCNP**.

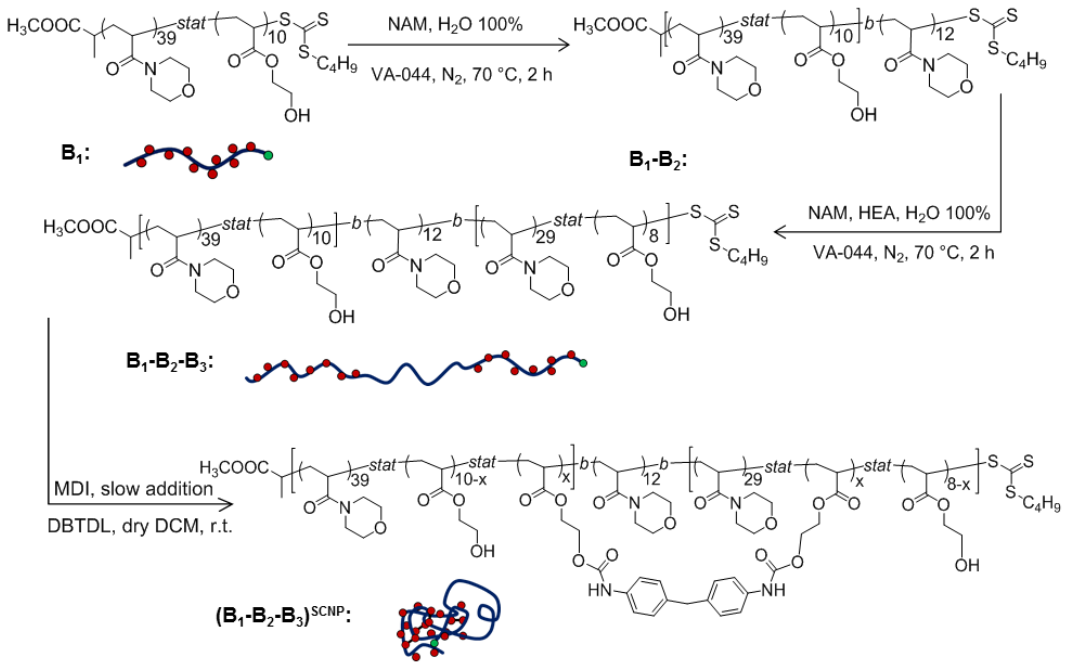

Scheme 3.3 Schematic representation of the folding of **B₁-B₂-B₃**.

In order to illustrate this assumption, a triblock linear copolymer of **B_1-B_2-B_3** (P(NAM_{39}-*stat*-HEA_{10})-*b*-$PNAM_{12}$-*b*-($PNAM_{29}$-*stat*-$PHEA_8$)) which has the same monomer composition as **B_1^{SCNP}-B_2-B_3** was synthesized (**Scheme 3.3, Figures 3.20**, **3.21** and **3.22**). This triblock copolymer was then folded using standard conditions. The folding process was studied by ^{1}H NMR spectroscopy and SEC analysis.

The ^{1}H NMR spectrum of the cross linked material of **$(B_1$-B_2-$B_3)^{SCNP}$** reveals a slight decrease of the amount of attached MDI as compared to **B_1^{SCNP}-B_2-B_3^{SCNP}**. However, a similar ratio between urethanes, urea and amines was observed (**Table 3.1**, **Figure 3.7**). Hence, a slightly decreased degree of cross linking (covalent and supra molecular) for **$(B_1$-B_2-$B_3)^{SCNP}$** as compared to **B_1^{SCNP}-B_2-B_3^{SCNP}** can be assumed.

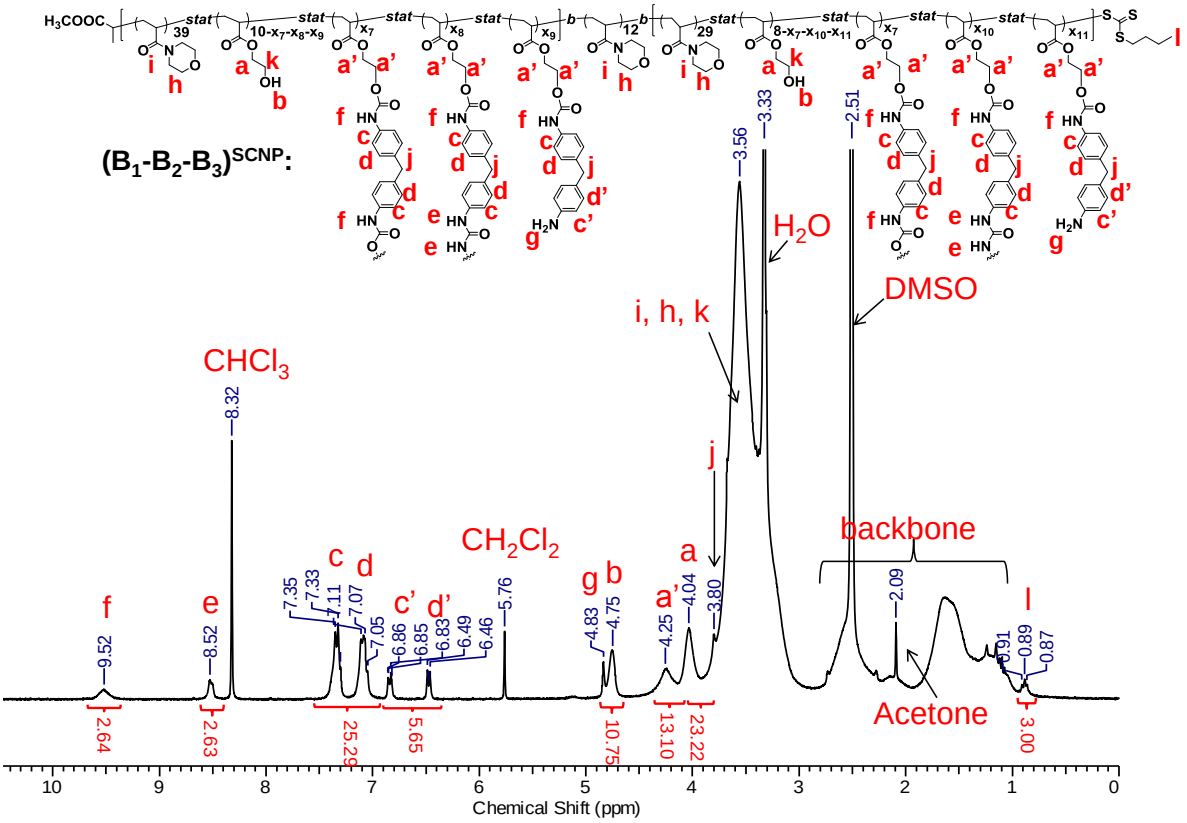

Figure 3.7 ^{1}H NMR spectrum (DMSO-d_6, 400MHz) of single chain nanoparticles **$(B_1$-B_2-$B_3)^{SCNP}$**.

The SEC trace of **$(B_1$-B_2-$B_3)^{SCNP}$** displays a mono-modal chromatogram possessing a shift to lower molar mass compared to the linear precursor **B_1-B_2-B_3** (from 12,100 g mol^{-1} to

8,400 g mol^{-1}, **Figure 3.8**, **Table 3.1**). Most importantly, the shift in hydrodynamic volume is more pronounced for **(B$_1$-B$_2$-B$_3$)^{SCNP}** as compared to **B$_1^{SCNP}$-B$_2$-B$_3^{SCNP}$** (**Figure 3.8**) indicating the formation of one SNCP instead of two particles connected by a P(NAM) block as assumed for **B$_1^{SCNP}$-B$_2$-B$_3^{SCNP}$**. This is further supported by the fact that the linear precursor (**B$_1$-B$_2$-B$_3$**) possesses a higher hydrodynamic volume as compared to **B$_1^{SCNP}$-B$_2$-B$_3$**. Additionally, the lower degree of cross linking as determined from ^{1}H-NMR spectroscopy in combination with the decreased hydrodynamic volume of **(B$_1$-B$_2$-B$_3$)^{SCNP}** compared to **B$_1^{SCNP}$-B$_2$-B$_3^{SCNP}$** illustrates the difference between the SCNP obtained by sequential and global folding. All the above results indicate the presence of two distinct folded subdomains within **B$_1^{SCNP}$-B$_2$-B$_3^{SCNP}$** linked by a P(NAM) spacer.

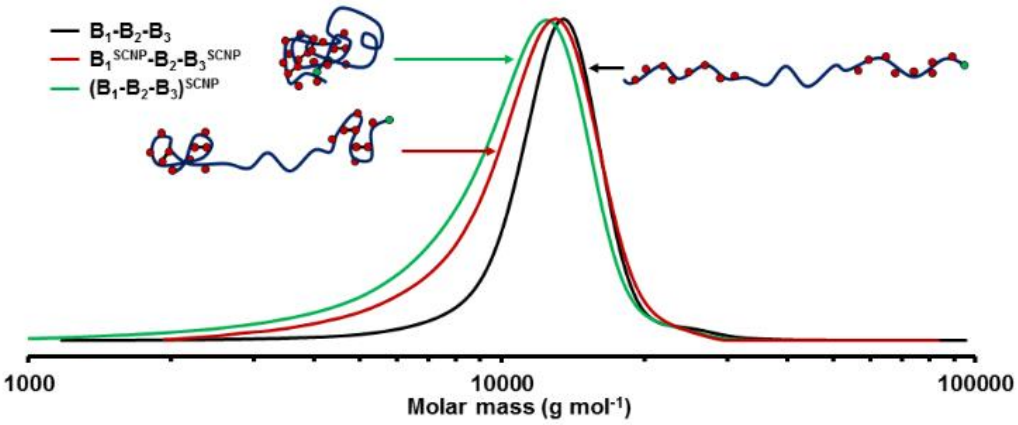

Figure 3.8 Overlay of SEC chromatograms (RI traces) obtained in $CHCl_3$ for **B$_1^{SCNP}$-B$_2$-B$_3^{SCNP}$, B$_1$-B$_2$-B$_3$,** and **B$_1$-B$_2$-B$_3$)^{SCNP}.**

3.2.3 Synthesis and folding of Penta-block copolymer (B$_1^{SCNP}$-B$_2$-B$_3^{SCNP}$-B$_4$-B$_5^{SCNP}$)

To explore the potential of the approach, a third chain-extension-folding cycle was attempted. The macro-CTA **B$_1^{SCNP}$-B$_2$-B$_3^{SCNP}$** containing two folded domains was first chain extended with a further spacer block (NAM, **B$_4$**, DP = 12). Again, a DP of 20 was targeted and

63% of monomer conversion was achieved after 24 h (**Figure 3.23**). The polymerization was continued after addition of HEA and NAM, to produce the last foldable block with conversions of 85% (NAM) and 84% (HEA), respectively (**B_5**, NAM_{41}-stat-HEA_8, **Figure 3.24**).

The SEC traces of both chain extensions displayed mono-modal distribution possessing a clear shift to higher molar mass from **B_1^{SCNP}-B_2-B_3^{SCNP}** to **B_1^{SCNP}-B_2-B_3^{SCNP}-B_4** and from **B_1^{SCNP}-B_2-B_3^{SCNP}-B_4** to **B_1^{SCNP}-B_2-B_3^{SCNP}-B_4-B_5**, respectively (**Figure 3.9**, **Table 3.1**).

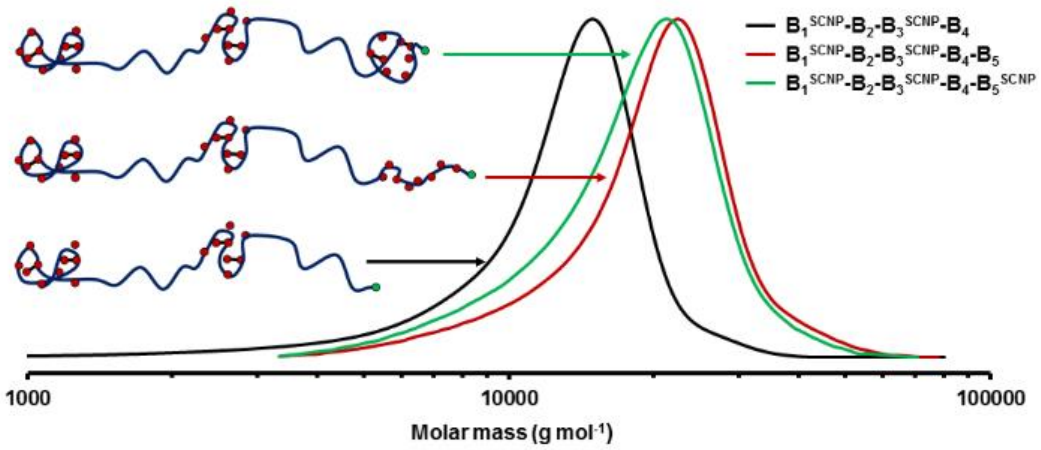

Figure 3.9 Overlay of SEC chromatograms (RI traces) obtained in $CHCl_3$ for: **B_1^{SCNP}-B_2-B_3^{SCNP}-B_4, B_1^{SCNP}-B_2-B_3^{SCNP}-B_4-B_5^{SCNP}**, and **B_1^{SCNP}-B_2-B_3^{SCNP}-B_4-B_5.**

The folding process of the 5th block was carried out using established conditions. After cross linking, the SEC trace in chloroform shows a shift toward lower molar mass species (from 17,500 g mol^{-1} to 16,000 g mol^{-1}, $Đ$ = 1.21, **Figure 3.9, Table 3.1**), indicating the formation of a third SCNP.

The obtained material was also characterized by ^{1}H NMR spectroscopy (**Figure 3.10**). Similar to the previous two folding process, the integrals of MDI associated aromatic peaks suggests the addition of two further cross linker molecules. In contrast to previous folding steps, the amount of resulting primary amine functions increased only slightly and more urethane bonds were formed, indicating a higher degree of covalent cross linking for the last

block, which could be the result of a lower overall amount of water during cross linking reaction.

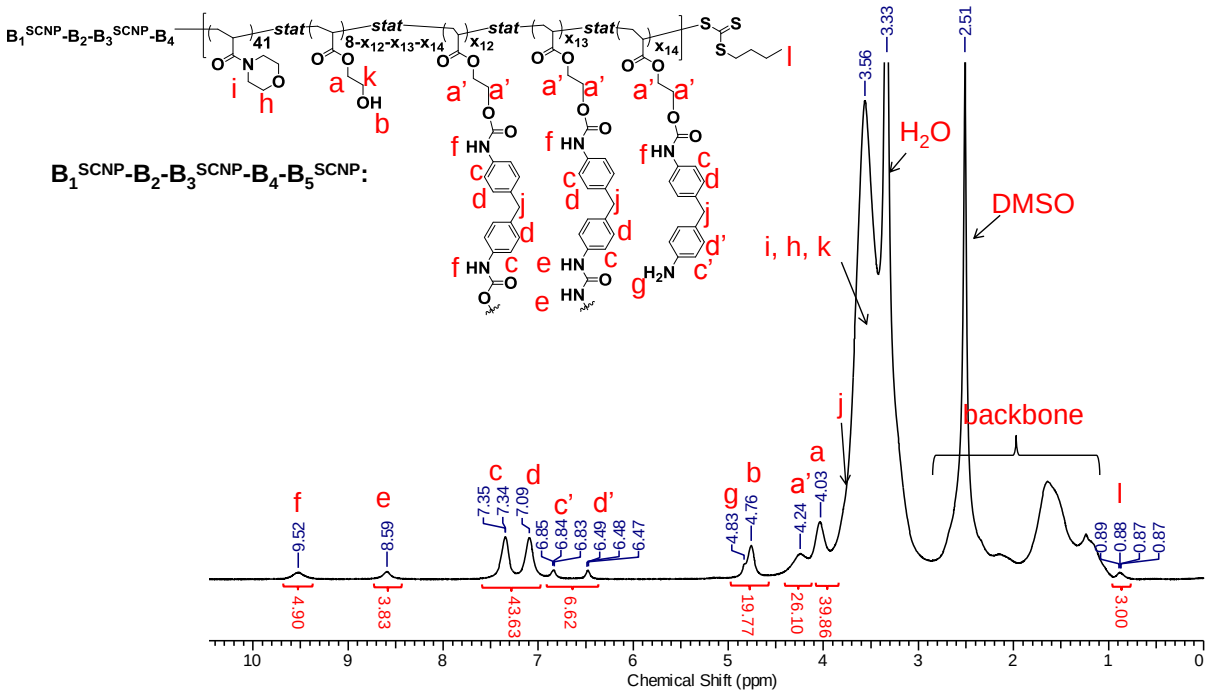

Figure 3.10 ^{1}H NMR spectrum (DMSO-d_6, 400MHz) of single chain nanoparticles **B_1^{SCNP}-B_2-B_3^{SCNP}-B_4-B_5^{SCNP}**.

Based on the above results, it can also be concluded that this folding process is only within the fifth block **B_5**. In order to demonstrate this, the penta-block based SCNP (**B_1^{SCNP}-B_2-B_3^{SCNP}-B_4-B_5^{SCNP}**) was dissolved in DMF (200 mg mL^{-1}) to break the hydrogen bonds stabilizing the SCNP structure, followed by the dilution with chloroform (to 0.7 mg mL^{-1}). The dilution of DMF with a solvent, which doesn't interfere with H-Bond formation should lead to the unspecific reformation of cross linking and a change in hydrodynamic volume. This was illustrated by comparing the SEC traces of the initial SCNP (**B_1^{SCNP}-B_2-B_3^{SCNP}-B_4-B_5^{SCNP}**) and the DMF annealed material in $CHCl_3$ (**Figure 3.11**). The change in elution behaviour shows that the partial interruption of H-bonds by the DMF leads to an increase in compaction after re-cross linking. These results indicate the existence of three individual folded SCNP within the polymer.

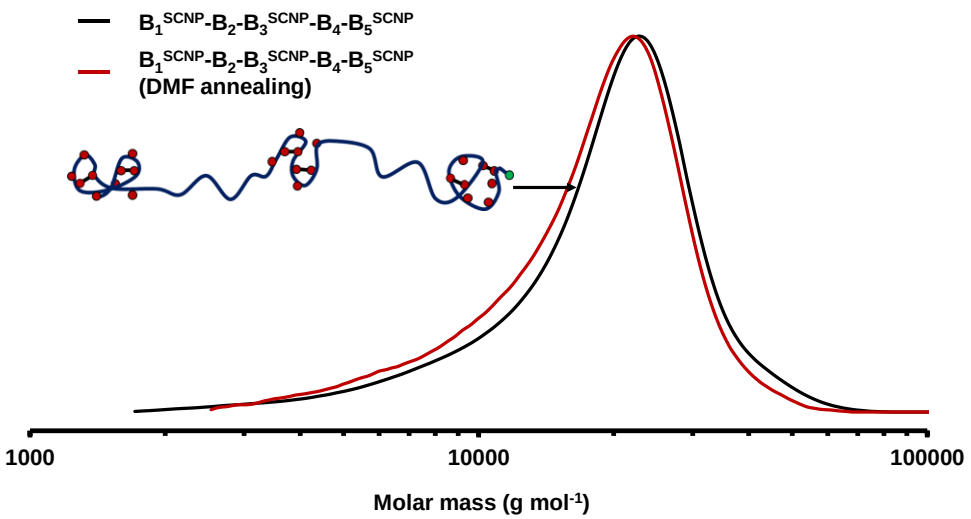

Figure 3.11 Overlay of SEC chromatograms (RI traces) obtained in $CHCl_3$ for penta-block based SCNP (**B_1^{SCNP}-B_2-B_3^{SCNP}-B_4-B_5^{SCNP}**) before and after treatment with DMF sample.

Having confirmed the formation of the penta-block based SCNP (**B_1^{SCNP}-B_2-B_3^{SCNP}-B_4-B_5^{SCNP}**) which has three individually cross-linked subdomains, the final material was also characterized by AFM. Diluted chloroform or dichloromethane solutions of **B_1^{SCNP}-B_2-B_3^{SCNP}-B_4-B_5^{SCNP}** at 1 µg mL^{-1} were drop-deposited onto freshly cleaved mica disc. **Figure 3.12** showed height map images of the cast surface with a scan size of 1 µm. This figure displays that these SCNPs have a height (from the particle peak to the surface of the mica disc) of around 6-8 nm. These size values are relatively high for the described materials,[26, 61] which could indicate aggregation, although similar heights have been reported for AFM profiles of SCNPs.[33] A stiffening of the nanostructure caused by the combination of covalent and supramolecular cross linking could explain the measured height profile of **B_1^{SCNP}-B_2-B_3^{SCNP}-B_4-B_5^{SCNP}** considering size determined by DLS for a single folded subdomain ($R_h \approx 3$ nm). However, the feature of three folded subdomains could not be observed in the image. One possible reason might be the insufficient length of the spacer block leading to an aggregation of the single domains after deposition. Furthermore, the complex sample casting process caused by the dewetting effects and evaporative self-assembly[31, 61, 62, 34] resulted the single

chain shrink. Nevertheless, the morphology of the SCNPs is expected to be the characteristic sparse “pearl necklace”shape which has been demonstrated by Pomposo and coworkers since the SCNPs were synthesized from the self-avoiding character of the folding blocks in good solvent.[63]

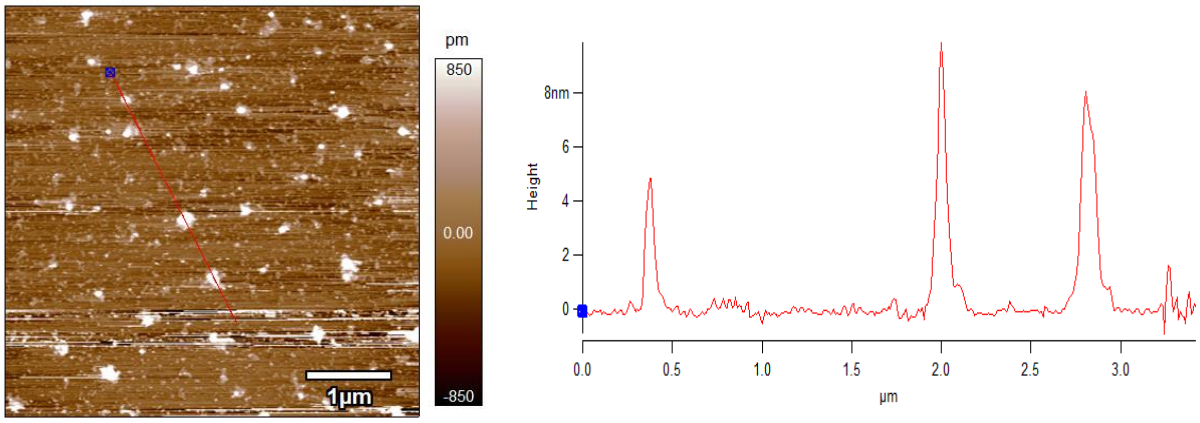

Figure 3.12 AFM topography image of penta-block based SCNP $\mathbf{B_1}^{\mathbf{SCNP}}\mathbf{\text{-}B_2\text{-}B_3}^{\mathbf{SCNP}}\mathbf{\text{-}B_4\text{-}B_5}^{\mathbf{SCNP}}$ (1 µm× 1 µm scan size, sample dissolved in chloroform).

3.3 Conclusions

In summary, a complex penta-block containing three individual SCNP segments with an overall dispersity of 1.21 was synthesized using RAFT polymerization. Foldable block consists of a mixture of NAM and HEA, while for polymerization of spacer blocks only NAM was used. The OH groups of HEA were cross-linked using a *bis*-isocyanate (MDI) to obtain covalently cross-linked SCNP, which in turn also resulted in the formation of urea, as well as amine functions in the cross-linked sections. These moieties were able to further stabilize the SCNP due to hydrogen bonding interactions which were evidenced by ^{1}H-NMR spectroscopy. Control experiments using mono-isocyanates, which are not able to cross link covalently, did solely result in urethane groups, which were not able to form SCNP by supramolecular interaction. Therefore, it was concluded that described SCNP are stabilized by a synergistic interaction between covalent and supramolecular cross linking.

A chain extension-folding sequence was used to create polymers chains having up to three individual SCNP segments. The cross linking between blocks was ruled out by control experiments using a non-sequential folding procedure. Dissolving the penta-block-tri-SCNP in DMF to interrupt supramolecular connections followed by the dilution in chloroform to reform hydrogen bonds revealed a decreased hydrodynamic volume of DMF annealed sample by SEC analysis in $CHCl_3$ which illustrates the importance of hydrogen bonding, as well as the existence of individual folded domains within the parent penta-block.

This strategy represents a highly versatile way to produce multi-block SCNP which enables the folding of individual domains within polymer chains. This feature is a further step on the way to copy nature's ability to synthesize highly defined bio-macromolecules with a distinct three dimensional structure. Further work will focus on the introduction of different functionalities enabling orthogonal folding and unfolding within single macromolecules.

3.4 Experimental

3.4.1 Materials

Milli-Q water was used as the solvent for polymerizations. 1, 4-Dioxane was obtained from Fisher Scientific and used as received. Silica gel for column chromatography was Merck Kieselgel 60 (230-400 mesh, ASTM). 4-acryloylmorpholine (NAM, Sigma-Aldrich, 97%) was filtered through a basic aluminium oxide (activated, basic, BrockmannI, standard grade, B150 mesh, 58Å) column before use to remove the radical inhibitor. 2-Hydroxyethyl acrylate (HEA, 96%) was obtained from Sigma Aldrich. HEA was purified following a previously reported protocol.[64] 2, 2′-Azobis[2-(2-imidazolin-2-yl)propane]dihydrochloride (VA-044, Wako) was used without further purification. Dimethyl 2, 2'-azobis(2-methylpropionate) (V601) was used without further purification. All polymerizations were carried out under a nitrogen atmosphere.

4, 4′-Methylenebis(phenyl isocyanate) (MDI, 98%) and *p*-Tolyl isocyanate was obtained from Sigma Aldrich and used as received. Diethyl ether (99.8%), anhydrous DCM (99.8%), methanol (99.6%), 1-(3-Dimethylaminopropyl)-3-ethylcarbodiimide hydrochloride (EDC •HCl, 98%), 4-dimethylaminopyridine (DMAP, 99%) and dibutyltin dilaurate (DBTDL, 95%) were obtained from Sigma Aldrich and used as received. Chloroform-*d* ($CDCl_3$, 99.8% D atom) and dimethyl sulfoxide-d6 (DMSO-d_6, 99.9% D atom) obtained from Sigma Aldrich were used for ^{1}H NMR analysis. 2-(((butylthio)-carbonothioyl)thio)propanoic acid (called (propanoic acid)yl butyl trithiocarbonate (PABTC) in this paper) was prepared according to a previously reported procedure.[65]

3.4.2 Methods

3.4.2.1 Nuclear Magnetic Resonance (NMR) spectroscopy (^{1}H NMR and ^{13}C NMR)

Spectra were recorded on a Bruker Avance III HD 400 spectrometer (400 MHz for proton and 100MHz for carbon) or a Bruker Avance III 600 (600 MHz for proton) at 27 °C in deuterated chloroform ($CDCl_3$) or deuterated DMSO (DMSO-d_6). Chemical shift values (δ) are reported in ppm. The residual proton signal of the solvent (δ_H = 7.26 ppm in $CDCl_3$, δ_H = 2.51 ppm in DMSO-d_6) was used as internal reference. For ^{13}C NMR, the carbon signal of the solvent (δ_C = 77.03 ppm in $CDCl_3$) was used as internal reference.

3.4.2.2 Size Exclusion Chromatography (SEC)

Number-average molar masses ($M_{n,SEC}$) and dispersity values ($Đ$) were determined using size exclusion chromatography with either $CHCl_3$ or DMF as an eluent. The $CHCl_3$ Agilent 390-LC MDS instrument was equipped with differential refractive index (DRI), and two wavelength UV detectors. The system was equipped with 2 x PLgel Mixed D columns (300 x

7.5 mm) and a PLgel 5 µm guard column. The eluent is $CHCl_3$ with 2 % TEA (triethylamine) additive. Samples were run at 1 mL min^{-1} at 30 °C. Poly(methyl methacrylate) ranging from MW = 550 g mol^{-1} to 955000 g mol^{-1} and polystyrene standards ranging from MW = 380 g mol^{-1} to 508000 g mol^{-1} (Agilent Easy Vials) were used for calibration. H_2O or Ethanol was used as a flow rate marker. Analyte samples were filtered through a PVDF membrane with 0.22 µm pore size before injection. Respectively, experimental molar mass ($M_{n,SEC}$) and dispersity ($Đ$) values of synthesized polymers were determined by conventional calibration using Agilent GPC/SEC software. The DMF Agilent 390-LC MDS instrument equipped with differential refractive index (DRI), viscometry (VS), dual angle light scatter (LS) and dual wavelength UV detectors. The system was equipped with 2 x PLgel Mixed D columns (300 x 7.5 mm) and a PLgel 5 µm guard column. The eluent is DMF with 5 mmol NH_4BF_4 additive. Samples were run at 1 mL min at 50 °C. Poly(methyl methacrylate) standards (Agilent EasyVials) ranging from MW = 550 g mol^{-1} to 955000 g mol^{-1} were used for calibration. Analyte samples were filtered through a nylon membrane with 0.22 µm pore size before injection. Respectively, experimental molar mass ($M_{n,SEC}$) and dispersity ($Đ$) values of synthesized polymers were determined by conventional calibration using Agilent GPC/SEC software.

3.4.2.3 Differential Scanning Calorimetry (DSC)

The experiments were performed to determine the thermal behavior of the synthesized polymers on a Mettler Toledo DSC1. In all tests, a scan rate of 10 K/min was used in the temperature range of -30 to 180 °C for three heating and cooling cycles. The T_g value is the maxima of the the first derivative of (d_H/d_T).

3.4.2.3 Dynamic Light Scattering (DLS)

The DLS measurements were performed on a MALVERN Instrument operating at 25 °C with a 633-nm laser module. Measurements were made at a detection angle of 173° (back scattering). The polymer solutions were prepared by dissolving the polymer samples in chloroform (1 mg/mL), which were filtered through a PVDF membrane with 0.22 μm pore size before being analysed.

3.4.2.4 Atomic Force Microscopy (AFM)

AFM images were acquired in AC mode on a Cypher S system (Oxford Instruments Asylum Research). The probes used were the AC160TS from Olympus probes with a nominal resonant frequency of 300 kHz and a spring constant of approximately 40 N m^{-1} on a Multimode AFM (Oxford Instruments Asylum Research). Images were acquired over a scan size of 1 μm at a pixel resolution of 512 and a scan rate of 1 Hz. Samples were diluted to 1 μg mL^{-1} in chloroform or dichloromethane and 10 μL of solution was drop-deposited onto freshly cleaved mica discs. The data were analyzed by the Asylum Research software.

3.4.2.5 Determination of monomer conversions

The conversions of the monomers were determined by comparing the integration of the vinyl protons (δ ~ 6.50–5.50 ppm) to the integration of the three methyl protons belonging to the Z group of the MPABTC chain transfer agent (–CH_2–CH_3) or by comparing the integration of the vinyl protons (δ ~ 6.50–5.50 ppm) before and after reaction using mesitylene as external reference.

3.4.2.6 General procedures for copolymer synthesis by RAFT polymerization

CTA, monomer and azoinitiator were charged into a flask having a magnetic stirring bar. The flask wass sealed with a rubber septum and degassed with nitrogen for 15 min. The solution was then allowed to stir at the desired temperature in a thermos-stated oil bath for the desired time. After reaction, the mixture is cooled down in cold water to room temperature and open under air. A sample is taken for ^{1}H NMR (to determine monomer conversion) and SEC analysis (to determine $M_{n.SEC}$ and $Đ$). See the supporting information for detailed procedure.

3.4.2.7 General procedures for the synthesis of single chain nanoparticles (SCNP)

The copolymer precursor was dissolved in dry DCM ($[OH]_0$= 0.01 M). MDI (0.5 eq. of n(-OH)) was dissolved in dry DCM (the volume of the solution of MDI was kept the same with the volume of the solution of the polymer). DBTDL was added to the solution of MDI as catalyst. Both the solution of copolymer precursor and MDI were degassed by N_2 for 5 min. Subsequently, the solution of the copolymer precursor was added to the solution of MDI (with vigorous stirring) at 2 mL h^{-1} using a syringe pump at room temperature. After addition of the solution of the copolymer precursor, the reaction mixture was left for 2 h to let the reaction to complete. Then excess amount of methanol was added to the reaction mixture to quench unreacted MDI. Subsequently, the reaction mixture was evaporated to dryness under reduced pressure. Then the crude product was dissolved in minimum amount of DCM and precipitated in diethyl ether. See the supporting information for detailed procedure.

3.4.3 Synthesis.

3.4.3.1 Synthesis of RAFT agent methoxy-(propanoic acid)yl butyl trithiocarbonate (MPABTC)

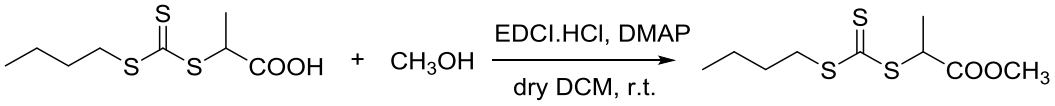

Scheme 3.4 Synthetic route of MPABTC.

(Propanoic acid)yl butyl trithiocarbonate (PABTC) (1.07 g, 4.49 mmol) was dissolved in 20 mL dry DCM. CH_3OH (0.22 g, 6.86 mmol) and 4-dimethylaminopyridine (DMAP, 0.11g, 0.90 mmol) were added to the above solution. 1-Ethyl-3-(3-dimethylaminopropyl)carbodiimide hydrochloride (EDC x HCl, 1.03 g, 5.37 mmol) was dissolved in 10 mL dry DCM and added dropwise to the above solution over 30 minutes. Then the reaction mixture was kept stirring for 24 hours at room temperature. Then the solvent was evaporated under reduced pressure. The crude product was dissolved in 100 mL DCM and transferred into a separating funnel and washed by H_2O (2 × 80 mL) and brine (80 mL). The organic layer was dried with $MgSO_4$, filtered and evaporated to dryness under reduced pressure. The crude product was purified by column chromatography [SiO_2, Hexane-EtOAc (10:3)] to afford MPABTC as a yellow liquid (0.90 g, 79 %). ^{1}H NMR (400 MHz, $CDCl_3$, ppm): δ= 0.92 (*t*, 3H, *J* = 8.0 Hz), 1.39-1.48 (*m*, 2H), 1.59 (*d*, 3H, *J* = 8.0 Hz), 1.63-1.72 (*m*, 2H), 3.35 (*t*, 2H, *J* = 8.0 Hz), 3.75 (*s*, 3H), 4.82 (*q*, 1H, *J* = 8.0 Hz); ^{13}C NMR (100 MHz, $CDCl_3$, ppm): δ= 222.04, 171.69, 52.88, 47.73, 36.99, 29.93, 22.07, 16.96, 13.60.

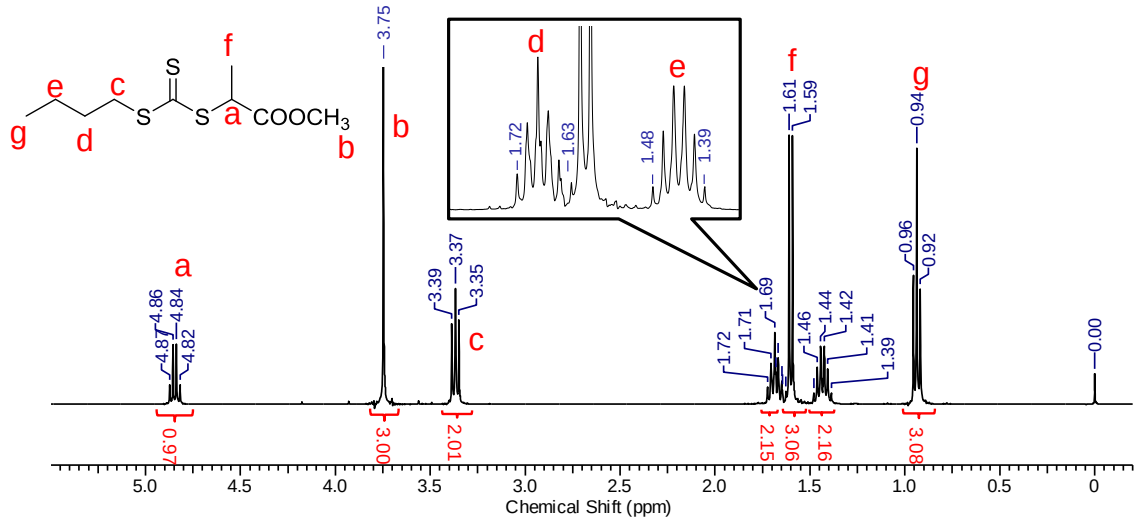

Figure 3.13 ^{1}H NMR spectrum (400 MHz, $CDCl_3$) of MPABTC.

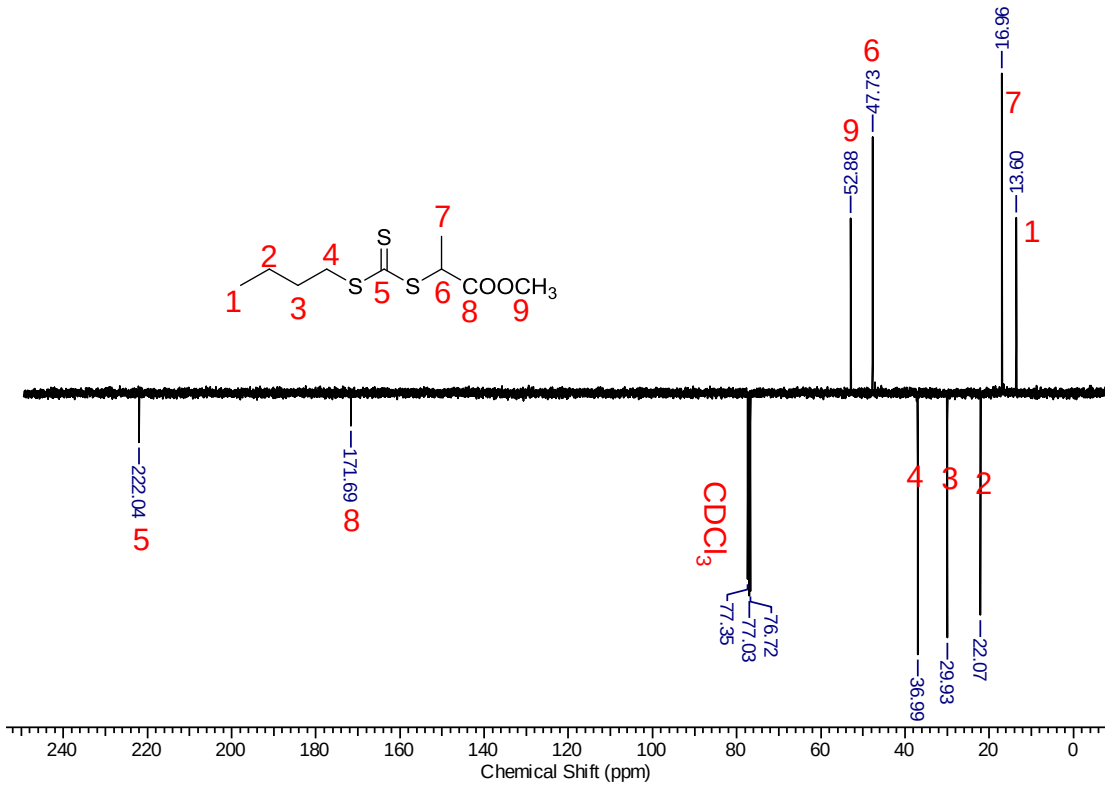

Figure 3.14 ^{13}C NMR spectrum (100 MHz, $CDCl_3$) of MPABTC.

3.4.3.2 Synthesis of linear copolymer B_1

MPABTC (0.076 g, 0.3 mmol, 1.0 eq.), NAM (1.70 g, 12 mmol, 40 eq.), HEA (0.35 g, 3 mmol, 10 eq.), VA-044 (0.5 mg, 0.0015 mmol, 0.005 eq.), 1, 4-dioxane (0.62 mL) and H_2O

(1.41 mL) were introduced into a flask equipped with a magnetic stirrer and sealed with a rubber septum. The flask was degassed by bubbling nitrogen through the solution for 15 minutes, and placed into a preheated oil bath at 70 ˚C. After 2 h, the reaction was stopped by cooling the mixture down using a cold water bath. Subsequently, a sample was taken from the reaction mixture for ^{1}H NMR analysis to determine the conversion. Then the solvent was removed under reduced pressure. And the crude polymer was dissolved in 1 mL of methanol and precipitated in diethyl ether (300 mL). The polymer was then filtered off and dried under vacuum to yield a yellow powder. The monomer conversion was determined after polymerization by ^{1}H NMR by comparing the integration of the vinyl protons (δ ~ 6.50–5.50 ppm) to the integration of the three methyl protons belonging to the Z group of the MPABTC chain transfer agent (–CH_2–CH_3) and the obtained monomer conversion was 98% for both monomers. The linear polymer **B$_1$** (Poly(NAM$_{39}$-*stat*-HEA$_{10}$)) was analyzed by SEC in $CHCl_3$. $M_{n,SEC}$ = 6200 g mol^{-1}, $Đ$ = 1.12. ^{1}H-NMR (400 MHz, DMSO-d_6, ppm): δ= 5.13 (*s*, *broad*, *weak*, CH-S), 4.76 (*s*, OH), 4.03 (*s*, –(C=O)–O–C***H*$_2$**–CH_2–OH), 3.57 (*s*, CH_2 polymer, –(C=O)–O-CH_2–C***H*$_2$**–OH polymer), 2.80-1.00 (*m*, CH and CH_2 backbone, CH_3 R-group, CH_2 Z-group), 0.87 (*t*, 3H, *J* = 8.0 Hz, CH_3 Z-group).

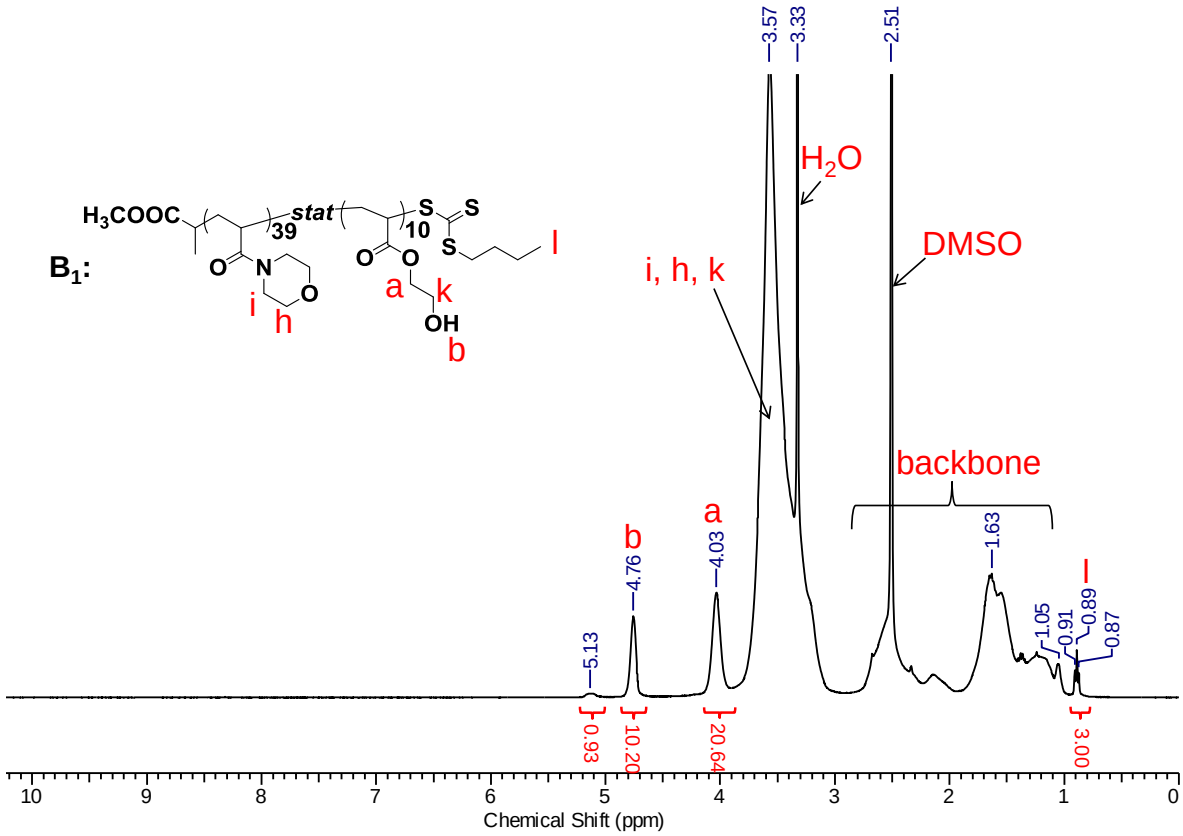

Figure 3.15 ^{1}H NMR spectrum (DMSO-d_6, 400MHz) of linear polymer **B$_1$**.

3.4.3.3 Synthesis of copolymer B_1^{SCNP}

The copolymer **B$_1$** (0.332 g, 0.048 mmol) was dissolved in 48 mL dry DCM. MDI (0.06 g, 0.24 mmol, 0.5 eq. of n(-OH)) was dissolved in 48 mL dry DCM. DBTDL (0.530 g, 0.5 mL, 0.83 mmol) was added to the solution of MDI as a catalyst. Both the solution of copolymer **B$_1$** and MDI were degassed by N_2 for 5 minutes. Then the solution of the copolymer **B$_1$** was added to the solution of MDI (with vigorous stirring) at 2 mL h^{-1} using a syringe pump at room temperature. After addition the reaction mixture was left for 2 h at room temperature. Subsequently, an excess of methanol (1.580 g, 2 mL, 49 mmol) was added to the reaction mixture to quench the unreacted MDI. After that the reaction mixture was evaporated to dryness under reduced pressure. The crude product was dissolved in DCM 1 mL and precipitated in diethyl ether (300 mL). The precipitate was then filtered and dried under

vacuum to yield a pale yellow powder (0.328 g). The $\mathbf{B_1}^{\mathbf{SCNP}}$ ([Poly(NAM_{39}-*stat*-HEA_{10})]^{SCNP}) was analyzed by SEC in $CHCl_3$. $M_{n,SEC}$ = 4800 g mol^{-1}, $Đ$ = 1.27. ^{1}H-NMR (400 MHz, DMSO-d_6, ppm): δ= 9.54 (*s*, *broad*,–NH–(C=O)–O–), 8.53 (*s*, –NH–(C=O)–NH–), 7.36-7.30 (*m*, CH, benzene ring), 7.13-7.05 (*m*, CH, benzene ring), 6.83 (*d*, CH, benzene ring, *J* = 8.0 Hz), 6.46 (*d*, CH, benzene ring, *J* = 8.0 Hz), 5.13 (*s*, *broad*, *weak*, CH–S), 4.85 (*s*, –NH_2), 4.78 (*s*, OH), 4.25 (*s*, –(C=O)–O-C***H*****$_2$**-C**H$_2$**-O-(C=O)-NH-), 4.03 (*s*, –(C=O)–O–C***H*****$_2$**–CH_2–OH), 3.79 (*s*, –CH_2–, corresponding to the reacted MDI), 3.56 (*s*, CH_2 polymer, –(C=O)–O–CH_2–C***H*****$_2$**–OH polymer), 2.80-0.94 (*m*, CH and CH_2 backbone, CH_3 R-group, CH_2 Z-group), 0.87 (*t*, 3H, *J* = 8.0 Hz, CH_3 Z-group).

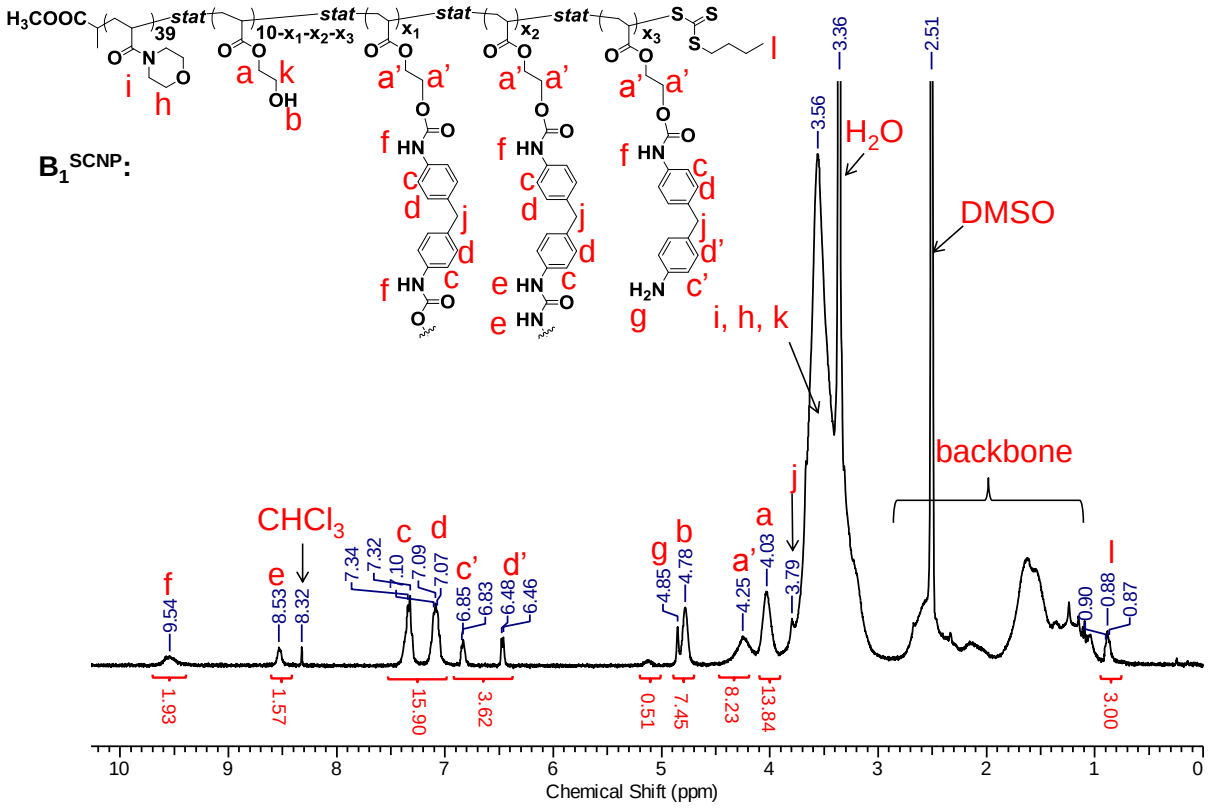

Figure 3.16 ^{1}H NMR spectrum (DMSO-d_6, 400MHz) of single chain nanoparticles $\mathbf{B_1}^{\mathbf{SCNP}}$.

3.4.3.4 Synthesis of B_1^{ctr}

The copolymer $\mathbf{B_1}$ (0.194 g, 0.028 mmol) was dissolved in 28 mL dry DCM. DBTDL (0.316 g, 0.296 mL, 0.50 mmol) was added to the solution as catalyst. *p*-Tolyl isocyanate

(0.037 g, 0.28 mmol, 1 eq. of n(-OH)) was added to the above solution. The mixture was degassed using N_2 for 5 minutes while stirring. Then the reaction mixture was kept stirring for 24 h at room temperature. An excess amount of methanol (1.580 g, 2 mL, 49 mmol) was added to the reaction mixture. After that the solvent was evaporated to dryness under reduced pressure. The crude product was dissolved in 1 mLof DCM and precipitated in diethyl ether (200 mL). The precipitate was filtered and dried under vacuum to yield a pale yellow powder (0.191 g). The $\mathbf{B_1^{ctr}}$ ([Poly(NAM$_{39}$-*stat*-HEA$_{10}$)]^{ctr}) was analyzed by SEC in $CHCl_3$. $M_{n,SEC}$ = 7500 g mol^{-1}, $Đ$ = 1.11. ^{1}H-NMR (400 MHz, DMSO-d_6, ppm): δ= 9.50 (*s*, *broad*,–NH–(C=O)–O–), 7.34 (*s*, CH, benzene ring), 7.08 (*s*, CH, benzene ring), 5.13 (*s*, *broad*, *weak*, CH–S), 4.75 (*s*, OH), 4.25 (*s*,–(C=O)–O-C***H***$_2$-C**H**$_2$-O-(C=O)-NH-), 4.03 (*s*, –(C=O)–O–C***H***$_2$–CH_2–OH), 3.54 (*s*, CH_2 polymer, –(C=O)–O–CH_2–C***H***$_2$–OH polymer), 2.80-0.94 (*m*, CH and CH_2 backbone, CH_3 R-group, CH_2 Z-group), 2.23 (*s*, benzene ring–CH_3, corresponding to the reacted *p*-Tolyl isocyanate), 0.87 (*broad*, 3H, CH_3 Z-group).

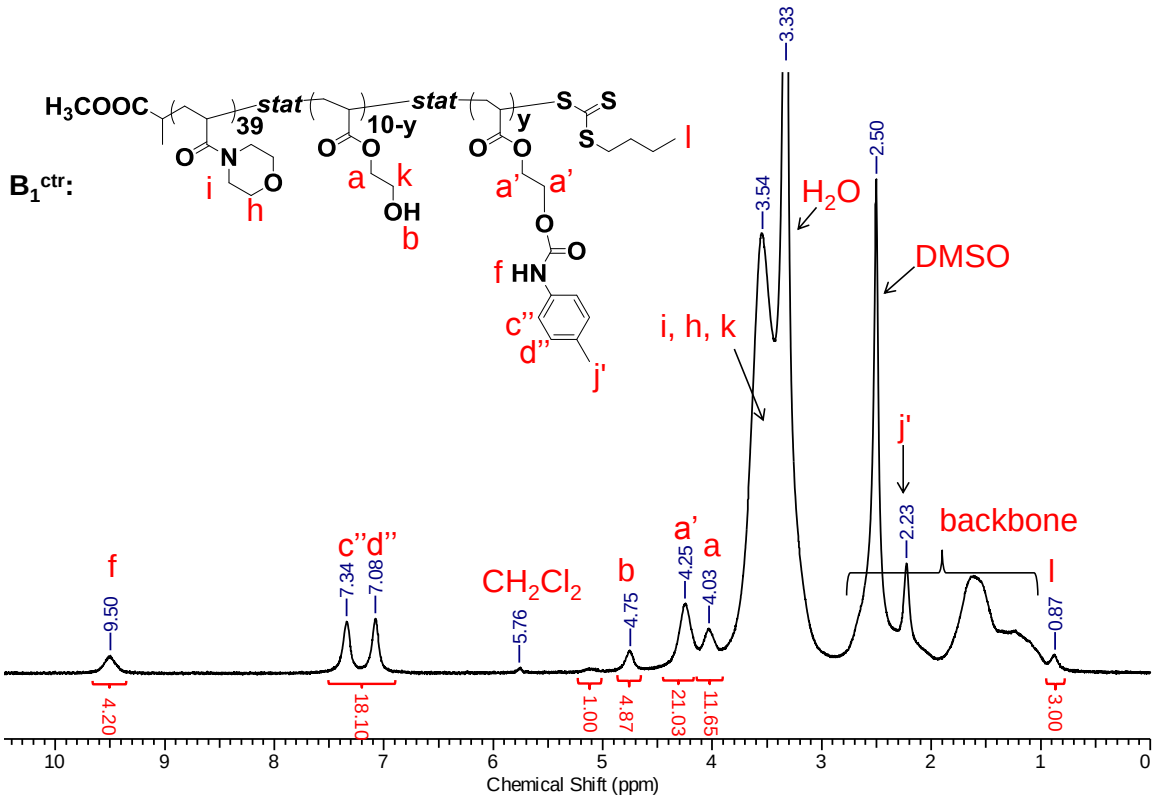

Figure 3.17 ^{1}H NMR spectrum (DMSO-d_6, 400MHz) of linear copolymer $\mathbf{B_1^{ctr}}$.

3.4.3.5 Synthesis of B_1^{SCNP}-B_2

B_1^{SCNP} (0.267 g, 0.035 mmol, 1.0 eq.), NAM (0.099 g, 0.7 mmol, 20 eq.), V-601 (0.083 mg, 0.00036 mmol, 0.01 eq.), 1, 4-dioxane (0.47 mL), mesitylene (0.01 mL, used as reference) were introduced into a flask equipped with a magnetic stirrer and sealed with a rubber septum. The flask was degassed purging with nitrogen for 15 minutes, and the flask was placed into a reheated oil bath at 70 ˚C. After 24 h, the reaction was stopped by cooling in a cold water bath. Subsequently, a sample was taken from the reaction mixture for the ^{1}H NMR and SEC analysis. The reaction mixture was used for the next chain extension without further purification. The monomer conversion was determined by ^{1}H NMR by comparing the integration of the vinyl protons (δ ~ 6.50–5.50 ppm) before and after reaction using mesitylene as reference, and the obtained monomer conversion was 62% for NAM. The polymer **B_1^{SCNP}-B_2** ([Poly(NAM$_{39}$-*stat*-HEA$_{10}$)]^{SCNP}-*b*-polyNAM$_{12}$) was analyzed by SEC in $CHCl_3$. $M_{n,SEC}$ = 7000 g mol^{-1}, $Đ$ = 1.19. ^{1}H-NMR (400 MHz, $CDCl_3$, ppm): δ= 7.37-6.91 (*m*, CH, benzene ring), 6.57 (*d*, CH, benzene ring, *J* = 8.0 Hz), 6.49 (*dd*, vinyl protons, *J* = 8.0, 16.0 Hz), 6.27 (*d*, vinyl protons, *J* = 20.0 Hz), 5.69 (*d*, vinyl protons, *J* = 8.0 Hz), 5.16 (*s*, *weak*, CH–S), 4.19 (*broad*, –(C=O)–O-C***H$_2$***-C**H$_2$**-O-(C=O)-NH-, –(C=O)–O–C***H$_2$***–CH$_2$–OH), 3.85-3.28 (*m*, –CH$_2$–, corresponding to the reacted MDI, CH$_2$ polymer, –(C=O)–O–CH$_2$–C***H$_2$***–OH polymer), 2.84-1.00 (*m*, CH and CH$_2$ backbone, CH$_3$ R-group, CH$_2$ Z-group), 0.93-0.90 (*m*, 3H, CH$_3$ Z-group).

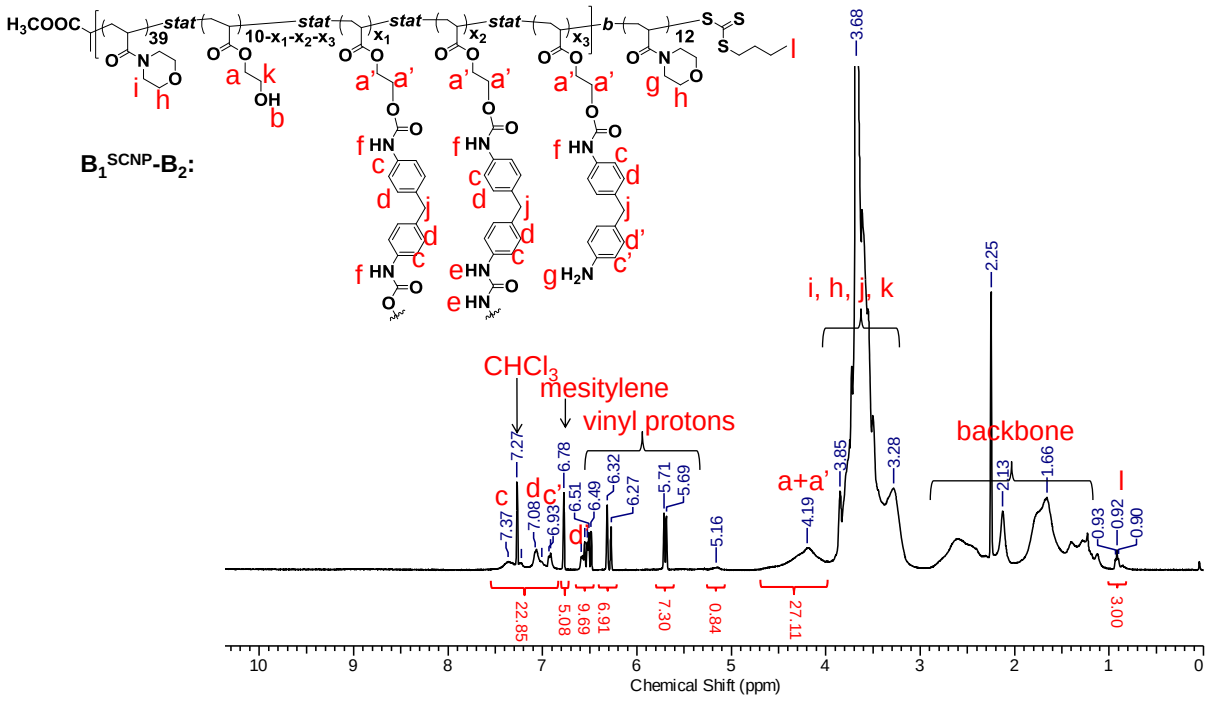

Figure 3.18 ^{1}H NMR spectrum ($CDCl_3$, 400MHz) of **B_1^{SCNP}-B_2** (reaction mixture, mesitylene was used as reference for the determination of conversion).

3.4.3.6 Synthesis of B_1^{SCNP}-B_2-B_3

NAM (0.149 g, 1.06 mmol), HEA (0.041 g, 0.35 mmol) and V-601 (0.143 mg, 0.00062 mmol) were added to the previous **B_1^{SCNP}-B_2** polymerization medium and is degassed by bubbling nitrogen through the solution for ca. 15 minutes, and the polymerization mixture is allowed to polymerize at 70 ˚C for 24 h with stirring. Then the reaction was stopped by placing the flask into cold water. Then a sample was taken from the reaction mixture for the ^{1}H NMR analysis. The monomer conversion was determined by ^{1}H NMR by comparing the integration of the vinyl protons (δ ~ 6.50–5.50 ppm) before and after reaction and the obtained monomer conversion was 77% for NAM and 76% for HEA. The resulting polymer mixture was diluted with 2 mL dioxane and precipitated in diethyl ether. The polymer was then filtered and dried under vacuum to yield a pale yellow powder (0.460 g). The polymer **B_1^{SCNP}-B_2-B_3** ([Poly(NAM_{39}-*stat*-HEA_{10})]^{SCNP}-*b*-polyNAM_{12}-*b*-poly(NAM_{29}-*stat*-HEA_8)) was analyzed by

SEC in $CHCl_3$. $M_{n,SEC}$ = 11100 g mol^{-1}, $Đ$ = 1.15. ^{1}H-NMR (600 MHz, DMSO-d_6, ppm): δ= 9.53 (*s, broad*,–NH–(C=O)–O–), 8.52 (*s*, –NH–(C=O)–NH–), 7.35-7.31 (*m*, CH, benzene ring), 7.11-7.05 (*m*, CH, benzene ring), 6.83 (*d*, CH, benzene ring, *J* = 8.0 Hz), 6.47 (*d*, CH, benzene ring, *J* = 8.0 Hz), 5.13 (*s, weak*, CH–S), 4.84 (*s*, –NH_2), 4.76 (*s*, OH), 4.25 (*s*, –(C=O)–O-C***H*****$_2$**-C**H$_2$**-O-(C=O)-NH-), 4.03 (*s*, –(C=O)–O–C***H*****$_2$**–CH_2–OH), 3.80 (*s*, –CH_2–, corresponding to the reacted MDI), 3.56 (*s*, CH_2 polymer, –(C=O)–O–CH_2–C***H*****$_2$**–OH polymer), 2.80-0.94 (*m*, CH and CH_2 backbone, CH_3 R-group, CH_2 Z-group), 0.87 (*t*, 3H, *J* = 8.0 Hz, CH_3 Z-group).

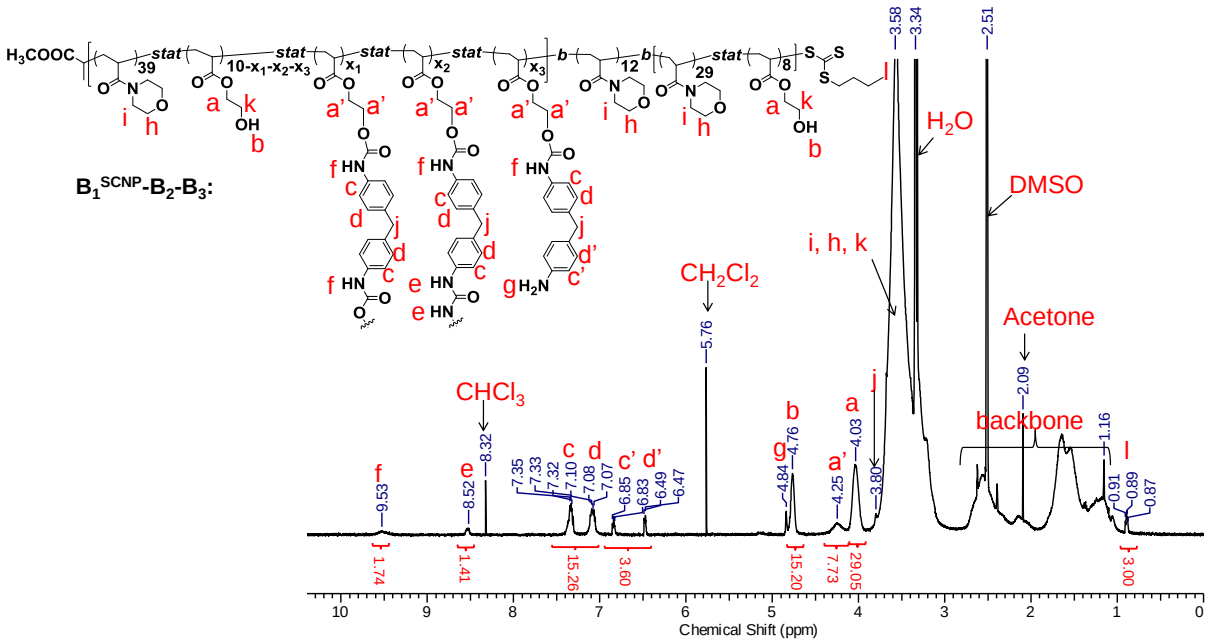

Figure 3.19 ^{1}H NMR spectrum (DMSO-d_6, 600MHz) of **B$_1^{SCNP}$-B$_2$-B$_3$**.

3.4.3.7 Synthesis of B_1^{SCNP}-B_2-B_3^{SCNP}

B$_1^{SCNP}$-B$_2$-B$_3^{SCNP}$ was synthesized under the conditions described for **B$_1^{SCNP}$** using **B$_1^{SCNP}$-B$_2$-B$_3$** (0.343 g, 0.024 mmol), 19 mL dry DCM, MDI (0.024 g, 0.096 mmol) and DBTDL (0.530 g, 0.5 mL, 0.83 mmol). The polymer **B$_1^{SCNP}$-B$_2$-B$_3^{SCNP}$** (0.340 g) ([poly(NAM_{39}-*stat*-HEA_{10})]^{SCNP}-*b*-polyNAM_{12}-*b*-[poly(NAM_{29}-*stat*-HEA_8)]^{SCNP}) was analyzed by SEC in $CHCl_3$. $M_{n,SEC}$ = 9400 g mol^{-1}, $Đ$ = 1.25. ^{1}H-NMR (600 MHz, DMSO-d_6,

ppm): δ= 9.53 (*s*, *broad*,–NH–(C=O)–O–), 8.56 (*s*, –NH–(C=O)–NH–), 7.35-7.31 (*m*, CH, benzene ring), 7.11-7.05 (*m*, CH, benzene ring), 6.85-6.83 (*m*, CH, benzene ring), 6.48-6.46 (*m*, CH, benzene ring), 5.13 (*s*, *weak*, CH–S), 4.84 (*s*, $–NH_2$), 4.76 (*s*, OH), 4.25 (*s*, –(C=O)–O-C***H*₂***-C**H*₂*-O-(C=O)-NH-), 4.03 (*s*, –(C=O)–O–C***H*₂***–CH_2–OH), 3.80 (*s*, –CH_2–, corresponding to the reacted MDI), 3.56 (*s*, CH_2 polymer, –(C=O)–O–CH_2–C***H*₂***–OH polymer), 2.80-0.94 (*m*, CH and CH_2 backbone, CH_3 R-group, CH_2 Z-group), 0.87-0.85 (*m*, 3H, CH_3 Z-group).

3.4.3.8 Synthesis of B_1-B_2

B_1 (0.414 g, 0.06 mmol, 1.0 eq.), NAM (0.102 g, 0.72 mmol, 12 eq.), VA-044 (0.161 mg, 0.0005 mmol, 0.008 eq.) and H_2O (0.8 g, 0.8 mL) were introduced into a flask equipped with a magnetic stirrer and sealed with a rubber septum. The flask is degassed by purging with nitrogen for 15 minutes, and the flask was placed into a preheated oil bath at 70 ˚C. After 2.3 h, the reaction was stopped by placing the flask into cold water. A sample was taken from the reaction mixture for the ^{1}H NMR analysis. The reaction mixture was used for the next chain extension to synthesize **B_1-B_2-B_3** without further purification. The monomer conversion was determined after polymerization by ^{1}H NMR by comparing the integration of the vinyl protons (δ ~ 6.50–5.50 ppm) before and after reaction and the obtained monomer conversion was 100% for NAM. The polymer **B_1-B_2** (P(NAM_{39}-*stat*-HEA_{10})-*b*-$PNAM_{12}$) was analyzed by SEC in $CHCl_3$. $M_{n,SEC}$ = 7800 g mol^{-1}, $Đ$ = 1.07. ^{1}H-NMR (400 MHz, DMSO-d_6, ppm): δ= 5.13 (*s*, *broad*, *weak*, CH-S), 4.84 (*s*, OH), 4.02 (*s*, –(C=O)–O–C***H*₂***–CH_2–OH), 3.56 (*s*, CH_2 polymer, –(C=O)–O-CH_2–C***H*₂***–OH polymer), 2.80-0.91 (*m*, CH and CH_2 backbone, CH_3 R-group, CH_2 Z-group), 0.88 (*t*, 3H, J = 8.0 Hz, CH_3 Z-group).

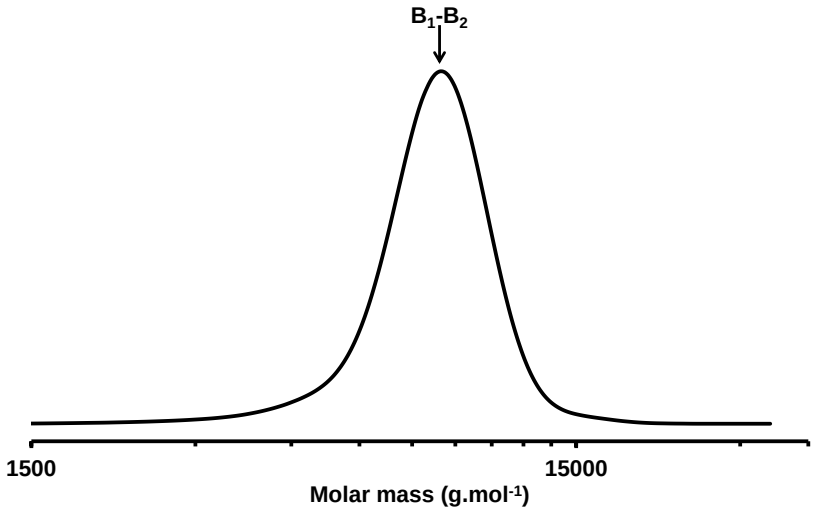

Figure 3.20 SEC chromatogram obtained in $CHCl_3$ for the copolymer of **B_1-B_2**.

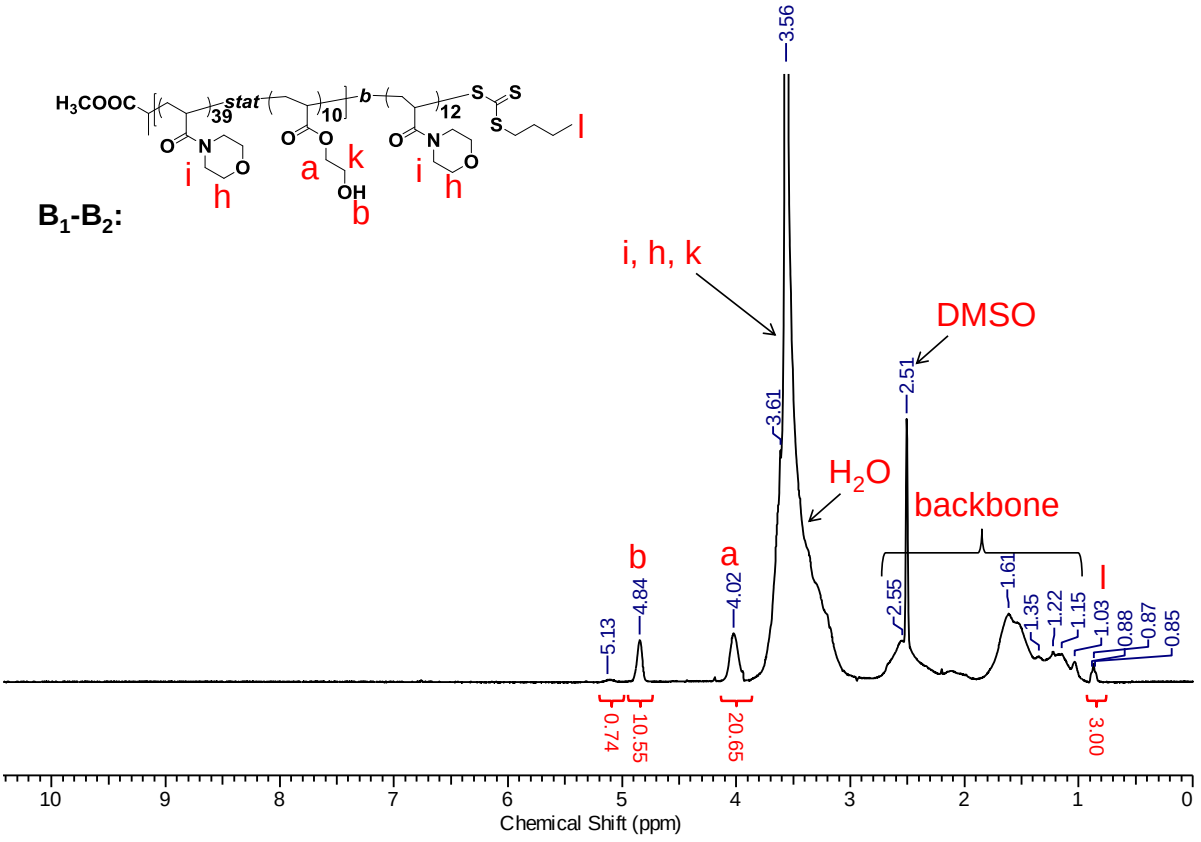

Figure 3.21 ^{1}H NMR spectrum (DMSO-d_6, 400MHz) of linear diblock copolymer **B_1-B_2** (reaction mixture).

3.4.3.9 Synthesis of B_1-B_2-B_3

The reaction mixture of **B_1-B_2** from the previous step was used directly for this synthesis. NAM (0.246 g, 1.74 mmol, 29 eq.), HEA (0.056 g, 0.48 mmol, 8 eq.) and VA-044 (0.309 mg, 9.56×10^{-4} mmol, 0.016 eq.) were added to the previous polymerization medium and sealed with a rubber septum. The flask is degassed by bubbling nitrogen through the solution for ca. 15 minutes, and then the flask was placed into a preheated oil bath at 70 ˚C. After 2 h, the reaction was stopped by placing the flask into cold water. Then a sample was taken from the reaction mixture for the ^{1}H NMR analysis. Then the solvent was removed under reduced pressure. And the crude polymer was dissolved in minimum amount of methanol and precipitated in diethyl ether. The polymer was then filtered and dried under vacuum to yield a yellow powder (0.790 g). The monomer conversion was determined after polymerization by ^{1}H NMR by comparing the integration of the vinyl protons (δ ~ 6.50–5.50 ppm) before and after reaction and the obtained monomer conversion was 99% for NAM and 100% for HEA. The polymer **B_1-B_2-B_3** (Poly(NAM_{39}-*stat*-HEA_{10})-*b*-PolyNAM_{12}-*b*-Poly(NAM_{29}-*stat*-HEA_8)) was analyzed by SEC in $CHCl_3$. $M_{n,SEC}$ = 12100 g mol^{-1}, $Đ$ = 1.10. ^{1}H-NMR (400 MHz, DMSO-d_6, ppm): δ= 4.76 (*s*, OH), 4.03 (*s*, –(C=O)–O–C***H*****$_2$**–CH_2–OH), 3.56 (*s*, CH_2 polymer, –(C=O)–O-CH_2–C***H*****$_2$**–OH polymer), 2.80-0.94 (*m*, CH and CH_2 backbone, CH_3 R-group, CH_2 Z-group), 0.91 (*t*, 3H, *J* = 8.0 Hz, CH_3 Z-group).

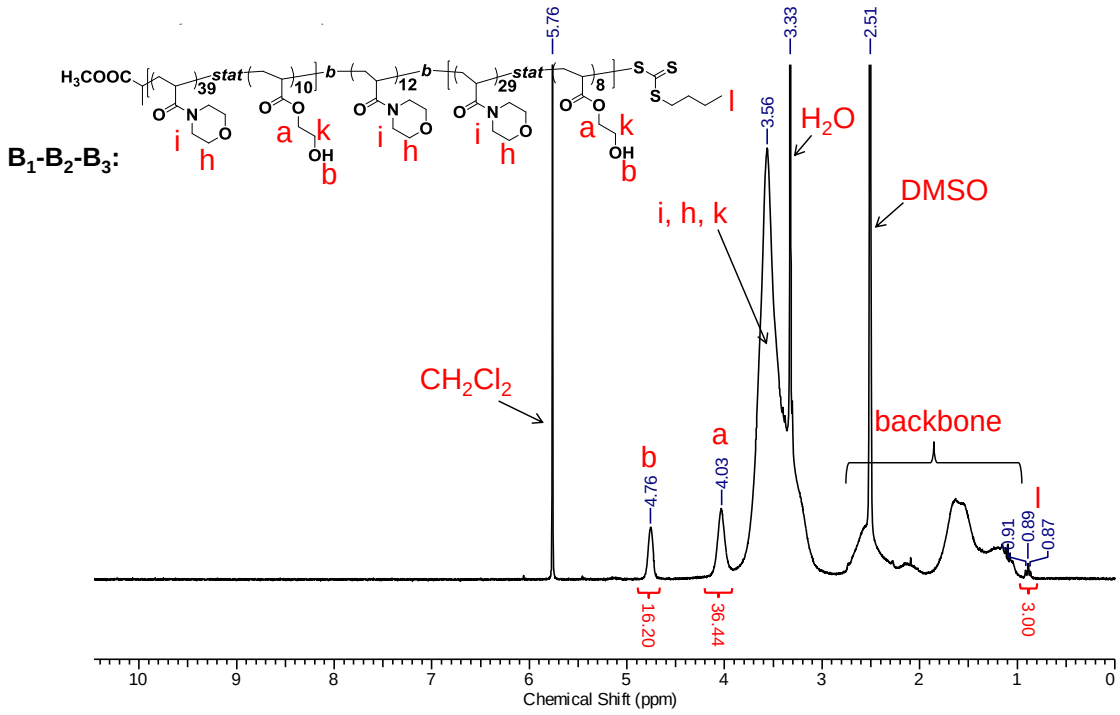

Figure 3.22 ^{1}H NMR spectrum (DMSO-d_6, 400MHz) of linear triblock copolymer **B_1-B_2-B_3**.

3.4.3.10 Synthesis of $(B_1$-B_2-$B_3)^{SCNP}$

$(B_1$-B_2-$B_3)^{SCNP}$ was synthesized under the conditions described for **B_1^{SCNP}** using **B_1-B_2-B_3** (0.096 g, 0.007 mmol) ,12 mL dry DCM, MDI (0.015 g, 0.06 mmol, 0.5 eq. of n(-OH)) and DBTDL (0.322 g, 0.3 mL, 0.51 mmol). The polymer (0.09 g) **(B_1-B_2-$B_3)^{SCNP}$**) **(**[Poly(NAM_{39}-*stat*-HEA_{10})-*b*-PolyNAM_{12}-*b*-Poly(NAM_{29}-*stat*-HEA_8)]^{SCNP}) was analyzed by SEC in $CHCl_3$. $M_{n,SEC}$ = 8400 g mol^{-1}, $Đ$ = 1.29. ^{1}H-NMR (400 MHz, DMSO-d_6, ppm): δ= 9.52 (*s, broad*,–NH–(C=O)–O–), 8.52 (*s*, –NH–(C=O)–NH–), 7.35-7.30 (*m*, CH, benzene ring), 7.11-7.05 (*m*, CH, benzene ring), 6.86-6.82 (*m*, CH, benzene ring), 6.49-6.46 (*m*, CH, benzene ring), 4.83 (*s*, –NH_2), 4.75 (*s*, OH), 4.25 (*s*, –(C=O)–O-C***H***$_2$-C**H**$_2$-O-(C=O)-NH-), 4.04 (*s*, –(C=O)–O–C***H***$_2$–CH_2–OH), 3.80 (*s*, –CH_2–, corresponding to the reacted MDI), 3.56 (*s*, CH_2 polymer, –(C=O)–O–CH_2–C***H***$_2$–OH polymer), 2.80-0.94 (*m*, CH and CH_2 backbone, CH_3 R-group, CH_2 Z-group), 0.91 (*t*, 3H, *J* = 8.0 Hz, CH_3 Z-group).

3.4.3.11 Synthesis of B_1^{SCNP}-B_2-B_3^{SCNP}-B_4

B_1^{SCNP}-B_2-B_3^{SCNP}-B_4 was synthesized under the conditions described for B_1^{SCNP}-B_2 using **B_1^{SCNP}-B_2-B_3^{SCNP}** (0.320 g, 0.02 mmol, 1.0 eq.), NAM (0.057 g, 0.4 mmol, 20 eq.), V-601 (0.101 mg, 0.00044 mmol, 0.022 eq.), 1, 4-dioxane (0.45 mL) and mesitylene (0.01 mL, used as reference) The monomer conversion was determined by ^{1}H NMR by comparing the integration of the vinyl protons (δ ~ 6.50–5.50 ppm) before and after reaction and the obtained monomer conversion was 63% for NAM. The polymer **B_1^{SCNP}-B_2-B_3^{SCNP}-B_4** ([Poly(NAM_{39}-*stat*-HEA_{10})]^{SCNP}-*b*-PolyNAM_{12}-*b*-[Poly(NAM_{29}-*stat*-HEA_8)]^{SCNP}-*b*-PolyNAM_{12}) was analyzed by SEC in $CHCl_3$. $M_{n,SEC}$ = 10700 g mol^{-1}, $Đ$ = 1.27. $Đ$ = 1.19. ^{1}H-NMR (400 MHz, $CDCl_3$, ppm): δ= 7.37-6.92 (*m*, CH, benzene ring), 6.58 (*d*, CH, benzene ring, *J* = 8.0 Hz), 6.49 (*dd*, vinyl protons, *J* = 8.0, 16.0 Hz), 6.28 (*d*, vinyl protons, *J* = 16.0 Hz), 5.69 (*d*, vinyl protons, *J* = 8.0 Hz), 5.15 (*s*, *weak*, CH–S), 4.19 (*broad*, –(C=O)–O-C***H₂***-C**H₂**-O-(C=O)-NH-, –(C=O)–O–C***H₂***–CH_2–OH), 3.85-3.29 (*m*, –CH_2–, corresponding to the reacted MDI, CH_2 polymer, –(C=O)–O–CH_2–C***H₂***–OH polymer), 2.92-1.00 (*m*, CH and CH_2 backbone, CH_3 R-group, CH_2 Z-group), 0.90-0.86 (*m*, 3H, CH_3 Z-group).

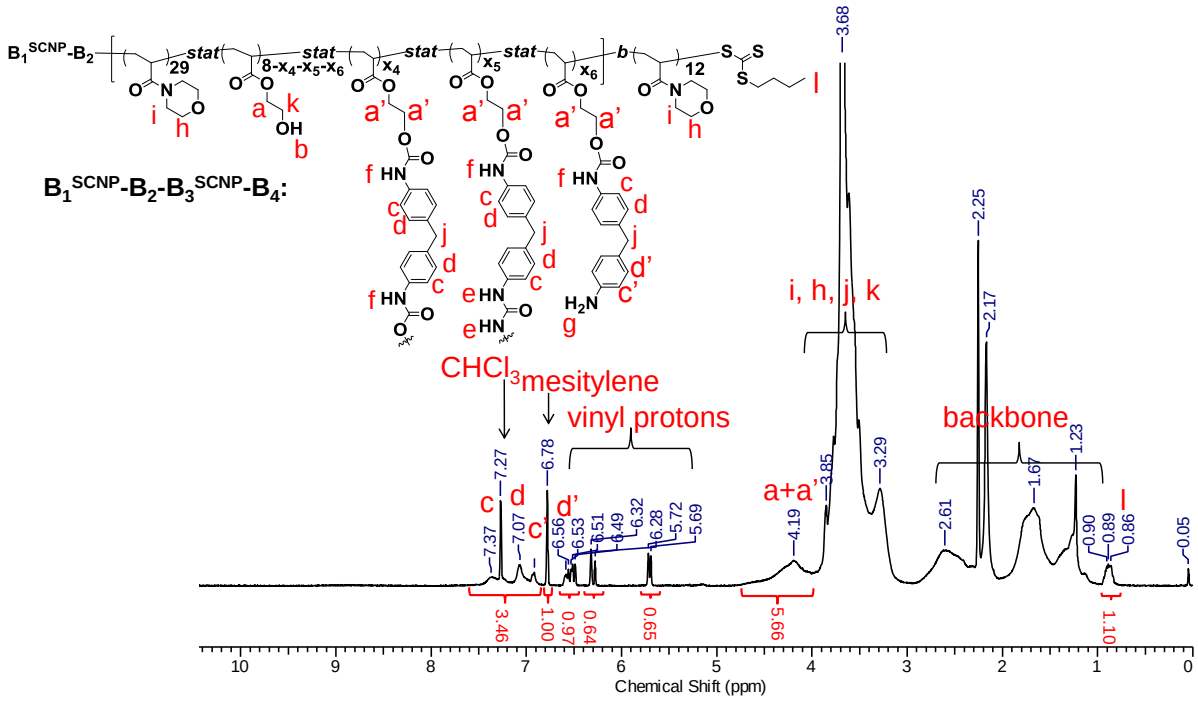

Figure 3.23 ^{1}H NMR spectrum ($CDCl_3$, 400MHz) of **B_1^{SCNP}-B_2-B_3^{SCNP}-B_4** (reaction mixture, mesitylene was used as reference for the determination of conversion).

3.4.3.12 Synthesis of B_1^{SCNP}-B_2-B_3^{SCNP}-B_4-B_5

B_1^{SCNP}-B_2-B_3^{SCNP}-B_4-B_5 was synthesized according to the procedure of B_1^{SCNP}-B_2-B_3 usingNAM (0.113 g, 0.8 mmol), HEA (0.023 g, 0.2 mmol) and V-601 (0.138 mg, 0.0006 mmol). The monomer conversion was determined after polymerization by ^{1}H NMR by comparing the integration of the vinyl protons (δ ~ 6.50–5.50 ppm) before and after reaction and the obtained monomer conversion was 85% for NAM and 84% for HEA. The polymer (0.380 g) **B_1^{SCNP}-B_2-B_3^{SCNP}-B_4-B_5** ([poly(NAM_{39}-*stat*-HEA_{10})]^{SCNP}-*b*-polyNAM_{12}-*b*-[poly(NAM_{29}-*stat*-HEA_8)]^{SCNP}-*b*-polyNAM_{12}-*b*-poly(NAM_{41}-*stat*-HEA_8)) was analyzed by SEC in $CHCl_3$. $M_{n,SEC}$ = 17500 g mol^{-1}, $Đ$ = 1.20. ^{1}H-NMR (600 MHz, DMSO-d_6, ppm): δ= 9.52 (*s, broad*,–NH–(C=O)–O–), 8.54 (*s*, –NH–(C=O)–NH–), 7.34-7.31 (*m*, CH, benzene ring), 7.11-7.05 (*m*, CH, benzene ring), 6.85-6.83 (*m*, CH, benzene ring), 6.48-6.47 (*m*, CH, benzene ring), 4.83 (*s*, –NH_2), 4.77 (*s*, OH), 4.24 (*s*, –(C=O)–O-C***H*****$_2$**-C**H**$_2$-O-(C=O)-NH-), 4.03 (*s*, –(C=O)–O–C***H*****$_2$**–CH_2–OH), 3.80 (*s*, –CH_2–, corresponding to the reacted MDI), 3.57

(*s*, CH_2 polymer, –(C=O)–O–CH_2–C***H*****$_2$**–OH polymer), 2.80-0.94 (*m*, CH and CH_2 backbone, CH_3 R-group, CH_2 Z-group), 0.90-0.88 (*m*, 3H, CH_3 Z-group).

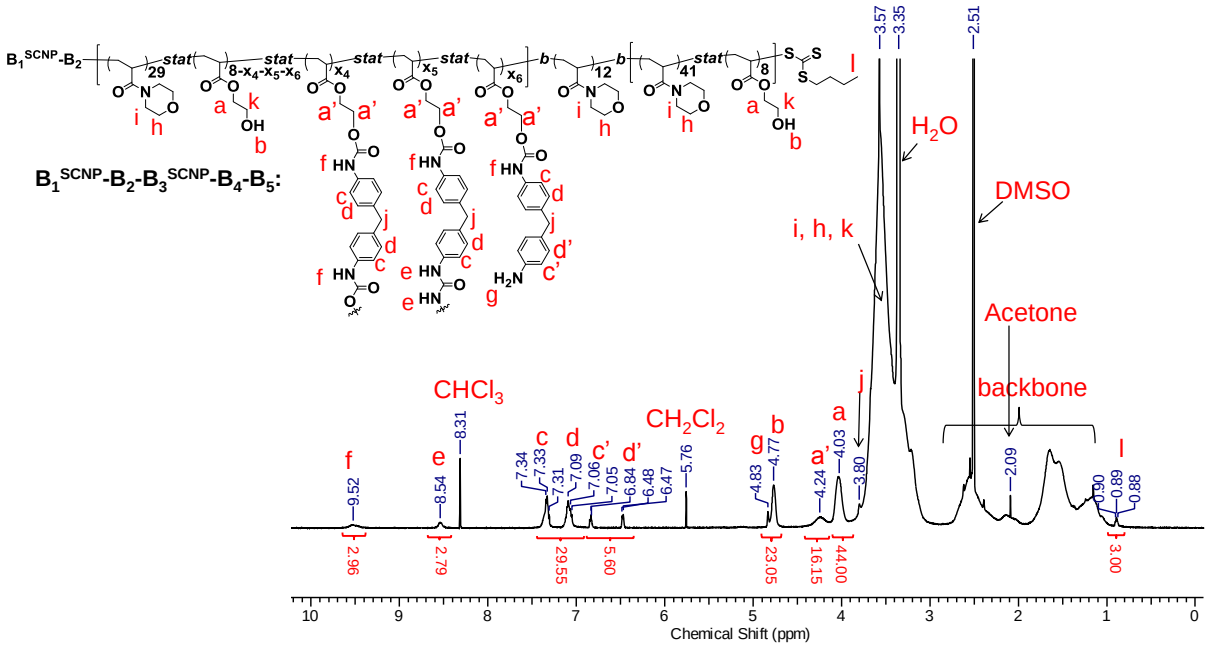

Figure 3.24 ^{1}H NMR spectrum (DMSO-d_6, 600MHz) of single chain nanoparticles **B_1^{SCNP}-B_2-B_3^{SCNP}-B_4-B_5**.

3.4.3.13 Synthesis of B_1^{SCNP}-B_2-B_3^{SCNP}-B_4-B_5^{SCNP}

B_1^{SCNP}-B_2-B_3^{SCNP}-B_4-B_5^{SCNP} was synthesized under the conditions described for **B_1^{SCNP}** using **B_1^{SCNP}-B_2-B_3^{SCNP}-B_4-B_5** (0.344 g, 0.014 mmol) 12 mL dry DCM, MDI (0.014 g, 0.056 mmol) and DBTDL (0.208 g, 0.2 mL, 0.33 mmol). The polymer (0.300 g) **B_1^{SCNP}-B_2-B_3^{SCNP}-B_4-B_5^{SCNP}** ([poly(NAM_{39}-*stat*-HEA_{10})]^{SCNP}-*b*-polyNAM_{12}-*b*-[poly(NAM_{29}-*stat*-HEA_8)]^{SCNP}-*b*-polyNAM_{12}-*b*-[poly(NAM_{41}-*stat*-HEA_8)]^{SCNP}) was analyzed by SEC in $CHCl_3$. $M_{n,SEC}$ = 16000 g mol^{-1}, $Đ$ = 1.21. ^{1}H-NMR (400 MHz, DMSO-d_6, ppm): δ= 9.52 (*s, broad*,–NH–(C=O)–O–), 8.59 (*s*, –NH–(C=O)–NH–), 7.35-7.34 (*m*, CH, benzene ring), 7.10-7.09 (*m*, CH, benzene ring), 6.85-6.83 (*m*, CH, benzene ring), 6.49-6.47 (*m*, CH, benzene ring), 4.83 (*s*, –NH_2), 4.76 (*s*, OH), 4.24 (*s*, –(C=O)–O-C***H*****$_2$**-C**H$_2$**-O-(C=O)-NH-), 4.03 (*s*, –(C=O)–O–C***H*****$_2$**–CH_2–OH), 3.79 (*s*, –CH_2–, corresponding to the reacted MDI), 3.56 (*s*, CH_2 polymer, –(C=O)–

O–CH_2–C***H*****$_2$**–OH polymer), 2.80-0.94 (*m*, CH and CH_2 backbone, CH_3 R-group, CH_2 Z-group), 0.89-0.87 (*m*, 3H, CH_3 Z-group).

3.4.4 Supporting Information

Table 3.2 Experimental conditions used and obtained conversions for the preparation of various polymers at 70 °C.

Polymer	$[CTA]_0/[I]_0$	$[I]_0$ (mol.L^{-1})	Reaction time (h)	Solvent	NAM $[M]_0$ (mol L^{-1})	NAM Conv.[a] (%)	NAM DP	HEA $[M]_0$ (mol L^{-1})	HEA Conv.[a] (%)	HEA DP
B_1	200	3.75 10^{-4} (VA-044)	2	H_2O/dioxane (70/30, v/v)	3	98	39	0.75	98	10
B_1^{SCNP}-B_2	97	6 10^{-4} (V601)	24	dioxane	1.17	62	12	-	-	-
B_1^{SCNP}-B_2-B_3	57	7.3 10^{-4} (V601)	24	dioxane	1.58	77	29	0.42	76	8
B_1-B_2	120	5.5 10^{-4} (VA-044)	2.3	H_2O	0.8	100	12	-	-	-
B_1-B_2-B_3	62	9.6 10^{-4} (VA-044)	2	H_2O	1.42	99	29	0.39	100	8
B_1^{SCNP}-B_2-B_3^{SCNP}-B_4	45	8 10^{-4} (V601)	24	dioxane	0.72	63	12	-	-	-
B_1^{SCNP}-B_2-B_3^{SCNP}-B_4-B_5	33	8 10^{-4} (V601)	24	dioxane	1.29	85	41	0.27	84	8

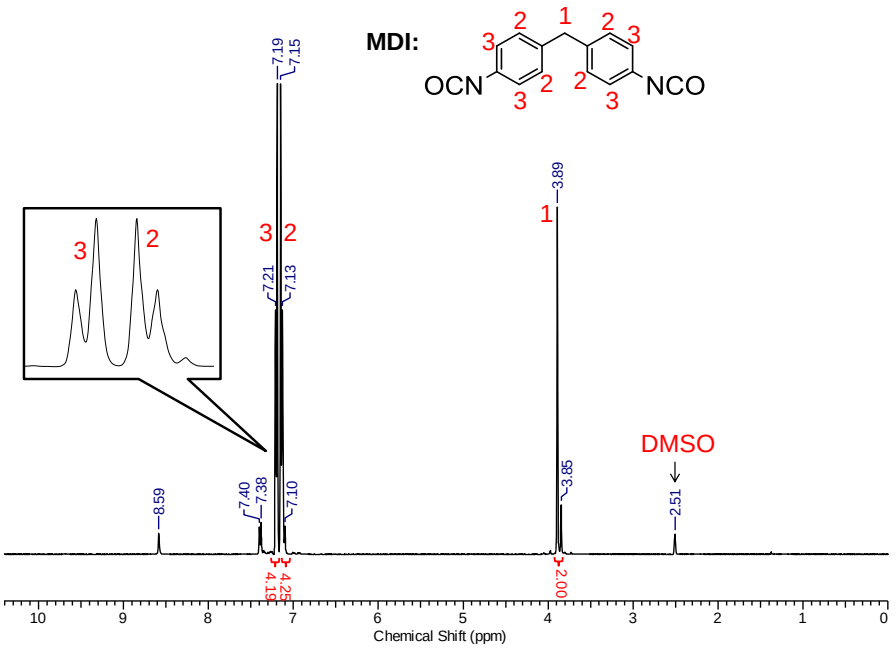

Figure 3.25 ^{1}H NMR spectrum (DMSO-d_6, 400MHz) of MDI.

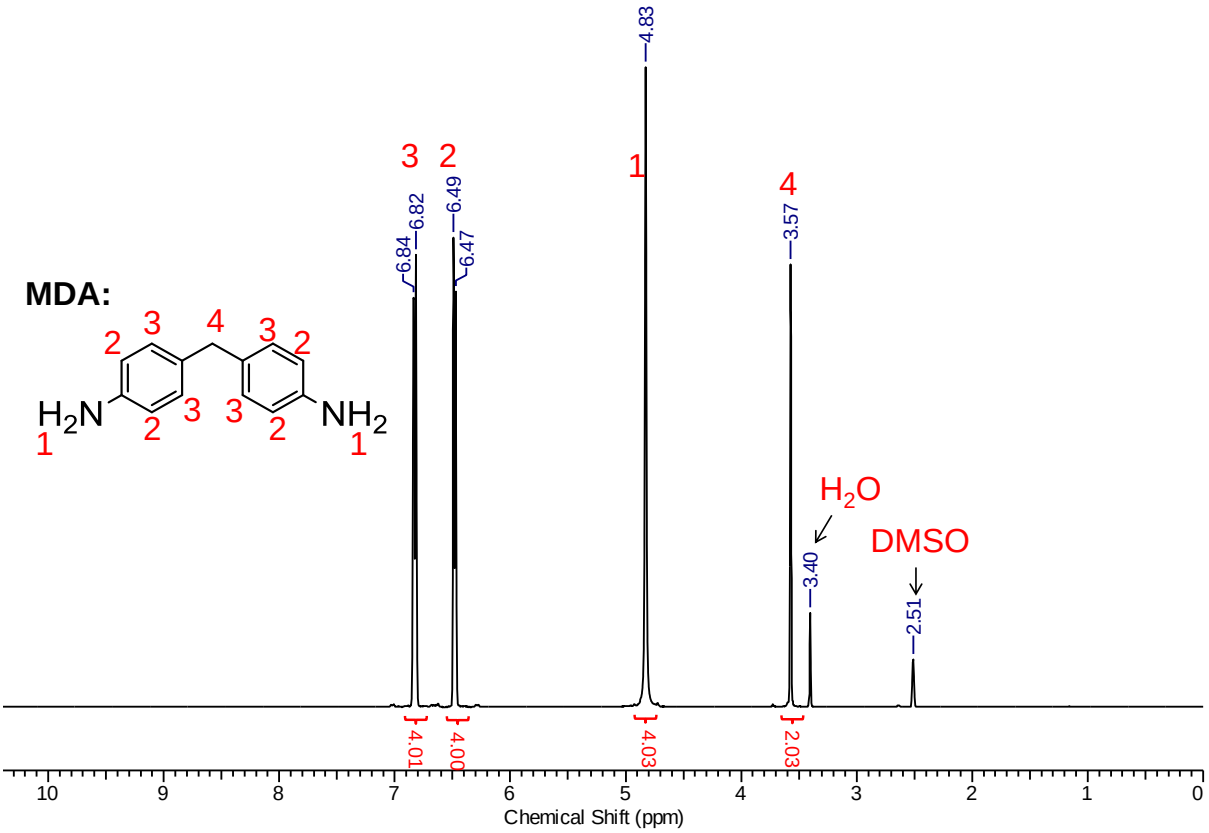

Figure 3.26 ^{1}H NMR spectrum (DMSO-d_6, 400MHz) of 4, 4'-methylenedianiline (MDA).

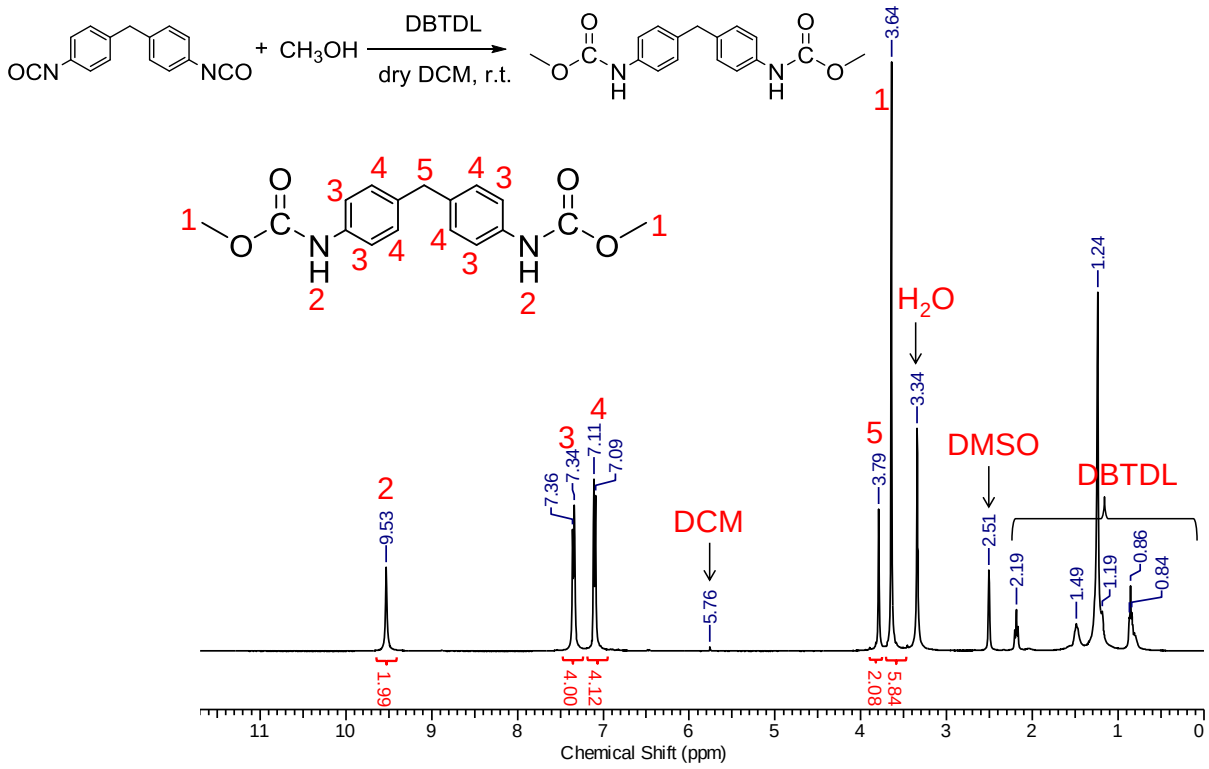

Figure 3.27 ^{1}H NMR spectrum (DMSO-d_6, 400MHz) of the crude product after MDI reacted with CH_3OH.

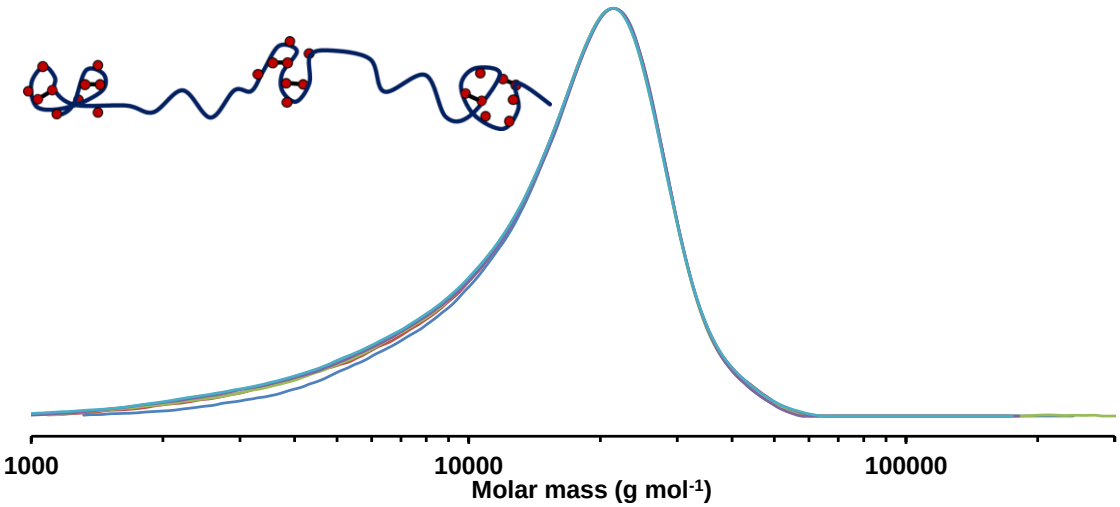

Figure 3.28 SEC chromatograms (RI traces) of $\mathbf{B_1^{SCNP}\text{-}B_2\text{-}B_3^{SCNP}\text{-}B_4\text{-}B_5^{SCNP}}$ analysed for 5 times in $CHCl_3$.

3.5 References

1. Gody, G.; Maschmeyer, T.; Zetterlund, P. B.and Perrier, S. Rapid and quantitative one-pot synthesis of sequence-controlled polymers by radical polymerization. *Nat. Commun.* **2013**, 4, 2505.

2. Anfinsen, C. B. Principles that Govern the Folding of Protein Chains. *Science* **1973**, 181 (4096), 223-230.

3. Dobson, C. M. Protein folding and misfolding. *Nature* **2003**, 426 (6968), 884-890.

4. Schmidt, B. V.; Fechler, N.; Falkenhagen, J.and Lutz, J. F. Controlled folding of synthetic polymer chains through the formation of positionable covalent bridges. *Nat. Chem.* **2011**, 3 (3), 234-238.

5. Mahon, C. S.and Fulton, D. A. Mimicking nature with synthetic macromolecules capable of recognition. *Nat. Chem.* **2014**, 6 (8), 665-672.

6. ter Huurne, G. M.; Gillissen, M. A. J.; Palmans, A. R. A.; Voets, I. K.and Meijer, E. W. The Coil-to-Globule Transition of Single-Chain Polymeric Nanoparticles with a Chiral Internal Secondary Structure. *Macromolecules* **2015**, 48 (12), 3949-3956.

7. Kirby, A. J. Enzyme Mechanisms, Models, and Mimics. *Angew. Chem. Int. Ed. Engl.* **1996**, 35 (7), 706-724.

8. Liu, Y.; Pauloehrl, T.; Presolski, S. I.; Albertazzi, L.; Palmans, A. R.and Meijer, E. W. Modular Synthetic Platform for the Construction of Functional Single-Chain Polymeric Nanoparticles: From Aqueous Catalysis to Photosensitization. *J. Am. Chem. Soc.* **2015**, 137 (40), 13096-105.

9. Ouchi, M.; Badi, N.; Lutz, J. F.and Sawamoto, M. Single-chain technology using discrete synthetic macromolecules. *Nat. Chem.* **2011**, 3 (12), 917-924.

10. Terashima, T.; Mes, T.; De Greef, T. F. A.; Gillissen, M. A. J.; Besenius, P.; Palmans, A. R. A.and Meijer, E. W. Single-Chain Folding of Polymers for Catalytic Systems in Water. *J. Am. Chem. Soc.* **2011**, 133 (13), 4742-4745.

11. Gillissen, M. A. J.; Voets, I. K.; Meijer, E. W.and Palmans, A. R. A. Single chain polymeric nanoparticles as compartmentalised sensors for metal ions. *Polym. Chem.* **2012**, 3 (11), 3166-3174.

12. Wulff, G.; Chong, B.-O.and Kolb, U. Soluble Single-Molecule Nanogels of Controlled Structure as a Matrix for Efficient Artificial Enzymes. *Angew. Chem. Int. Ed.* **2006**, 45 (18), 2955-2958.

13. Hanlon, A. M.; Lyon, C. K.and Berda, E. B. What Is Next in Single-Chain Nanoparticles? *Macromolecules* **2016**, 49 (1), 2-14.

14. Pomposo, J. A. Bioinspired single-chain polymer nanoparticles. *Polym. Int.* **2014**, 63 (4), 589-592.

15. Altintas, O.and Barner-Kowollik, C. Single-Chain Folding of Synthetic Polymers: A Critical Update. *Macromol. Rapid Commun.* **2016**, 37 (1), 29-46.

16. Lyon, C. K.; Prasher, A.; Hanlon, A. M.; Tuten, B. T.; Tooley, C. A.; Frank, P. G.and Berda, E. B. A brief user's guide to single-chain nanoparticles. *Polym. Chem.* **2015**, 6 (2), 181-197.

17. Mavila, S.; Eivgi, O.; Berkovich, I.and Lemcoff, N. G. Intramolecular Cross-Linking Methodologies for the Synthesis of Polymer Nanoparticles. *Chem. Rev.* **2015**.

18. Altintas, O.and Barner-Kowollik, C. Single chain folding of synthetic polymers by covalent and non-covalent interactions: current status and future perspectives. *Macromol. Rapid Commun.* **2012**, 33 (11), 958-971.

19. Sanchez-Sanchez, A.and Pomposo, J. A. Single-Chain Polymer Nanoparticles via Non-Covalent and Dynamic Covalent Bonds. *Particle & Particle Systems Characterization* **2014**, 31 (1), 11-23.

20. Gonzalez-Burgos, M.; Latorre-Sanchez, A.and Pomposo, J. A. Advances in single chain technology. *Chem. Soc. Rev.* **2015**, 44 (17), 6122-6142.

21. Huo, M.; Wang, N.; Fang, T.; Sun, M.; Wei, Y.and Yuan, J. Single-chain polymer nanoparticles: Mimic the proteins. *Polymer* **2015**, 66, A11-A21.

22. Aiertza, M.; Odriozola, I.; Cabañero, G.; Grande, H.-J.and Loinaz, I. Single-chain polymer nanoparticles. *Cell. Mol. Life Sci.* **2012**, 69 (3), 337-346.

23. Cheng, C.-C.; Chang, F.-C.; Yen, H.-C.; Lee, D.-J.; Chiu, C.-W.and Xin, Z. Supramolecular Assembly Mediates the Formation of Single-Chain Polymeric Nanoparticles. *ACS Macro Letters* **2015**, 4 (10), 1184-1188.

24. Foster, E. J.; Berda, E. B.and Meijer, E. W. Metastable Supramolecular Polymer Nanoparticles via Intramolecular Collapse of Single Polymer Chains. *J. Am. Chem. Soc.* **2009**, 131 (20), 6964-6966.

25. Mes, T.; van der Weegen, R.; Palmans, A. R.and Meijer, E. W. Single-chain polymeric nanoparticles by stepwise folding. *Angew. Chem. Int. Ed. Engl.* **2011**, 50 (22), 5085-5089.

26. Berda, E. B.; Foster, E. J.and Meijer, E. W. Toward Controlling Folding in Synthetic Polymers: Fabricating and Characterizing Supramolecular Single-Chain Nanoparticles. *Macromolecules* **2010**, 43 (3), 1430-1437.

27. Hosono, N.; Palmans, A. R. A.and Meijer, E. W. "Soldier-Sergeant-Soldier" triblock copolymers: revealing the folded structure of single-chain polymeric nanoparticles. *Chem. Commun.* **2014**, 50 (59), 7990-7993.

28. Altintas, O.; Krolla-Sidenstein, P.; Gliemann, H.and Barner-Kowollik, C. Single-Chain Folding of Diblock Copolymers Driven by Orthogonal H-Donor and Acceptor Units. *Macromolecules* **2014**, 47 (17), 5877-5888.

29. Altintas, O.; Lejeune, E.; Gerstel, P.and Barner-Kowollik, C. Bioinspired dual self-folding of single polymer chains via reversible hydrogen bonding. *Polym. Chem.* **2012**, 3 (3), 640-651.

30. Stals, P. J. M.; Gillissen, M. A. J.; Paffen, T. F. E.; de Greef, T. F. A.; Lindner, P.; Meijer, E. W.; Palmans, A. R. A.and Voets, I. K. Folding Polymers with Pendant Hydrogen Bonding Motifs in Water: The Effect of Polymer Length and Concentration on the Shape and Size of Single-Chain Polymeric Nanoparticles. *Macromolecules* **2014**, 47 (9), 2947-2954.

31. van Roekel, H. W. H.; Stals, P. J. M.; Gillissen, M. A. J.; Hilbers, P. A. J.; Markvoort, A. J.and de Greef, T. F. A. Evaporative self-assembly of single-chain, polymeric nanoparticles. *Chem. Commun.* **2013**, 49 (30), 3122-3124.

32. Beck, J. B.; Killops, K. L.; Kang, T.; Sivanandan, K.; Bayles, A.; Mackay, M. E.; Wooley, K. L.and Hawker, C. J. Facile Preparation of Nanoparticles by Intramolecular Crosslinking of Isocyanate Functionalized Copolymers. *Macromolecules* **2009**, 42 (15), 5629-5635.

33. Hansell, C. F.; Lu, A.; Patterson, J. P.and O'Reilly, R. K. Exploiting the tetrazine-norbornene reaction for single polymer chain collapse. *Nanoscale* **2014**, 6 (8), 4102-7.

34. Wong, E. H. H.; Lam, S. J.; Nam, E.and Qiao, G. G. Biocompatible Single-Chain Polymeric Nanoparticles via Organo-Catalyzed Ring-Opening Polymerization. *ACS Macro Letters* **2014**, 3 (6), 524-528.

35. Beck, J. B.; Killops, K. L.; Kang, T.; Sivanandan, K.; Bayles, A.; Mackay, M. E.; Wooley, K. L.and Hawker, C. J. Facile Preparation of Nanoparticles by Intramolecular Cross-Linking of Isocyanate Functionalized Copolymers. *Macromolecules* **2009**, 42 (15), 5629-5635.

36. Sugai, N.; Heguri, H.; Yamamoto, T.and Tezuka, Y. A Programmed Polymer Folding: Click and Clip Construction of Doubly Fused Tricyclic and Triply Fused Tetracyclic Polymer Topologies. *J. Am. Chem. Soc.* **2011**, 133 (49), 19694-19697.

37. Song, C.; Li, L.; Dai, L.and Thayumanavan, S. Responsive single-chain polymer nanoparticles with host–guest features. *Polym. Chem.* **2015**, 6 (26), 4828-4834.

38. Sanchez-Sanchez, A.; Fulton, D. A.and Pomposo, J. A. pH-responsive single-chain polymer nanoparticles utilising dynamic covalent enamine bonds. *Chem. Commun.* **2014**, 50 (15), 1871-1874.

39. Whitaker, D. E.; Mahon, C. S.and Fulton, D. A. Thermoresponsive Dynamic Covalent Single-Chain Polymer Nanoparticles Reversibly Transform into a Hydrogel. *Angew. Chem. Int. Ed.* **2013**, 52 (3), 956-959.

40. Shishkan, O.; Zamfir, M.; Gauthier, M. A.; Borner, H. G.and Lutz, J.-F. Complex single-chain polymer topologies locked by positionable twin disulfide cyclic bridges. *Chem. Commun.* **2014**, 50 (13), 1570-1572.

41. Badi, N.and Lutz, J. F. Sequence control in polymer synthesis. *Chem. Soc. Rev.* **2009**, 38 (12), 3383-90.

42. Lutz, J.-F. Sequence-controlled polymerizations: the next Holy Grail in polymer science? *Polym. Chem.* **2010**, 1 (1), 55.

43. Lutz, J.-F.; Ouchi, M.; Liu, D. R.and Sawamoto, M. Sequence-Controlled Polymers. *Science* **2013**, 341 (6146), 628-636.

44. Gody, G.; Maschmeyer, T.; Zetterlund, P. B.and Perrier, S. Exploitation of the Degenerative Transfer Mechanism in RAFT Polymerization for Synthesis of Polymer of High Livingness at Full Monomer Conversion. *Macromolecules* **2014**, 47 (2), 639-649.

45. Gody, G.; Maschmeyer, T.; Zetterlund, P. B.and Perrier, S. Pushing the Limit of the RAFT Process: Multiblock Copolymers by One-Pot Rapid Multiple Chain Extensions at Full Monomer Conversion. *Macromolecules* **2014**, 47 (10), 3451-3460.

46. Lutz, J.-F. Polymer chemistry: A controlled sequence of events. *Nat. Chem.* **2010**, 2 (2), 84-85.

47. Roy, R. K.and Lutz, J. F. Compartmentalization of single polymer chains by stepwise intramolecular cross-linking of sequence-controlled macromolecules. *J. Am. Chem. Soc.* **2014**, 136 (37), 12888-91.

48. Harth, E.; Horn, B. V.; Lee, V. Y.; Germack, D. S.; Gonzales, C. P.; Miller, R. D.and Hawker, C. J. A Facile Approach to Architecturally Defined Nanoparticles via Intramolecular Chain Collapse. *J. Am. Chem. Soc.* **2002**, 124 (29), 8653-8660.

49. Gody, G.; Rossner, C.; Moraes, J.; Vana, P.; Maschmeyer, T.and Perrier, S. One-Pot RAFT/"Click" Chemistry via Isocyanates: Efficient Synthesis of α-End-Functionalized Polymers. *J. Am. Chem. Soc.* **2012**, 134 (30), 12596-12603.

50. Pomposo, J. A.; Perez-Baena, I.; Buruaga, L.; Alegría, A.; Moreno, A. J.and Colmenero, J. On the Apparent SEC Molecular Weight and Polydispersity Reduction upon Intramolecular Collapse of Polydisperse Chains to Unimolecular Nanoparticles. *Macromolecules* **2011**, 44 (21), 8644-8649.

51. Tuten, B. T.; Chao, D.; Lyon, C. K.and Berda, E. B. Single-chain polymer nanoparticles via reversible disulfide bridges. *Polym. Chem.* **2012**, 3 (11), 3068-3071.

52. Murray, B. S.and Fulton, D. A. Dynamic Covalent Single-Chain Polymer Nanoparticles. *Macromolecules* **2011**, 44 (18), 7242-7252.

53. Buurma, N. J.; Cook, J. L.; Hunter, C. A.; Low, C. M. R.and Vinter, J. G. The role of functional group concentration in solvation thermodynamics. *Chemical Science* **2010**, 1 (2), 242-246.

54. Catrouillet, S.; Fonteneau, C.; Bouteiller, L.; Delorme, N.; Nicol, E.; Nicolai, T.; Pensec, S.and Colombani, O. Competition Between Steric Hindrance and Hydrogen Bonding in the Formation of Supramolecular Bottle Brush Polymers. *Macromolecules* **2013**, 46 (19), 7911-7919.

55. Liu, J. W.; Mackay, M. E.and Duxbury, P. M. Molecular Dynamics Simulation of Intramolecular Cross-Linking of BCB/Styrene Copolymers. *Macromolecules* **2009**, 42 (21), 8534-8542.

56. Higashijima, T.; Tasumi, M.and Miyazawa, T. ^{1}H Nuclear magnetic resonance studies of melanostatin: Dependence of the chemical shifts of NH protons on temperature and concentration. *FEBS Letters* **1975**, 57 (2), 175-178.

57. Boileau, S.; Bouteiller, L.; Laupretre, F.and Lortie, F. Soluble supramolecular polymers based on urea compounds. *New Journal of Chemistry* **2000**, 24 (11), 845-848.

58. Mecerreyes, D.; Lee, V.; Hawker, C. J.; Hedrick, J. L.; Wursch, A.; Volksen, W.; Magbitang, T.; Huang, E.and Miller, R. D. A Novel Approach to Functionalized Nanoparticles: Self-Crosslinking of Macromolecules in Ultradilute Solution. *Adv. Mater.* **2001**, 13 (3), 204-208.

59. Cherian, A. E.; Sun, F. C.; Sheiko, S. S.and Coates, G. W. Formation of Nanoparticles by Intramolecular Cross-Linking: Following the Reaction Progress of Single Polymer Chains by Atomic Force Microscopy. *J. Am. Chem. Soc.* **2007**, 129 (37), 11350-11351.

60. Zhong, M.and Matyjaszewski, K. How Fast Can a CRP Be Conducted with Preserved Chain End Functionality? *Macromolecules* **2011**, 44 (8), 2668-2677.

61. Altintas, O.; Willenbacher, J.; Wuest, K. N. R.; Oehlenschlaeger, K. K.; Krolla-Sidenstein, P.; Gliemann, H.and Barner-Kowollik, C. A Mild and Efficient Approach to Functional Single-Chain Polymeric Nanoparticles via Photoinduced Diels–Alder Ligation. *Macromolecules* **2013**, 46 (20), 8092-8101.

62. Rabani, E.; Reichman, D. R.; Geissler, P. L.and Brus, L. E. Drying-mediated self-assembly of nanoparticles. *Nature* **2003**, 426 (6964), 271-274.

63. Pomposo, J. A.; Perez-Baena, I.; Lo Verso, F.; Moreno, A. J.; Arbe, A.and Colmenero, J. How Far Are Single-Chain Polymer Nanoparticles in Solution from the Globular State? *ACS Macro Letters* **2014**, 3 (8), 767-772.

64. Coca, S.; Jasieczek, C. B.; Beers, K. L.and Matyjaszewski, K. Polymerization of acrylates by atom transfer radical polymerization. Homopolymerization of 2-hydroxyethyl acrylate. *J. Polym. Sci., Part A: Polym. Chem.* **1998**, 36 (9), 1417-1424.

65. Ferguson, C. J.; Hughes, R. J.; Nguyen, D.; Pham, B. T. T.; Gilbert, R. G.; Serelis, A. K.; Such, C. H.and Hawkett, B. S. Ab Initio Emulsion Polymerization by RAFT-Controlled Self-Assembly. *Macromolecules* **2005**, 38 (6), 2191-2204.

Chapter 4 *Self-assembly and Dis-assembly of Stimuli Responsive Tadpole-like Single Chain Nanoparticles using a Switchable Hydrophilic/Hydrophobic Boronic Acid Cross-linker*

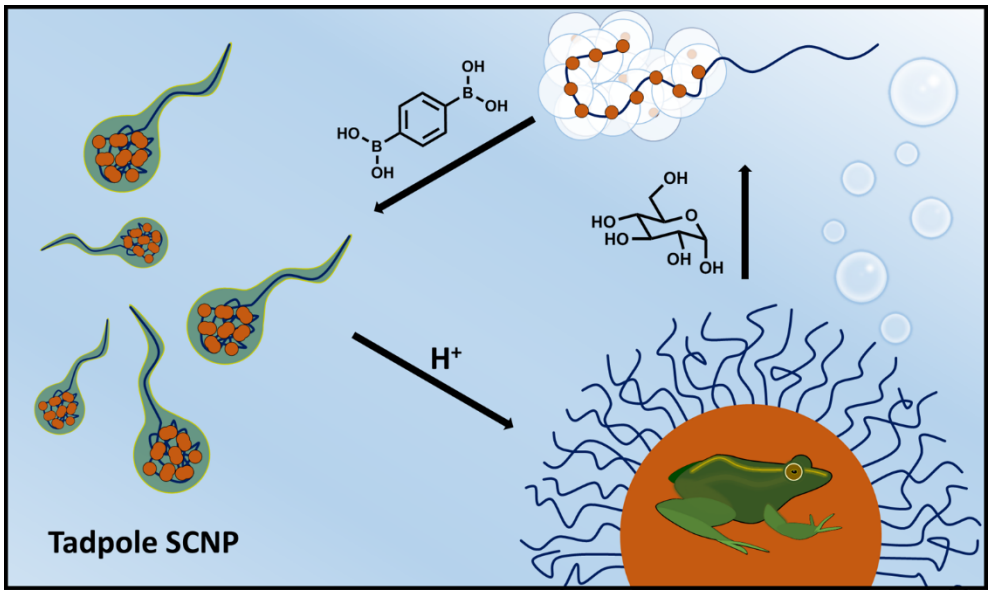

Living systems are driven by molecular machines that are composed of folded polypeptide chains, which are assembled together to form a multimeric complex. Although replicating this kind of systems is highly desirable, their complexity imposes a synthetic challenge, therefore generating synthetic polymers to mimic the process of these assemblies is a more appealing approach. This chapter demonstrates a linear polymer programmable for stepwise folding and assembly to higher-order structures. To achieve this, a diblock copolymer composed of 4-acryloylmorpholine and glycerol acrylate was synthesised via reversible addition fragmentation chain transfer polymerisation (Đ < 1.22). Both intramolecular folding and intermolecular assembly was driven by pH responsive cross-linker, benzene-1,4-diboronic acid. The resulting intramolecular folded single chain nanoparticles were well defined (Đ <

1.16) and successfully assembled into a multimeric structure (D_h = 245 nm) at neutral pH with no chain entanglement. The assembled multimer was observed with a spherical morphology as confirmed by TEM and AFM. These structures were capable of unfolding and disassembling either at low pH or in the presence of sugar. This work offers new perspective for the generation of adaptive smart materials.

4.1 Introduction

Nature uses the sophisticated machinery of the cell to confer precision on its biopolymers (e.g. proteins) in one-dimension through their primary sequences, and in three-dimensions (3D) via their subsequent secondary and tertiary structures, as well as their molecular organisation into multimeric complexes, all of which are imperative for the polymers to perform their specific biological functions. The 3D architectures of proteins originate from the controlled dynamic folding process of a single-stranded polypeptide chain and further self-assembling into selectively tailored molecular assemblies and interfaces which interact and respond to their environment.[1-4] Folding a single linear polymer chain into a single chain nanoparticle (SCNP) has been utilized as a versatile way of constructing polymeric nanoparticles to copy nature's ability to form well-defined structures and is a rapidly expanding research area in polymer science.[5-30] SCNPs can not only mimic the delicate controlled folding process of proteins with controlled size and morphology,[31-33] but can also self-assemble into more complexed 3D structures.[34] Furthermore stimuli-responsive polymeric nanoparticles, also called "smart" or "intelligent" nanoparticles that are capable of conformational and chemical changes by adapting the external stimuli[35, 36] have increasingly attracted interest due to their diverse range of applications in delivery and release of drugs,[37, 38] diagnostics,[39] sensors.[40] Dynamic covalent chemistry is a very suitable candidate for building intelligent materials which can be responsive to the environmental changes, such as pH or input stimuli.[33, 41-44] Boronic acid containing macromolecules have been widely utilized as an effective route toward bioresponsive architectures and a large body of research has been carried out.[45-51] Boronic acid derivatives reversibly react with 1, 2- and 1, 3-diols (*i.e.* saccharides) to form boronic or boronate ester depending on the environmental pH.[52] At high pH, the anionic boronate ester is hydrophilic (**Scheme 4.1a**). Upon acidification the boronate moieties will be converted to neutral/hydrophobic groups (**Scheme 4.1b**).[53, 54] Sumerlin *et al.* reported a novel example of

boronic acid containing triply-responsive "schizophrenic" diblock copolymers which displayed self-assembly in response to changes in temperature, pH, and the concentration of diol.[52]

The self-assembly of amphiphilic diblock copolymers have attracted considerable interest to generate stimuli responsive nanoparticles with tailored structures.[35, 55, 56] The structure and properties of superparticles formed by self-assembled SCNPs have been proved to be entirely different from traditional block copolymer micelles.[57] Zhao *et al.*[58] and Chen *et al.*[57] reported the first examples of self-assembly and disassembly of diblock single chain Janus nanoparticles (SCJNPs). However, these self-assemblies were obtained either in organic solvent or requiring the involvement of organic solvent to assist the solubility of the hydrophobic part, which will limit the application in physiological conditions. Besides, the disassembly was achieved by utilizing the ultra-sonication which will also circumvent its wide use due to the destructive effect of sonication.[59]

This work describes a novel synthesis of completely water soluble SCNPs from a 1,2-diol pendant linear precursor polymer, using a boronic acid cross linker and utilising the aforementioned pH dependency of boronate esters to promote self-assembly. In contrast to the studies of Zhao *et al.* and Chen *et al.*, self-assembly was achieved without the need for switching solvents and also new to this field is the dis-assembly of the SCNPs back to the linear precursor using pH and sugars as chemical stimuli.

4.2 Results and Discussion

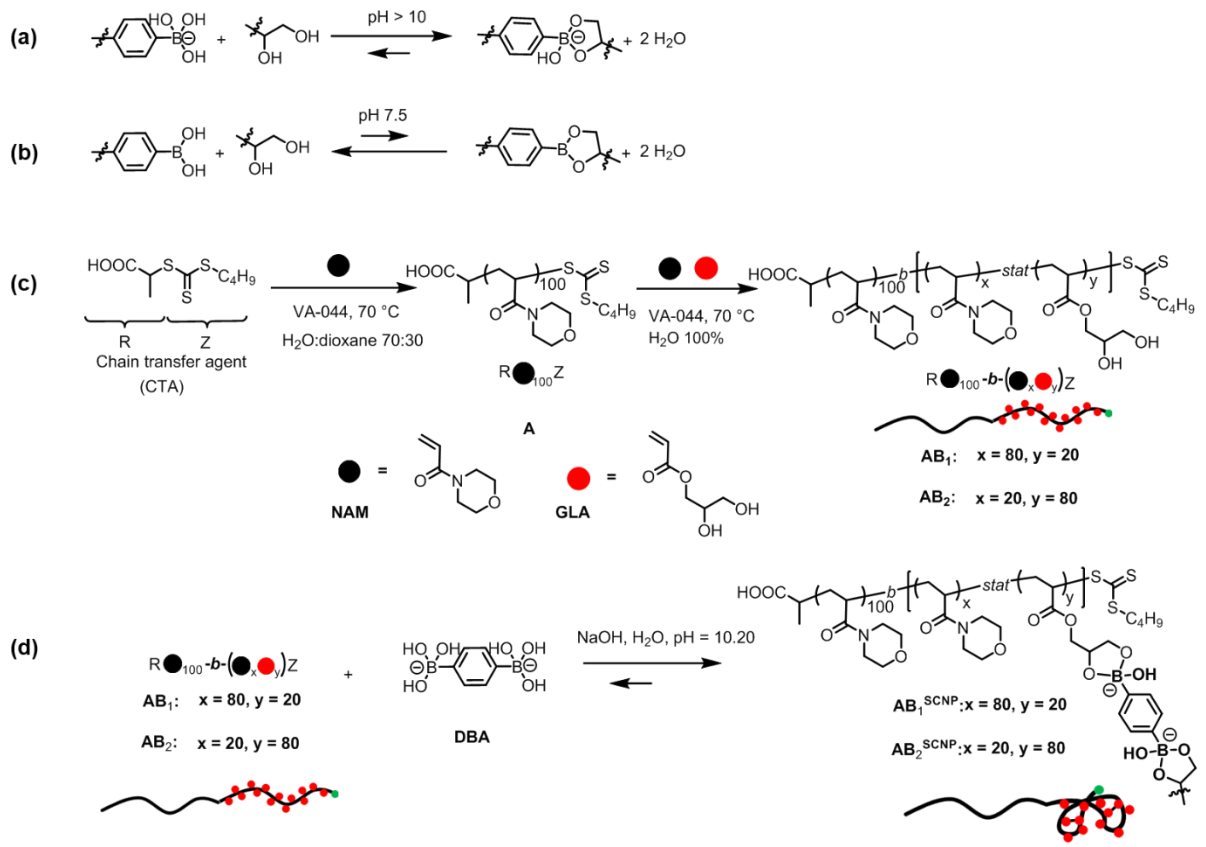

Scheme 4.1 a) Equilibrium formation of boronate esters from 1,2-diols at high pH in water; b) Equilibrium formation of boronic esters from 1,2-diols at neutral pH in water; c) Schematic representation of the synthesis of hydrophilic diblock copolymers of **AB_1** and **AB_2** by RAFT polymerization. d) Schematic representation of the synthesis of tadpole-like SCNPs.

In the present study, 4-acryloylmorpholine (NAM) and glycerol acrylate (GLA, synthesized by adapting the published procedure,[60] **Scheme 4.2**, **Figures 4.22** and **4.23**) were used as monomers to fabricate water soluble, 1,2-diol-containing copolymers. Two diblock copolymers were designed with an initial hydrophilic block of poly(NAM) (Block A), comprising 100 units, to impart water solubility for the later self-assembled structure followed by a statistical hydrophilic segment of NAM/GLA (Block B, 100 units in total) able to react with a suitable diboronic acid cross-linker to form tadpole-like SCNPs. In order to investigate

the effect of the relative molar fractions of the hydrophobic block for self-assembly behaviour of the SCNPs, two different compositions of B block copolymers were synthesized: PolyNAM$_{100}$-*b*-Poly(NAM$_{80}$-*stat*-GLA$_{20}$) (**AB$_1$**) and PolyNAM$_{100}$-*b*-Poly(NAM$_{20}$-*stat*-GLA$_{80}$) (**AB$_2$**). As illustrated in **Scheme 4.1c**, optimized RAFT conditions as previously described for the synthesis of water soluble multiblock copolymers (azoinitiator: VA-044 at 70 °C in H_2O),[61] were applied to provide a fast (within 2 hours) and quantitative monomer conversion while maintaining high control over molar mass, narrow dispersity, and high theoretical livingness. 2-[(Butylthio-carbonothioyl)thio]propanoic acid [called (propanoic acid)yl butyl trithiocarbonate (PABTC) in this chapter] and 2, 2′-azobis[2-(2-imidazolin-2-yl)propane]dihydrochloride (VA-044) were used as the chain transfer agent (CTA) and the initiator respectively.

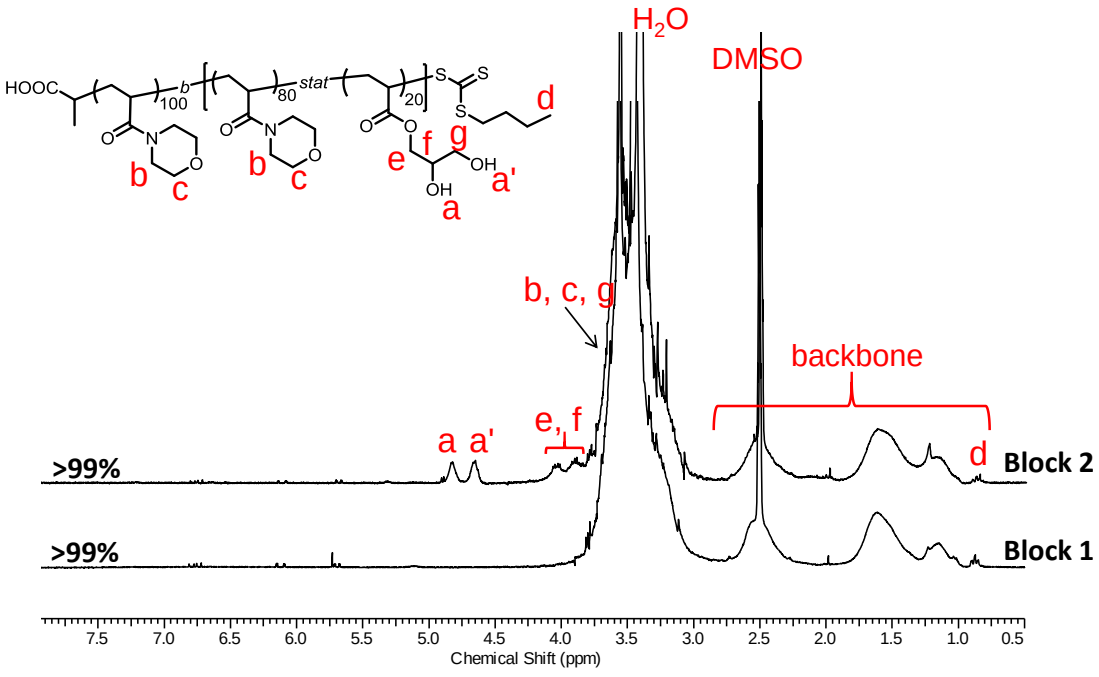

Figure 4.1 ^{1}H NMR spectrum (DMSO-d_6, 300MHz) of **AB$_1$** (PNAM$_{100}$-*b*-P(NAM$_{80}$-*stat*-GLA$_{20}$)) showing the monomer conversion for each block after iterative RAFT polymerization.

After 2 h polymerization for each block (See the experimental for a detailed procedure), near quantitative monomer conversion (> 99%) was obtained and confirmed by ^{1}H NMR

spectroscopy analysis for both diblock copolymers (**Figures 4.1** and **4.2**). ^{1}H NMR spectroscopy of both diblock copolymer confirmed the presence of the peaks associated with each segment, especially the presence of the diol functional group at 4.81 and 4.64 ppm (**Figures 4.1** and **4.2**, signals **a** and **a'**).

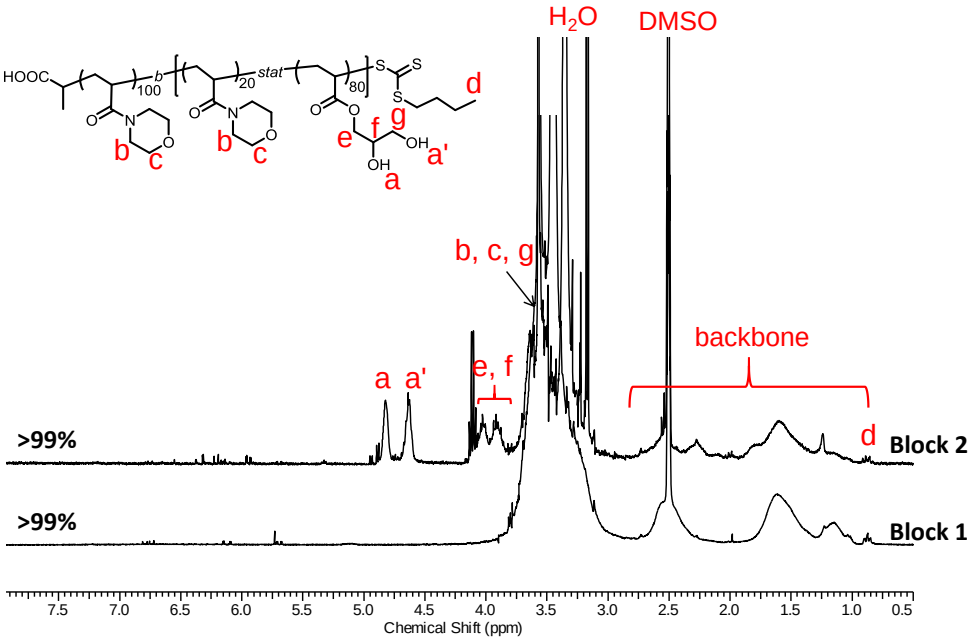

Figure 4.2 ^{1}H NMR spectrum (DMSO-d_6, 300MHz) of **AB$_2$** (PNAM$_{100}$-*b*-P(NAM$_{20}$-*stat*-GLA$_{80}$)) showing the monomer conversion for each block after iterative RAFT polymerization.

Size exclusion chromatography (SEC) in DMF revealed a shift towards higher molar mass confirming the successful chain extension after polymerization (**Figures 4.3** and **4.4**). While a narrow dispersity was detected for both copolymers [PNAM$_{100}$-*b*-(PNAM$_{80}$-GLA$_{20}$), **AB$_1$**, $Đ$ = 1.14; PNAM$_{100}$-*b*-(PNAM$_{20}$-GLA$_{80}$), **AB$_2$**, $Đ$ = 1.22, **Table 4.1**), it needs to be noted that, for the **AB$_2$** copolymer, a low molar mass tail was observed in the chromatogram (**Figure 4.4**). This is due to low re-initiation efficiency of a polyacrylamide macroCTA towards acrylate monomer considering the large amount of the acrylate monomer in the second block.[62] The high molecular weight shoulder evident in the SEC trace of **AB$_2$** copolymer (**Figure 4.4**) is likely associated to the copolymerization of macromonomer formed by the propagating radical

undergoing backbiting β-scission during the radical polymerization of acrylates,[63, 64] which will not affect the following cross-linking reaction.

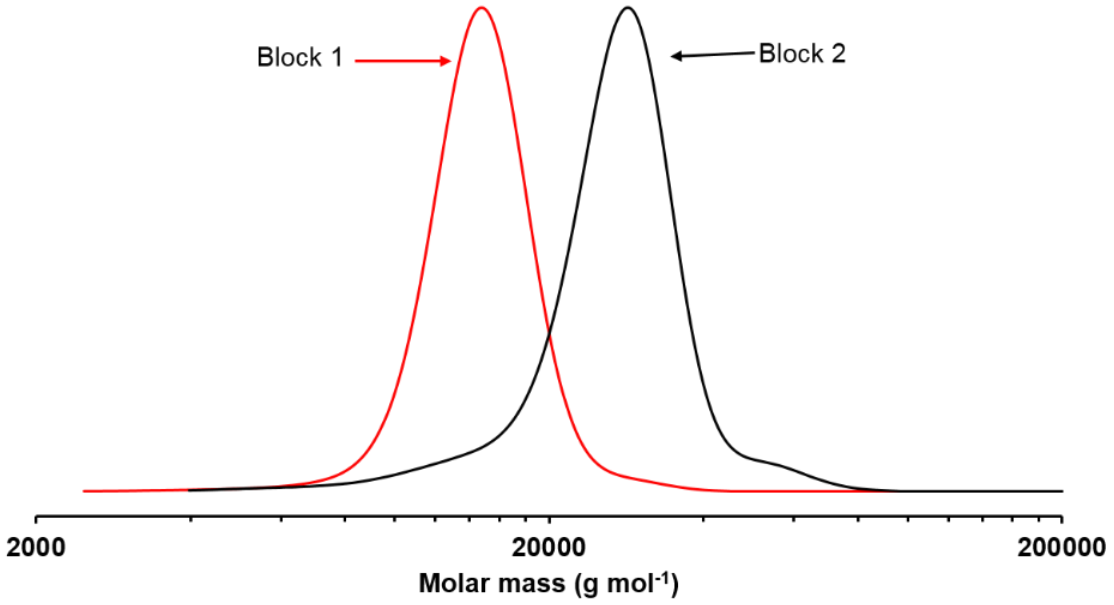

Figure 4.3 Molecular weight distributions (SEC RI traces in DMF) for successive block extensions of the diblock copolymer **AB$_1$** (PNAM$_{100}$-*b*-P(NAM$_{80}$-*stat*-GLA$_{20}$).

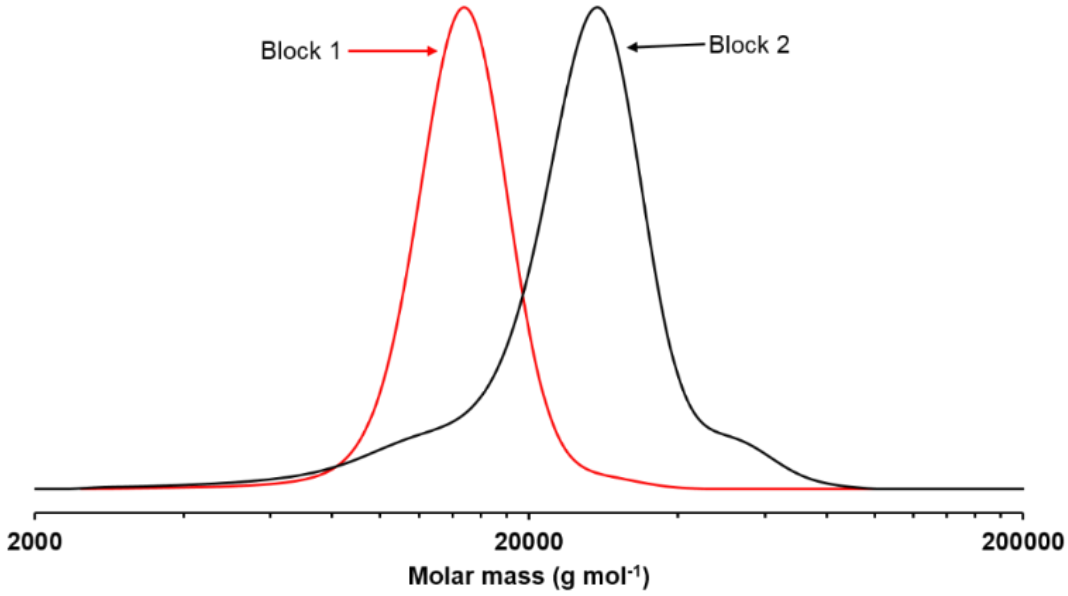

Figure 4.4 Molecular weight distributions (SEC RI traces in DMF) for successive block extensions of the diblock copolymer **AB$_2$** (PNAM$_{100}$-*b*-P(NAM$_{20}$-*stat*-GLA$_{80}$).

Table 4.1 Characterization of the linear copolymers, SCNPs by ^{1}H NMR spectroscopy, DMF-SEC, DLS and DSC.

Sample	Composition	$M_{n,th}$[a]	$M_{p,SEC}$[b]	$M_{n,SEC}$[b]	$Đ$[b]	$<G>$[c]	D_h[d]	PDI[d]	T_g[e]
		g mol^{-1}	g mol^{-1}	g mol^{-1}			nm		°C
A	$PNAM_{100}$	14400	14800	14100	1.07	-	-	-	-
AB_1	$PNAM_{100}$-*b*-$P(NAM_{80}$-*stat*-$GLA_{20})$	28600	27200	23700	1.14	-	7.7	0.07	147.9
AB_1^{SCNP}	$PNAM_{100}$-*b*-$[P(NAM_{80}$-*stat*-$GLA_{20})]^{SCNP}$	-	24400	19900	1.17	0.90	6.1	0.05	172.4
AB_2	$PNAM_{100}$-*b*-$P(NAM_{20}$-*stat*-$GLA_{80})$	28900	27700	22100	1.22	-	6.5	0.08	95.8
AB_2^{SCNP}	$PNAM_{100}$-*b*-$[P(NAM_{20}$-*stat*-$GLA_{80})]^{SCNP}$	-	23700	20300	1.16	0.86	5.0	0.08	172.6

[a] $M_{n,th} = [M]_0 \times p \times M_M/[CTA]_0 + M_{CTA}$, p is the monomer conversion determined by ^{1}H NMR spectroscopy.

[b] Determined by SEC in DMF with PMMA used as molecular weight standards, M_p represents the maximum peak value of the size-exclusion chromatogram.

[c] Folding parameter $<G> = M_{p,SCNP}/M_{p,linear}$, the molecular weight variation caused by the cross-linking reaction (*e.g.* the increased DBA units) was not taken into account.

[d] Hydrodynamic diameter (D_h) and size distributions were measured by dynamic light scattering (DLS) in H_2O. See experimental part for details.

[e] Glass transition temperature: determined by the second heating curve of DSC.

As shown in **Scheme 4.1d**, the folding of the linear polymers to synthesize the tadpole-like SCNPs was carried out applying a continuous addition method (by adding the solution of one reactant dropwise to the solution of the other reactant) developed by Hawker *et al*..[31] For this system, the solution of cross-linker benzene-1,4-diboronic acid (DBA, 0.5 equivalent per diol group) was added drop-wise (*i.e.* 15 minutes for **AB_1**, 30 minutes for **AB_2**, see the Supporting Information for a detailed procedure) into a premade basic aqueous solution (pH = 10) of the linear polymer precursor to fold the second block. In order to investigate whether the single chain folding was successful, SEC, dynamic light scattering (DLS), and differential scanning calorimetry (DSC) analysis were performed.

SEC is an ideal technique to monitor any changes in the hydrodynamic volume of a polymer chain allowing to distinguish between linear precursors, SCNP and intermolecular

cross linked species.[65-68] Comparing the SEC chromatograms of the obtained materials with their parent linear copolymers, a shift towards lower molar mass (*i.e.* smaller hydrodynamic volume, **Figure 4.5**) was observed for both cross-linking reactions, suggesting the successful formation of single chain polymeric nanoparticles **AB$_1$^{SCNP}** and **AB$_2$^{SCNP}**. These results are consistent with previous literature about the intramolecular cross linking of a single polymer chain.[33, 43, 69-73]

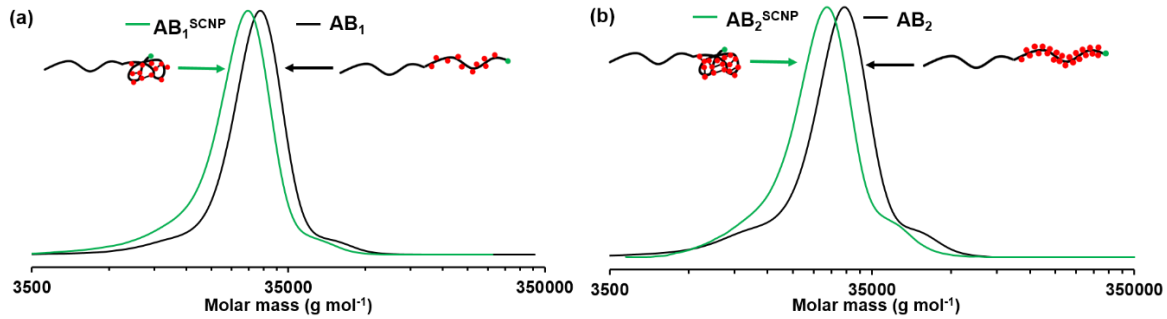

Figure 4.5 SEC chromatograms (RI traces) obtained in DMF for: (a) **AB$_1$** and **AB$_1$^{SCNP}**; (b) **AB$_2$** and **AB$_2$^{SCNP}**.

The folding parameter <*G*> calculated according to the method of Lutz *et al.*,[65] by comparison of the maximum peak values of the linear precursor and the compacted polymer chains, was obtained to be 0.90 and 0.86 for **AB$_1$^{SCNP}** and **AB$_2$^{SCNP}**, respectively (**Table 4.1**). These values closely match those of tadpole-like (P-shaped) macromolecules reported by Lutz *et al.*.[65] The relatively smaller <*G*> value of **AB$_2$^{SCNP}** is likely due to the more significant extent of folding of **AB$_2$** given the relative more amount of cross-linkable units.

The folding process is further illustrated by DLS analysis. Since the intensity of the scattered light is related to the sixth power of the radius of the scattering particles, thus the nanometer ranged SCNPs produce only a small amount of scattered light compared to larger aggregates which might be present (even in a very small amount) in solution.[74] This can result in nonoptimal measuring conditions and thus it is often difficult to obtain reliable number average hydrodynamic diameter (D_h). Therefore, only the number-weighted distributions for

the linear polymers and corresponding SCNPs are displayed. DLS measurements revealed a characteristic decrease in D_h of **AB$_1$^{SCNP}** and **AB$_2$^{SCNP}** compared to the corresponding linear precursor, which further indicates the intramolecular collapse and the formation of SCNPs (**Figure 4.6**). The average hydrodynamic diameter decreased from 7.7 nm for **AB$_1$** to 6.1 nm for **AB$_1$^{SCNP}** and from 6.5 nm for **AB$_2$** to 5.0 nm for **AB$_2$^{SCNP}** (**Table 4.1**).

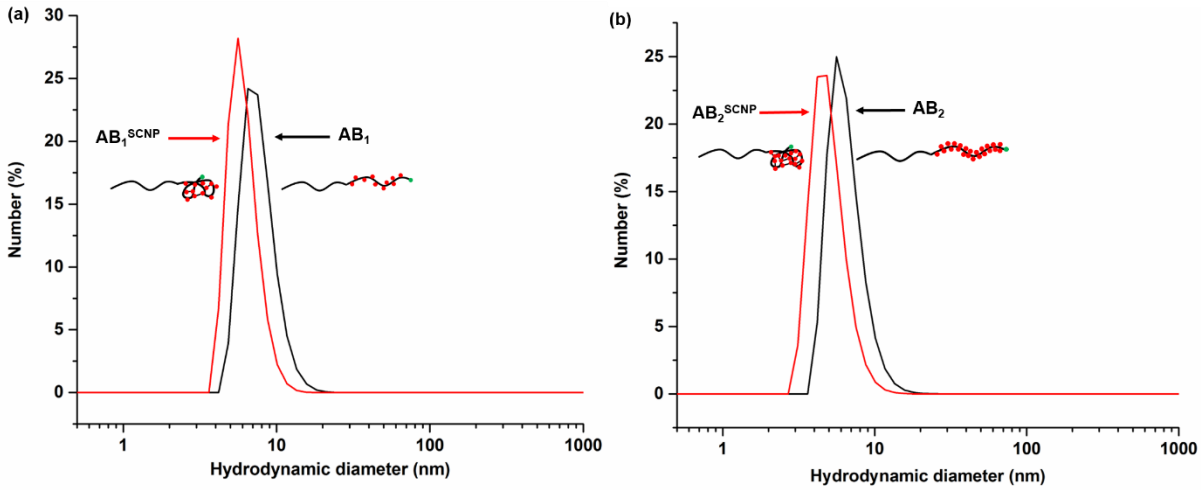

Figure 4.6 Hydrodynamic size distributions obtained by DLS in H_2O for (a) **AB$_1$** and **AB$_1$^{SCNP}** (pH = 10.02); (b) **AB$_2$** and **AB$_2$^{SCNP}** (pH = 10.20).

DSC analysis was also conducted to demonstrate the successful formation of SCNPs. Compared to the linear polymer, the chain mobility of SCNPs will decrease, resulting in an increased glass transition temperature (T_g) value.[31, 75-77] The T_g value of the **AB$_1$^{SCNP}** increased significantly to 172.4 °C from the initial value of 147.9 °C for linear polymer **AB$_1$** (**Table 4.1**, **Figure 4.7a** , note that signal at 90 °C is a measurement artefact, see the following text for a detailed explanation). During the DSC analysis, the signal around 90 °C displaying the character of a T_g exists in the DSC curves of both **AB$_1$** and **AB$_1$^{SCNP}**. In order to demonstrate this is an artefact due to the analytical instrument rather than a real T_g, the homopolymer PolyNAM$_{100}$ (**A**) and the statistical copolymer Poly(NAM$_{80}$-*stat*-GLA$_{20}$) (**B$_1$**) were analysed by DSC. Again, a signal around 90 °C was observed for both polymers (see **Figure 4.7b**). Since no phase separation should exist in the homopolymer **A** and the statistical copolymer, each

copolymer should only displays one T_g, 159.2 °C for homopolymer **A** (PolyNAM$_{100}$) and 132.1 °C for the statistical copolymer (Poly(NAM$_{80}$-*stat*-GLA$_{20}$)). Based on these results, it can be concluded that the signal around 90 °C is an instrument artefact.

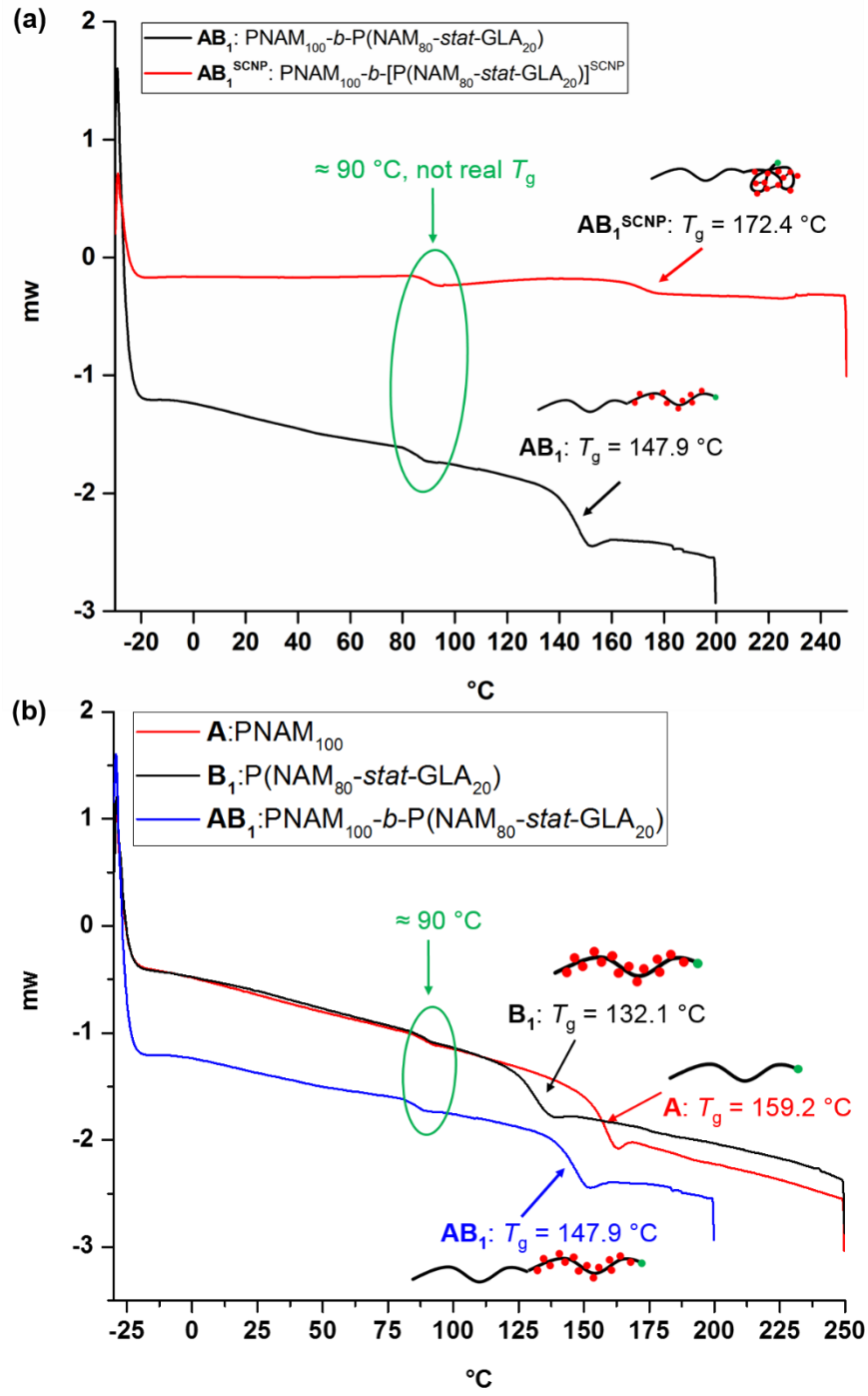

Figure 4.7 DSC curves of (a) the linear copolymer **AB$_1$** and folded polymer **AB$_1^{SCNP}$**; (b) homopolymer **A**, statistical copolymer **B$_1$**, and linear copolymer **AB$_1$**

On the other hand, the linear copolymer **AB$_2$** contains a larger fraction of GLA in the second block (**B$_2$**) which leads to a broader glass transition process and a decreased T_g (95.8 °C, **Table 4.1**, **Figure 4.8**) compared to **AB$_1$** (147.9 °C). The disappearance of the T_g value at 95.8 °C and the characteristic glass transition process with the T_g value of 172.6 °C (**Figure 4.8**) indicate the successful compaction of **AB$_2$** leading to the formation of **AB$_2^{SCNP}$**. The more dramatic change of T_g for **AB$_2^{SCNP}$** should be caused by the higher degree of compaction which is consistent with the SEC results.

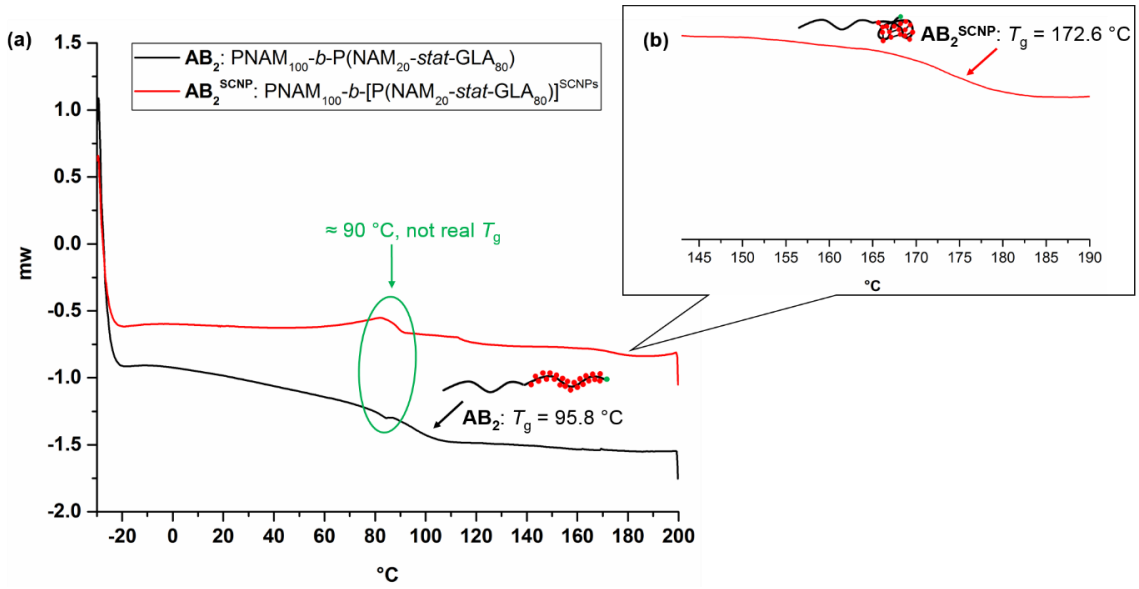

Figure 4.8 DSC curves of (a) the linear copolymer **AB$_2$** and the folded polymer **AB$_2^{SCNP}$**; (b) a zoomed in figure of the folded polymer **AB$_2^{SCNP}$**.

Due to the wide pH ranges present in biological and physiological systems the application of pH-responsive polymeric nanoparticles for controlled encapsulation and release is of great interest.[78] The self-assembly behaviour of the tadpole-like SCNPs was investigated by varying the environmental pH. At high pH, the cross-linker exists as hydrophilic anionic boronate esters (**Scheme 4.1a** and **4.1d**),[52, 79] therefore both segments of the diblock copolymers are hydrophilic. As the pH is lowered to neutral (pH ≈ 7.5), the majority of the cross-linker will become neutral boronic ester and hydrophobic, causing the tadpole-like SCNPs to be amphiphilic. This transition will lead to the folded "head" block to self-assemble into a

hydrophobic core while the hydrophilic "tail" segment of NAM constitutes the shell. If the pH is further lowered to acidic condition, the boronic esters will be hydrolysed (**Scheme 4.1b**).[79] The self-assembly behaviour of tadpole-like SCNPs adapting the pH changes was monitored by DLS analysis. When the pH of the aqueous solution of the $\mathbf{AB_1}^{\mathbf{SCNP}}$ was gradually lowered from basic (pH = 10.02) to acidic (pH = 2.36), the particles displayed similar sizes across the whole range and no self-assembly was observed (**Figure 4.9** and **Table 4.2**).

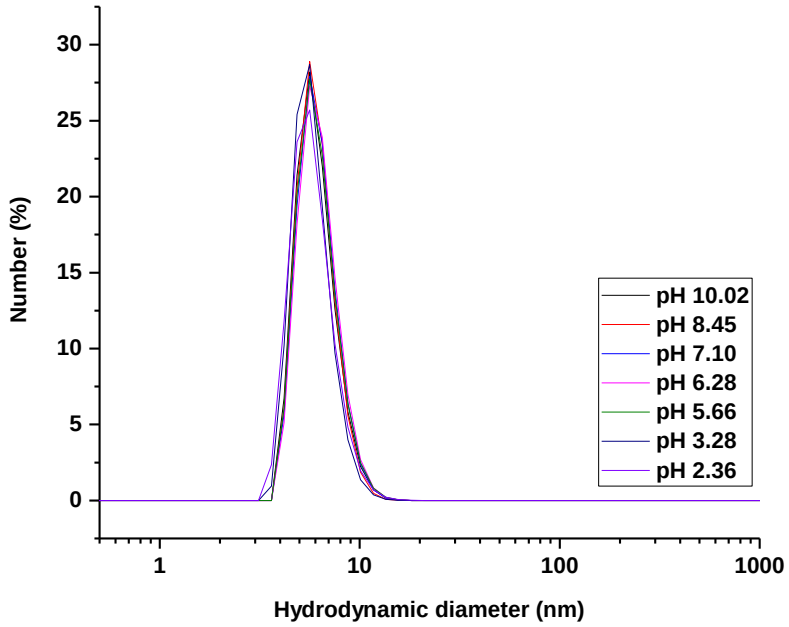

Figure 4.9 Average hydrodynamic size distributions of $\mathbf{AB_1}^{\mathbf{SCNP}}$ at different pH values obtained by DLS in H_2O.

Table 4.2 Hydrodynamic sizes of $\mathbf{AB_1}^{\mathbf{SCNP}}$ at different pH values obtained by DLS in H_2O.

pH	D_h (nm)	PDI
10.02	6.1	0.05
8.45	6.1	0.05
7.10	6.2	0.05
6.28	6.3	0.05
5.66	6.2	0.06
3.28	5.8	0.05
2.36	5.9	0.06

On the other hand, when the pH of the aqueous solution of the **AB_2^{SCNP}** was lowered from basic to neutral, multimolecular aggregates were observed which indicated the occurrence of self-assembly. The hydrodynamic diameters of **AB_2^{SCNP}** increased from 5.0 nm (at pH 10.20) to 111 nm and 245 nm at pH 8.00 and 7.60, respectively (**Table 4.3**, **Figures 4.10** and **4.11**), revealing the aggregate size could vary depending on the pH. Upon further lowering the pH to acidic, DLS displayed the dissociation of the aggregates and hydrolysis of the boronic esters leading to the formation of polymers with slightly bigger sizes than **AB_2^{SCNP}** at basic condition (**Table 4.3**, **Figure 4.11**). This phenomena is consistent with the assumption that assembled micellar structures were formed, composed of a hydrophilic PolyNAM shell and a hydrophobic core, the size of which gradually increases when the pH was decreased as the anionic/hydrophilic boronate esters groups were converted to neutral/hydrophobic boronic esters groups. Once the pH-value reached to a critical level, the hydrolysis of boronic esters started occurring and led the dissociation of the micelles. It is noteworthy that at acidic condition (pH ≈ 2), **AB_1^{SCNP}** still displays a similar size as basic condition, whereas **AB_2^{SCNP}** shows an increased size value. ^{1}H NMR and SEC studies were utilized to investigate the transition further.

Table 4.3 Hydrodynamic sizes of **AB_2^{SCNP}** at different pH values obtained by DLS in H_2O.

pH	D_h (nm)	PDI
10.20	5.0	0.08
8.89	5.0	0.06
8.00	111.2	0.04
7.60	245.5	0.02
6.55	6.3	0.04
4.40	6.8	0.04
3.08	6.6	0.05
2.50	6.5	0.07

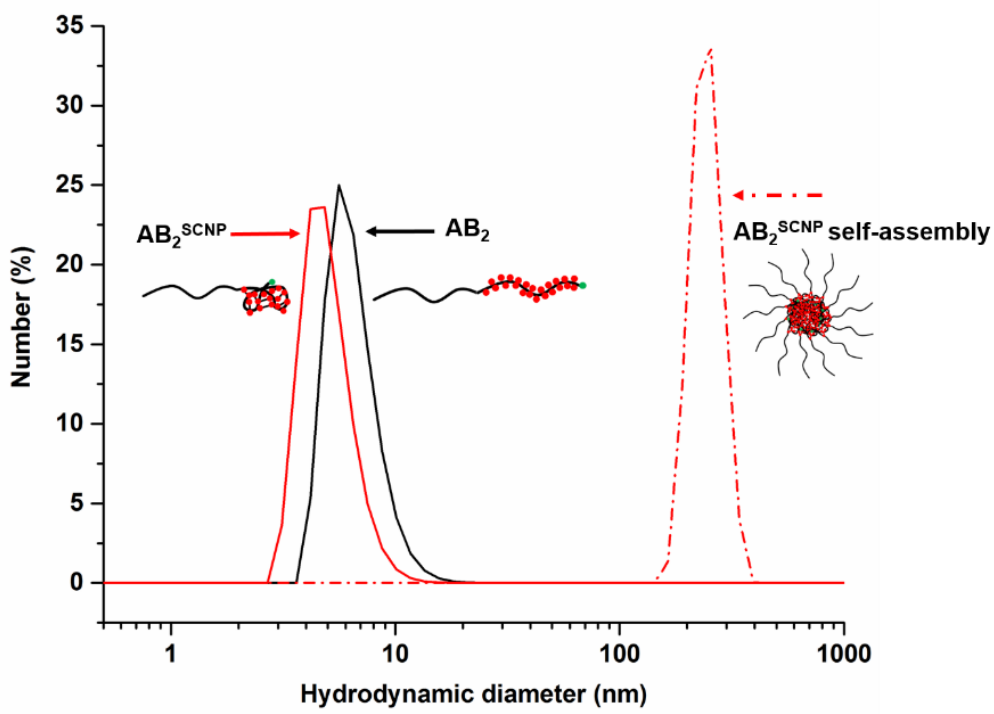

Figure 4.10 Hydrodynamic size distributions obtained by DLS in H_2O for: **AB_2**, **AB_2^{SCNP}** at pH = 10.20, and **AB_2^{SCNP}** self-assembly at pH = 7.60.

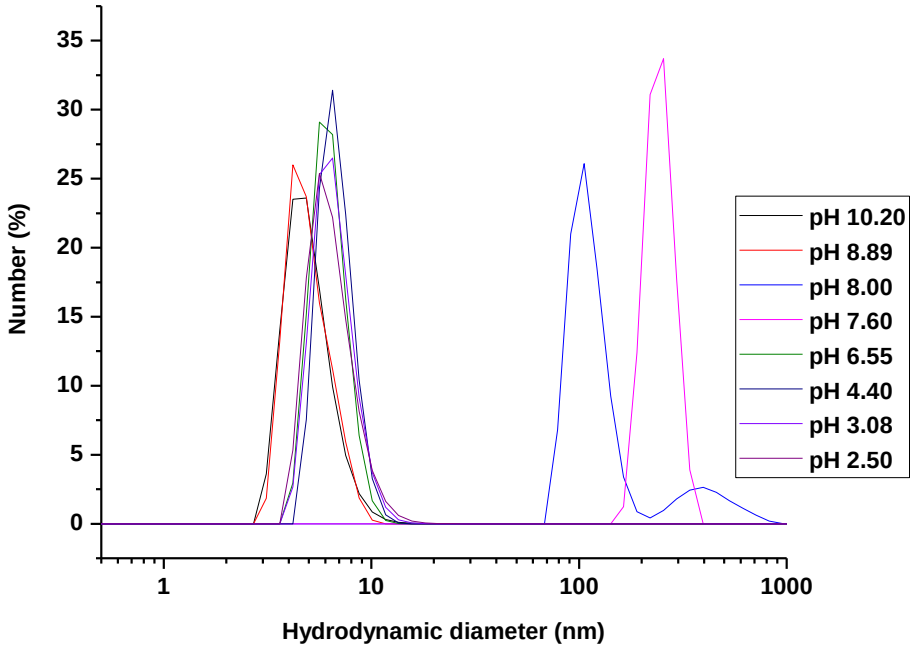

Figure 4.11 Hydrodynamic size distributions of **AB_2^{SCNP}** at different pH values obtained by DLS in H_2O.

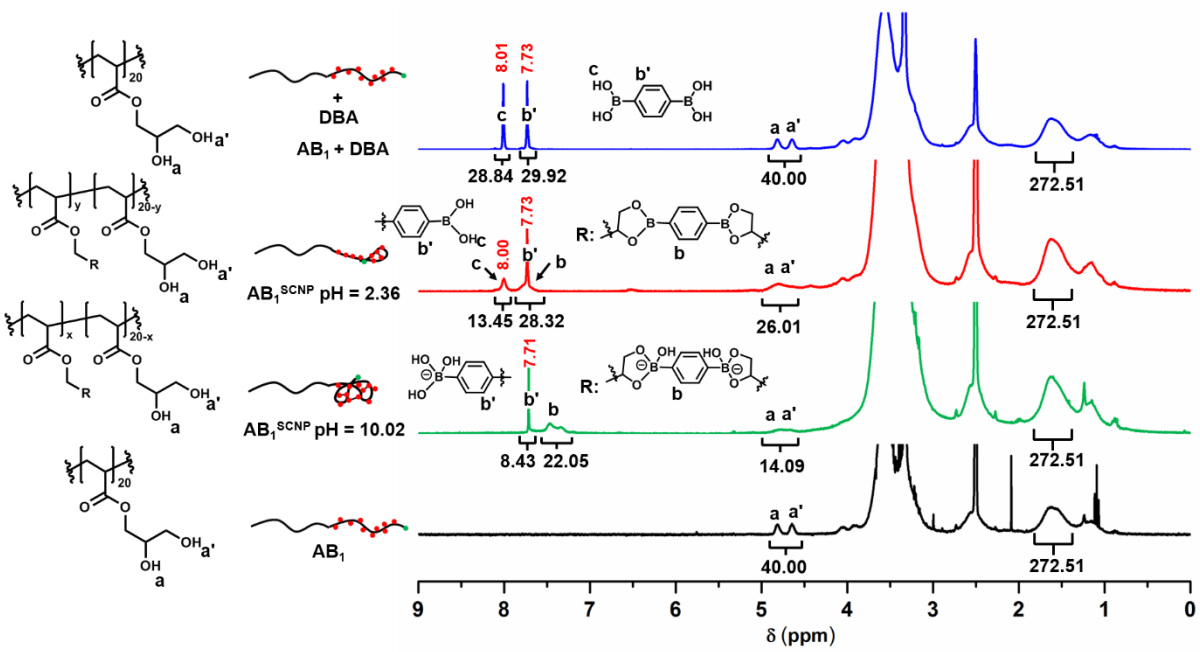

Figure 4.12 ^{1}H NMR spectra (300 MHz, DMSO-d_6) of: (from bottom to top) linear copolymer **AB$_1$**, folded copolymer **AB$_1^{SCNP}$** at pH = 10.02, folded copolymer **AB$_1^{SCNP}$** at pH = 2.36, and linear copolymer **AB$_1$** mixed with free DBA cross-linker in DMSO-d_6.

In order to be able to monitor the hydrolysis of boronic esters, DMSO-d_6 was used to observe the appearance of O***H*** groups of GLA unit. ^{1}H NMR spectroscopy investigation of **AB$_1$** and **AB$_1^{SCNP}$** in DMSO-d_6 was examined first (**Figure 4.12**, the integral of the peaks between δ = 1.90 and 1.30 ppm was used as internal reference, see the experimental part for how to integrate these peaks).

The spectrum of **AB$_1^{SCNP}$** at pH 10.02 revealed the appearance of signals associated with cross linked DBA (peak **b**; for a comparison with free DBA mixed with free linear polymer **AB$_1$**, see the top spectrum in **Figure 4.12**; for a comparison with free DBA and free DBA at pH ≈ 10, see **Figures 4.24** and **4.25**, respectively). The spectrum displayed the signals of unreacted diol groups (peaks **a** and **a'**) which is probably due to the high steric hindrance after the folding of the polymer.[68, 70] The ^{1}H NMR spectroscopy of **AB$_1^{SCNP}$** in acidic condition (pH = 2.36) revealed that the integral of the signals associated with the free diol (peaks **a** and **a'**)

increased to 26.01 from 14.09 (for pH = 10.02), indicating 46 % [(26.01-14.09) ÷ (40.00-14.09) = 46%] hydrolysis of the total number of boronic esters. Similarly the integration of aromatic protons (peaks **b** + **b'**) and O***H*** groups (peak **c**) corresponding to DBA cross-linker also demonstrates equivalent value for hydrolysis. This equates between 100% and 53% of the cross-linker still attached to the polymer backbone depending on the number of DBA existing as a mono-boronic ester (100%, meaning all the DBA units were attached to the polymer backbone by one side) and di-boronic ester [53%, in this case all the O*H* groups (peak c) corresponding to DBA cross-linker belong to free DBA units, therefore the amount of the cross-linker still being attached to the polymer backbone is 28.32 – 13.45 = 14.87. The percentage of the attached DBA is therefore calculated to be 14.87 ÷ 28.32 = 53%] respectively. It is noteworthy the signals of aromatic protons (peak **b**) corresponding to the DBA cross-linker attached to the polymer chain shifted downfield at lower pH. This is consistent with the fact that boronate esters are negatively charged at high pH causing a rich electron environment (low chemical shift) around the aromatic ring and poor electron environment (high chemical shift) when uncharged at low pH.

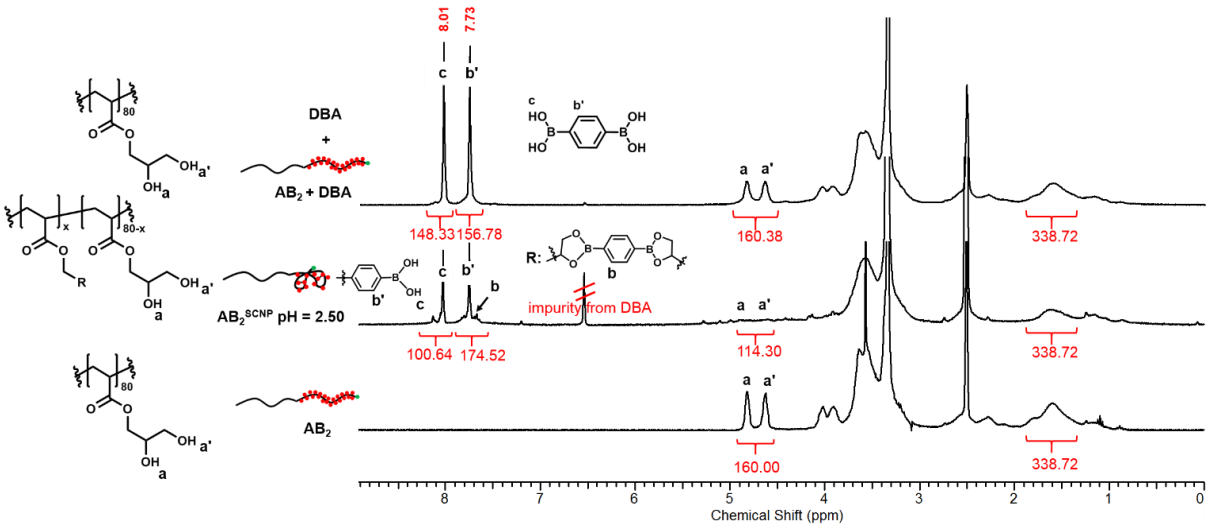

Figure 4.13 ^{1}H NMR spectra (300 MHz, DMSO-d_6) of linear polymer **AB$_2$** (bottom), folded polymer **AB$_2^{SCNP}$** at pH = 2.50 (middle), and linear polymer **AB$_2$** mixed with free DBA cross-linker in DMSO-d_6 (top). The integration

of the peaks between δ = 2.00 and 1.28 ppm was used as internal reference (see the experimental for how to integrate these peaks).

AB_2^{SCNP} was found to be insoluble in the NMR solvent used for this investigation, due to the high density of anionic boronate ester formed (see **Figure 4.26** for DBA at pH ≈ 10 in DMSO-d_6). However, the ^{1}H NMR spectrum of **AB_2^{SCNP}** in acidic condition (pH = 2.50, **Figure 4.13**) also displays similar profile to that of **AB_1^{SCNP}**, revealing between 84 % and 42 % (see the following text for the detailed calculation) of DBA cross-linker still attached to the polymer backbone. The method for the calculation of the percentage of DBA cross-linker attached to the polymer backbone is as following: As **AB_2^{SCNP}** at pH ≈ 10 was not fully soluble in DMSO, we were not able to obtain the ^{1}H NMR spectrum at this pH. Therefore, the diol units (peaks a and a') could not be used as reference and the percentage of DBA cross-linker attached to the backbone was calculated according to the integration of peaks c, b', and b. As aforementioned, peak c corresponds to the hydrolysed DBA units and as shown in the above figure, the integration of peak c equals peak b'. The percentage of hydrolysed DBA cross-linker: $(\text{hydrolyzed DBA}) = \frac{\int b'}{\int b+b'} \times 100\% = \frac{\int c}{\int b+b'} \times 100\%$. Therefore, $n(\text{hydrolyzed DBA}) = \frac{100.64}{174.52} \times 100\% = 57.6\%$. If both sides of the DBA were hydrolyzed, then the percentage of attached DBA is 42% (1 - 57.6% = 42.4%). If only one side of the DBA was hydrolysed, then the percentage of attached DBA is 84% (42% × 2 = 84%). Therefore, the percentage of DBA cross-linker attached to the polymer backbone is between 84% and 42%.

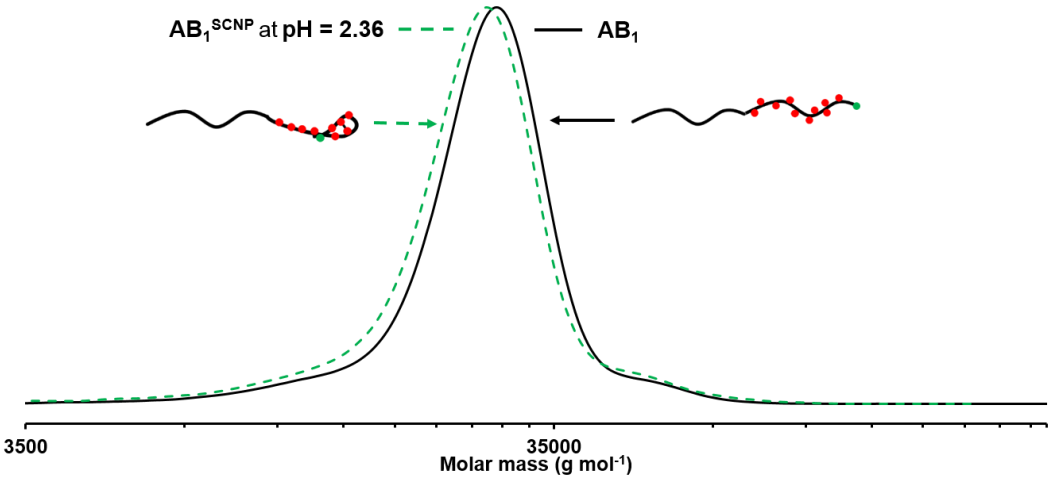

Figure 4.14 SEC chromatograms (RI traces) obtained in DMF for: **AB$_1$** ($M_{p,SEC}$ = 27200 g mol^{-1}, $M_{n,SEC}$ = 23700 g mol^{-1}, $Đ$ = 1.14) and **AB$_1$^{SCNP}** at pH = 2.36 ($M_{p,SEC}$ = 26100 g mol^{-1}, $M_{n,SEC}$ = 22000 g mol^{-1}, $Đ$ = 1.19, <G> = 0.96).

SEC analysis of the **AB$_1$^{SCNP}** at acidic condition (pH = 2.36) displays slightly smaller hydrodynamic volume compared to linear precursor **AB$_1$** (<G> = 0.96, **Figure 4.14**) but higher hydrodynamic volume than **AB$_1$^{SCNP}** at pH = 10.02 which is consistent with the hydrolysis of the boronic esters. This minor shift is likely to be associated with the low amount of residual intramolecular cross-linking. It is noteworthy that SEC analysis of self-assembled **AB$_2$^{SCNP}** at around neutral condition (pH = 7.60) demonstrates the retention of tadpole-like SCNPs structure with no apparent intermolecular exchange of the DBA cross-linker, despite the close proximity of the hydrophobic "heads" in solution and dynamic nature of the boronic ester (**Figure 4.15**). Moreover, a smaller compaction parameter (<G> = 0.78, **Table 4.4**) compared to **AB$_2$^{SCNP}** at pH = 10.20 (<G> = 0.86) was observed. This is because the anionic boronate esters are more solvated due to the solvent screening the charge, hence neutralising the charge reduces the swelling. The SEC trace of the **AB$_2$^{SCNP}** in acidic conditions (pH = 2.50) shows a shift towards higher molar mass compared to **AB$_2$^{SCNP}** at pH =7.60, suggesting the hydrolysis of the boronic esters (**Figure 4.15**). However, compared to the linear precursor, it still displays lower molar mass distribution indicating intramolecular cross-linking (<G> = 0.88, **Table 4.4**).

These results are consistent with the ^{1}H NMR analysis. The more pronounced compaction displayed by **AB$_2$^{SCNP}** compared to **AB$_1$^{SCNP}** in acidic condition is likely due to the increased amount of cross-linker in **AB$_2$^{SCNP}** which caused the de-crosslinking to be less efficient.

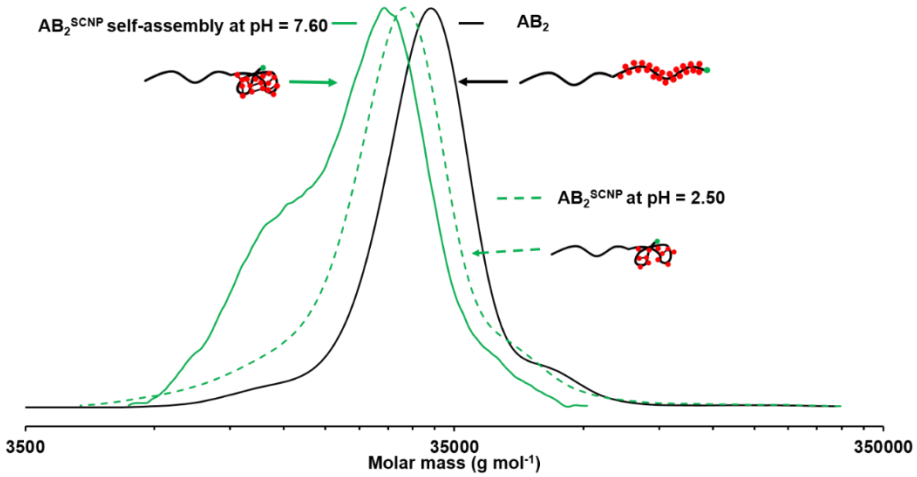

Figure 4.15 SEC chromatograms (RI traces) obtained in DMF for: **AB$_2$**, **AB$_2$^{SCNP}** self-assembly at pH = 7.60, and **AB$_2$^{SCNP}** at pH = 2.50. These samples were run in the same calibration which is different to those in **Figure 4.5** due to the recalibration of the SEC system when the analysis was carried out.

It is interesting to notice that while DMF-SEC of **AB$_1$^{SCNP}** in acidic condition (pH = 2.36) only shows a minor shift towards lower molar mass compared to **AB$_1$** (**Figure 4.14**) but DLS still displays similar size to **AB$_1$^{SCNP}** in basic condition (**Table 4.2**, **Figure 4.9**); whereas **AB$_2$^{SCNP}** in acidic condition (pH = 2.50) reveals a relatively big shift toward lower molar mass compared to **AB$_2$** by DMF-SEC (**Figure 4.15**) but displays bigger size distribution than **AB$_2$^{SCNP}** in basic condition in DLS (**Table 4.3**, **Figure 4.11**). This is probably due to the hydrophobicity of the remaining DBA cross-linker attached to **AB$_1$^{SCNP}** in acidic condition causing the chains to collapse in H_2O leading to the smaller size as reflected by DLS. On the other hand, considering there are still relative high amount of DBA cross-linkers in **AB$_2$^{SCNP}** in acidic condition as illustrated by DMF-SEC (**Figure 4.15**), these hydrophobic DBA cross-linkers will still cause the aggregation of **AB$_2$^{SCNP}** to a certain extent which caused bigger sizes than **AB$_2$^{SCNP}** in basic condition but are insufficient for self-assembly into bigger particles.

Therefore, it is reasonable to assume $\mathbf{AB_2}^{\mathbf{SCNP}}$ in acidic condition in H_2O is composed of small self-assembled aggregates consisting of amphiphilic tadpole-like SCNPs with a low degree compaction. The reason why $\mathbf{AB_1}^{\mathbf{SCNP}}$ did not self-assemble into micellar structures was hypothesized due to the low amount of the boronate ester compared to $\mathbf{AB_2}^{\mathbf{SCNP}}$ as a result of the low diol content of $\mathbf{AB_1}$, and therefore insufficient hydrophobicity to promote self-assembly.

Transmission electron microscopy (TEM) and atomic force microscopy (AFM) imaging were employed to further explore the morphology of the nanoparticles formed by self-assembly of $\mathbf{AB_2}^{\mathbf{SCNP}}$ at pH 7.60 in aqueous solution. Spherical nano-objects with diameter sizes of around 38 (± 6.6) nm were visualized by TEM (**Figure 4.16**). AFM also revealed nanoparticles with similar diameter values to TEM (**Figure 4.17**, samples used for TEM and AFM were diluted by 10 times after self-assembly of $\mathbf{AB_2}^{\mathbf{SCNP}}$at pH = 7.60). The relatively small size compared to the values obtained by DLS analysis could be due to a shrinking of the samples in dry state, whereas water-swollen structures were observed in aqueous solution using DLS.

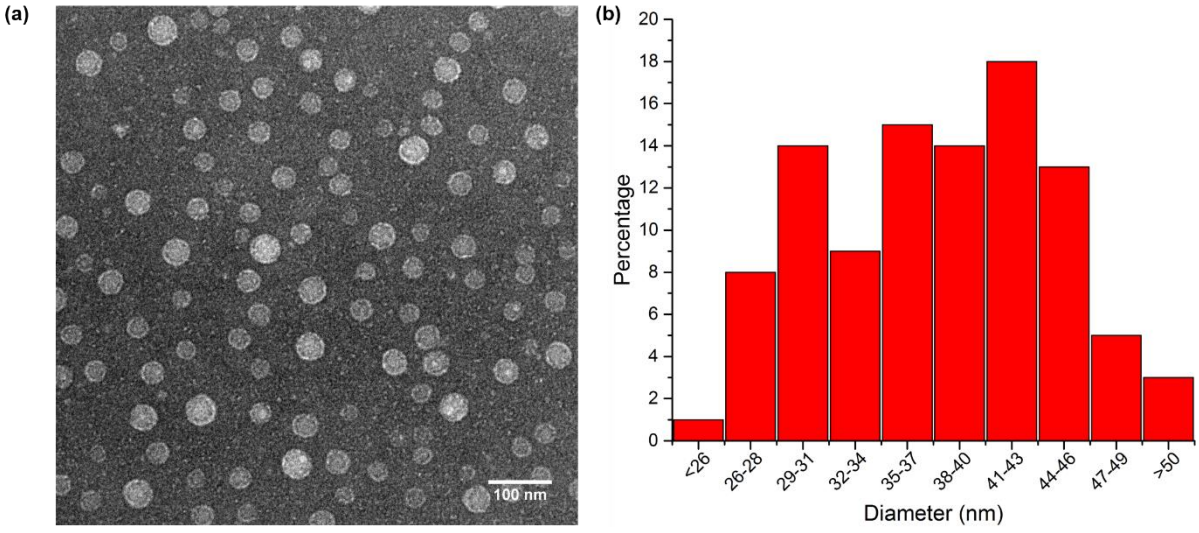

Figure 4.16 Representative image of nanoparticles formed by the self-assembly of $\mathbf{AB_2}^{\mathbf{SCNP}}$ obtained by TEM (a) and size distributions of nanoparticles analyzed from TEM results (b).

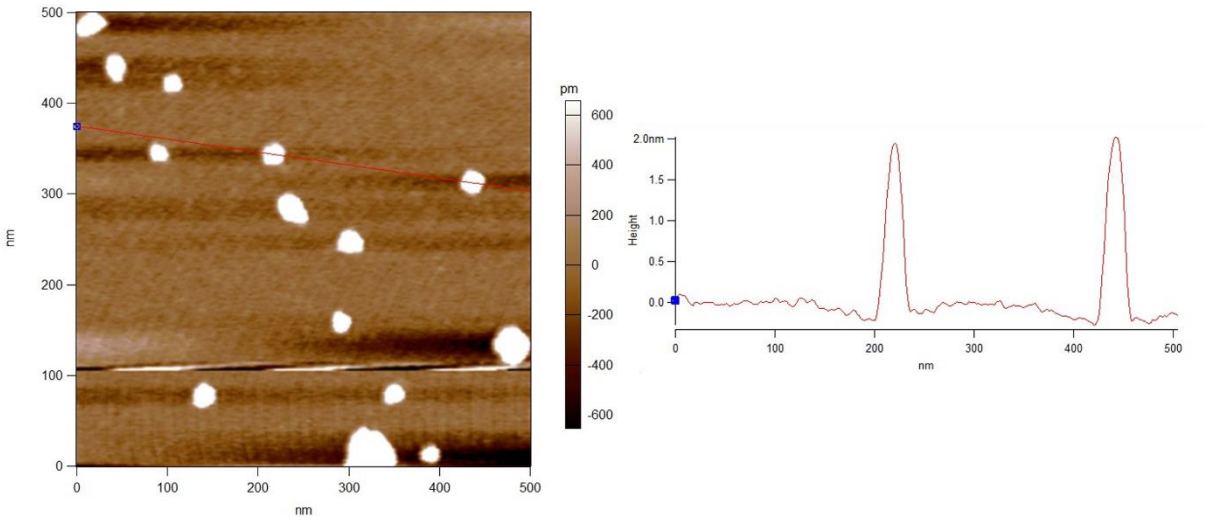

Figure 4.17 Representative AFM topography image of nanoparticles formed by the self-assembly of $\mathbf{AB_2}^{\mathbf{SCNP}}$. The red line in the topography image shows the analyzed particles.

In addition to the pH responsive nature, the diol responsiveness of the tadpole-like SCNPs and the self-assembled micelles was also investigated in order to exploit the potential applications in sensors for sugars.[80] Due to the reversibility of the cyclic boronate/boronic esters formed by the boronic acid groups with 1,2- and 1,3-diols,[52, 80] the free diol containing molecules will competitively react with boronic ester *via* transesterification. Upon the addition of glucose to the aqueous solution of the $\mathbf{AB_1}^{\mathbf{SCNP}}$ and $\mathbf{AB_2}^{\mathbf{SCNP}}$ at basic condition, decross-linking of the SCNPs was triggered leading to polymers with similar sizes to the respective linear precursor as detected by DLS (**Figures 4.18** and **4.19**). SEC analysis of the SCNPs samples treated with sugar also revealed similar molar mass distributions to the corresponding linear copolymers (**Figures 4.20** and **4.21**).

Addition of glucose to the solution of micelles formed by self-assembly of $\mathbf{AB_2}^{\mathbf{SCNP}}$ at pH 7.60 caused the disruption of self-assembled structure and led the formation of unimers as displayed by DLS showing similar hydrodynamic diameter to the linear $\mathbf{AB_2}$ (**Figure 4.19**). In addition to the DLS results, dissociation was also illustrated by SEC (**Figure 4.21**) analysis which shows similar molar mass distribution to $\mathbf{AB_2}$ precursor for the disassembled sample.

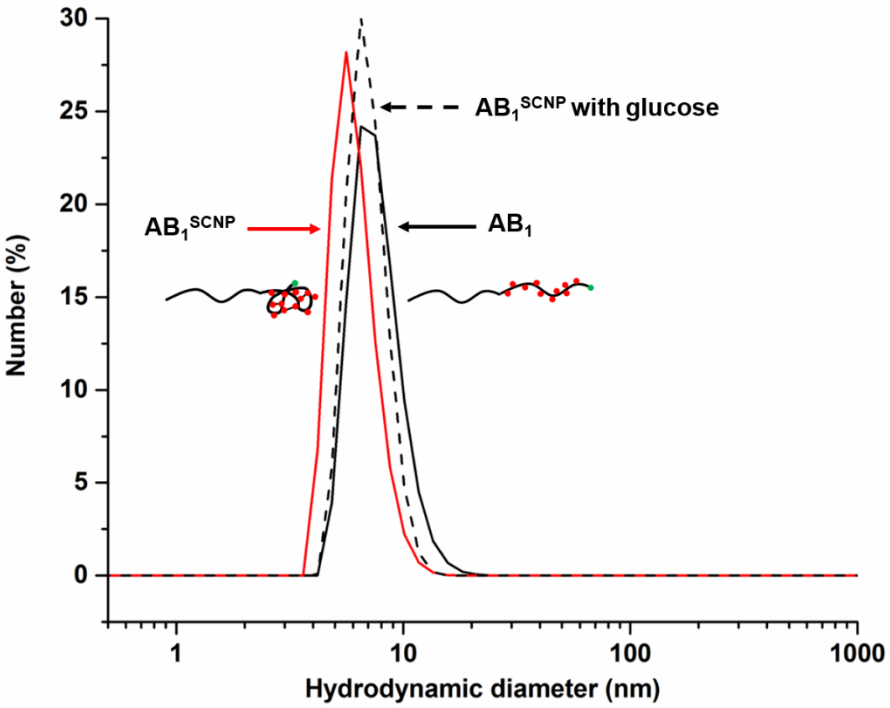

Figure 4.18 Hydrodynamic size distributions obtained by DLS in H_2O for: **AB_1^{SCNP}** at pH = 10.02, **AB_1^{SCNP}** with addition of glucose at pH = 10.02, and linear copolymer **AB_1**.

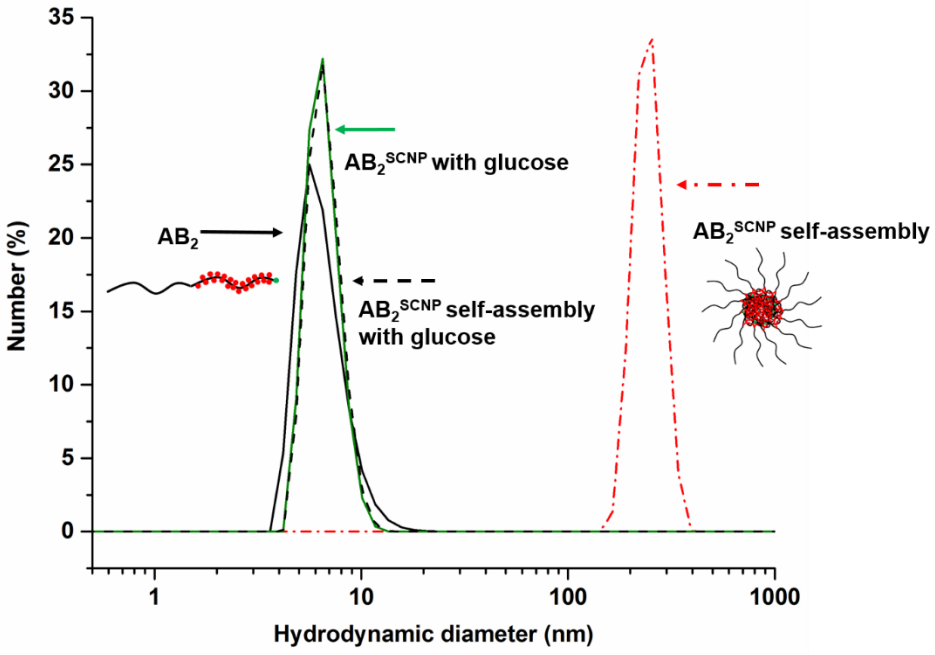

Figure 4.19 Hydrodynamic size distributions obtained by DLS in H_2O for: linear copolymer **AB_2**, **AB_2^{SCNP}** with addition of glucose at pH = 10.20, **AB_2^{SCNP}** self-assembly with addition of glucose at pH = 7.60, and **AB_2^{SCNP}** self-assembly at pH = 7.60.

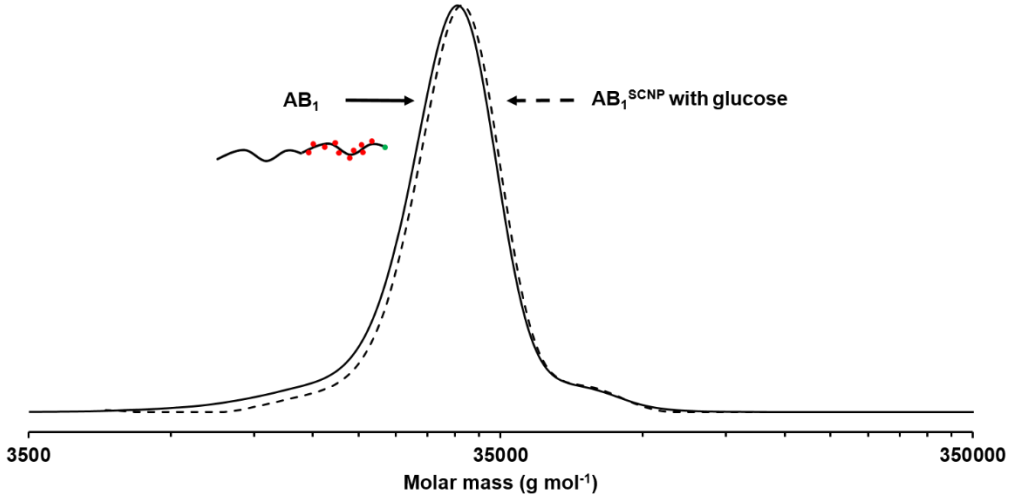

Figure 4.20 SEC chromatograms (RI traces) obtained in DMF for: **AB$_1$** (solid) and **AB$_1^{SCNP}$** with addition of glucose at pH = 10.02 (dash). These samples were run in the same calibration which is different to those in **Figure 1** due to the recalibration of the SEC system when the analysis was carried out.

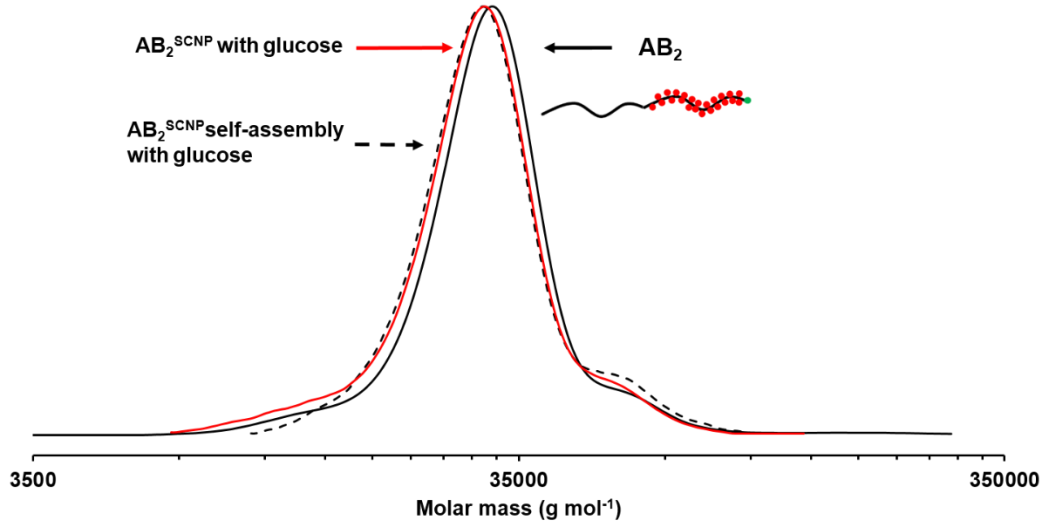

Figure 4.21 SEC chromatograms (RI traces) obtained in DMF for: **AB$_2^{SCNP}$** self-assembly with addition of glucose at pH = 7.60 (black dash), **AB$_2^{SCNP}$** with addition of glucose at pH = 10.20 (red), and linear copolymer **AB$_2$** (black solid). These samples were run in the same calibration which is different to those in **Figure 4.5** due to the recalibration of the SEC system when the analysis was carried out.

4.3 Conclusions

In summary, tadpole-like SCNPs were synthesised using a pH responsive DBA cross-linker and suitable linear polymer precursors, which exhibited self-assembly due to the hydrophobic nature of cross-linker past its isoelectric point. The assembled SCNPs displayed spherical morphology as characterised by TEM and AFM. The intramolecular folding of individual SCNPs was intact and no chain entanglement occurred after self-assembly according to the SEC. The volume fraction of cross-linkable GLA in the second block was found to play a crucial role in the self-assembly of the SCNP, as sufficient hydrophobicity is required to promote the "head" group to drive self-assembly. The dissociation of assemblies can be triggered by varying the environmental pH or exposing to an external stimuli as demonstrated by addition of glucose. The use of boronic acid containing polymers for pH dependent self-assembly has been demonstrated elsewhere, however, forming a SCNP with boronic acid cross-linker and taking advantage of its stimuli-responsive properties to drive self-assembly, has not been reported. The present study demonstrates the ability of synthetic polymers to mimic folding of natural polypeptide chains and assembly into a higher-order structures found in natural multiprotein complexes, which also display a stimuli responsive character.

4.4 Experimental

4.4.1 Materials

1, 4-Dioxane was obtained from Fisher Scientific and used as received. Anhydrous Tetrahydrofuran (THF, ≥99.9%), Dichloromethane (DCM, ≥99.5%), Isopropyldiene glycerol (98%), triethylamine (99%), benzene-1,4-diboronic acid (DBA, ≥95.0%) were obtained from Sigma Aldrich and used as received. 4-Acryloylmorpholine (NAM, Sigma-Aldrich, 97%) was

filtered through a basic aluminium oxide (activated, basic, BrockmannI, standard grade, B150 mesh, 58Å) column before use to remove the radical inhibitor. 2, 2′-azobis[2-(2-imidazolin-2-yl)propane]dihydrochloride (VA-044, Wako) was used without further purification. dimethyl sulfoxide-d6 (DMSO-d_6, 99.9% D atom) obtained from Sigma Aldrich were used for ^{1}H NMR analysis. 2-(((butylthio)-carbonothioyl)thio)propanoic acid (called (propanoic acid)yl butyl trithiocarbonate (PABTC) in this paper) was prepared according to a previously reported procedure.[81] Glycerol acrylate **(**GLA) was synthesized by adapting to the published procedure.[60] Carbon coated copper (300 mesh) TEM grids were obtained from EM Resolutions (Saffron Walden, U.K.) and used as received. Mica discs for AFM were purchased from Agar Scientific Ltd, U.K. and freshly cleaved before use.

4.4.2 Methods

4.4.2.1 Nuclear Magnetic Resonance (NMR) spectroscopy

^{1}H NMR Spectra were recorded on a Bruker Avance III AV 300 spectrometer (300 MHz) or an HD 400 spectrometer (400 MHz) at 27 °C in deuterated DMSO (DMSO-d_6). Chemical shift values (δ) are reported in ppm. The residual proton signal of the solvent (δ_H = 2.51 ppm) was used as internal reference.

4.4.2.2 Size Exclusion Chromatography (SEC)

Number-average molar masses ($M_{n,SEC}$) and dispersity values ($Đ$) were determined using size exclusion chromatography with DMF as an eluent. The DMF Agilent 390-LC MDS instrument equipped with differential refractive index (DRI), viscometry (VS), dual angle light scatter (LS) and dual wavelength UV detectors. The system was equipped with 2 x PLgel Mixed D columns (300 x 7.5 mm) and a PLgel 5 µm guard column. The eluent is DMF with 5 mmol NH_4BF_4 additive. Samples were run at 1 mL/min at 50 °C. Poly(methyl methacrylate)

standards (Agilent EasyVials) ranging from MW = 1010 g mol^{-1} to 955000 g mol^{-1} were used for calibration. Analyte samples were filtered through a nylon membrane with 0.22 μm pore size before injection. Respectively, experimental molar mass ($M_{n,SEC}$) and dispersity ($Đ$) values of synthesized polymers were determined by conventional calibration using Agilent GPC/SEC software.

4.4.2.3 Differential Scanning Calorimetry (DSC)

The experiments were performed to determine the thermal behavior of the synthesized polymers on a Mettler Toledo DSC1. In all tests, a scan rate of 10 K/min was used for three heating and cooling cycles. The glass transition temperature (T_g) value is the maxima of the first derivative of (d_H/d_T) the second heating run.

4.4.2.4 Transmission Electron Microscopy (TEM)

Samples were prepared by placing a carbon coated copper grid onto a 20 μL droplet of aqueous nanoparticles in a petri dish and allowed to air-dry overnight. The grid was then stained with an aqueous solution of uranyl acetate (0.2 wt%) and allowed to air-dry overnight. TEM images were acquired using a JEOL 2100 transmission electron microscope operating at a 200 kV accelerating voltage. Images were captured using Digital Micrograph® and analysed with ImageJ. Size distributions were produced by measuring at least 100 particles in ImageJ.

4.4.2.5 Atomic Force Microscopy (AFM)

AFM images were acquired in AC mode on a Cypher S system (Asylum Research). The probes used were the AC160TS from Olympus probes with a nominal resonant frequency of 300 kHz and a spring constant of approximately 40 N m^{-1} on a Multimode AFM (Asylum Research). Images were acquired at a pixel resolution of 512 and a scan rate of 1 Hz. The data were analysed by the Asylum Research software.

4.4.2.6 Dynamic Light Scattering (DLS)

Hydrodynamic diameters (D_h) and size distributions were determined by DLS on a MALVERN Zetasizer Nano ZS operating at 20 °C with a 633 nm laser module. Measurements were made at a detection angle of 173° (back scattering). Measurements were repeated three times with automatic attenuation selection and measurement position. The results were analysed using Malvern DTS 6.20 software, using the multiple narrow modes setting. PDI values were calculated using equation 4.1.

$$\text{PDI} = \frac{\sigma^2}{d^2} \qquad \text{(Equation 4.1)}$$

where σ is standard deviation, and d is the diameter.

4.4.2.7 Determination of monomer conversions

The conversions of the monomers were determined by comparing the integration of the vinyl protons (δ ~ 6.50–5.50 ppm) to the integration of the three methyl protons belonging to the Z group of the PABTC chain transfer agent (–CH_2–C$\underline{\boldsymbol{H_3}}$) before and after polymerization.

Calculation of $M_{n,th}$. The theoretical number average molar mass ($M_{n,th}$) is calculated using Equation 4.2.

$$M_{n,th} = \frac{[M]_0\, p M_M}{[CTA]_0} + M_{CTA} \qquad \text{(Equation 4.2)}$$

where $[M]_0$ and $[CTA]_0$ are the initial concentrations (in mol L^{-1}) of monomer and chain transfer agent respectively; p is the monomer conversion as determined by ^{1}H NMR, M_M and M_{CTA} are the molar masses (g mol^{-1}) of the monomer and chain transfer agent respectively.

4.4.2.8 General procedures for copolymer synthesis by RAFT polymerization

A typical synthesis of the first block is the following: CTA, monomer, solvent (1, 4-dioxane and deionized water) and azoinitiator were charged into a flask having a magnetic stirring bar. The flask was sealed with a rubber septum and degassed with nitrogen for ca. 15 minutes. The solution was then allowed to stir at 70 ˚C in a thermo-stated oil bath for the desired time. A sample was taken for ^{1}H NMR (to determine monomer conversion) and SEC analysis (to determine $M_{n.SEC}$ and $Đ$). After reaction, the mixture is cooled down in cold water to room temperature and open to air.

Typical synthesis of the following block: Monomer, initiator and solvent is added to the previous polymerization medium and well mixed. The mixture is then degassed by bubbling nitrogen through the solution for ca. 15 minutes, and the polymerization mixture was allowed to polymerize at 70 ˚C for the desired time with stirring. A sample was withdrawn from the polymerization medium using a degassed syringe for ^{1}H NMR and SEC analysis. After reaction, the mixture is cooled down in cold water to room temperature and open to air.

4.4.2.9 Integration in the ^{1}H NMR spectroscopy of the purified polymers of AB_1, AB_2, AB_1^{SCNP} and AB_2^{SCNP} at different pH values

Due to the high DP of the polymers, the integration of the three methyl protons belonging to the Z group of the PABTC chain transfer agent (–CH_2–CH_3) will not be accurate. Therefore, the integration of the diol of **AB_1** and **AB_2** after precipitation was used as internal reference respectively to integrate the peaks between δ = 1.90 and 1.30 ppm for **AB_1** and the peaks between δ = 2.00 and 1.28 ppm for **AB_2** and this integration was used as internal reference respectively for **AB_1^{SCNP}** and **AB_2^{SCNP}** at different pH values. Considering the targeted DPs

and the quantitative conversion of the monomers, the integration of the diol peaks was assumed to be 40 for **AB$_1$** and 160 for **AB$_2$**.

4.4.2.10 Self-assembly behaviour study of AB$_1^{SCNP}$ and AB$_2^{SCNP}$ depending on the pH changes by DLS measurements, TEM, AFM, ^{1}H NMR, and SEC analysis

A 1% weight solution of **AB$_1^{SCNP}$** and **AB$_2^{SCNP}$** were prepared separately by dissolving the respective SCNPs in deionized water. The initial pH values of the resulting solutions were found to be 10.02 for **AB$_1^{SCNP}$** and 10.20 for **AB$_2^{SCNP}$** without adjusting. The pH of the resulting solutions were then adjusted to the certain values as displayed in **Tables S1** and **S2** using 1 M HCl solution. The hydrodynamic diameters (D_h) and size distributions of each pH value were measured by DLS. The solution of **AB$_1^{SCNP}$** at pH 2.36 was freeze dried to remove the solvent and the obtained material was used for ^{1}H NMR and SEC analysis. Part of the solution of **AB$_2^{SCNP}$** at pH 7.60 (when the self-assembly occurred) was taken for SEC, TEM, AFM, and sugar responsive analysis. The solution of **AB$_2^{SCNP}$** at pH 2.50 was freeze dried to remove the solvent and the obtained material was used for ^{1}H NMR and SEC analysis.

4.4.2.11 Sugar responsive study of AB$_1^{SCNP}$, AB$_2^{SCNP}$, and AB$_2^{SCNP}$self-assembly at pH 7.60

Glucose (10 eq. of n(diol)) was added to the solution of **AB$_1^{SCNP}$** and **AB$_2^{SCNP}$** (1% weight in H_2O) at pH ≈ 10 and the solution of **AB$_2^{SCNP}$**self-assembly at pH 7.60. The hydrodynamic diameters (D_h) and size distributions of the resulting solutions were measured by DLS. The solutions were then freeze dried to remove the solvent and the obtained materials were used for SEC analysis.

4.4.3 Synthesis

4.4.3.1 Synthesis of glycerol acrylate (GLA)

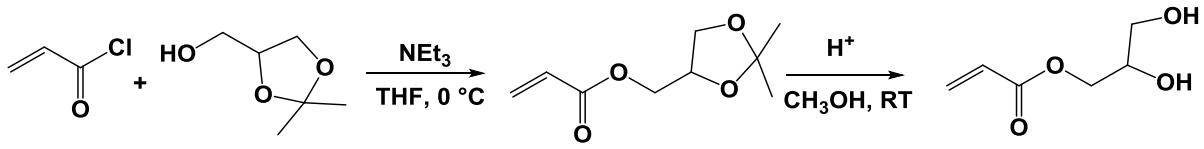

Scheme 4.2 Synthetic route of GLA

First step: Isopropyldiene glycerol (19.95 g, 151 mmol, 1 eq), NEt_3 (22.97 g, 227 mmol, 1.5 eq), 0.25 g of hydroquinone (inhibitor), and 200 mL of dried THF were added to a 2 L round bottom flask. Acryloyl chloride (16.4 g, 182 mmol, 1.2 eq) was dissolved in 35 mL of dry THF and added drop wise to the above mixture with stirring in an ice bath over one hour. The mixture was then stirred for 24 hours and filtered. The solvent was removed to obtain a pale yellow solid which was dissolved in 150 mL of DCM and then 100 mL of water was added. The organic phase was extracted with DCM (2 × 100 mL). The organic layer was combined and washed once with 100 mL of brine. The organic phase was dried with magnesium sulphate, filtered, and the solvent was removed to obtain a yellow oil. Half amount of this yellow oil was distilled at 50 ˚C under vacuum (0.35 mba) to obtain 7.2 g intermediate (solketal acrylate monomer, **SA**). ^{1}H NMR (**Figure S1**, 400 MHz, DMSO-d_6, ppm): δ = 6.38 (*dd*, 1H, J_1 = 16.0 Hz, J_2 = 4.0 Hz), 6.23 (*dd*, 1H, J_1 = 16.0 Hz, J_2 = 8.0 Hz), 5.99 (*dd*, 1H, J_1 = 8.0 Hz, J_2 = 4.0 Hz), 4.33-4.27 (*m*, 1H), 4.23 (*dd*, 1H, J_1 = 12.0 Hz, J_2 = 4.0 Hz), 4.11 (*dd*, 1H, J_1 = 8.0 Hz, J_2 = 4.0 Hz), 4.05 (*dd*, 1H, J_1 = 8.0 Hz, J_2 = 4.0 Hz), 3.72 (*dd*, 1H, J_1 = 8.0 Hz, J_2 = 4.0 Hz), 1.33 (*s*, 3H), 1.28 (*s*, 3H).

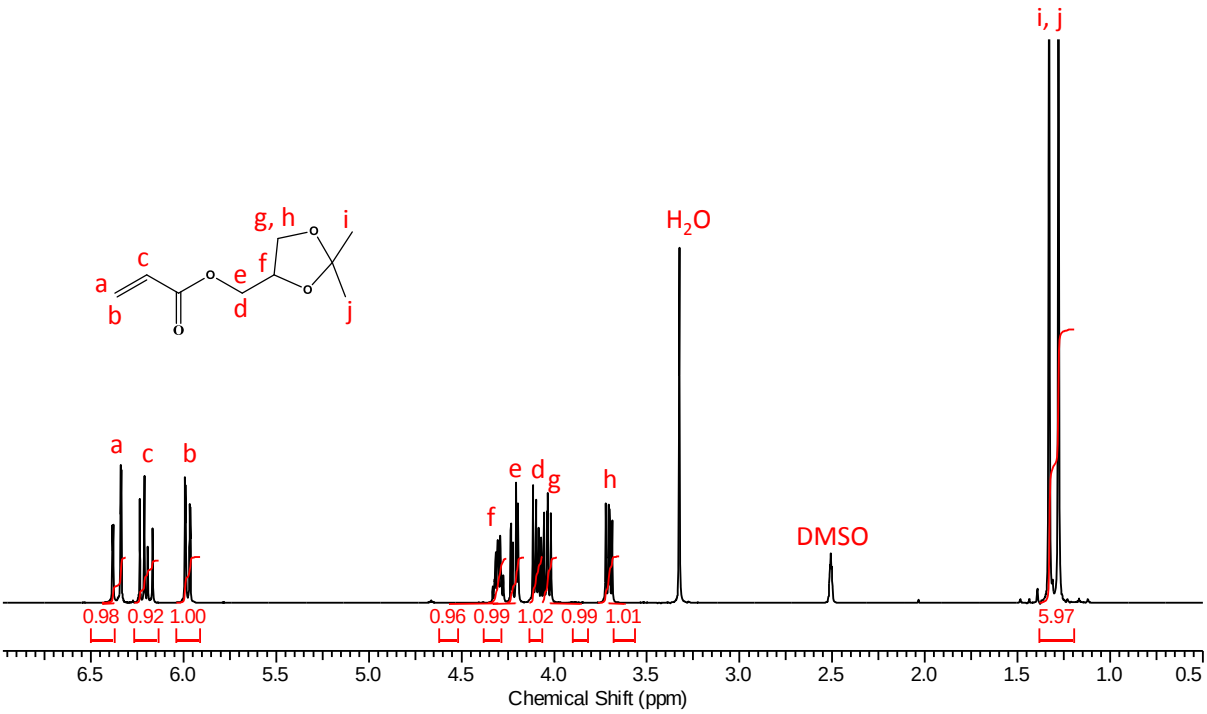

Figure 4.22 ^{1}H NMR spectrum (DMSO-d_6, 400 MHz) of **SA**.

Second step: Solketal acrylate monomer (5 g, 27 mmol) was dissolved in 130 mL of methanol in a 250 mL round bottom flask. Amberlyst resin (2.7 g) was added to the above solution and the resultant mixture was stirred for 24 hours at room temperature. The reaction mixture was then filtered to remove the amberlyst resin and the solvent was removed under reduced pressure to obtain a light brown oil which was then purified by flash column chromatography using chloroform and methanol mixture as the eluent to obtain 2.08 g of product (GLA, colorless liquid). ^{1}H NMR (**Figure S2**, 300 MHz, DMSO-d_6, ppm): δ = 6.38 (*dd*, 1H, J_1 = 18.0 Hz, J_2 = 3.0 Hz), 6.23 (*dd*, 1H, J_1 = 18.0 Hz, J_2 = 12.0 Hz), 5.97 (*dd*, 1H, J_1 = 12.0 Hz, J_2 = 3.0 Hz), 4.94 (*d*, 1H, J = 6.0 Hz), 4.68 (*t*, 1H, J = 6.0 Hz), 4.17 (*dd*, 1H, J_1 = 12.0 Hz, J_2 = 3.0 Hz), 4.03 (*dd*, 1H, J_1 = 12.0 Hz, J_2 = 6.0 Hz), 3.73-3.64 (*m*, 1H), 3.39-3.36 (*m*, 2H).

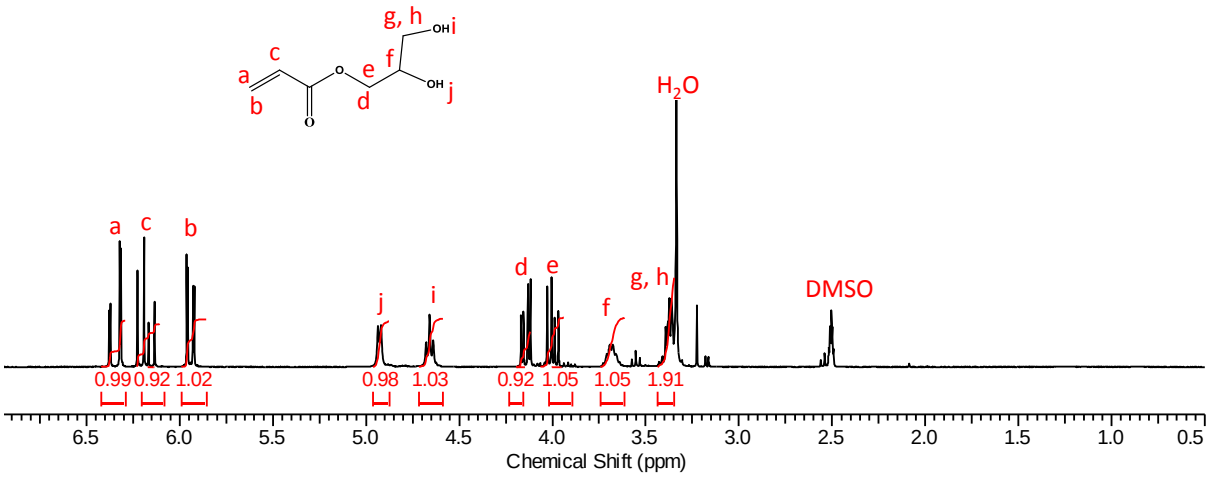

Figure 4.23 ^{1}H NMR spectrum (DMSO-d_6, 300 MHz) of **GLA**.

4.4.3.2 Synthesis of linear copolymer AB$_1$

Synthesis of first block **A**: PABTC (13.5 mg, 0.057 mmol, 1.0 eq.), NAM (800 mg, 5.7 mmol, 100 eq.), VA-044 (0.09 mg, 2.8E-04 mmol, 0.0049 eq., 45.8 µL, 2 mg/mL in H_2O), 1, 4-dioxane (0.353 mL) and H_2O (0.777 mL) were introduced into a flask equipped with a magnetic stirrer and sealed with a rubber septum. The flask was degassed by bubbling nitrogen through the solution for 15 minutes, and placed into a preheated oil bath at 70 ˚C. After 2 h, the reaction was stopped by cooling the mixture down using a cold water bath. Subsequently, a sample was taken from the reaction mixture for ^{1}H NMR and SEC analysis. ^{1}H-NMR (300 MHz, DMSO-d_6, ppm): δ = 5.11 (*s*, *broad*, *weak*, CH-S), 3.86-2.89 (*m*, broad, CH_2 polymer), 2.80-0.96 (*m*, CH and CH_2 backbone, CH_3 R-group, CH_2 Z-group), 0.89 (*t*, 3H, *J* = 6.0 Hz, CH_3 Z-group).

Chain extension of first block **A** to obtain **AB$_1$**: The reaction mixture from the last step was used directly for the chain extension. NAM (640 mg, 4.5 mmol, 80 eq.), GLA (166 mg, 1.14 mmol, 20 eq.), VA-044 (0.30 mg, 9.3E-04 mmol, 0.0016 eq., 150.6 µL, 2 mg/mL in H_2O), and H_2O (1.025 mL) were introduced into the previous polymerization medium and sealed with a rubber septum. The flask was degassed by bubbling nitrogen through the solution for 15

minutes, and placed into a preheated oil bath at 70 ˚C. After 2 h, the reaction was stopped by cooling the mixture down using a cold water bath. Subsequently, a sample was taken from the reaction mixture for ^{1}H NMR and SEC analysis. ^{1}H-NMR (300 MHz, DMSO-d_6, ppm): δ = 4.81 (*s*, OH), 4.64 (*s*, OH), 4.04 (*s*, –(C=O)–O–C***H₂***–(CHOH)-CH_2OH), 3.92 (*s*, –(C=O)–O–CH_2–(C***H***OH)-CH_2OH), 3.83-2.86 (*m*, broad, CH_2 polymer, –(C=O)–O–CH_2–(CHOH)-C***H₂***OH), 2.80-0.96 (*m*, CH and CH_2 backbone, CH_3 R-group, CH_2 Z-group), 0.90 (*t*, 3H, *J* = 6.0 Hz, CH_3 Z-group).

4.4.3.3 Synthesis of linear copolymer AB_2

Synthesis of first block **A**: The first block was synthesized using exactly the same procedure with the synthesis of **AB_1**.

Chain extension of first block **A** to obtain **AB_2**: The reaction mixture from the last step was used directly for the chain extension. NAM (160.9 mg, 1.14 mmol, 20 eq.), GLA (657.6 mg, 4.5 mmol, 80 eq.), VA-044 (0.30 mg, 9.3E-04 mmol, 0.0016 eq., 150.6 µL, 2 mg/mL in H_2O), and H_2O (1.025 mL) were introduced into the previous polymerization medium and sealed with a rubber septum. The flask was degassed by bubbling nitrogen through the solution for 15 minutes, and placed into a preheated oil bath at 70 ˚C. After 2 h, the reaction was stopped by cooling the mixture down using a cold water bath. Subsequently, a sample was taken from the reaction mixture for ^{1}H NMR and SEC analysis. ^{1}H-NMR (300 MHz, DMSO-d_6, ppm): δ= 4.82 (*s*, OH), 4.62 (*s*, OH), 4.02 (*s*, –(C=O)–O–C***H₂***–(CHOH)-CH_2OH), 3.91 (*s*, –(C=O)–O–CH_2–(C***H***OH)-CH_2OH), 3.79-3.07 (*m*, broad, CH_2 polymer, –(C=O)–O–CH_2–(CHOH)-C***H₂***OH), 2.83-0.95 (*m*, CH and CH_2 backbone, CH_3 R-group, CH_2 Z-group), 0.89 (*t*, 3H, *J* = 6.0 Hz, CH_3 Z-group).

4.4.3.4 Single chain nanoparticles (SCNP) synthesis

The copolymer precursor was dissolved in deionized water (1 mg/mL for **AB$_1$** and 0.5 mg/mL for **AB$_2$**) and the pH of the solution was adjusted to pH ≈ 10 using 1 M NaOH aqueous solution. DBA (0.5 eq. of n(diol), 0.5 mg/mL) was dissolved in pH ≈ 10 NaOH aqueous solution. The DBA solution was added drop wise to the solution of respective linear precursor in 15 minutes for the synthesis of **AB$_1$**^{SCNP} and 30 minutes for the synthesis of **AB$_2$**^{SCNP} in order to avoid the intermolecular cross-linking considering the relative large amount of diol in **AB$_2$**. After addition of the solution of DBA, the reaction mixture was freeze dried to remove water to afford the products as white solids.

4.4.4 Appendix: Supporting Information

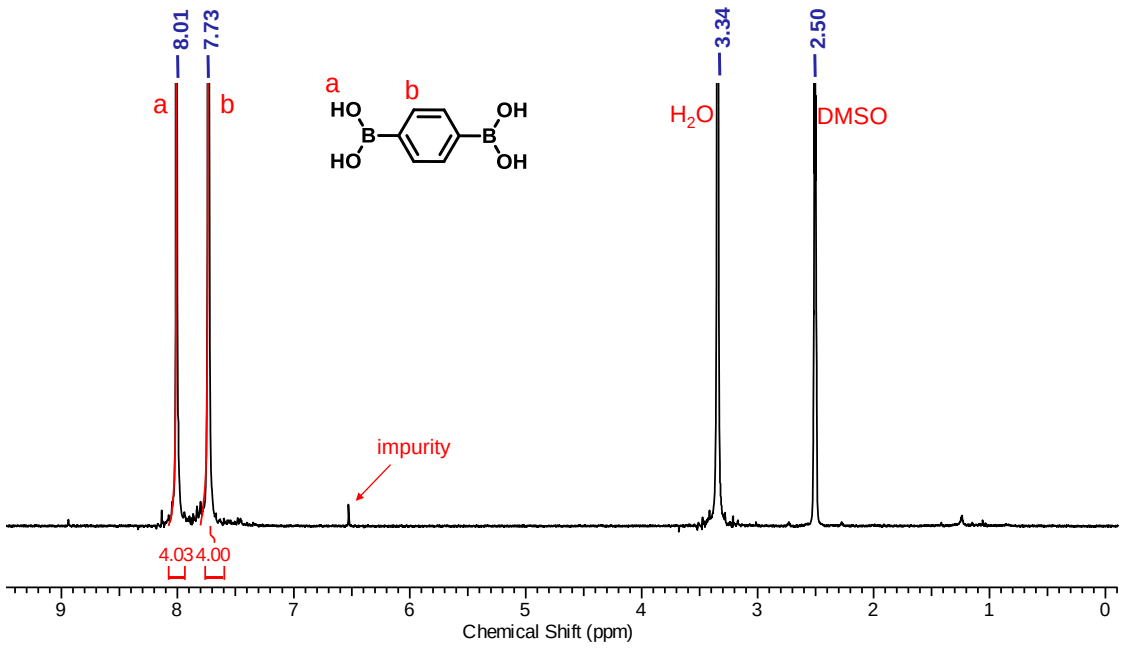

Figure 4.24 ^{1}H NMR spectrum (DMSO-d_6, 300 MHz) of free DBA.

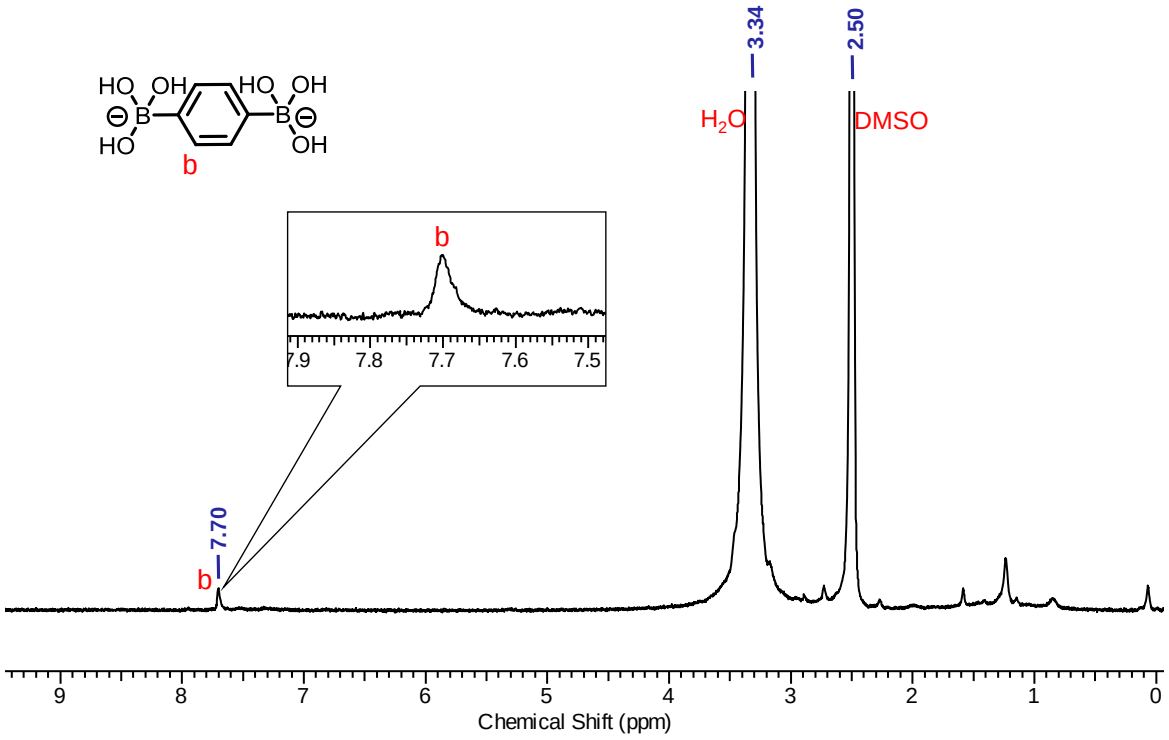

Figure 4.25 ^{1}H NMR spectrum (DMSO-d_6, 300 MHz) of free DBA at pH ≈ 10.

Figure 4.26 The picture shows that the negatively charged free DBA **(**pH ≈ 10) is not soluble in DMSO-d_6. The negatively charged free DBA was made by dissolving DBA in the solution of NaOH in H_2O and the pH was adjusted to pH ≈ 10 and freeze dried.

Table 4.4 Characterization of the linear copolymers, SCNPs at different conditions by DMF-SEC*.

sample	Composition	$M_{n,th}$[a] g mol^{-1}	$M_{p,SEC}$[b] g mol^{-1}	$M_{n,SEC}$[b] g mol^{-1}	$Đ$[b]	$<G>$[c]
AB_1	$PNAM_{100}$-*b*-P(NAM_{80}-*stat*-GLA_{20})	28600	28600	25100	1.13	-
AB_1^{SCNP} with addition of glucose	$PNAM_{100}$-*b*-[P(NAM_{80}-*stat*-GLA_{20})]^{SCNP}	-	29100	27000	1.08	-
AB_2	$PNAM_{100}$-*b*-P(NAM_{20}-*stat*-GLA_{80})	28900	30800	28200	1.16	-
AB_2^{SCNP} self-assembly at pH 7.60	$PNAM_{100}$-*b*-[P(NAM_{20}-*stat*-GLA_{80})]^{SCNP}	-	24100	18800	1.17	0.78
AB_2^{SCNP} at pH 2.50	$PNAM_{100}$-*b*-[P(NAM_{20}-*stat*-GLA_{80})]^{SCNP}	-	27100	23200	1.16	0.88
AB_2^{SCNP} with addition of glucose	$PNAM_{100}$-*b*-[P(NAM_{20}-*stat*-GLA_{80})]^{SCNP}		29900	26500	1.14	-
AB_2^{SCNP} self-assembly at pH 7.60 with addition of glucose	$PNAM_{100}$-*b*-[P(NAM_{20}-*stat*-GLA_{80})]^{SCNP}		29600	28000	1.12	-

* These samples were run in the same calibration which is different to those in **Figure 4.5** due to the recalibration of the SEC system when the analysis was carried out.

[a] $M_{n,th} = [M]_0 \times p \times M_M/[CTA]_0 + M_{CTA}$, p is the monomer conversion determined by ^{1}H NMR.

[b] Determined by SEC in DMF with PMMA used as molecular weight standards, M_p represents the maximum peak value of the size-exclusion chromatogram.

[c] Folding parameter $<G> = M_{p,SCNP}/M_{p,linear}$, the molecular weight variation caused by the cross-linking reaction (*e.g.* the attached DBA units) was not taken into account.

4.5 References

1. Anfinsen, C. B. Principles that Govern the Folding of Protein Chains. *Science* **1973**, 181 (4096), 223-230.

2. Dobson, C. M. Protein folding and misfolding. *Nature* **2003**, 426 (6968), 884-890.

3. Mahon, C. S.and Fulton, D. A. Mimicking nature with synthetic macromolecules capable of recognition. *Nat. Chem.* **2014**, 6 (8), 665-672.

4. Stuart, M. A. C.; Huck, W. T. S.; Genzer, J.; Muller, M.; Ober, C.; Stamm, M.; Sukhorukov, G. B.; Szleifer, I.; Tsukruk, V. V.; Urban, M.; Winnik, F.; Zauscher, S.; Luzinov, I.and Minko, S. Emerging applications of stimuli-responsive polymer materials. *Nat Mater* **2010**, 9 (2), 101-113.

5. Hanlon, A. M.; Lyon, C. K.and Berda, E. B. What Is Next in Single-Chain Nanoparticles? *Macromolecules* **2016**, 49 (1), 2-14.

6. Lyon, C. K.; Prasher, A.; Hanlon, A. M.; Tuten, B. T.; Tooley, C. A.; Frank, P. G.and Berda, E. B. A brief user's guide to single-chain nanoparticles. *Polym. Chem.* **2015**, 6 (2), 181-197.

7. Ouchi, M.; Badi, N.; Lutz, J. F.and Sawamoto, M. Single-chain technology using discrete synthetic macromolecules. *Nat. Chem.* **2011**, 3 (12), 917-924.

8. Altintas, O.and Barner-Kowollik, C. Single-Chain Folding of Synthetic Polymers: A Critical Update. *Macromol. Rapid Commun.* **2016**, 37 (1), 29-46.

9. Altintas, O.and Barner-Kowollik, C. Single chain folding of synthetic polymers by covalent and non-covalent interactions: current status and future perspectives. *Macromol. Rapid Commun.* **2012**, 33 (11), 958-971.

10. Gonzalez-Burgos, M.; Latorre-Sanchez, A.and Pomposo, J. A. Advances in single chain technology. *Chem. Soc. Rev.* **2015**, 44 (17), 6122-6142.

11. Pomposo, J. A. Bioinspired single-chain polymer nanoparticles. *Polym. Int.* **2014**, 63 (4), 589-592.

12. Sanchez-Sanchez, A.; Perez-Baena, I.and Pomposo, J. A. Advances in click chemistry for single-chain nanoparticle construction. *Molecules* **2013**, 18 (3), 3339-3355.

13. Mavila, S.; Eivgi, O.; Berkovich, I.and Lemcoff, N. G. Intramolecular Cross-Linking Methodologies for the Synthesis of Polymer Nanoparticles. *Chem. Rev.* **2016**, 116 (3), 878-961.

14. Huo, M.; Wang, N.; Fang, T.; Sun, M.; Wei, Y.and Yuan, J. Single-chain polymer nanoparticles: Mimic the proteins. *Polymer* **2015**, 66, A11-A21.

15. Zhang, J.; Gody, G.; Hartlieb, M.; Catrouillet, S.; Moffat, J.and Perrier, S. Synthesis of Sequence-Controlled Multiblock Single Chain Nanoparticles by a Stepwise Folding–Chain Extension–Folding Process. *Macromolecules* **2016**, 49 (23), 8933-8942.

16. Hosono, N.; Kushner, A. M.; Chung, J.; Palmans, A. R. A.; Guan, Z.and Meijer, E. W. Forced Unfolding of Single-Chain Polymeric Nanoparticles. *J. Am. Chem. Soc.* **2015**, 137 (21), 6880-6888.

17. Mes, T.; van der Weegen, R.; Palmans, A. R.and Meijer, E. W. Single-chain polymeric nanoparticles by stepwise folding. *Angew. Chem. Int. Ed. Engl.* **2011**, 50 (22), 5085-5089.

18. Hosono, N.; Palmans, A. R. A.and Meijer, E. W. "Soldier-Sergeant-Soldier" triblock copolymers: revealing the folded structure of single-chain polymeric nanoparticles. *Chem. Commun.* **2014**, 50 (59), 7990-7993.

19. Altintas, O.; Krolla-Sidenstein, P.; Gliemann, H.and Barner-Kowollik, C. Single-Chain Folding of Diblock Copolymers Driven by Orthogonal H-Donor and Acceptor Units. *Macromolecules* **2014**, 47 (17), 5877-5888.

20. Altintas, O.; Lejeune, E.; Gerstel, P.and Barner-Kowollik, C. Bioinspired dual self-folding of single polymer chains via reversible hydrogen bonding. *Polym. Chem.* **2012**, 3 (3), 640-651.

21. Wong, E. H. H.; Lam, S. J.; Nam, E.and Qiao, G. G. Biocompatible Single-Chain Polymeric Nanoparticles via Organo-Catalyzed Ring-Opening Polymerization. *ACS Macro Letters* **2014**, 3 (6), 524-528.

22. Beck, J. B.; Killops, K. L.; Kang, T.; Sivanandan, K.; Bayles, A.; Mackay, M. E.; Wooley, K. L.and Hawker, C. J. Facile Preparation of Nanoparticles by Intramolecular Cross-Linking of Isocyanate Functionalized Copolymers. *Macromolecules* **2009**, 42 (15), 5629-5635.

23. Shishkan, O.; Zamfir, M.; Gauthier, M. A.; Borner, H. G.and Lutz, J.-F. Complex single-chain polymer topologies locked by positionable twin disulfide cyclic bridges. *Chem. Commun.* **2014**, 50 (13), 1570-1572.

24. Altintas, O.; Willenbacher, J.; Wuest, K. N. R.; Oehlenschlaeger, K. K.; Krolla-Sidenstein, P.; Gliemann, H.and Barner-Kowollik, C. A Mild and Efficient Approach to Functional Single-Chain Polymeric Nanoparticles via Photoinduced Diels–Alder Ligation. *Macromolecules* **2013**, 46 (20), 8092-8101.

25. Hanlon, A. M.; Martin, I.; Bright, E. R.; Chouinard, J.; Rodriguez, K. J.; Patenotte, G. E.and Berda, E. B. Exploring structural effects in single-chain "folding" mediated by intramolecular thermal Diels-Alder chemistry. *Polym. Chem.* **2017**.

26. Lambert, R.; Wirotius, A.-L.and Taton, D. Intramolecular Quaternization as Folding Strategy for the Synthesis of Catalytically Active Imidazolium-Based Single Chain Nanoparticles. *ACS Macro Letters* **2017**, 489-494.

27. Nguyen, T.-K.; Lam, S. J.; Ho, K. K. K.; Kumar, N.; Qiao, G. G.; Egan, S.; Boyer, C.and Wong, E. H. H. Rational Design of Single-Chain Polymeric Nanoparticles That Kill Planktonic and Biofilm Bacteria. *ACS Infectious Diseases* **2017**, 3 (3), 237-248.

28. Fischer, T. S.; Schulze-Sünninghausen, D.; Luy, B.; Altintas, O.and Barner-Kowollik, C. Stepwise Unfolding of Single-Chain Nanoparticles by Chemically Triggered Gates. *Angew. Chem. Int. Ed.* **2016**, 55 (37), 11276-11280.

29. Knöfel, N. D.; Rothfuss, H.; Willenbacher, J.; Barner-Kowollik, C.and Roesky, P. W. Platinum(II)-Crosslinked Single-Chain Nanoparticles: An Approach towards Recyclable Homogeneous Catalysts. *Angew. Chem. Int. Ed.* **2017**, 56 (18), 4950-4954.

30. Aiertza, M.; Odriozola, I.; Cabañero, G.; Grande, H.-J.and Loinaz, I. Single-chain polymer nanoparticles. *Cell. Mol. Life Sci.* **2012**, 69 (3), 337-346.

31. Harth, E.; Horn, B. V.; Lee, V. Y.; Germack, D. S.; Gonzales, C. P.; Miller, R. D.and Hawker, C. J. A Facile Approach to Architecturally Defined Nanoparticles via Intramolecular Chain Collapse. *J. Am. Chem. Soc.* **2002**, 124 (29), 8653-8660.

32. Berda, E. B.; Foster, E. J.and Meijer, E. W. Toward Controlling Folding in Synthetic Polymers: Fabricating and Characterizing Supramolecular Single-Chain Nanoparticles. *Macromolecules* **2010**, 43 (3), 1430-1437.

33. Murray, B. S.and Fulton, D. A. Dynamic Covalent Single-Chain Polymer Nanoparticles. *Macromolecules* **2011**, 44 (18), 7242-7252.

34. Hosono, N.; Gillissen, M. A. J.; Li, Y.; Sheiko, S. S.; Palmans, A. R. A.and Meijer, E. W. Orthogonal Self-Assembly in Folding Block Copolymers. *J. Am. Chem. Soc.* **2013**, 135 (1), 501-510.

35. Penfold, N. J. W.; Lovett, J. R.; Verstraete, P.; Smets, J.and Armes, S. P. Stimulus-responsive non-ionic diblock copolymers: protonation of a tertiary amine end-group induces vesicle-to-worm or vesicle-to-sphere transitions. *Polym. Chem.* **2017**, 8 (1), 272-282.

36. Cobo, I.; Li, M.; Sumerlin, B. S.and Perrier, S. Smart hybrid materials by conjugation of responsive polymers to biomacromolecules. *Nat Mater* **2015**, 14 (2), 143-159.

37. Surnar, B.and Jayakannan, M. Stimuli-Responsive Poly(caprolactone) Vesicles for Dual Drug Delivery under the Gastrointestinal Tract. *Biomacromolecules* **2013**, 14 (12), 4377-4387.

38. Du, J.; Fan, L.and Liu, Q. pH-Sensitive Block Copolymer Vesicles with Variable Trigger Points for Drug Delivery. *Macromolecules* **2012**, 45 (20), 8275-8283.

39. Sun, X.and James, T. D. Glucose Sensing in Supramolecular Chemistry. *Chem. Rev.* **2015**, 115 (15), 8001-8037.

40. Gillissen, M. A. J.; Voets, I. K.; Meijer, E. W.and Palmans, A. R. A. Single chain polymeric nanoparticles as compartmentalised sensors for metal ions. *Polym. Chem.* **2012**, 3 (11), 3166-3174.

41. Rowan, S. J.; Cantrill, S. J.; Cousins, G. R. L.; Sanders, J. K. M.and Stoddart, J. F. Dynamic Covalent Chemistry. *Angew. Chem. Int. Ed.* **2002**, 41 (6), 898-952.

42. Whitaker, D. E.; Mahon, C. S.and Fulton, D. A. Thermoresponsive Dynamic Covalent Single-Chain Polymer Nanoparticles Reversibly Transform into a Hydrogel. *Angew. Chem. Int. Ed.* **2013**, 52 (3), 956-959.

43. Sanchez-Sanchez, A.; Fulton, D. A.and Pomposo, J. A. pH-responsive single-chain polymer nanoparticles utilising dynamic covalent enamine bonds. *Chem. Commun.* **2014**, 50 (15), 1871-1874.

44. Sanchez-Sanchez, A.and Pomposo, J. A. Single-Chain Polymer Nanoparticles via Non-Covalent and Dynamic Covalent Bonds. *Particle & Particle Systems Characterization* **2014**, 31 (1), 11-23.

45. Brooks, W. L. A.and Sumerlin, B. S. Synthesis and Applications of Boronic Acid-Containing Polymers: From Materials to Medicine. *Chem. Rev.* **2016**, 116 (3), 1375-1397.

46. Ren, J.; Zhang, Y.; Zhang, J.; Gao, H.; Liu, G.; Ma, R.; An, Y.; Kong, D.and Shi, L. pH/Sugar Dual Responsive Core-Cross-Linked PIC Micelles for Enhanced Intracellular Protein Delivery. *Biomacromolecules* **2013**, 14 (10), 3434-3443.

47. Coumes, F.; Woisel, P.and Fournier, D. Facile Access to Multistimuli-Responsive Self-Assembled Block Copolymers via a Catechol/Boronic Acid Ligation. *Macromolecules* **2016**, 49 (23), 8925-8932.

48. Cambre, J. N.and Sumerlin, B. S. Biomedical applications of boronic acid polymers. *Polymer* **2011**, 52 (21), 4631-4643.

49. Deng, C. C.; Brooks, W. L. A.; Abboud, K. A.and Sumerlin, B. S. Boronic Acid-Based Hydrogels Undergo Self-Healing at Neutral and Acidic pH. *ACS Macro Letters* **2015**, 4 (2), 220-224.

50. De, P.; Gondi, S. R.; Roy, D.and Sumerlin, B. S. Boronic Acid-Terminated Polymers: Synthesis by RAFT and Subsequent Supramolecular and Dynamic Covalent Self-Assembly. *Macromolecules* **2009**, 42 (15), 5614-5621.

51. Bapat, A. P.; Roy, D.; Ray, J. G.; Savin, D. A.and Sumerlin, B. S. Dynamic-Covalent Macromolecular Stars with Boronic Ester Linkages. *J. Am. Chem. Soc.* **2011**, 133 (49), 19832-19838.

52. Roy, D.; Cambre, J. N.and Sumerlin, B. S. Triply-responsive boronic acidblock copolymers: solution self-assembly induced by changes in temperature, pH, or sugar concentration. *Chem. Commun.* **2009**, (16), 2106-2108.

53. Edwards, J. O.; Morrison, G. C.; Ross, V. F.and Schultz, J. W. The Structure of the Aqueous Borate Ion. *J. Am. Chem. Soc.* **1955**, 77 (2), 266-268.

54. Lorand, J. P.and Edwards, J. O. Polyol Complexes and Structure of the Benzeneboronate Ion. *J. Org. Chem.* **1959**, 24 (6), 769-774.

55. Blanazs, A.; Armes, S. P.and Ryan, A. J. Self-Assembled Block Copolymer Aggregates: From Micelles to Vesicles and their Biological Applications. *Macromol. Rapid Commun.* **2009**, 30 (4-5), 267-277.

56. Mai, Y.and Eisenberg, A. Self-assembly of block copolymers. *Chem. Soc. Rev.* **2012**, 41 (18), 5969-5985.

57. Zhou, F.; Xie, M.and Chen, D. Structure and Ultrasonic Sensitivity of the Superparticles Formed by Self-Assembly of Single Chain Janus Nanoparticles. *Macromolecules* **2014**, 47 (1), 365-372.

58. Wen, J.; Yuan, L.; Yang, Y.; Liu, L.and Zhao, H. Self-Assembly of Monotethered Single-Chain Nanoparticle Shape Amphiphiles. *ACS Macro Letters* **2013**, 2 (2), 100-106.

59. Smagowska, B.and Pawlaczyk-Łuszczyńska, M. Effects of Ultrasonic Noise on the Human Body—A Bibliographic Review. *Int. J. Occup. Saf. Ergonomics* **2013**, 19 (2), 195-202.

60. Sousa, S. C. O.; Junior, C. G. L.; Silva, F. P. L.; Andrade, N. G.; Barbosa, T. P.and Vasconcellos, M. L. A. A. Microwave-promoted morita-baylis-hillman reactions: efficient synthesis of new monoacylglycerols (MAGs) as potential anti-parasitic compounds. *J. Braz. Chem. Soc.* **2011**, 22, 1634-1643.

61. Gody, G.; Maschmeyer, T.; Zetterlund, P. B.and Perrier, S. Pushing the Limit of the RAFT Process: Multiblock Copolymers by One-Pot Rapid Multiple Chain Extensions at Full Monomer Conversion. *Macromolecules* **2014**, 47 (10), 3451-3460.

62. Martin, L.; Gody, G.and Perrier, S. Preparation of complex multiblock copolymers via aqueous RAFT polymerization at room temperature. *Polym. Chem.* **2015**, 6 (27), 4875-4886.

63. Postma, A.; Davis, T. P.; Li, G.; Moad, G.and O'Shea, M. S. RAFT Polymerization with Phthalimidomethyl Trithiocarbonates or Xanthates. On the Origin of Bimodal Molecular Weight Distributions in Living Radical Polymerization. *Macromolecules* **2006**, 39 (16), 5307-5318.

64. Moad, G.and Barner-Kowollik, C., The Mechanism and Kinetics of the RAFT Process: Overview, Rates, Stabilities, Side Reactions, Product Spectrum and Outstanding Challenges. In *Handbook of RAFT Polymerization*, Wiley-VCH Verlag GmbH & Co. KGaA: 2008; pp 51-104.

65. Schmidt, B. V.; Fechler, N.; Falkenhagen, J.and Lutz, J. F. Controlled folding of synthetic polymer chains through the formation of positionable covalent bridges. *Nat. Chem.* **2011**, 3 (3), 234-238.

66. Pomposo, J. A.; Perez-Baena, I.; Buruaga, L.; Alegría, A.; Moreno, A. J.and Colmenero, J. On the Apparent SEC Molecular Weight and Polydispersity Reduction upon Intramolecular Collapse of Polydisperse Chains to Unimolecular Nanoparticles. *Macromolecules* **2011**, 44 (21), 8644-8649.

67. Foster, E. J.; Berda, E. B.and Meijer, E. W. Metastable Supramolecular Polymer Nanoparticles via Intramolecular Collapse of Single Polymer Chains. *J. Am. Chem. Soc.* **2009**, 131 (20), 6964-6966.

68. Tuten, B. T.; Chao, D.; Lyon, C. K.and Berda, E. B. Single-chain polymer nanoparticles via reversible disulfide bridges. *Polym. Chem.* **2012**, 3 (11), 3068-3071.

69. Roy, R. K.and Lutz, J. F. Compartmentalization of single polymer chains by stepwise intramolecular cross-linking of sequence-controlled macromolecules. *J. Am. Chem. Soc.* **2014**, 136 (37), 12888-91.

70. Beck, J. B.; Killops, K. L.; Kang, T.; Sivanandan, K.; Bayles, A.; Mackay, M. E.; Wooley, K. L.and Hawker, C. J. Facile Preparation of Nanoparticles by Intramolecular Crosslinking of Isocyanate Functionalized Copolymers. *Macromolecules* **2009**, 42 (15), 5629-5635.

71. Heiler, C.; Offenloch, J. T.; Blasco, E.and Barner-Kowollik, C. Photochemically Induced Folding of Single Chain Polymer Nanoparticles in Water. *ACS Macro Letters* **2017**, 6 (1), 56-61.

72. Hanlon, A. M.; Chen, R.; Rodriguez, K. J.; Willis, C.; Dickinson, J. G.; Cashman, M.and Berda, E. B. Scalable Synthesis of Single-Chain Nanoparticles under Mild Conditions. *Macromolecules* **2017**, 50 (7), 2996-3003.

73. Pomposo, J. A.; Rubio-Cervilla, J.; Moreno, A. J.; Lo Verso, F.; Bacova, P.; Arbe, A.and Colmenero, J. Folding Single Chains to Single-Chain Nanoparticles via Reversible Interactions: What Size Reduction Can One Expect? *Macromolecules* **2017**, 50 (4), 1732-1739.

74. Hassan, P. A.; Rana, S.and Verma, G. Making Sense of Brownian Motion: Colloid Characterization by Dynamic Light Scattering. *Langmuir* **2015**, 31 (1), 3-12.

75. Mecerreyes, D.; Lee, V.; Hawker, C. J.; Hedrick, J. L.; Wursch, A.; Volksen, W.; Magbitang, T.; Huang, E.and Miller, R. D. A Novel Approach to Functionalized Nanoparticles: Self-Crosslinking of Macromolecules in Ultradilute Solution. *Adv. Mater.* **2001**, 13 (3), 204-208.

76. Cherian, A. E.; Sun, F. C.; Sheiko, S. S.and Coates, G. W. Formation of Nanoparticles by Intramolecular Cross-Linking: Following the Reaction Progress of Single Polymer Chains by Atomic Force Microscopy. *J. Am. Chem. Soc.* **2007**, 129 (37), 11350-11351.

77. Song, C.; Li, L.; Dai, L.and Thayumanavan, S. Responsive single-chain polymer nanoparticles with host–guest features. *Polym. Chem.* **2015**, 6 (26), 4828-4834.

78. Du, J.and O'Reilly, R. K. Advances and challenges in smart and functional polymer vesicles. *Soft Matter* **2009**, 5 (19), 3544-3561.

79. Roy, D.and Sumerlin, B. S. Glucose-Sensitivity of Boronic Acid Block Copolymers at Physiological pH. *ACS Macro Letters* **2012**, 1 (5), 529-532.

80. Fang, H.; Kaur, G.and Wang, B. Progress in Boronic Acid-Based Fluorescent Glucose Sensors. *Journal of Fluorescence* **2004**, 14 (5), 481-489.

81. Ferguson, C. J.; Hughes, R. J.; Nguyen, D.; Pham, B. T. T.; Gilbert, R. G.; Serelis, A. K.; Such, C. H.and Hawkett, B. S. Ab Initio Emulsion Polymerization by RAFT-Controlled Self-Assembly. *Macromolecules* **2005**, 38 (6), 2191-2204.

Chapter 5 *Conclusions & Outlook*

The aim of this thesis was to employ reversible addition fragmentation chain transfer (RAFT) polymerization to synthesize sequence controlled multiblock copolymers (MBCPs) in order to understand the relationship between the monomer sequence of a polymer chain and the resulting microstructure and functionality. The obtained materials were used to investigate the self-assembly of block copolymers in the bulk or in solution which leads to the formation of different types of objects with a tailored microstructure.

In order to provide a fundamental guidance for the synthesis of polymeric materials with certain physical property, an experimental study was focused on the self-assembly of sequence controlled MBCPs in the bulk. A series of MBCPs were synthesized by RAFT polymerization. Their glass transition temperatures (T_gs) were characterized by differential scanning calorimetry (DSC). Small Angel X-ray Spectroscopy (SAXS) analysis was also applied to investigate the microphase separation of the MBCPs. DSC and SAXS analyses showed that microdomain space was a characteristic size of inhomogeneity which decreased when lowering the size of the blocks. This study provided fundamental understanding of the relationship between the glass transition temperatures and the number of segments whilst maintaining the overall degree of polymerization. This work also demonstrated the enormous potential of multiblock architectures to tune the physical properties and morphologies.

Sequence controlled synthetic polymers have proven to possess great potential in tuning the microstructure of polymeric systems and to generate nanostructured materials. The specific activity of biopolymers (e.g. proteins) can be traced back to their highly defined tertiary structure, which is primarily a result of a perfectly controlled folding process of polypeptide chain. The investigation of folding sequence controlled copolymers to fabricate materials with

a distinct microstructure to mimic the elegant folding process of biopolymers was carried out. A chain extension-folding sequence was utilized to create a complex pentablock polymer chain having up to three individually folded segments, separated by non-functional spacer blocks. The linear precursor which is decorated with pendent hydroxyl units was synthesized by RAFT polymerization. These sections were folded using an isocyanate cross-linker to form single chain nanoparticles (SCNPs) prior to chain extension. This strategy represents a highly versatile way to produce multiblock SCNPs which enables the folding of specific domains within polymer chains. This feature is a further step on the way to copy nature's ability to synthesize highly defined biomimetic macromolecules with a distinct three dimensional (3D) structure.

The 3D architecture of proteins originate from their controlled folding process of a single-stranded polypeptide chain which further self-assemble into selectively tailored quaternary structure. These multimeric complexes can interact and respond to the environment to perform specific biological functions. In order to mimic the higher order level of self-assembly of folded biopolymers, the stepwise folding of a well-defined linear polymer chain followed by intermolecular self-assembly was investigated. Tadpole like SCNPs was prepared by folding of the cross-linkable block of a diblock copolymer and then self-assembled into micelles at neutral pH. These structures were capable of unfolding and disassembling either at low pH or in the presence of sugar. This study displays the folded synthetic polymer chains capable of self-assembling into a higher-ordered structure which is responsive to external stimuli and brings polymer chemistry closer to the responsive nature of biopolymers.

Multiblock copolymers exhibit tremendous potential in terms of tuning the microstructure to generate synthetic materials with desired sizes, structures, properties and functionalities. The increased understanding of RAFT mechanism will greatly expand the versatility of this approach for the preparation of novel functional materials. In future, more

effort should be devoted to the synthesis of highly complex polymeric structures in a more efficient and convenient way. The development of multiblock copolymers will bring the high precision of sequence of biopolymers in reach. The advances of sequence controlled polymers will offer more opportunities for the construction of biomimetic nano-structures.